Christian Doppler Laboratorium für metallurgische Grundlagen von Stranggießprozessen
Lehrstuhl für Metallurgie, Department Metallurgie
Montanuniversität Leoben

Formulation of a Hot Tearing Criterion for the Continuous Casting Process

An der Montanuniversität Leoben eingereichte Dissertation zur Erlangung des akademischen Grades eines Doktors der montanistischen Wissenschaften

vorgelegt von Dipl.-Ing. Robert F. Pierer
Leoben, September 2007

Erstbegutacher: Univ.-Prof. Dipl.-Ing. Dr. mont. Wilfried Krieger
Lehrstuhl für Metallurgie, Department Metallurgie
Montanuniversität Leoben
Zweitbegutachter: Univ.-Prof. Dipl.-Ing. Dr. mont. Bruno Buchmayr
Lehrstuhl für Umformtechnik, Department Product Engineering
Montanuniversität Leoben

Acknowledgments

First of all, my special thanks go to Ass. Prof. Dr. Christian Bernhard due to many reasons. He gave me the opportunity for writing this thesis within the *Christian Doppler Laboratory for Metallurgical Fundamentals of Continuous Casting Processes*. As the supervisor of this laboratory, our discussions (not only of scientific nature), his contributions and support accompanied me during the last years. Furthermore, the presentation of the investigations at international conferences and the publications in various journals were only possible because of his assistance. The success of the present thesis is certainly a result of the excellent team work. I also appreciated the time we spent aside from working hours, but always coming back to scientific discussions late in the day.

I would also like to thank my Ph. D. supervisor Univ. Prof. Dr. Wilfried Krieger – the supervisor of the *Chair of Metallurgy* – his assistance is also highly appreciated. Thanks also go to all colleagues from the department, especially the hard-working men from the workshop who supported me in the accomplishment of the laboratory experiments.

Univ. Prof. Dr. Bruno Buchmayr, my second Ph.D. supervisor, is the one who gave the essential hints for improving the quality of the present thesis. Thank you for the final discussion and comments on the work.

The financial background was provided by the Austrian Ministry for Economy and Labour in the framework of the Christian Doppler Laboratories and the industrial partner of this work, *Siemens VAI Metals Technologies GmbH & Co.* My contact person from the industry – Dr. Christian Chimani – as well as his colleagues were always aivalable for discussions. In addition, Christian's invaluable contributions to the publications made the papers 'more sophisticated'. Again, thanks a lot for the excellent collaboration during the whole project.

Finally, I would also like to mention a couple of persons who more or less contributed to the success of the present thesis. From Markus Lechner I learned how the internet works, of course only concerning job-related things such as 'literature search'. Bernd Linzer showed me the importance and the correct approach to meetings or other events with respect to being 'on time'. Jürgen Reiter is the one who consequently tried to get to the bottom of possibilities and feasibility of things. Thank you for the excellent metallographic work. Augustin Karasangabo showed me that nothing is as it seems to be. 'Merci beaucoup' to my friend from another world showing me what the word liberal really stands for. Sebastian Michelic – a very young colleague with a big future – improved my English, mathematics, physics and coding. 'Please note' that without your help nothing would really work. Special thanks go to Gerhard Wieser who introduced me to the big, wide world of microsegregation modelling. The LaTeX-style of the present thesis comes from very

old friends of mine, Johann and Georg Wurzenberger. Furthermore, thanks to Birgit Färber who was my proof reader. Last but not least, thanks go to Lisa and her endless patience. Our 'after business' discussions and your unusual technical understanding played a decisive role in the progress of the work. Again, thank you for your 'backing' and your patience during the completion of this work.

Affidavit

I hereby declare that the following Ph. D. Thesis has been written only by the undersigned and without any assistance from third parties.

Furthermore, I confirm that no sources have been used in the preparation of this thesis other than those indicated in the work itself.

Robert F. Pierer
Leoben, September 2007

Contents

List of Symbols

Latin Letters

A	s^{-1}	coefficient in Eq. 3.11
A_m	mm^2	area of the mushy zone
A_s	mm^2	area of the solidified shell
a	mm	crack length
b	μm	liquid film thickness
c_P	%	equivalent carbon content
c_p	J/kgK	heat capacity
d	μm	grain size
d_{grain}	μm	grain diameter
d_{cavity}	μm	cavity diameter
d_C	μm	critical diameter
D_{min}	$-$	minimum fracture strain in Eq. 3.19
E	N/m^2	*Young's* modulus
f_L	$-$	fraction of liquid
f_S	$-$	fraction of solid
${}^C f_S$	$-$	critical fraction of solid
G	K/m	temperature gradient
G_{mod}	N/m^2	shear modulus
g	m/s^2	gravity constant
H	J/kg	enthalpy
ΔH_{LS}	J/K	latent heat
h	m	height
I_C	$-$	crack index
K	Ns/m^2	constitutive parameter in Eq. 3.41
K_P	N/m^2	plastic resistance in the *Hollomon* equation
k	W/Km	thermal conductivity
L	m	length unit in Eq. 3.33
l	μm	gage length in Eq. 3.32
l_0	μm	half grain size in Eq. 3.32
Δl_{BTR}	mm	length of the brittle temperature range

m	$-$	coefficient in Eq. 3.11
m_p	$-$	microstructure parameter in Eq. 3.30
m^*	$-$	strain rate exponent in Eq. 3.18 and Eq. 3.41
n^*	$-$	brittle temperature range exponent in Eq. 3.18
n	$-$	strain-hardening exponent
p_m	Pa	metallostatic pressure
p_0	Pa	atmospheric pressure
p_C	Pa	cavitation pressure
p_r	$-$	reserve of plasticity
Δp_ε	Pa	pressure drop due to deformation
Δp_{sh}	Pa	pressure drop due to shrinkage
Q	J/mol	activation energy for deformation
q	MW/m^2	heat flux density
R	$J/Kmol$	gas constant
R_S	m/s	solidification velocity of solidus isotherm
r	m	radius
r_{tb}	m	radius of the test body
r_0	m	inner radius of the induction furnace
S_C	$-$	cracking susceptibility coefficient
${}^T S_C$	$-$	total cracking susceptibility coefficient
${}^S S_C$	$-$	specific cracking susceptibility coefficient
s	mm	shell thickness
s_{coat}	mm	coating thickness
T	℃	temperature
$\dot{T}$	K/s	cooling rate
T_L	℃	liquidus temperature
T_S	℃	solidudus temperature
T_{SB}	℃	steel bath temperature
T_{coal}	℃	coalescence temperature
T_{coh}	℃	coherency temperature
ΔT_B	℃	brittle temperature range
ΔT_{LS}	℃	solidification interval
ΔT_{SA}	℃	temperature range of preferable strain accumulation
t	s	time
t_A	s	time of strain accumulation
t_C	s	casting time
t_f	s	local solidification time
Δt_{BTR}	s	time interval within the brittle temperature range

v	m/s	velocity
v_C	m/min	casting speed
v_{prop}	mm/s	propagation velocity
v_T	m/s	solidification velocity in Eq. 3.22
$W_{\Delta T_B}$	MPa	difference of deformation energy in the brittle temperature range

Greek Letters

α	$-$	ratio between solid-liquid and solid-gas interfacial energy
β	MPa^{-1}	coefficient in Eq.3.18
β_{sh}	%	shrinkage factor
γ_{GB}	mJ/m^2	grain boundary energy
γ_{SL}	mN/m	solid-liquid interfacial tension
γ_{LG}	mN/m	surface tension
γ_{SG}	mJ/m^2	solid-gas surface energy
γ_{fr}	mJ/m^2	effective fracture surface energy
γ_P	mJ/m^2	specific plastic deformation energy
$\Delta\varepsilon_{res}$	$-$	reserve of strain in Eq. 3.19
$\Delta\varepsilon_{free}$	$-$	linear free shrinkage strain in Eq. 3.19
$\Delta\varepsilon_{app}$	$-$	apparent strain in Eq. 3.19
ε_A	$-$	accumulated strain
ε_C	$-$	critical strain of hot tearing
$\varepsilon_{C,A}$	$-$	critical accumulated strain of hot tearing
ε_{eff}	$-$	effective strain
ε_{fr}	$-$	fracture strain
ε_P	$-$	strain due to the process
$\varepsilon_{P,A}$	$-$	accumulated strain due to the process
ε_p	$-$	effective plastic strain
ε_{sh}	$-$	shrinkage strain
ε_{th}	$-$	thermal strain
ε_{tol}	$-$	tolerable strain
$\varepsilon_{\theta\theta}$	$-$	circumferential plastic strain
$\dot{\varepsilon}$	s^{-1}	strain rate
$\dot{\varepsilon}_p$	s^{-1}	effective plastic strain rate
$\dot{\varepsilon}_C$	s^{-1}	critical strain rate
η	$Pa \cdot s$	viscosity
η_H	$-$	hardening parameter
θ	$^\circ$	dihedral angle
κ	m^2	permeability
λ_1	μm	primary dendrite arm spacing
λ_2	μm	secondary dendrite arm spacing

ν	$-$	*Poisson's* ratio
ρ	kg/m^3	density
σ	N/m^2	stress
σ_{fr}	N/m^2	fracture stress
σ_C	N/m^2	critical (fracture) stress
σ_P	N/m^2	stress due to the process
σ_{max}	N/m^2	maximum stress
σ_{min}	N/m^2	minimum stress
σ_0	N/m^2	flow stress of fully solidified steel
φ	$-$	coefficient in Eq. 3.18

Superscripts, Subscripts

A	accumulation
$init$	initiation
L	liquid
M	mushy zone
P	process
$prop$	propagation
S	solid
γ	austentite
δ	δ-ferrite

Abbreviations

ATL	average tear length
ATL_0	initial average tear length
BTR	brittle temperature range
DfI	distance from interface
GM	Gaussian mean
HCS	hot tearing (cracking) coefficient
HT	holding time
LHT	length of hot tears
LIT	liquid impenetrable temperature
NHT	number of hot tears
SD	standard deviation
SPV	maximum volumetric flow rate
$SSCT$	submerged split chill tensile
SRG	velocity of volumetric solidification shrinkage
ZDT	zero ductility temperature
ZST	zero strength temperature

1 Introduction

A continuous casting machine is principally a metallurgical machine, and a good machine must be designed by metallurgists and not by mill builders.[a]
IRVING ROSSI

[a]Irving Rossi, Concast and Daedomorphy, (1978).

The problem of hot tearing in the continuous casting process has been an important area of research for several decades. At the Chair of Metallurgy at the University of Leoben, hot tearing of steels has been investigated for 20 years. The great interest in this subject matter can be explained by the trend towards higher casting speed for enhanced caster productivity and the development of new steel grades showing a possibly higher hot tearing sensitivity.

Hot tearing criteria in continuous casting are mainly based on critical values of stress or strain, because these approaches enable the quantification of deformation limits. The stresses and strains in the process originate from both, thermal and mechanical loads, which result mainly from[1] contraction and phase transformation, temperature gradients along the surface or across the shell, friction between strand and mould, bending and straightening as well as bulging and soft reduction.

Using sophisticated mechanical strand models, the strain and strain rates within the solidification interval (mushy zone) due to the above mentioned loads can be calculated exactly. Thus, using a strain-based criterion seems to be the most promising approach. However, the accuracy of such a criterion strongly depends on the "quality of critical strain values", which are necessary for the quantification of hot tearing. For determining critical values of hot tearing, mainly experiments were carried out. Critical stress data are rather rare in the literature, most publications focus on the evaluation of critical strain values. Similarly to the different testing equipments used, the results of critical strains differ in the relevant literature[2–7]. Especially at carbon contents lower than 0.3 $wt.\text{-}\%C$, values of the critical strain show a very high scatter band. Nevertheless, taking into account the brittle temperature range* and the strain rate and using different experimentally determined results, Won *et al.*[8] proposed an empirical equation of the critical strain of hot tearing. In a first estimation of the critical strain, the proposed empirical equation is certainly a good

*The brittle or critical temperature range is defined as a certain temperature range within the mushy zone where hot tears tend to occur. A detailed consideration will be carried out later in the work.

approximation. However, for certain steel grades it can also be shown that calculated values differ from experimentally determined results[9].

Furthermore, the consideration of solely a critical strain and consequently only the initiation of hot tears are not sufficient to provide a basis for the enhancement of the caster design. A further mechanism of hot tearing – the tear propagation (growth) – must be considered. Therefore, the aim of the present thesis is to perform a series of experiments under continuous casting conditions to make a step forward in the description of hot tearing. These experiments will be conducted using the continuously modified and improved *Submerged Split Chill Tensile (SSCT)-test*. Based on experimentally determined results, a new hot tearing criterion taking into account the influence of the chemical composition, the strain rate and the solidification conditions will be developed.

Chapter 2 provides a comprehensive literature study illustrating the most important influencing parameters as well as the basic theories of hot tearing. An important intention of the following work is the theoretical review of the phenomenon of hot tearing not only in conjunction with the continuous casting process of steel. Many hot tearing criteria found in the literature were partly developed in the field of welding or have their origin in die casting of aluminum alloys or other materials. These hot tearing criteria are summarised in *Chapter 3*. Subsequently, selected hot tearing criteria are applied to laboratory experiments to predict the expected hot tearing tendency. The calculation procedures and the results – the hot tearing susceptibility – are illustrated in *Chapter 4*. Using these results and considering the demands on the final cast product, the major requirements to a process related hot tearing criterion will be deduced in *Chapter 5*. Based on these considerations the concept behind the new hot tearing criterion will be introduced in *Chapter 6*. As already suggested, the developed model is a strain-based hot tearing criterion which assumes that a certain temperature range exists within the solidification interval where strain can be accumulated. Before presenting the results of the experimental investigations, the applied testing method will be described in *Chapter 7* together with the procedure of the metallographic analysis. The main part of the present work is the illustration and interpretation of the experimental results in conjunction with the developed hot tearing model. This will be done in *Chapter 8*, where the phenomenon of hot tearing is investigated in terms of the hot tearing susceptibility (critical strain of tear initiation) and the evolution of the initiated tears (tear propagation).

Therefore, the used approach is contrasted against common hot tearing models. This approach does not only consider whether hot tearing takes place or not, it also takes into account the strain-dependent severity of hot tearing.

2 Hot Tearing

Like the anatomist, the metallurgist has been more concerned with form and function that with origins.[a]
C. S. Smith

[a]Technical Publication No. 2387, Class E, Metals Technology, (1948).

The following chapter provides a comprehensive literature study, which is subdivided into five sections. The first section gives an overview on *Definitions of Hot Tearing* according to different authors and research fields. After this, the *Basic Theories of Hot Tearing Mechanisms* are summarised. Three theories, which were already developed 60 years ago are examined in detail. Nevertheless, these considerations are fundamental and represent the background of all hot tearing models developed later. Basically, this chapter focuses on the subject from a theoretical point of view and not from the view point of continuous casting of steel. Therefore, studies dealing with the problem of hot tearing in other processes – such as direct-chill casting or die casting of aluminium alloys or other materials together with studies in the field of welding – are also considered. In a further section (*Factors Controlling Hot Tearing)* the most important parameters affecting hot tearing are discussed. *Further Comments on Hot Tearing* as well as the section *Summary and Conclusions* complete this chapter.

2.1 Definition of Hot Tearing

The literature provides many terms regarding the phenomenon of crack formation at temperatures close to the solidus temperature such as *hot tearing*, *hot cracking*, *hot shortness* or *solidification cracking*. Additionally, the term *internal cracking* – meaning crack formation during solidification – is often used in the field of continuous casting. However, this phenomenon is still of great interest in the continuous casting process due to the permanent tendency towards enhanced casting productivity and increasing quality demands, as well as the development of new steel grades.

Terms and definitions in conjunction with cracks and fracture are specified, for example, in the *Stahl-Eisen-Prüfblatt 1100* [10]. In this document, hot cracks, solidification cracks, melting cracks and shrinkage cracks are considered as *cracks and fractures caused by heat*, which are subdivided

into *manufacturing induced cracks and fractures*. Since the literature often does not distinguish between these types of cracks, the following definitions should be mentioned[10,11]:

> *Hot cracks are intergranular separations which might form during casting, welding or hot forming when the temperatures of sub-areas of the material are between solidus (T_S) and liquidus (T_L) together with simultaneously acting tensile stresses. Their occurrence is linked to the presence of low-melting grain boundary zones in conjunction with local shrinkage.*

Depending on how hot cracks are generated, it will further be distinguished between solidification and melting cracks[11–13]:

> *Solidification cracks are hot cracks, which occur at the end of solidification under acting tensile stresses due to shrinkage. Melting cracks are intercrystalline hot cracks, which are developed due to re-melting phases at grain boundaries together with simultaneously acting tensile stresses.*

In the present study, only crack formation during solidification will be investigated. Thus, the term *melting crack* can be eliminated immediately. Likewise, the definition of *solidification cracks* is not adequate in the continuous casting process, where further stresses need to be considered in addition to shrinkage. However, the definition of *hot cracks* already includes very important facts regarding the phenomenon of hot tearing in the continuous casting process.

Besides the above mentioned definitions, other definitions can be found in the literature. For example, Langlais and Gruzleski[14] use the term *hot tear* in the field of aluminium alloys:

> *Hot tearing is defined by the formation of a macroscopic fissure in a casting as a result of strains and the associated stresses, generated during cooling, at a temperature above the non-equilibrium solidus. The hot tear nucleates and grows interdendritically within the solidifying material.*

According to Eskin *et al.*[15] the phenomenon of hot tearing represents the formation of an irreversible crack (failure) in the still semi-solid casting. Campbell[16] has proposed the following definition:

> *A hot tear is almost certainly a uniaxial tensile failure in a weak material.*

The derived consequences and the deductions of this definition as well as the general considerations of hot tearing in the work of Campbell will be discussed later. The definition according to Langlais and Gruzleski[14] is similar to the definition of hot cracks, whereas the latter two ones describe the problem of hot tearing from a more general point of view.

Finally, Bernhard[17,18] provides the following statement regarding hot tearing during continuous casting:

> *In continuous casting of steels, hot tearing generally results from an overcritical, perpendicularly oriented tensile straining of a columnar solidifying mushy zone. The hot tears that are initiated propagate along interdendritic paths and/or primary grain boundaries.*

The term *mushy zone* (solidification range) corresponds to the temperature range between T_L and T_S and is the solid/liquid two-phase region between fully liquid and fully solid states.

This definition was suggested for the continuous casting process as it also considers that hot tears can only be found in the columnar structure of the product. Due to the very detailed description of the phenomenon of hot tearing in the continuous casting process the latter definition seems to be the most appropriate one and will be used in the present work. Furthermore, the terms ***hot tearing*** and ***hot tear*** are used in the present thesis in order to ensure a consistent terminology.

However, none of the above mentioned definitions distinguish between open and segregated (healed, filled) hot tears. Likewise, considering the description of the microscopic characteristics of hot tears, the segregated hot tears are not mentioned in the relevant literature. In this context, Eskin and Katgerman[19] summarised the findings from the literature[19,20,16,21]:

> *The fracture of hot tears shows a bumpy surface covered with a smooth layer and sometimes with solid bridges that connect or have connected both sides of the crack.*

Furthermore, freely solidified dendritic or grain boundary surfaces are a typical feature[11]. Generally, a spheroidisation of crystals can be obtained with increasing hot tearing tendency. Fig. 2.1a shows an occasionally occurring earing in the hot tearing surface, which indicates a partial bonding of the hot tears (Fig. 2.1b). Furthermore, stable phases (sulphides, phosphides, silicides or carbonitrides, etc.) can mostly be found on the hot tear surface (see Fig. 2.1c and d)[11].

Chapter 5, will point out that – in contrast to the casting of eutectic alloys – both open and segregated hot tears can degrade the quality of the continuously cast steel product. Depending on further processing and the demands on the final product, both types of hot tears have to be seen as potential defects.

Summarising it can be concluded that hot tearing occurs within the mushy zone, for this tensile stresses are necessary. In fact, industrial and fundamental studies of hot tearing show that this phenomenon occurs in the mushy zone at the end of solidification, independent of the material[15]. The temperature range of hot tearing is further restricted between T_S and the temperature, which corresponds to a fraction of solid (f_S) greater than $85-95$ %[15]. Yamanaka *et al.*[22], for example, demonstrate by experimental investigations of steel that hot tearing takes place between $f_S = 0.80$ and 0.99 %*.

The second important fact is the consideration of segregated hot tears, which are neclected in the definitions of hot tearing. Based on the requirements to a process related hot tearing criterion, the definition of Bernhard[17,18] will be modified in Chapter 5 with respect to segregated hot tears.

*In the next section, the necessity of microsegregation models to determine the fraction of solid as a function of temperature will be discussed. These values strongly depend on the used microsegregation analysis.

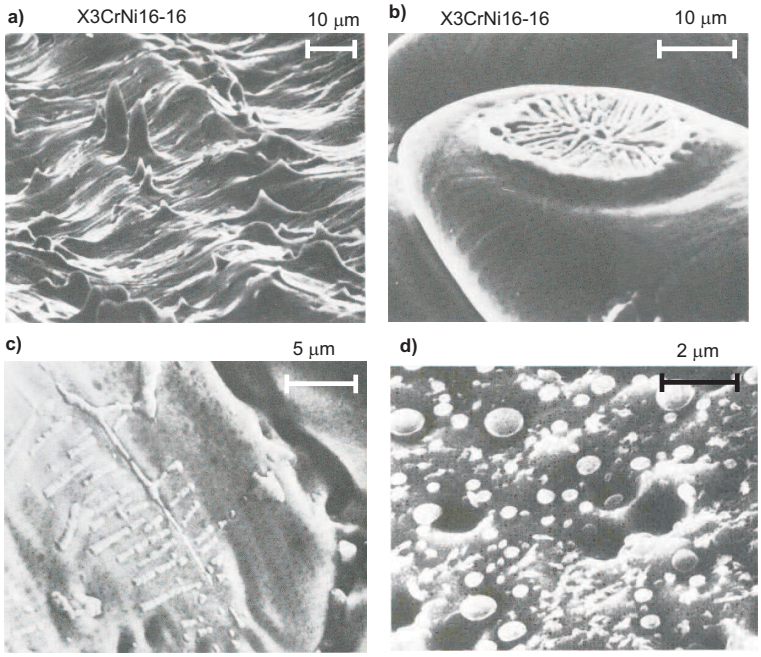

Figure 2.1: *a) Earing in the hot tearing surface, b) fracture in the interdendritic contact zone c) hot tearing surface with dendritic sulphides and d) disk-like sulphides.*[11]

2.2 Basic Theories of Hot Tearing Mechanisms

In the literature various investigations have been conducted to explain the mechanism of hot tearing in casting. However, according to Langlais and Gruzleski[14], basically three different theories can be distinguished, which are summarised in the following sections:

2.2.1 The Shrinkage Brittleness Theory

This theory was first proposed by Verö[23], and was mainly applied in the field of Al-Si alloy systems[24–26]. During the liquid-solid state and the solidification progress, the primary crystals come into contact (coherency temperature) and form a coherent network, which is illustrated in Fig. 2.2. Generally, the mushy zone can be classified into different stages, based on the permeability of the solid network. From a certain point in the mushy zone, the dendrites start to interact with each other. At first, an uninterrupted liquid film still exists between the dendrites. After this, dendrites contact each other and form bridges and finally, a continuous solid phase is formed[15]. A review of the literature[15,16,27–29] leads to a consideration of three different regions within the mushy zone, which are schematically illustrated in Fig. 2.2:

Liquid or viscous flow: Stage 1 corresponds to the formation of primary dendrites at the beginning of solidification, where the movement of the liquid is very easy.

Vulnerable region: The temperature where the secondary dendrite arms start to interact is called the *coalescence temperature*. In this stage the liquid is distributed as an interdendritic film.

With increasing solid fraction, the liquid is isolated in pockets or immobilised by surface tension. However, the permeability of the solid network is sufficient to avoid pore formation.

Coherent region: At the final stage of solidification only isolated drops (liquid pockets) remain and liquid feeding is no longer possible.

The theory postulates that during the cooling from coherent temperature to solidus temperature (*coherent region*) a contraction strain develops that initiates hot tears. It is also stated that in the presence of more than a certain critical portion of liquid any incipient hot tears between primary crystals are healed by liquid feeding.

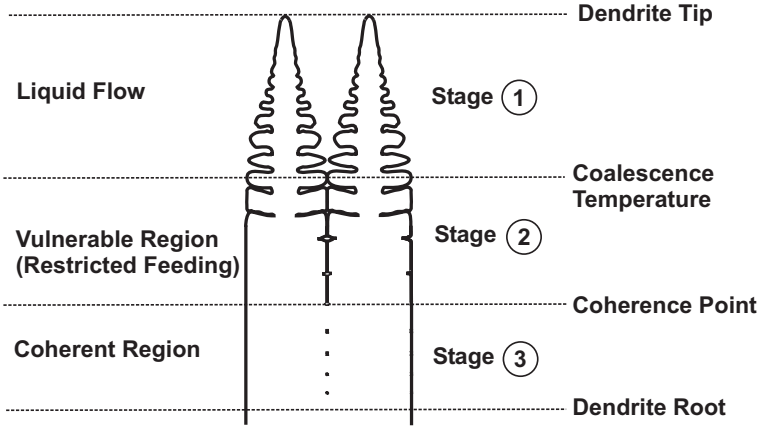

Figure 2.2: *Schematic illustration of the three different stages within the mushy zone*

This theory was later taken up by Russian investigators[30–33] introducing the ***Brittle Temperature Range*** (BTR or ΔT_B) in the field of hot tearing in welds. The upper and lower temperature limits are defined by the coherency temperature and by the temperature at which imposed loads can be absorbed. Generally, the hot tearing tendency is directly related to the extent of the brittle temperature range and consequently to any factor that influences this parameter. A lower hot tearing sensitivity is associated with a more narrow brittle temperature range.

According to several researchers[8,34–37] it was also found that in continuous casting of steels hot tears tend to occur in the brittle temperature range† due to thermal contraction, mechanical deformation and δ/γ phase transformation. Furthermore, the formation of hot tears during continuous casting is generally related to the interaction between a reduced ductility of the solidifying steel in the mushy zone and tensile stresses, which are caused by different mechanisms (bulging, bending, misalignment, etc.). Fig. 2.3 illustrates the characteristics of the strength and the ductility within the mushy zone as well as the parameters ZST, ZDT and LIT:

†In conjunction with crack formation during continuous casting – according to Suzuki *et al.*[38] – three characteristic brittle temperature ranges are distinguished. The mechanisms behind the different brittle temperature ranges were further enhanced by Wolf[39] and Thomas *et al.*[40]. However, regarding hot tearing only the brittle temperature range within the mushy zone is of importance.

Zero Ductility Temperature (ZDT): The reduction of area, as a measure of ductility used in hot tensile tests, remains zero as long as a liquid film exists between dendrites. The first increase in ductility during solidification is identified by the ZDT and is associated with a fraction of solid between 0.98 and 1[22,41,42].

Zero Strength Temperature (ZST): The ramification of secondary dendrite arms and the capillary forces of the residual liquid between the dendrites enable the solidifying material to transmit forces perpendicular to the solidification direction below ZST. This temperature corresponds to f_S of around $0.65 - 0.80$[41,42]. Similar to the definition of ZDT, also this definition results from hot tensile tests needed to explain the measured strength above solidus.

Liquid Impenetrable Temperature (LIT): Below LIT the remaining liquid cannot flow freely. Hence, interdendritic separations cannot be refilled by residual liquid. The reason for this is that the dendrite arms are too compacted and resist feeding of the liquid.

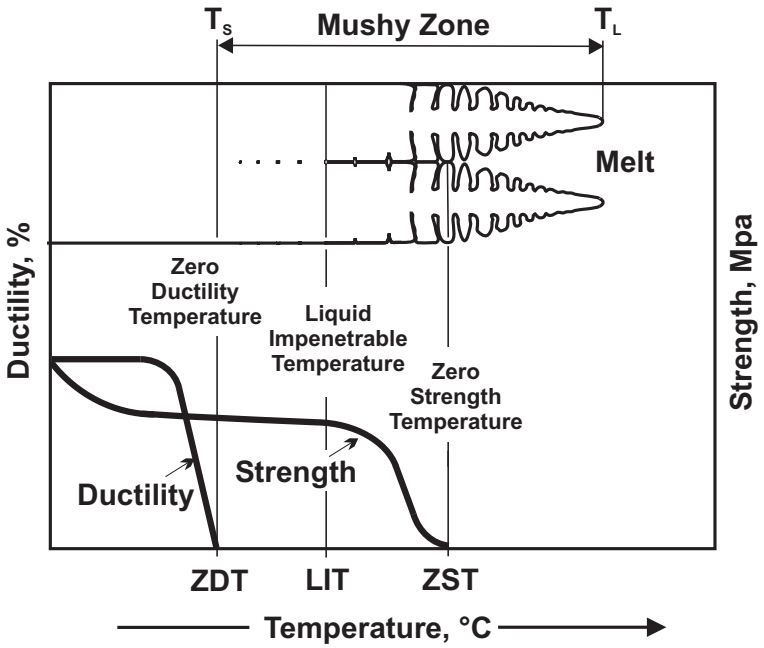

Figure 2.3: *Schematic illustration of the mushy zone together with characteristic temperatures (according to Won* et al.*[8]).*

The terms ZDT and ZST and the corresponding f_S result from experimental work using conventional hot tensile tests. In the literature many studies using this experimental procedure can be found. These publications often investigate the influence of chemical composition, cooling rate and strain rate on resulting characteristic values of the experiment. A more detailed description of the conventional hot tensile test can be found in the relevant literature (see for example references in[43]).

In contrast to ZDT and ZST, LIT is based on theoretical considerations of hot tearing, considering only open hot tears. This assumption is based on the concept of Clyne *et al.*[27,44,35] where the

mushy zone is divided into the *mass and feeding zone* and the *cracking zone*. Hot tears formed in the feeding zone are refilled with surrounding liquid, whereas hot tears formed in the cracking zone cannot be refilled. The fraction of solid in the boundary between the two zones is assumed to be 0.90 %.

Considering the large number of investigations using the hot tensile test under continuous casting conditions, it is not surprising that hot tearing is mainly related to results from these experiments. Consequently, considerations of hot tearing during continuous casting are often associated with ZST, LIT and ZDT. Therefore, these characteristic temperatures are used for defining the brittle temperature range.

In order to investigate hot tearing under continuous casting conditions, Yamanaka *et al.*[22] conducted experiments using a uni-directional tensile test of a cylindrical ingot with a liquid core. This investigation showed that hot tears occured in a certain temperature range. By applying a solidification analysis the corresponding f_S was found in the range of 0.80 and 0.99, which is in good agreement with the values of Kobayashi[45]. Kobayashi analysed the data presented by Schmidtmann and Rakoski[46,47] and indicated that f_S of 0.80 and 0.99 correspond to ZST and ZDT, respectively. Based on these findings a first definition of the brittle temperature range was carried out between these two characteristic temperatures:

$$\Delta T_B = ZST - ZDT = T(f_S = 0.8) - T(f_S = 0.99) \tag{2.1}$$

In order to take into account only open hot tears, Kim *et al.*[48] follow the concept of Clyne and Davies[27]. The latter two define a temperature region where hot tears cannot be refilled with liquid because the dendrite arms are compact enough to resist feeding of the liquid. They proposed a fraction of solid above liquid feeding is restricted to 0.9. Therefore, Kim et al.[48] point out that hot tears formed between ZST and LIT can be refilled with surrounding liquid and leave no hot tear. Finally, the brittle temperature is defined between LIT and ZDT ($\Delta T_B = LIT - ZDT = T(f_S = 0.9) - T(f_S = 0.99)$).

Considering the definition of ΔT_B, the calculation of this parameter requires the determination of the fraction of solid as a function of temperature. In this context, microsegregation plays an important role, since this phenomenon strongly influences the characteristics of f_S as a function of temperature. In order to calculate the temperature dependence of the fraction of solid, different models can be found in the literature. The earliest description is based on the Scheil equation, which neglects back diffusion[49]. Further analytical models are suggested by Brody and Flemings[50], Clyne and Kurz[51], Ohnaka[52] and Kobayashi[53]. A direct finite difference method was published by Ueshima *et al.*[54]. However, a detailed description of the theoretical background of this phenomenon[‡] as well as the existing microsegregation models would go beyond the scope of the present thesis. Nevertheless, it is undoubted that the redistribution of the alloying elements influences hot tearing.

[‡]See for example Kurz and Fisher[55]

Therefore, a first assessment of elements influencing the hot tearing susceptibility can be done in terms of ΔT_B, which consequently depends on the microsegregation of solute elements. Heavy segregating elements, such as sulphur or phosphorus widen ΔT_B and increase the hot tearing susceptibility. Elements that reduce the solute enrichment (e.g. interdendritic MnS precipitation) show a positive effect on the hot tearing susceptibility. In other words, an increasing tendency of hot tearing is generally associated with a high ΔT_B, which implies a large volume of material and a long time interval where hot tears may occur:

$$\Delta l_{BTR} = \frac{\Delta T_B}{G}, \qquad \Delta t_{BTR} = \frac{\Delta T_B}{\dot{T}} \tag{2.2}$$

In these equations, Δl_{BTR} is the length of the brittle temperature range and Δt_{BTR} denotes the time interval during which a volume element moves through the brittle range within the mushy zone. The parameters G and $\dot{T}$ are the temperature gradient and the cooling rate, respectively. Considering the equations for Δl_{BTR} and Δt_{BTR} a further assessment of the parameters G and $\dot{T}$ with respect to hot tearing can be done. Assuming that the hot tearing tendency depends on the length and the time where hot tears may form during directional solidification, the equations state that an increasing temperature gradient as well as an increasing solidification rate decrease the hot tearing susceptibility.

However, the size of the brittle temperature range is not the only material property that influences the hot tearing susceptibility. Zhang and Singer[56] have shown that hot tearing of directionally solidified Ni-based superalloys cannot be explained by ΔT_B only. Some of these alloys show similar freezing behavior but a different hot tearing resistance[57]. Investigations of five different Ni-based alloys have clearly shown that an increasing ΔT_B does not increase the hot tearing tendency.

2.2.2 The Strain Theory

The first to investigate hot tearing of steel was Pellini[58] in the 1950's. Pellini proposed the *Strain Theory* to explain the mechanism of hot tearing. The author assumes that materials associated with an existing liquid film can only sustain a certain amount of strain before tearing. The total strain that develops during the presence of a liquid film therefore depends on the strain rate and the time of film life. The strain theory is schematically illustrated in Fig. 2.4.

Bishop *et al.*[59,60] continued the work of Pellini by investigating the hot tearing of steel. By conducting radiographic studies of the development of hot tears in casting and by conducting strength tests during the solidification of test bars, the liquid *film stage concept* of hot tearing was confirmed for the case of steels. Furthermore, based on these studies the authors point out the following general assumptions and conclusions regarding the hot tearing problem[60]:

- All alloys pass through a critical temperature range of hot tearing during the process of solidification.

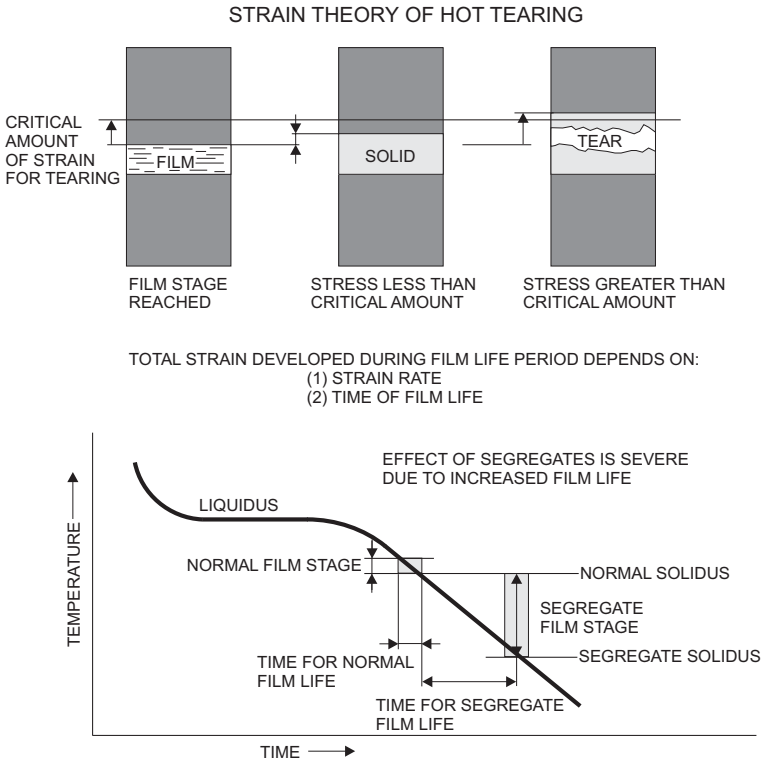

Figure 2.4: *Strain theory of hot tearing according to Pellini[58], schematically*

- The time-rate of extension during the presence of a liquid film (*film stage condition*) is the primary mechanical factor that determines hot tearing.
- A further important critical factor is represented by the specific linear contraction rate. Metals showing high contraction rates at solidus temperature are generally more prone to hot tearing.
- The sensitivity to hot tearing is increased by the presence of low-melting segregates due to the increasing film life time.
- Coarse grain size results in a high concentration of strain per boundary and therefore leads to hot tearing, while fine grain size leads to a decrease in strain concentration. Consequently, finer grains decrease the hot tearing tendency.

2.2.3 The Generalised Theory

The *Generalised Theory* by Borland[61] was developed to explain the mechanism of hot tearing as a combination of the *Shrinkage-Brittleness Theory* and the *Strain Theory*. The main objective was to modify both theories and explain how the liquid quantity and distribution during solidification affects hot tearing. In doing so, Borland suggested the *dihedral angle concept* as an important factor controlling the morphology of the liquid films. Therefore, it is necessary to establish a relationship between the interfacial energies and the liquid distribution at the grain boundaries, which was first discussed by Smith[62]. The ***wettability*** as well as the shape and distribution of grain boundaries

are expressed by the dihedral angle θ. The relationship between θ, the relative interfacial energies of the grain-to-grain interface itself and the grain-to-particle interface is illustrated in Fig. 2.5. The relation between the area of the boundary occupied by the liquid, θ and the fraction of liquid requires complicated geometrical calculations (see references[63–65]).

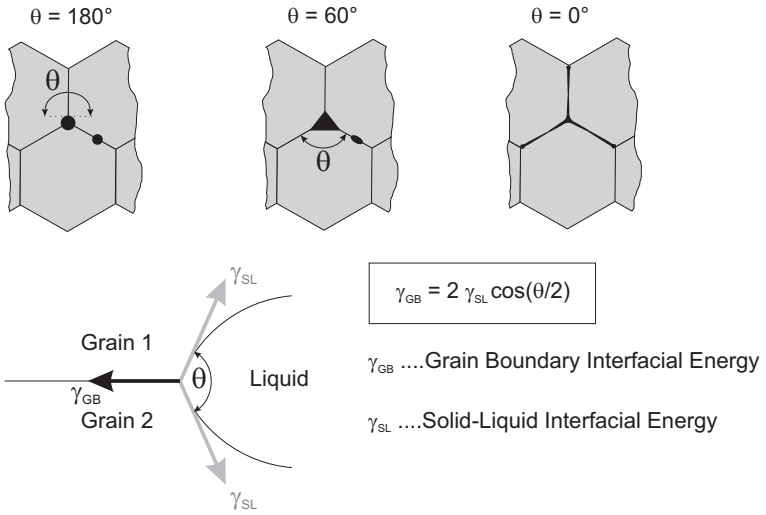

Figure 2.5: *Shape and distribution of the liquid phase at the grain boundaries as a function of θ and the relation between θ and surface energies according to Smith[62].*

According to Borland[61,66], the most likely event of hot tearing in industrial welding can be described by the breaking of solid-solid bridges of grain surfaces covered by liquid, whereas extensive solid-solid bridges prevent cracking. The author pointed out that for hot tearing not only a wide brittle temperature range should exist (*shrinkage-brittleness theory*), and the alloy should pass through a liquid-solid stage (*strain theory*), but the liquid distribution between grains should also allow stresses to build up[61]. The application of this theory requires the relationship between the dihedral angle and the temperature under non-equilibrium conditions. Therefore, Borland conducted experiments mainly on Al-Sn alloys, which were known to be hot tearing sensitive.

Several studies[66–68] illustrate that in addition to the amount of residual liquid, the distribution of the liquid at the grain boundaries has an important influence on hot tearing. A continuous liquid film along grain boundaries provides good conditions for crack propagation, but does not necessarily advance the tear initiation (e.g. $\theta = 0°$ in Fig. 2.5). In contrast, hot tears mainly develop at the interfaces of liquid phases with a very high dihedral angle (e.g. $\theta = 180°$ in Fig. 2.5). Hence, a higher amount of liquid phases (higher dihedral angle) results in a higher damage compared to a continuous liquid film (lower dihedral angle) along grain boundaries.

The importance of θ and the wettability of the grain boundary in conjunction with hot tearing was also mentioned by Campbell[16], referring to the study of Frederickson and Lehtinen[69]. In Al-Sn alloys the liquid Sn wetted the grain boundaries of Al, causing a brittle tensile failure, whereas in Al-Cd alloys the liquid Cd at the grain boundaries did not wet and spread, but remained as compact pools. Investigations of the fractured surface show a ductile fracture in this case.

The three above described theories can be summarised as follows. The *Shrinkage-Brittleness Theory* states that hot tearing takes place within a temperature interval where solid-solid bridges form. It is assumed that hot tearing includes the breaking of these solid-solid bridges. According to the *Strain Theory*, hot tearing is described by the separation of a solid-liquid mass in the absence of solid-solid bridges. The latter prevents hot tearing. The *Generalised Theory* refers to regions of high stresses between grains or highly localised strains due to the liquid distribution between grains. The concept of this theory is that hot tearing takes place after a small number of solid-solid bridges were formed.

Finally, it should be mentioned that these theories have their origin in die casting and/or welding, where the stresses and strains result from constrained shrinkage. This is in contrast to continuous casting, where the strain causing hot tearing can come from a number of sources, as pointed out previously. Therefore, the mushy zone morphology as well as the external characteristics of the process have to be considered. Up to now, no agreement on the exact mechanism of hot tearing has been reached. However, the main parameters influencing hot tearing were extensively investigated in the past. The following section summarises these factors.

2.3 Factors Controlling Hot Tearing

According to the relevant literature (for example[61,70]) it is accepted that the various parameters affecting hot tearing can be grouped in metallurgical or mechanical factors. The latter involve stress, strain and strain rate and will be discussed later in the present thesis. In the following the most important metallurgical factors are summarised.

2.3.1 Metallurgical Parameters

Brittle Temperature Range: This parameter was already discussed in the previous section. The width of the brittle temperature range (Δl_{BTR}) and consequently the influence of the temperature gradient G was illustrated. Furthermore, the deleterious effect of sulphur and phosphorous on hot tearing was mentioned. However, it was also pointed out that the width of the brittle temperature range cannot be the only parameter that affects hot tearing.

Liquid Feeding (Back-Filling): This phenomenon consistently appears in the relevant literature (for example in the *Shrinkage-Brittleness Theory* or in conjunction with LIT) meaning the drawing of liquid back through the mushy zone to feed solidification shrinkage[70]. This phenomenon plays an important role in foundry practise, where risers are used in order to feed hot spots to avoid tear formation. Thus, understanding only open hot tears as potential defects, the phenomenon of liquid feeding is considered in many hot tearing criteria[27,71–74]. However, based on the definition of a hot tear (see section 2.1), Campbell has made the following deductions[16] with respect to liquid feeding:

> *Theories which are based on feeding difficulties can almost certainly be dismissed instantly. Feeding difficulties result in hydrostatic stress in the residual liquid, causing pores or even layer porosity. If the stress exceeds a level of defect nucleation, the liquid separates and expands to create the pores along the dendrites. The dendrites themselves are not affected by pulling apart, but continue to bridge the newly formed volume defect. This is in contrast to hot tearing, where the dendrites open up a pathway first.*

Furthermore, according to Campbell a very important aspect is that dendrites which have separated but still contain residual liquid have always contained liquid. In the literature the terms *healed hot tears* can be found frequently, referring to tears containing residual liquid, but implying that the tears were once empty and refilled by an inflow of liquid. As a result, Campbell indicated that the term *healed hot tear* is misleading and would be better discontinued[16]. A more explicit denotation is *filled hot tear*, referring to a constituted region of segregate (*segregated hot tear*), but only an open (empty) hot tear has to be seen as a major defect[16]. However, as already mentioned above, in continuously cast products also the segregated hot tears must be considered. The reasons for this will be specified later in this work.

Apart from these statements, Campbell[16] has published a comprehensive study on the phenomenon of hot tearing. In this study, the important parameters, which have to be considered are wettability, pre-tear extension, tear initiation as well as tear growth. Wettability was already discussed in conjunction with the *Generalised Theory*. Tear initiation and growth will be discussed in the following section in combination with another important parameter, grain boundaries.

Pre-Tear Extension: Campbell pointed out that the problem starts when the grains (dendrites) collide with each other, but are still largely surrounded by the residual liquid. Thus, he considers a model of hot tearing based on hexagonal and square grains as illustrated in Fig. 2.6. Based on this model, it can be shown that for $3-6$ % of residual liquid phase, the extension prior to the impingement of the grains is $1-2$ %. This shows that the pre-tear extension is proportional to the amount of existing liquid, which was often confirmed by experiments. In addition, the extension is inversely proportional to the grain size for a given amount of liquid. Campbell further stated that with increasing amounts of residual liquid and finer grains, more strain can be accommodated by grain boundary sliding. Burton and Greenwood[75] have shown that grain boundary sliding is the preferred deformation mechanism of the solid if a liquid film exists on grain boundaries and stresses are below a critical value. Therefore, the extension of the solid prior to fracture results from the effects of grain boundary sliding and the extension due to the opening of cracks[76]. However, if the grains are in contact, some deformation of the grains takes place. Such a deformation is confined to the surface of the sliding grains, which was found by Novikov and Novik[77]. In addition, the recovery of the grains is very fast at temperatures close to the melting point, therefore no work hardening occurs.

It can be summarised that the total extension due to grain boundary sliding, independent of an existing liquid film, is approximately $1-2$ % . Higher strains occur during the extension of the crack itself[16].

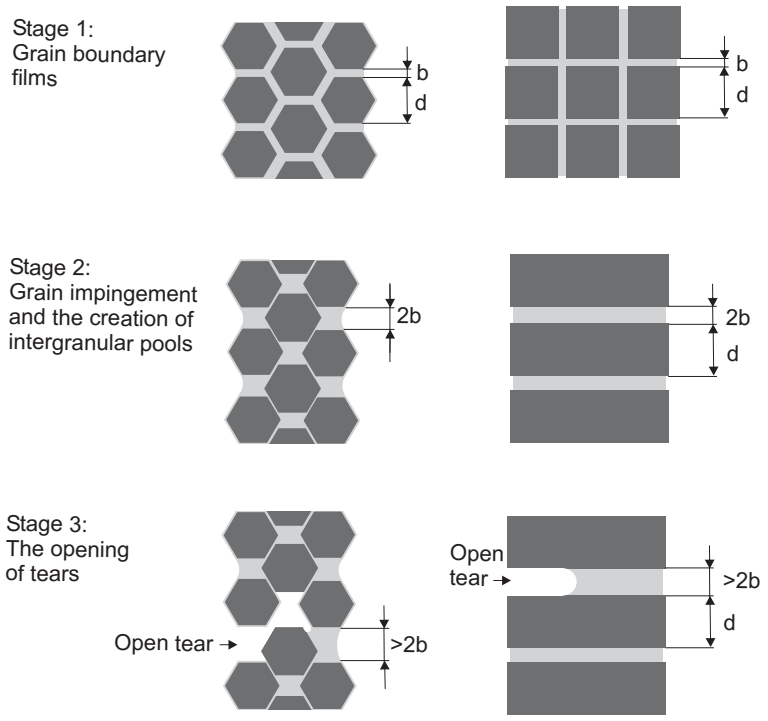

Figure 2.6: *Model of hot tearing using hexagonal and square grains according to Campbell*[16].

Primary Grain Boundaries: Generally, the literature agrees that hot tearing occurs along primary grain boundaries. An explanation for this can be found in the preferential segregation of solute elements at grain boundaries. A further important parameter is the number of grain boundaries. Considering, for example, a coarse grain size including only one boundary leads to the concentration of strain in this liquid film, whereas finer grains including many boundaries result in a more widely distributed strain. Campbell quantifies this fact by dividing the length of a certain range – where a strain exists – by the diameter of the grains.

When considering grain boundaries, ***tear initiation*** is an important aspect. Dendrites within the grain are interconnected. However, if residual liquid exists between the grains, dendrites from neighboring grains do not show such links. Therefore, it can be concluded that hot tears can only start at grain boundaries, not within grains. In this case, the boundaries perpendicular to the tensile stress represent favorable oriented grain boundaries (for the case of columnar grains) which provide conditions for easy initiation of hot tears[16].

Furthermore, Campbell refers to a very important investigation using a simple technique. A transparent cell on a microscope enables the study of the solidification similar to the solidification of a metal. The cell was shaped to provide a sharp corner, around which the solidifying material could be stretched. The outcome of this study was that no matter how much the material was stretched, it was not possible to create a hot tear. Only in the presence of a small inclusion or a bubble near the corner a hot tear nucleates immediately and spreads away from the corner. Thus,

the mechanism of hot tearing requires a nucleus to initiate a crack, which explains much of the scattered nature and the results of the work on the topic[16].

Tear initiation and ***tear growth*** have to be considered as two different phenomena. It is obvious that the tear growth also takes place along such favorable oriented grain boundaries. Spittle and Crushway[21] observe that the linear boundary formed by two columnar crystals represents an easy growth route of a hot tear. This was confirmed by Warrington and McCartney[78] by determining that fine equiaxed grains also promote easy growth directions for hot tearing. A possible explanation for these findings is that owing to the very short paths – due to the fine grain size – the crack propagation remains almost perpendicular to the applied stress. Conversely, a coarse equiaxed structure shows an increasing resistance to crack propagation, because the crack is forced to propagate in directions which do not correspond to the stress direction. Additionally, the plastic work necessary for the deformation of grains tends to increase. Hence, the amount of plastic work, which is expended during crack propagation is of particular importance. It is in the order of at least 10^{-4} times greater than the work required to create the newly formed surface of a hot tear. Thus, Campbell deduced that criteria based on the effect of surface energy as the limiting parameter for crack propagation are not relevant for hot tearing of metals.

In absence of a favorably oriented grain boundary, the further crack propagation for a coarse structure can be caused by transgranular tear growth across the grain, which blocks the crack path. This behaviour was observed by Davies[79] using Sn-Pb alloys. A further possibility is either tear initiation at a short distance ahead in a favorable oriented grain boundary (re-nucleation), or more likely, the crack travels around the grain. Such a behaviour of tear growth was found in investigations of Al-Sn alloys[69].

2.3.2 Mechanical Parameters

The mechanical factors affecting hot tearing involve stress, strain and strain rate. Both, stresses and strains play an important role in the phenomenon of hot tearing. In continuous casting of steel a lot of effort has been taken to determine critical strain and stress values of hot tearing. Critical values of strain were mainly determined experimentally using different testing methods, whereas values of critical stress are rather rare in the relevant literature. Instead, several models were developed to calculate the fracture stress of hot tearing. Both, the summary of experimentally determined critical strain as well as the calculation procedures of critical stress of hot tearing are illustrated in the next chapter. The following section deals with the influence of the strain rate on hot tearing.

In the literature different effects of the **strain rate** on hot tearing can be found. Pellini's[58] idea concerning the effect of the strain rate has already been mentioned. Results of investigations in the field of continuous casting are briefly summarised as follows.

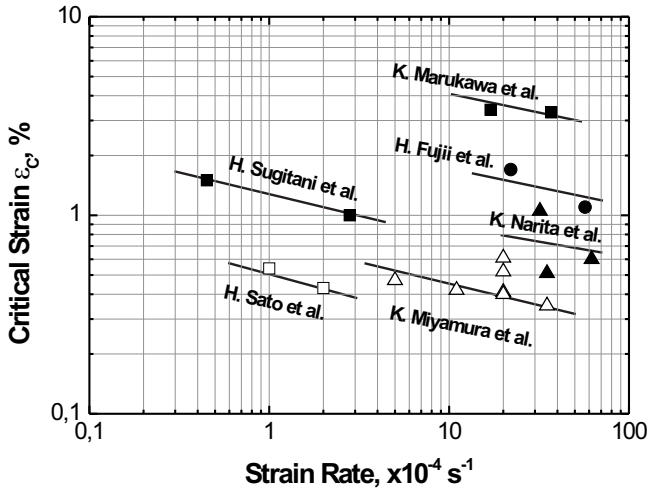

Figure 2.7: *Relation between values of the critical strain as a function of strain rate[3].*

In most studies the strain rate shows a negative effect on hot tearing. The effect of the strain rate on the critical strain as found by different researchers is shown in Fig. 2.7.[§] It can be seen that the critical strain generally decreases with an increasing strain rate. However, it can also be seen that the values of the critical strain at a strain rate of e.g. $1 \cdot 10^{-3}$ s^{-1} varies between 0.5 % and 3 %. This can be explained by the different testing methods used and different investigated steel grades. Besides the illustrated results in Fig. 2.7, further investigations regarding the effect of the strain rate on hot tearing have been performed. Miyazaki *et al.*[2] use bending tests of small-sized ingots for systematic investigations applying different strain rates. The detailed results together with the chemical composition are presented later in the present thesis. A very interesting outcome of these investigations is that with increasing carbon content, and consequently an increasing ΔT_B, the effect of the strain rate on hot tearing tends to decrease. This means that the critical strain of hot tearing of a 0.22 $wt.$-%C steel ranges between approximately 0.8 and 1.5 % for strain rates of $3 \cdot 10^{-3}$ and $1 \cdot 10^{-3}$ s^{-1}, respectively. Applying the same strain rates, the critical strain of a 1.04 $wt.$-%C steel remains nearly constant ($\sim$ 0.6 %). Laboratory experiments with isothermal conditions[80] show an exception of the negative effect of the strain rate. Yamanaka *et al.*[22,81] conducted experiments in order to investigate the influence of the strain rate using steels containing 0.15 $wt.$-%C. At a strain rate of $3 \cdot 10^{-4}$ s^{-1} the critical strain of hot tearing reaches a constant value of 1.6 %. The results of Yamanaka can be summarised as follows. Hot tearing occurs when the total amount of strain within a certain critical temperature range exceeds the critical strain, independent of strain rate and manner of deformation. In addition, the experiments carried out by Yu *et al.*[82] show no influence of the strain rate on hot tearing. The critical strain for peritectic steels is independent of

[§]This figure is taken from the work of Nagata *et al.*[3]. The references of the different researchers can be found in this work.

the strain rate within the range of $5 \cdot 10^{-4}$ and $5 \cdot 10^{-3}$ s^{-1}, which was also found for low carbon steels.

2.4 Further Comments on Hot Tearing

The comprehensive studies of Campbell were already mentioned several times in the present thesis. On the basis of his definition, some deductions were made. The problem of theories which are based on feeding difficulties was already illustrated in conjunction with the phenomenon of *liquid feeding*. Further deductions are[16]:

- Relevant theories of hot tearing explain the weakening of the material casting structure along interdendritic and grain boundaries during solidification.
- Hot tearing has to be understood in terms of hot tear initiation by exceeding a certain critical stress.

The phenomenon of hot tearing according to Campbell can be summarised as follows. Hot tearing is a process depending on nucleation. Tear growth occurs at favorably oriented grain boundaries (perpendicular to the stress direction). Only if a hot tear becomes empty it represents a major defect in the casting material.

However, Campbell mainly refers to die casting of non-ferrous alloys and therefore his considerations cannot be easily be transferred to continuous casting of steel.

Likewise, Sigworth[83] reviewed and analysed the available literature on hot tearing of castings. First of all, the author also mentions the problem concerning criteria which are based on feeding difficulties. Such criteria were published by Feurer[84] as well as by Niyama[85]. According to Sigworth the first problem is that the effect of strain is ignored, and the second is that the liquid hydrostatic tension was the only operating mechanism. However, investigations from practical experience show that this is not the case. Therefore, a better theoretical basis for hot tearing must also be developed. Thus, it would be beneficial to consider some scientific information on liquid metal embrittlement (LME). The problem of LME is defined as the brittle fracture – or loss in ductility – of a usually ductile material in presence of liquid metal. This definition is sometimes modified by the necessity of an external load or the presence of internal residual stresses. In hot tearing no liquid metal is introduced to the solid as in LME, instead, a portion of the alloy is molten. In order to underline the similarity between LME and hot tearing, Sigworth refers to the influence of the grain size on hot tearing. From theoretical considerations, which are also confirmed by experiments, it is known that smaller grain sizes are more ductile and more resistant to hot tearing. The same dependence on grain size was found in LME[86,87].

The liquid metal embrittlement is often approached by employing *Griffith's* crack theory, or its modified form. The original criterion considers a defect or a small crack as a stress concentrator and therefore as the initiator of fracture. Williams and Singer[76] modified *Griffith's* criterion with

respect to hot tearing by considering the liquid film in the mushy zone as a crack. In doing so, the authors argue that the final liquid is the weakest point and the stress concentrator within the mushy zone. The Griffith approach assumes that the strain energy stored in the material (under tension) is released as energy needed to create a new surface area when cracks grow. *Griffith's* theory is applied to ductile materials, even though the surface energy calculated from the observed fracture stress is $10-100$ times too large. This means that most of the fracture energy is consumed in plastic deformation at the root of the growing crack tip. However, in the presence of certain liquid metals, the ductility nearly vanishes, the fracture stress decreases considerably and the surface energy – calculated from *Griffith's* crack theory – is very close to measured surface free energies[87–89]. The liquid metal embrittlement (or hot tearing) is therefore caused by the fact that the surface free energy between liquid and solid (at grain boundaries) is sufficiently small. Hence, it is energetically very easy to create liquid cracks, which was shown most clearly in the study of Kelly and Stoloff[88]. In addition, similar to hot tearing, it has also been observed in LME that the embrittlement is related to the dihedral angle. As illustrated in Fig. 2.5, the dihedral angle is a function of the relative surface energies of the solid grain boundaries and the liquid. The increasing embrittlement due to the liquid with a decreasing dihedral angle was found, for example, in Al-Sn[76] systems and in a number of other metal systems[87].

The statements of Sigworth[83] can be summarised in the following way. Criteria based on feeding difficulties are not adequate to describe the phenomenon of hot tearing. An essential part of Sigworth's work is the consideration of scientific backgrounds of liquid metal embrittlement in the field of hot tearing.

2.5 Summary and Conclusions

Summarising, a lot of effort has been taken to understand the hot tearing phenomenon. In a first section, definitions of hot tearing were illustrated. Generally, the literature only considers open hot tears as a potential defect. Considerations of segregated hot tears cannot be found in the relevant literature. The definition of Bernhard[17,18] accounts for the most important features of hot tearing in the continuous casting process. Later on, this definition will be modified with respect to segregated (filled) hot tears.

Three basic theories which try to describe the mechanisms of hot tearing were presented. The *shrinkage-brittleness* refers to a region within the mushy zone where hot tearing occurs due to shrinkage. The mechanism of hot tearing is the breaking of solid-solid bridges. Based on this theory the term brittle temperature range was introduced, which was also used in conjunction with hot tearing in the continuous casting process. From a more theoretical point of view, the mushy zone is divided into three regions, the *liquid flow*, the *vulnerable* and the *coherent region*. The latter describes the above mentioned brittle temperature range. In the field of continuous casting, the brittle temperature range results from experimentally determined parameters of ZST and ZDT ($\Delta T_B = ZST - ZDT$ or $\Delta T_B = LIT - ZDT$), whereas the liquid impenetrable temperature is based

on theoretical considerations of hot tearing. The determination of these characteristic temperatures is done by conducting conventional hot tensile tests. In these tests, the testing specimen were fully ruptured in all cases, which makes an adequate interpretation of the determined characteristic temperatures rather difficult with respect to hot tearing. In addition, the brittle temperature range cannot be the only parameter affecting hot tearing. However, using the brittle temperature range a first estimation of the hot tearing susceptibility can be done. An increasing brittle temperature range increases the hot tearing susceptibility, which consequently results in a higher tendency to hot tearing in carbon steels with increasing carbon content.

The *strain theory* states that hot tearing occurs when an accumulated strain at existing liquid films at grain boundaries reaches a critical value. Therefore, the accumulated strain depends on the strain rate and the time of film life. The mechanism of hot tearing is the separation of solid-liquid mass in the absence of dendritic coalescence. This concept (strain accumulation within a certain temperature range) is the basic principle of the strain-based hot tearing criterion developed in the present thesis. By the use of an accumulated strain, a critical strain of hot tearing can be defined which directly considers the effect of the strain rate. Moreover, this concept explains the different findings regarding the effect of strain rate. The concept behind the model will be presented later in Chapter 6.

The *generalised theory* combines the previous ones considering liquid quantity and distribution on grain boundaries during solidification. The mechanism of hot tearing is described by the breaking of just formed solid-solid bridges. The wettability and the dihedral angle are the major factors controlling hot tearing. Furthermore, the ratio between the solid-liquid and grain boundary interfacial energies play an important role in this theory. However, data on the above mentioned parameters are rather rare and the effect of the dihedral angle on hot tearing is very difficult to quantify.

The parameters influencing hot tearing are metallurgical and mechanical ones. The most important metallurgical factors are the brittle temperature range (already discussed before) and the influence of primary grain boundaries on tear initiation and growth. Tear initiation and growth occur along primary grain boundaries. The number of grain boundaries (finer grains vs. coarser grains) strongly influences the strain distribution and consequently the extent and sensitivity to hot tearing, respectively. Finally, the problem of liquid feeding (back filling) in combination with hot tearing criteria based on feeding difficulties was also discussed. The mechanical factors controlling hot tearing are strain, stress and train rate. As already mentioned before, the major findings with respect to the strain rate result from experiments with isothermal conditions where no influence of this parameter on hot tearing was observed. The parameters strain and stress will be treated in detail in the next chapter.

Based on the mechanisms of hot tearing, a large number of of hot tearing criteria were developed. The aim of these criteria is to quantify the phenomenon of hot tearing or at least to indicate the susceptibility of hot tearing. The next chapter gives a detailed summary of the existing hot tearing models from literature.

3 Hot Tearing Criteria

Truth is ever to be found in the simplicity, and not in the multiplicity and confusion of things.[a]
SIR ISAAC NEWTON

[a]The Religion of Isaac Newton, Frank E. Manuel (1974).

A comprehensive study of hot tearing criteria for aluminium alloys was published by Eskin *et al.*[15]. In this study the hot tearing models are classified as *stress-based*, *strain-based* and *strain rate-based* criteria. Models that cannot be allocated to this classification are termed as *criteria based on other principles*. In a further publication eight different criteria were implemented in a finite-element method simulation of direct-chill casting of aluminium alloys and were evaluated[90]. The criteria used in this study were classified as non-mechanical aspects such as feeding difficulties, criteria based only on mechanical aspects, and those that combine these features.

The present thesis follows the classification according to Eskin *et al.*[15]. However, Eskin *et al.* consider only hot tearing criteria which were mainly developed in the field of aluminium alloys. The following sections give a detailed overview of existing hot tearing models from literature considering different theoretical approaches. Of course, models in the field of continuous casting of steel are included. Most hot tearing criteria for continuous casting of steels are strain-based models, which compare the strain of the process to a critical strain of hot tearing. The latter is mainly determined using laboratory experiments.

3.1 Stress-Based Hot Tearing Criteria

These models are based on the assumption that a semi-solid body will fracture if the applied stress σ_a exceeds the strength of the material. Two different types of these hot tearing criteria can be distinguished. The first type assumes that the material has a critical limit (stress) at which it fails. This type of criterion is further subdivided into those which assume that the liquid film trapped between the grain boundaries is the limiting parameter (***Case A***), and those which take into account the strength of the solidified material (***Case B***). The second type of the stress-based criteria considers that the material contains defects or weak points (***Case C***). Whether the material will fracture or not depends on e.g. stress, or the initial defect dimension. Furthermore, a consideration of the parameters grain diameter, viscosity or liquid fraction is possible.

3.1.1 Stress-Based Criteria – Case A

A hot tearing criterion based on the liquid film trapped between the grain boundaries as the limiting parameter was published by **Rogberg**[20]. This model assumes that two grains are separated by a thin liquid film with the thickness b as illustrated in Fig. 3.1. The tensile strength (fracture stress, σ_{fr}) to overcome the attraction due to surface tension (γ_{LG}) is expressed by*:

$$\sigma_{fr} = \frac{2 \cdot \gamma_{LG}}{b} \tag{3.1}$$

This model assumes a uniform distribution of liquid and no influence of sliding on the fracture stress. Regarding the surface tension in Eq. 3.1 it is assumed that the liquid and the atmosphere are in contact. Rogberg[20] applied two different values of surface tension ($1.8\,J/m^2$ and $1.0\,J/m^2$) together with measured values of fracture stress to determine the liquid film thickness. In doing so, Rogberg reported values of b between $0.25 - 2\,\mu m$.

Dickhaus *et al.*[92] modified this approach and applied the criterion in the field of continuous casting of Al-alloys. The liquid film thickness was determined based on the geometric conditions as illustrated in Fig. 3.1b:

$$b = \frac{(1 - f_S) \cdot d}{2} \tag{3.2}$$

In Eq. 3.2, f_S is the already mentioned solid fraction (ratio of grain volume and volume of liquid) and d is the average thickness of the solidifying grain.

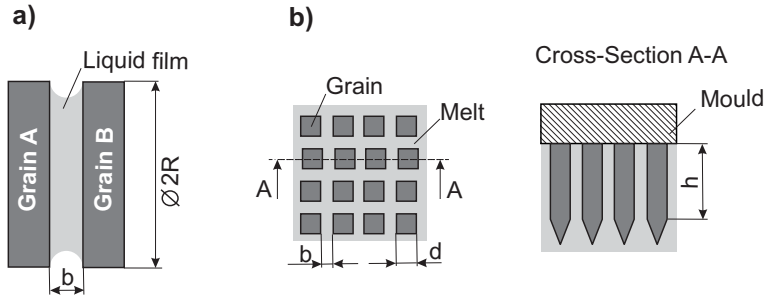

Figure 3.1: *a) Model of two grains separated by a liquid film*[20,91] *and b) schematic illustration of columnar crystals used to predict the liquid film thickness b according to Dickhaus* et al.[92].

However, this model is based on the assumption that the liquid films cover the grain/dendrite surface extensively. In order to describe the fracture of solid-liquid components in welds, Borland[61,67] pointed out the following statement. If the liquid phase is contained internally and is not open to the surface, the following possibilities can be distinguished:

- Separation at the solid-liquid interface: $\gamma_{LG} + \gamma_{SG} - \gamma_{SL}$.

*From an extensive literature review it appears that this expression was first applied on the problem of hot tearing by Saveiko[91]

- Separation within the liquid: $2\,\gamma_{LG}$.
- Penetration of liquid into the solid (e.g. presence of liquid along grain boundaries): $2\,\gamma_{SL} - \gamma_{GB}$.

Eliminating the separation within the liquid and applying the energy balance of the remaining possibilities makes it possible to determine, whether the separation takes place at the solid-liquid interface or along grain boundaries. A detailed derivation can be found in the literature[61,67]. However, introducing the dihedral angle in the interfacial energies leads to the important finding that, for a low dihedral angle, the separation along grain boundaries is more likely to ocurr.

An extension of Eq. 3.1 was proposed by **Lahaie and Bouchard**[93] taking into account the fraction of solid, the fracture strain ε_{fr} and a microstructure parameter m_p. The geometric model assumes that the microstructure of the semisolid material perpendicular to the growth direction can be reasonably idealised by hexagonal grains, as illustrated in Fig. 3.2a. The assumed deformation mechanism is illustrated in Fig. 3.2b. Based on this geometry the strain can be calculated as:

$$\varepsilon = \frac{b_h - b}{a_{hex}\sqrt{3}} \tag{3.3}$$

Eq. 3.3 is related to the side length of the hexagons a_{hex}. Laheie and Bouchard did not use the primary arm spacing λ_1 to define the strain but $a_{hex}\sqrt{3}$. Since λ_1 is the center-to-center distance between two adjacent grains, it is clear that this length is more representative for the microstructure under stress. Therefore, more recently Larouche *et al.*[94] modified this equation, where b_h is the thickness of the horizontal channels and m is a microstructure parameter:

$$\varepsilon = \frac{b_h - b}{\lambda_1} \quad \text{with} \quad b = \lambda_1 \cdot (1 - f_S^{m_p}) \tag{3.4}$$

These redefined equations change the hot tearing criterion in the original publication. Due to the fact that λ_1 is the more representative parameter, the latter equations are applied to the stress-based hot tearing criterion proposed by Lahaie and Bouchard[93]. This model assumes that tear initiation is the critical step. Once it occurs, propagation of the crack will follow until fracture. Furthermore, it is assumed that the liquid capillaries and the atmosphere are in contact (semi-solid body with constrained capillaries at its free surfaces).

The model was developed for direct-chill casting of aluminium alloys. The authors stated that hot tearing in direct-chill cast ingots is a surface defect and that the initiation of the tear may be at or near the free surface of the ingot. The relationship between the surface tension and the liquid film thickness (Eq. 3.1) together with the strain lead to the following expression:

$$\sigma_{fr} = \frac{4 \cdot \gamma_{LG}}{3 \cdot b} \left[1 + \frac{\varepsilon}{1 - f_S^{m_p}}\right]^{-1} \tag{3.5}$$

In order to consider the influence of microstructure on hot tearing, Eq. 3.5 can be applied to equiaxed and columnar grains by adjusting m_p (1/3 for equiaxed and 1/2 for columnar structure).

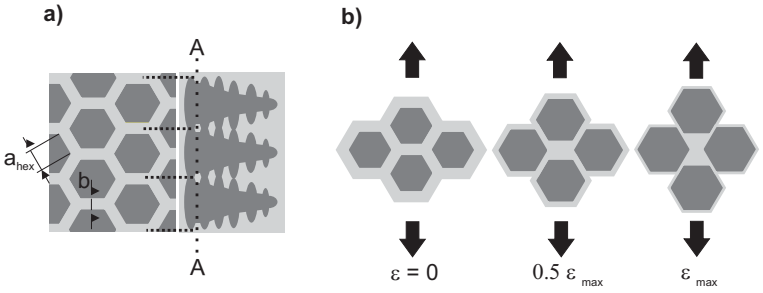

Figure 3.2: *a) Idealised microstructure of a dendritic solidification and b) the schematic illustration of the deformation within the mushy zone according to Lahaie and Bouchard[93].*

According to Drucker[95] the stress on the body is 2/3 the stress in each horizontal channel, and this factor is included in the criterion. Inserting the fracture strain ε_{fr} into Eq. 3.5 finally results in the fracture stress σ_{fr}. This fracture strain is defined in the model of Lahaie and Bouchard[93] as the maximum strain that is limited due to the viscous flow of the intergranular liquid from the inclined channels to the horizontal ones. Assuming furthermore a limiting thickness b_{limit} in the inclined channels to ensure the liquid flow due to the effect of the viscosity, the maximum strain is:

$$\varepsilon_{max} = 2 \cdot \frac{b - b_{limit}}{\lambda_1} \tag{3.6}$$

By inserting the equation of the liquid film thickness into Eq. 3.6 it can easily be shown that the maximum strain is independent of λ_1 ($b_{limit} \gg \lambda_1$), but a function of f_S. Hence, the second term of Eq. 3.5 is only a function of f_S. Assuming a constant surface tension as well as a constant value of f_S, the fracture stress σ_{fr} decreases with increasing liquid film thickness or λ_1, respectively (Eq 3.4). In terms of the grain size, the model predicts a decreasing fracture strain with an increasing grain size, but again, the fracture strain is independent of the grain size. Due to the influence of the microstructure parameter m_p on the film thickness, the value ε_{max} is lower in the case of an equiaxed structure. In contrast to this, the fracture stress shows higher values, when applying a value of $m_p = 1/3$ (equiaxed structure).

The models discussed above are based on the requirement that the solidifying crystals (dendrites) are sufficiently separated by a liquid film. Thus, the mechanical properties of the system are defined by the weakest element, namely the liquid film. As soon as a sustainable framework of crystals (continuous solid network of dendrites/grains) exists, the properties of the liquid become less important compared to the strength of the continuous solid network. During continuous casting of steels, the liquid steel immediately solidifies by forming a solid skin shell. Hence, the case that the liquid film covers the grain/dendrite surface extensively along the total solidified steel shell does not apply in the continuous casting process of steel. However, the considerations of the interfacial energies between solid-liquid and/or along grain boundaries as illustrated by Borland[61,67] are of particular interest for hot tearing. A further interesting point is the principle of maximum strain assuming the above illustrated hexagonal grains. Neglecting the limiting liquid film thickness, the value ε_{max} only depends on f_S. For a columnar microstructure this leads to a maximum strain

(prior to impingement of grains) of $1-3\,\%$ for a f_S between $0.97-0.99$, as also pointed out by Campbell[16].

3.1.2 Stress-Based Criteria – Case B

A second approach of the stress-based hot tearing criteria considers the strength of the solidified material within the mushy zone. In the field of continuous casting of steel, some authors[36,96,97] estimated the possibility of cracking in comparison with the maximum principal stress and/or the transverse stress along the wide and narrow face of the cast product. Some researchers[37,98] proposed that the hot tearing occurs in the mushy zone, when the maximum principal stress exceeds the yield stress at that temperature.

Kim *et al.*[37] proposed the ***cracking susceptibility coefficient*** S_C to predict the effects of operating conditions on the continuous casting process:

$$S_C = \begin{cases} \frac{\sigma_{max}(T)}{\sigma_C(T)} & \text{for} \quad ZDT \leq T \leq ZST \\ 0 & \text{for} \quad ZST \leq T \leq T_L \quad \text{or} \quad \sigma_{max}(T) < 0 \end{cases} \tag{3.7}$$

In Eq. 3.7, σ_{max} denotes the calculated maximum principal stress and σ_C is the critical fracture stress at temperatures between ZDT and ZST. Therefore, hot tears can originate from the region, where S_C exceeds 1. The possibility of hot tearing increases with increasing S_C. The maximum principal stress – developed during the continuous casting process within the product – is calculated using thermo-mechanical computer models. The determination of the critical fracture stress of pure δ-phase and γ-phase is illustrated in the following section[8,36,37,99].

Since the liquid phase has no mechanical strength, the description of the thermo-mechanical behavior between ZST and ZDT is done by treating the mushy zone as a porous material. Thus, the yield criterion proposed by Lee and Kim[100] is applied. In this approach the relative density, the critical relative density as well as the yield stress of the porous metal were replaced by the solid fraction, the critical solid fraction ${}^{C}f_S$ and the yield stress of the mushy zone σ_Y, respectively:

$$\eta_H = \frac{\sigma_Y^2}{\sigma_0^2} = \left[\frac{f_S - {}^{C}f_S}{1 - {}^{C}f_S}\right]^2 \quad \text{at} \quad ZDT \leq T \leq ZST \tag{3.8}$$

In Eq. 3.8, η_H is the hardening parameter due to the solidification and σ_0 is the flow stress of the fully solidified steel. At ZST the fraction of solid becomes ${}^{C}f_S$. The hardening parameter represents the geometrical effect of growing dendrite arms on the strength of steels. As the solid fraction increases from ${}^{C}f_S$ to 1.0, the hardening parameter increases from 0 to 1. Assuming an axial loading of a composite structure of parallel plates, σ_0 can be calculated using the rule of mixture for δ-Fe and γ-Fe:

$$\sigma_0 = {}^{\delta}f_S \cdot {}^{\delta}\sigma + {}^{\gamma}f_S \cdot {}^{\gamma}\sigma \tag{3.9}$$

In Eq. 3.9, the parameters ${}^{\delta}f_S$ and ${}^{\gamma}f_S$ represent the fraction of δ-Fe and γ-Fe, respectively. Inserting Eq. 3.9 into Eq. 3.8 and assuming critical values for all stresses, the following expression for the critical fracture stress σ_C can be used:

$$\sigma_C = \left[\frac{f_S - {}^{C}f_S}{1 - {}^{C}f_S}\right] \cdot ({}^{\delta}f_S \cdot {}^{\delta}\sigma_C + {}^{\gamma}f_S \cdot {}^{\gamma}\sigma_C) \quad \text{for} \quad ZDT \leq T \leq ZST \tag{3.10}$$

This equation shows a linear increase of the critical stress between ZST and ZDT. Below the critical solid fraction, the critical stress of the mushy zone becomes zero ($\eta_H = 0$). At $f_S = 1$ σ_C corresponds to σ_0. In Eq. 3.10, the terms ${}^{\delta}\sigma_C$ and ${}^{\gamma}\sigma_C$ denote the critical fractures stresses of the fully solidified ($f_S = 1$) δ-phase and γ-phase, respectively. The determination of these parameters is done by calculating the flow stress for each Fe-phase as a function of the strain. Thus way, a group of researchers[8,36,37,99,101,102] from Seoul National University applied the constitutive equation proposed by Han *et al.*[103]in their studies in the field of continuous casting. Han *et al.* combined the *Hollomon* equation ($\sigma = K_P \cdot \varepsilon_p^n$) with the modified relationship between the effective plastic strain rate $\dot{\varepsilon}_p$ and the flow stress suggested by Garofalo[104], where A, β and m are constants, Q is the activation energy for deformation and R is the gas constant:

$$\dot{\varepsilon_p} = A \cdot \exp\left(\frac{-Q}{R \cdot T}\right) \cdot [\sinh(\beta \cdot K_P)]^{1/m} \tag{3.11}$$

The *Hollomon* equation was used by Uehara *et al.*[105], modeling continuous casting of low-carbon steels. In this study, it was assumed that the strain hardening exponent n depends on the strain rate and the temperature via the *Zener-Hollomon* parameter. The plastic resistance K_P was assumed to be constant. Inserting K_P from the *Hollomon* equation as well as a critical strain for hot tearing ε_C into Eq. 3.11 finally leads to the critical stress σ_C^i ($i = \delta$ *or* $i = \gamma$):

$$\sigma_C^i = \frac{\varepsilon_C^{n^i}}{\beta^i} \cdot \sinh^{-1}\left[\frac{\dot{\epsilon}}{A^i} \cdot \exp\left(\frac{Q^i}{R \cdot T}\right)\right]^{m^i} \tag{3.12}$$

The material parameters necessary to calculate σ_C are illustrated in Tab. 3.1 for the two Fe-phases[101]. By using Eq. 3.12 and Eq. 3.10 the critical stress for hot tearing can be determined, which is necessary to calculate the cracking susceptibility coefficient S_C in Eq. 3.7.

Phase	β, MPa^{-1}	$n, -$	A, s^{-1}	$Q, kJ/mol$	$m, -$
$\beta - Fe$	0.0933	0.0379	$6.754 \cdot 10^8$	216.9	0.1028
$\gamma - Fe$	0.0381	0.2100	$1.192 \cdot 10^{10}$	373.4	0.2363

Table 3.1: *Parameters necessary to calculate the fracture stress using Eq. 3.10.*

A very important parameter, which has not been discussed up to now, is the critical strain for hot tearing. The detailed description of the procedure to determine this parameter will be presented

later. The critical strain, ε_C, results from an empirical relationship, considering the strain rate and the brittle temperature range.

The crack susceptibility coefficient S_C represents the instantaneous possibility of hot tearing at a certain position within the cast product. In order to estimate the possibility of hot tearing of the whole strand, **Kim**[106] proposed the ***total crack susceptibility*** ${}^{T}S_C$:

$$ {}^{T}S_C = \int_{A_m} \int_{0}^{t_C} S_C \cdot \mathrm{d}t \cdot \mathrm{d}A'_m \tag{3.13} $$

In this equation, A_m represents the area of the mushy zone in the brittle temperature range and t_C is the casting time. Using this approach, Kim determined the possibility of hot tearing at various carbon and sulphur contents in continuously cast beam blanks. With increasing casting speed the dwelling time of the strand within the mould decreases. Consequently, Eq. 3.13 shows a decreasing hot tearing susceptibility. However, the possibility of hot tearing generally rises with increasing casting speed. In order to take into account the influence of casting speed on hot tearing within the mould, Won *et al.*[99] proposed the specific crack susceptibility coefficient ${}^{S}S_C$, where A_s is the area of the solidified shell:

$$ {}^{S}S_C = \frac{{}^{T}S_C}{\int_{A_s} \int_{0}^{t_C} \mathrm{d}t \cdot \mathrm{d}A'_s} \tag{3.14} $$

This parameter shows the average possibility of hot tearing of the whole strand within the mould during continuous casting. Won *et al.*[99] investigated the influence of carbon content, slab width, narrow face taper and casting speed. The calculated maximum hot tearing susceptibility was found between 0.1 and 0.14 $wt.\text{-}\%C$. An increasing slab width as well as an increasing casting speed lead to an increasing ${}^{S}S_C$ in the regions of wide center, corner and off-corner. An increasing narrow face taper leads to a decreasing hot tearing susceptibility along the region of the wide face.

The latest hot tearing criterion published by Won *et al.*[8] is based on the above described calculations of the critical stress for the two Fe-phases (Eq. 3.12). The approach is based on the deformation energy accumulated over the brittle temperature range between LIT and ZDT. The difference of deformation energy within ΔT_B – qualitatively proportional to the possibility of hot tearing – is expressed as follows:

$$ W_{\Delta T_B} = \int_{0}^{\varepsilon_C} (\sigma_{ZDT} - \sigma_{LIT}) \cdot \mathrm{d}\varepsilon \tag{3.15} $$

The parameters σ_{ZDT} and σ_{LIT} must be calculated using Eq. 3.10. Applying this model, Won *et al.*[8] predict a maximum of $\Delta W_{\Delta T_B}$ and therefore the highest probability of hot tearing at a carbon content of 0.12 $wt.\text{-}\%C$.

3.1.3 Stress-Based Criteria – Case C

Besides models assuming that material has a critical stress at which it fails, a stress-based criterion can be found in the literature taking into account a fracture mechanics approach. **Williams and Singer**[76] modified *G*riffith's cracking theory for application as a hot tearing criterion. This idea was already presented in the previous chapter. Again, the volume of liquid in the final stage of solidification acts as crack initiator in terms of the weakest point and stress concentrator within the mushy zone. According to Williams and Singer, the critical stress to propagate the liquid crack is as follows:

$$\sigma_C = \sqrt{\frac{8 \cdot G_{mod} \cdot \gamma_{fr}}{\pi \cdot (1-\nu) \cdot a}} \tag{3.16}$$

The *Griffith* criterion considers the shear modulus G_{mod}, the effective fracture surface energy[†] γ_{fr}, the *Poisson's* ratio ν and the crack length a. For truly brittle fracture the effective fracture surface energy ($\gamma_{fr} = 2\gamma_{SL} - \gamma_{GB}$) results from the solid-liquid interface energy and from the grain boundary energy[107]. According to Skok[108], the *Griffith* criterion is applicable to fracture of brittle materials. Regarding metallic materials, it is not possible to create conditions without plastic strain in the fracture process. Therefore, the *Griffith* criterion was revised and applied to metallic materials by considering the specific plastic deformation energy γ_P. If any plastic deformation occurs at the crack tip, the specific plastic deformation energy must be added ($\gamma_{fr} = 2\gamma_{SL} - \gamma_{GB} + \gamma_P$). Apart from these rather unknown parameters, the crack length must be known. In order to overcome this lack of data, Williams and Singer determined l at the triple point grain boundaries as a function of the grain size, the dihedral angle and the fraction of liquid based on an equiaxed solidification structure. After validating their model in experiments (Al-Zn alloys), which show grain boundary sliding as the main deformation mechanism above T_S, the model was modified for a boundary at 45° to the stress axis. The effective fracture surface energy was used as a fitting parameter in the calculations of the fracture stress. The effect of grain size on the fracture stress calculated with this model and illustrated in their work shows an increase of σ_C with increasing grain diameter. However, Eskin *et al.*[15] pointed out that this is rather doubtful, because casting practice shows less hot tearing susceptibility in fine grain structures.

Summarising, three different approaches were discussed:

- **Case A:** Models based on the liquid film trapped between the grain boundaries as the limiting parameter, e.g. Rogberg[20] or Lahaie and Bouchard[93]. The important parameters are surface tension, interfacial energies, grain boundary energy, liquid film thickness and primary dendrite arm spacing.
- **Case B:** Models based on the strength of the solidified material within the mushy zone, e.g. the studies from the research group at Seoul National University. Important parameters

[†] At this point the energy balance due to separation of grain boundaries, stated by Borland[61,67] should be considered.

represent the critical fraction of solid, where stresses develop first, as well as the necessary material parameters in the constitutive equations.

- **Case C:** Models based on a fracture mechanics approach (*Griffith* criterion), e.g. Williams and Singer[76].

3.2 Strain-Based Hot Tearing Criteria

Approaches of strain-based hot tearing criteria which are mainly applied on Al-Cu alloys are summarised in the following section. A further section focuses on experimentally determined critical strain of hot tearing in the field of continuous casting.

3.2.1 Models Applied on Aluminium Alloys

A strain-based criterion for Al-alloys considering only the strain within the mushy zone due to shrinkage ε_{sh} was proposed by **Novikov and Grushko**[109]. A *reserve of plasticity* p_r is defined, which is the integrated difference between the elongation to failure (ε_C or ε_{fr}) and the linear shrinkage within ΔT_B:

$$p_r = \frac{1}{\Delta T_B} \int_{T_{coh}}^{T_S} (\varepsilon_{fr} - \varepsilon_{sh}) \cdot \mathrm{d}T \tag{3.17}$$

This equation shows that the brittle temperature range is defined between the coherency temperature T_{coh} and the solidus temperature. The hot tearing susceptibility can be expressed by $1/p_r$.

Likewise, **Magnin** *et al.*[110] use such a model for the prediction of hot tearing of an Al–Cu alloy. The authors propose that hot tearing occurs when the maximum plastic strain exceeds the experimentally determined fracture strain in the mushy zone. Finally, the hot tearing susceptibility results from the quotient of the circumferential plastic strain ($\varepsilon_{\theta\theta}$) at T_S and the experimentally determined fracture strain close to T_S. If this quotient is greater than 1, a hot tear will develop.

Zhao *et al.*[111] adopted this approach to predict hot tearing in an Al–Cu alloy. The shrinkage stress is measured and transformed to a critical strain for the formation of a hot tear. The determined strain resulting from experiments is finally compared to the ductility described by Magnin *et al.*. The temperature range where the ductility is lower than the strain induced by solidification shrinkage is considered as potentially hazardous for hot tearing.

Obviously, the strain-based criteria require an experimentally determined critical (or fracture) strain. Hence, the quality of these types of criteria strongly depends on the critical strain of hot tearing. Therefore, the next section gives an overview of the determination of critical strains of hot tearing in the field of continuous casting.

3.2.2 Critical Strain of Hot Tearing

The quantification of limits of hot tearing is an important requirement for hot tearing in the continuous casting process. Therefore, this section focuses on results of this parameter in the field of continuous casting of steel. In the literature, various publications based on laboratory experiments as well as on in-plant trials can be found. The latter were first carried out by Tarmann and Poppmaier[112]. Similar investigations were conducted by **Miyazaki** *et al.*[2]. They deformed 300 *mm* squared blooms using a squeezing test (*roll-squeeze-test*) for the purpose of estimating the influence of roll misalignment on crack formation. The investigated steel grades are illustrated in Tab. 3.2.

Steel No.	C	Si	Mn	P	S	Mn/S	ΔT_B	ε_C	$\dot{\varepsilon}$
1	0.16	0.21	0.45	0.023	0.015	30	49	> 0.8	-
2	0.15	0.03	1.21	0.051	0.051	6	113	0.25	$4.0 \cdot 10^{-4}$
3	0.40	0.28	0.77	0.024	0.020	38	75	0.6	$1.0 \cdot 10^{-3}$
4	0.43	0.27	0.72	0.021	0.023	31	78	0.7	$1.1 \cdot 10^{-3}$
5	0.60	0.22	0.48	0.024	0.023	21	127	0.35	$6.0 \cdot 10^{-4}$
6	0.64	1.69	0.92	0.020	0.014	66	160	> 0.8	-

Table 3.2: *Chemical composition of steels for the squeezing test (in wt.-%) according to Miyazaki[2], Mn/S ratio, calculated brittle temperature range (in* °C*) and the experimentally determined critical strain (in %) and strain rate (in* s^{-1}*) of hot tearing.*

The obtained results can be summarized as follows. Generally, the steels show very high S contents. The Mn/S ratio and the calculated brittle temperature range (microsegregation model according to Ueshima *et al.*[54]) are illustrated in Tab. 3.2. In addition, the determined critical strain together with the calculated (finite element analysis) strain rate are presented in Tab. 3.2.

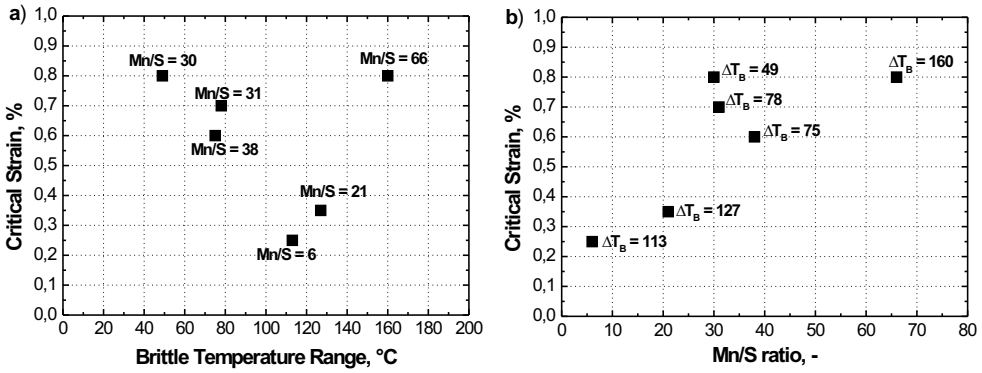

Figure 3.3: *a) Critical strain as a function of the brittle temperature range and b) the Mn/S ratio according to Miyazaki* et al.*[2].*

Fig. 3.3a shows the experimentally determined critical strain as a function of the brittle temperature range. It can be seen from this diagram that the critical strain tends to decrease with increasing brittle temperature range. However, steel number 6 with 0.64 $wt.\text{-}\%C$ and the highest value of ΔT_B shows no hot tears up to a strain of 0.8 %. In that case the brittle temperature range as a measure of the hot tearing sensitivity obviously can not describe the characteristics of the critical strain of hot tearing. A second important parameter is the Mn/S ratio, illustrated in Fig. 3.3b. Steel 6 with the highest value of ΔT_B shows the highest value of Mn/S. Generally, an increasing Mn/S ratio tends to increase the critical strain of hot tearing.

Steel No.	C	Si	Mn	P	S	Mn/S	ΔT_B
1	0.20	0.21	0.45	0.023	0.015	43	51
2	0.44	0.03	1.21	0.051	0.051	40	72
3	0.42	0.28	0.77	0.024	0.020	56	68
4	0.62	0.27	0.72	0.021	0.023	28	98
5	1.04	0.22	0.48	0.024	0.023	27	140

Table 3.3: *Chemical composition of steels for the bending test (in wt.-%) according to Miyazaki[2], Mn/S ratio, calculated brittle temperature range (in* ℃*).*

In order to determine critical strains using laboratory experiments, mainly the bending test is used. With this apparatus, an *in-situ* solidifying strand shell is deformed by applying a defined strain on the liquid-solid interface. Along with the squeezing test, Miyazaki *et al.*[2] also conducted bending tests of small-sized ingots. Using this experiment, systematic investigations with different strain rates were carried out. The chemical composition of the tested ingots can be seen in Tab. 3.3, together with the Mn/S ratio and the brittle temperature range.

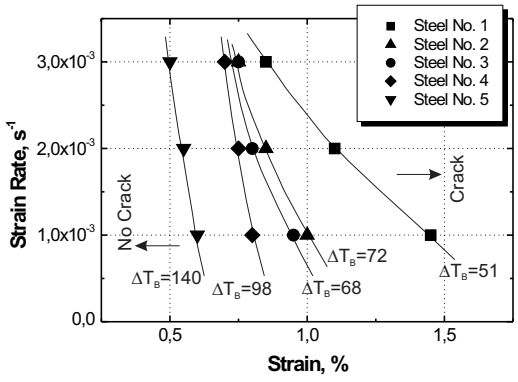

Figure 3.4: *Strain rate vs. critical strain curves for the initiation of hot tears according to Miyazaki* et al.*[2]*

In Fig. 3.4, the values of the critical strain resulting from the bending test are summarised according to the illustration found in the study of Miyazaki *et al.*[2]. The influence of the strain rate on the critical strain of hot tearing can be seen. However, it is very interesting that with an

increasing brittle temperature range – also illustrated in Fig. 3.4 – the influence of the strain rate apparently vanishes. The influence of the brittle temperature range on the critical strain of hot tearing can already be identified in this figure. An increasing brittle temperature range decreases the critical strain. An overview of the critical strain versus the brittle temperature range and the Mn/S ratio is presented in Fig. 3.5.

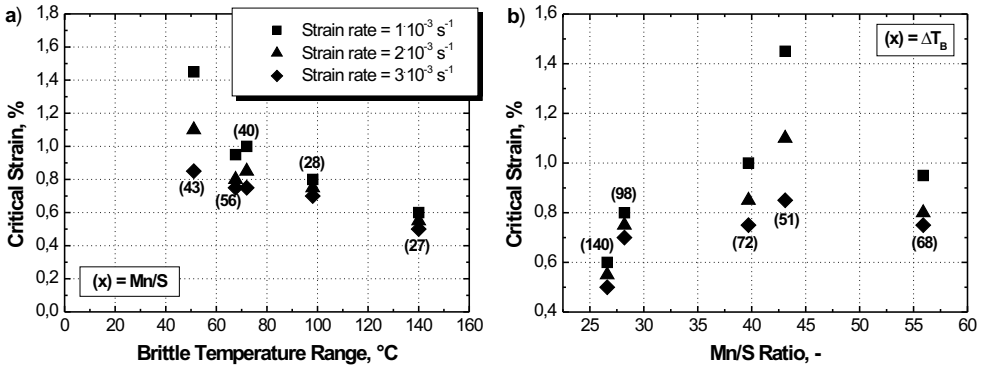

Figure 3.5: *a) Critical strain as a function of the brittle temperature range and b) the Mn/S ratio according to Miyazaki* et al.*[2].*

Nagata *et al.*[3] evaluated the results of carbon steels (0.15 $wt.\text{-}\%C$) from different testing arrangements using the bending test. Typical strain rates under continuous casting conditions range between $10^{-3} - 10^{-4}\ s^{-1}$ [113]. Applying this range of the strain rate, the evaluated critical strains of hot tearing in Nagata's study are between 0.5 and 4.0 % (see Fig. 2.7). It can be concluded that the results of such experiments strongly depend on the testing arrangement. Consequently, these results can not be transferred unrestrictedly to the conditions of the continuous casting process.

Matsumiya *et al.*[4] used an *in-situ* melt-bending test method. The chemical composition of the tested steel grades, the Mn/S ratio, the brittle temperature range and the determined critical strain are summarised in Tab. 3.4. The strain rate at the solidification front is $5 \cdot 10^{-4}\ s^{-1}$. In Fig. 3.6, the critical strain of hot tearing determined by Matsumiya *et al.*[4] is illustrated over the brittle temperature range and the Mn/S ratio. These results show a clear influence of the brittle temperature range on the critical strain, a decreasing critical strain with an increasing brittle temperature range. However, the distinct influence of the Mn/S ratio found by Miazaki *et al.* cannot be seen in Fig. 3.6b. At Mn/S ratios up to 50, the values of the critical strain range between 1.1 and 3.7 %.

Wünnenberg and Flender[5,6] developed an experiment, where an ingot shell is deformed using a deformation tool connected to the piston rod of a double-acting air cylinder. A detailed illustration of the experimental set-up, is provided by Wünnenberg and Flender. In this study, the influence of carbon content ($0.09\ wt.\text{-}\% - 1.16\ wt.\text{-}\%$) is investigated using a basic steel composition with $1.55\ wt.\text{-}\%Mn$ and $0.025\ wt.\text{-}\%S$. The strain rate is $1.7 \cdot 10^{-3}\ s^{-1}$. Fig. 3.7a again shows the dependence of the measured critical strain on the brittle temperature range. The influence of

Steel No.	C	Si	Mn	P	S	Mn/S	ΔT_B	ε_C
1	0.042	0.011	0.224	0.020	0.010	22	12	3.7
2	0.088	0.013	0.476	0.014	0.018	26	29	2.0
3	0.150	0.183	0.500	0.016	0.011	46	34	3.0
4	0.181	0.349	1.360	0.019	0.003	453	24	2.0
5	0.230	0.220	0.440	0.024	0.014	31	67	1.4
6	0.640	0.230	0.770	0.016	0.015	51	72	1.1

Table 3.4: *Chemical composition of steels for the* in-situ *melt-bending test (in wt.-%)according to Matsumiya[4], Mn/S ratio, calculated brittle temperature range (in* °C*) and the experimentally determined critical strain (in %) of hot tearing.*

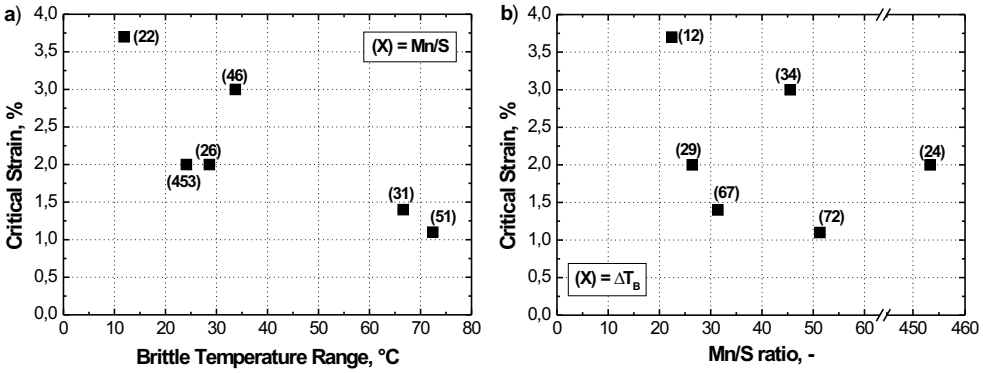

Figure 3.6: *a) Critical strain as a function of the brittle temperature range and b) the Mn/S ratio according to Matsumiya* et al.*[4].*

the brittle temperature range on the critical strain is obvious. An increasing brittle temperature range decreases the critical strain of hot tearing. Due to the constant Mn/S ratio of the tested steel grades (Mn/S=62), an illustration of the critical strain is not useful. However, Wünnenberg and Flender[5,6] investigated the influence of the Mn/S ratio in separate test series, but no critical strain was determined in these investigations. Nevertheless, the authors defined a crack index considering the number of cracks, the mean crack opening, the mean crack length and the mean spacing between adjoining cracks. Therefore, Fig. 3.7b shows the results of the crack index as a function of the Mn/S ratio instead of the critical strain. The deformation in all cases is approximately 3 %. Assuming that the crack index is in inverse proportion to the critical strain, the results of Fig. 3.7b show an increasing critical strain with increasing Mn/S ratio. These results refer to two test series. The first with a constant sulphur content (0.025 $wt.\text{-}\%S$) but varying manganese content, and the second with a higher manganese content (1.55 $wt.\text{-}\%Mn$) but varying sulphur content. Comparing the crack index at a Mn/S ratio of approximately 40, higher sulphur contents show negative effects on hot tearing at the same values of Mn/S, .

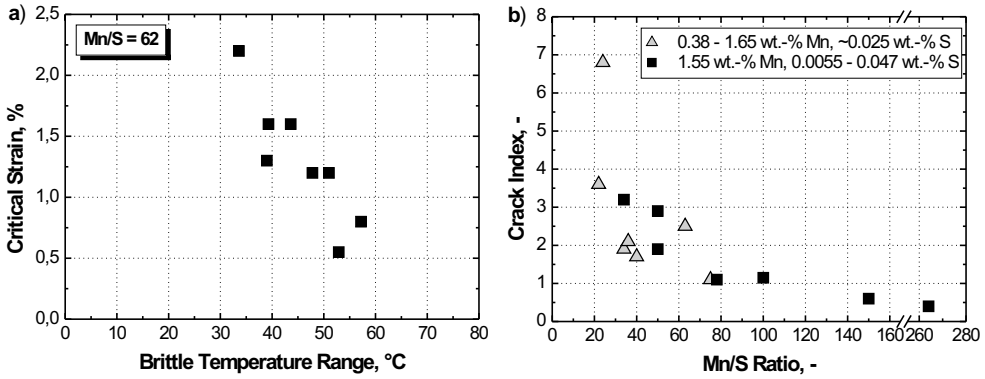

Figure 3.7: *a) Critical strain as a function of the brittle temperature range and b) crack index versus Mn/S ratio according to Wünnenberg and Flender[5].*

Wintz *et al.*[7] conducted bending tests using a similar testing arrangement as Flender[6]. A solidifying ingot is deformed by a punch, generating a controlled strain within the mushy zone. The tested steel grades together with the Mn/S ratio, the brittle temperature range and the critical strain are illustrated in Tab. 3.5. The critical strain as a function of the brittle temperature range and the Mn/S ratio is shown in Fig. 3.8. The influence of both the brittle temperature range and the Mn/S ratio on the critical strain shows more or less the expected tendency. An increasing brittle temperature range leads to a decreasing critical strain, and an increasing Mn/S ratio reduces the proneness to hot tearing (critical strain increases). In particular, the influence of phosphorus on the critical strain was investigated. Increasing the phosphorus content from 0.03 to 0.1 *wt.*-% reduces the critical strain at a carbon content between 0.15 and 0.18 *wt.*-% from 1.0 to 0.8 %. At carbon contents of about 0.40 *wt.*-%, the critical strain decreases from 1.0 to 0.3 %, when increasing the phosphorus content. The reason for that is the increasing amount of austenite during solidification, which leads to an increasing segregation of phosphorous.

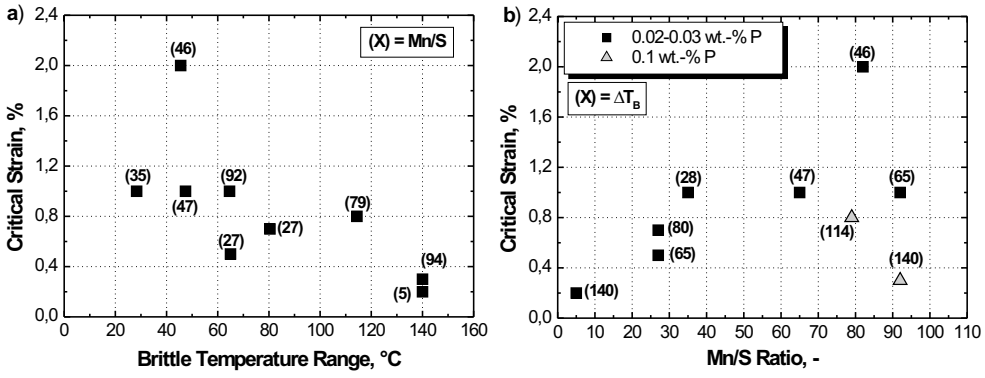

Figure 3.8: *a) Critical strain as a function of the brittle temperature range and b) the Mn/S ratio according to Wintz* et al.*[7].*

Steel No.	C	Mn	P	S	Al	Mn/S	ΔT_B	ε_C
1	0.11	0.46	0.02	0.013	0.07	35	28	1.0
2	0.11	1.23	0.03	0.015	0.12	82	46	2.0
3	0.20	0.48	0.03	0.018	0.08	27	65	0.5
4	0.18	1.30	0.03	0.020	0.04	65	47	1.0
5	0.36	0.46	0.03	0.017	0.13	27	80	0.7
6	0.41	1.10	0.03	0.012	0.09	92	65	1.0
7	0.17	0.50	0.03	0.097	0.12	5	140	1.0
8	0.15	1.10	0.10	0.014	0.07	79	114	0.8
9	0.40	1.10	0.10	0.012	0.08	94	140	0.3

Table 3.5: *Chemical composition of steels for the ingot bending test (in wt.-%) according to Wintz* et al.*[7], Mn/S ratio, calculated brittle temperature range (in* °C*) and the experimentally determined critical strain (in %) of hot tearing.*

Apart from the bending tests, some researchers use uni-directional tensile tests of cylindrical ingots with a liquid core. In the previous section, results of this apparatus were already mentioned in connection with the temperature range of hot tearing. One of these researchers are Yamanaka *et al.*[22,81], who conducted a test series mainly on a 0.15 $wt.\text{-}\%C$ steel (0.60 $wt.\text{-}\%Mn$, 0.02 $wt.\text{-}\%P$ and 0.012 $wt.\text{-}\%S$). In these tests a tensile strain was continuously or intermittently applied to the ingot shell. Contrary to the already discussed studies, which show a clear influence of the strain rate on hot tearing, the results of Yamanaka *et al.* show no strain rate-dependence at strain rates greater than $3 \cdot 10^{-4}\ s^{-1}$. In this case, the resulting critical strain is 1.6 %. At lower strain rates ($< 3 \cdot 10^{-4}\ s^{-1}$), the critical strain sharply increases, i.e. the critical strain is 3.2 % at a strain rate of $1.1 \cdot 10^{-4}\ s^{-1}$. A further important result of this study was that hot tearing is independent of the deformation mode, no matter whether continuous or intermittent.

An experiment which allows the observation of hot tearing during tensile testing was used by Kinefuchi *et al.*[96] and Nakayama *et al.*[114]. As a result, they found that the critical strain of a 0.16 $wt.\text{-}\%C$ steel (1.46 $wt.\text{-}\%Mn$, 0.019 $wt.\text{-}\%P$ and 0.002 $wt.\text{-}\%S$) is between 0.2 % and 0.5 %, and that the critical strain decreases with increasing strain rate.

Mizukami *et al.*[115] applied *in-situ* tensile tests to determine values of the critical strain between ZST and ZDT. The results can be summarised as follows. The critical strain varies from zero at ZST to about 1 % at ZDT in the brittle temperature range. Furthermore, it was found that the critical strain is independent of strain rate and carbon content. The authors reason that these findings result from the lack of liquid in front of the crack.

As illustrated, many researches determined the critical strain of hot tearing in the field of continuous casting of steels. Different testing equipments were used with the result of just as many different values of the critical strain. This fact is illustrated in Fig. 3.9, summarising the previously discussed results as a function of the equivalent carbon content ($c_P = [\%C] + 0.04 \cdot [\%Mn] + 0.1 \cdot [\%Ni] - 0.14 \cdot [\%Si]$[116]). Generally, it can be seen that various values exist at equivalent carbon contents of approximately 0.12, 0.20, 0.40 and 0.60 $wt.\text{-}\%$. At an equivalent carbon content of

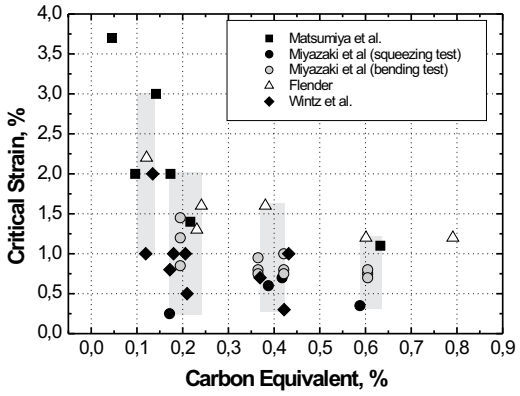

Figure 3.9: *The critical strain of hot tearing as a function of the equivalent carbon content according to different researchers*

nearly 0.12 *wt.*-% the values range from 0.2 to 3 %. Certainly, it can be assumed that the reason for this is the strain rate. Nevertheless, it is interesting to note that with increasing carbon content the scatter band tends to decrease.

Kim *et al.*[37] as well as Won *et al.*[8] proposed an empirical relationship to calculate the critical strain of hot tearing taking into account the brittle temperature range and the strain rate:

$$\varepsilon_C = \frac{\varphi}{\dot{\varepsilon}^{m^*} \cdot {\Delta T_B}^{n^*}} \tag{3.18}$$

In Eq. 3.18, φ denotes a coefficient, m^* is the strain rate exponent and n^* stands for the brittle temperature range exponent. Considering this equation, the critical strain decreases with increasing strain rate and increasing brittle temperature range. The latter depends on the cooling rate and on the content of solute elements: An increasing cooling rate as well as an increasing content of solute elements (e.g. sulphur and/or phosphorus) widen the brittle temperature range, thus decreasing the critical strain. It is well known that heavy segregating elements increase the hot tearing susceptibility and thus, decrease the critical strain of hot tearing. However, the decreasing critical strain with increasing cooling rate is questionable, since the hot tearing tendency generally decreases with increasing cooling rate.

In order to determine the necessary fitting parameters in Eq. 3.18, many experimental data are used (see references in Kim *et al.* and Won *et al.*). These data of critical strain were best fitted by a nonlinear fitting method, resulting in $\varphi = 0.02821$, $m^* = 0.3131$ and $n^* = 0.8638$[8].

3.3 Strain Rate-Based Hot Tearing Criteria

Eskin *et al.*[15] stated that the more complex the shape of the casting, the higher the strain. Therefore, hot tearing criteria that are merely based on the comparison of the ductility of semi-

solid materials and their solidification shrinkage cannot be used for the hot tearing prediction of complex castings[15].

Prokhorov[30] published a hot tearing model considering the configuration of the solidifying body. In this model, the hot tearing susceptibility is determined by the shrinkage and the apparent strain rate in the mushy zone in relation to the fracture strain rate. Therefore, the effects of the surrounding configuration are accounted for by the apparent strain rate. Furthermore, the model assumes that during solidification the material passes through a brittle temperature range, which is defined between the solidus temperature and the coherence temperature. The minimum fracture strain in this range is called D_{min}. Finally, Prokhorov considers the difference between D_{min} and the sum of the linear free shrinkage $\Delta\varepsilon_{free}$ and the apparent strain $\Delta\varepsilon_{app}$ within ΔT_B. A reserve of hot tearing strain $\Delta\varepsilon_{res}$ is defined by the minimum value within this interval and the expression is divided by the brittle temperature range:

$$\frac{\Delta\varepsilon_{res}}{\Delta T_B} = \frac{D_{min}}{\Delta T_B} - \frac{\Delta\varepsilon_{free}}{\Delta T_B} - \frac{\Delta\varepsilon_{app}}{\Delta T_B} \tag{3.19}$$

Since the strain rate is $\dot{\varepsilon} = (\Delta\varepsilon \cdot \dot{T})/\Delta T_B$, where $\dot{T}$ is the cooling rate, Eq. 3.19 leads to:

$$\dot{\varepsilon}_{res} = \dot{\varepsilon}_{min} - \dot{\varepsilon}_{free} - \dot{\varepsilon}_{app} \tag{3.20}$$

The formulation of the hot tearing criterion is achieved using Eq. 3.20. A hot tear will form during solidification if $\dot{\varepsilon}_{res} \leq 0$, or

$$\dot{\varepsilon}_{min} \leq \dot{\varepsilon}_{free} + \dot{\varepsilon}_{app} \tag{3.21}$$

This criterion can be used for both a qualitative (Eq. 3.20) and a quantitative (Eq. 3.21) prediction of hot tearing. Suyitno *et al.*[90] applied this criterion on direct-chill casting of Al-alloys and stated that Eq. 3.21 is very sensitive to the constitutive behavior of the mushy zone. Therefore, a more qualitative prediction is used by considering the hot tearing susceptibility, which is given by the inverse reserve strain rate ($\dot{\varepsilon}_{res}^{-1}$). The values of $\dot{\varepsilon}_{free}$ and $\dot{\varepsilon}_{app}$ are determined by an FEM analysis and values of D_{min} must be taken from the literature.

A further hot tearing criterion based on the strain rate was developed for Al-alloys by **Rappaz** *et al.*[71]. The *"RDG-criterion"* is based on the mass balance within a volume element in the mushy zone for a columnar solidification in the x-direction:

$$\frac{\partial(\rho_L \cdot f_L \cdot v_{L,x})}{\partial x} + \frac{\partial(\rho_S \cdot f_S \cdot v_{S,y})}{\partial y} - v_T \left[\frac{\partial(\rho_S \cdot f_S)}{\partial x} + \frac{\partial(\rho_L \cdot f_L)}{\partial x}\right] = 0 \tag{3.22}$$

The term v_T means the solidification velocity, ρ is the density and v is the velocity, where the subscripts L and S denote solid and liquid phase.

Fig. 3.10 shows the principle of the hot tearing model together with the mass balance within a volume element. The liquid has to flow from right to left in order to compensate for shrinkage and

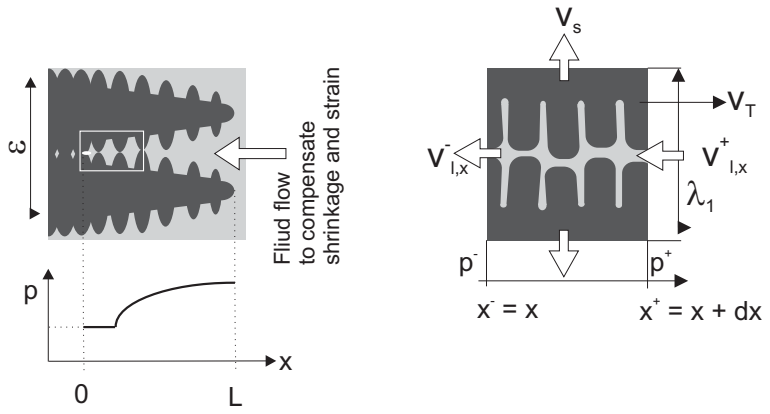

Figure 3.10: *Hot tearing model and mass balance within a volume element according to Rappaz* et al.*[71]*

deformation. The pressure in the interdendritic liquid (schematically illustrated in the bottom of Fig. 3.10) decreases along the mushy zone from the metallostatic pressure p_m near the dendritic tip. If the pressure falls below a cavitation pressure p_C, a hot tear will form:

$$p_m - p_C = \Delta p_\varepsilon + \Delta p_{sh} \tag{3.23}$$

The terms on the right hand side of Eq. 3.23 are the pressure drop contributions due to deformation and shrinkage, respectively. A detailed description of the derivation of these two parameters can be found in the literaure[71]. The following expressions were used by Rappaz *et al.*:

$$\Delta p_\varepsilon = \frac{180 \cdot \eta \cdot (1+\beta_{sh}) \cdot \dot{\varepsilon}}{\lambda_2^2 \cdot G} \int_{T_S}^{T_L} \frac{f_S^2 \cdot \int f_S \cdot \mathrm{d}T}{G \cdot (1-f_S)^3} \mathrm{d}T \tag{3.24}$$

$$p_{sh} = \frac{180 \cdot \eta \cdot \beta_{sh} \cdot v_T}{\lambda_2^2 \cdot G} \int_{T_S}^{T_L} \frac{f_S^2}{(1-f_S)^2} \mathrm{d}T \tag{3.25}$$

The term G is the temperature gradient, λ_2 is the secondary dendrite arm spacing, β_{sh} denotes the shrinkage factor and η is the viscosity. According to Rappaz *et al.*[71] the upper and lower boundary correspond to T_L and T_S, respectively. A later publication[117] adapts the model to the conditions of continuous casting of steels. In this study the temperature range between the coalescence temperature and the solidus temperature are applied as integration limits. The case of steel is more complicated due to the presence of a peritectic reaction. Therefore, the two different phases (ferrite, δ and austenite, γ) must be considered. Thus, Eq. 3.24 and Eq. 3.25 must be rewritten:

$$\Delta p_\epsilon = \frac{180 \cdot \eta \cdot \dot{\varepsilon}}{\lambda_2^2 \cdot G} \cdot \left[(1+\beta_{sh}^\gamma) \cdot B_\gamma + (1+\beta_{sh}^\delta) \cdot B_\delta \right] = K_{RDG} \cdot \dot{\varepsilon} \cdot B \tag{3.26}$$

$$B_i = \int_{T_{coal}}^{T_L} \frac{f_S^2 \cdot \int_{T_{coal}}^{T} f_i \cdot \mathrm{d}T}{G \cdot (1 - f_S)^3} \mathrm{d}T \qquad (i = \delta \text{ or } \gamma) \tag{3.27}$$

$$\Delta p_{sh} = \frac{180 \cdot \eta \cdot v_T}{\lambda_2^2 \cdot G} \cdot \left[\beta_{sh}^{\gamma} \cdot A_\gamma + \beta_{sh}^{\delta} \cdot A_\delta \right] = K_{RDG} \cdot v_T \cdot A \tag{3.28}$$

$$A_i = \int_{T_{coal}}^{T_L} \frac{(f_i^0 - f_i) \cdot f_S^2}{(1 - f_S)^3} \mathrm{d}T \qquad (i = \delta \text{ or } \gamma) \tag{3.29}$$

The term f_i^0 denotes the amount of ferrite ($i = \delta$) or the amount of austenite ($i = \gamma$) at the end of solidification. These equations are valid for the assumption of a constant temperature gradient as well as a constant strain rate within the mushy zone.

Inserting the contributions of the deformation and the shrinkage in Eq. 3.23 together with a value of the cavitation pressure allows the determination of the maximum or critical strain rate ($\dot{\varepsilon}_C$). Finally, the calculation of the reciprocal value of the maximum strain rate shows the hot tearing susceptibility.

In addition, **Braccini** *et al.*[118,119] proposed a hot tearing criterion based on the strain rate. They use the strain rate to describe the crack initiation and the crack propagation. The problem of hot tearing is simplified for a columnar and an equiaxed structure as illustrated in Fig. 3.11.

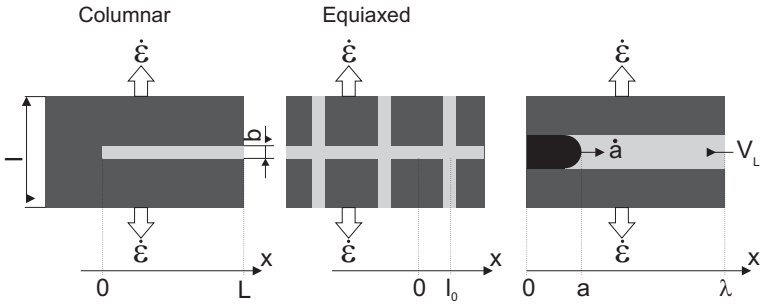

Figure 3.11: *Simplified mushy zone (columnar and equiaxed) according to the hot tearing model proposed by Braccini* et al.

In both cases – columnar and equiaxed structure – the system is subject to a deformation, which is represented by the strain rate. Braccini *et al.* conclude that the strain rate and the stresses generated in the mushy zone (M) and in the liquid film (L) can be determined using series models:

$$\sigma_L = \sigma_M \qquad \text{and} \qquad \dot{\varepsilon} = (1 - \frac{b}{l}) \cdot \dot{\varepsilon}_M + \frac{b}{l} \cdot \dot{\varepsilon}_L \tag{3.30}$$

The terms b and l are illustrated in Fig. 3.11 and denote the liquid film thickness and the gage length, respectively. Eq. 3.30 describes the constitutive behavior of the mushy zone ($\sigma_M = K(T, f_S) \cdot \dot{\varepsilon}_M^m$), whereas in the liquid only the hydrostatic part is considered ($\sigma_L = -\bar{p}$). In these

equations, K represents a constitutive parameter which is a function of temperature and fraction of solid, m is the strain rate sensitivity coefficient and $\bar{p}$ denotes the average pressure in the liquid. Similar to the RDG-criterion[71], the hot tear initiation is defined by the pressure drop within the mushy zone ($\Delta p = p_m - \sigma$). A hot tear nucleates if the pressure drop is equal to a critical value $p_m - p_C$, where p_C is the cavitation pressure and p_m the metallostatic pressure. The critical strain rate of hot tear initiation results from Eq. 3.30. The critical strain rate for hot tear propagation can be derived from the expansion velocity $\dot{a}$, which reaches a positive value for insufficient liquid feeding:

$$\dot{b} \cdot (l_0 - a) = \dot{a} \cdot b - v_L \cdot b \tag{3.31}$$

In Eq. 3.31, l_0 is the half grain size, a is the length of the tear and v_L is the liquid flow entering the liquid film. Finally, Braccini *et al.*[118] derived the critical strain rate for hot tear propagation $\dot{\varepsilon}_C^{prop}$, which results in the critical strain rate of hot tear initiation, when inserting $a = 0$:

$$\dot{\varepsilon}_C^{prop} = \left(1 - \frac{b}{l}\right) \cdot \left[\frac{l_0 - a}{l_0} \cdot \left(\frac{2/3 p_c - p_m}{K(T, f_s)}\right)\right] + \frac{b}{l} \cdot \frac{2 \cdot \kappa}{(l_0 - a)^2} \cdot \frac{p_C}{\eta} \tag{3.32}$$

The terms κ and η are the permeability of the mushy zone and the viscosity of the liquid, respectively.

3.4 Criteria Based on Other Principles

The hot tearing model proposed by **Feurer**[84] is a non-mechanical criterion that focuses on feeding and shrinkage during solidification. The model considers the influence of alloy composition and solidification conditions on the dendrite arm spacing. The principle is based on the comparison of the maximum volumetric flow rate (SPV) and the velocity of volumetric solidification shrinkage (SRG) caused by the density differences between solid and liquid phase. The maximum volumetric flow rate per unit volume through a dendritic network is formulated as follows, where V is a volume element of the solidifying mush with constant mass and t is the time:

$$SPV = \left(\frac{\partial ln V}{\partial t}\right)_{feeding} = \frac{\kappa}{\eta \cdot L^2} \cdot (p_0 + p_m - p_C) \tag{3.33}$$

In Eq. 3.33, κ is the permeability of the mushy zone ($\kappa = (f_l^2 \cdot \lambda_2^2)/(24 \cdot \pi \cdot c^2)$, c is the tortuosity constant of the dendritic network), η is the viscosity of the liquid, L denotes the length of the porous network and p_0 is the atmospheric pressure. The metallostatic pressure p_m and the cavitation pressure p_C can be calculated according to Feurer as follows:

$$p_m = (\rho_L \cdot f_L + \rho_S \cdot f_S) \cdot g \cdot h \qquad \text{and} \qquad p_C = \frac{4 \cdot \gamma_{SL}}{\lambda_2} \tag{3.34}$$

The term γ_{SL} denotes the solid-liquid interface energy, g is the gravity constant and h denotes the distance to the melt surface.

The volumetric solidification shrinkage velocity (SRG) is expressed as follows:

$$SRG = \left(\frac{\partial lnV}{\partial t}\right)_{shrinkage} = -\frac{1}{\bar{\rho}} \cdot \frac{\partial}{\partial t} \cdot (\rho_L \cdot f_L + \rho_S \cdot f_S) \tag{3.35}$$

Finally, the hot tearing criterion states that hot tearing is possible once the volumetric solidification shrinkage velocity is greater than the maximum volumetric flow rate per unit volume through a dendritic network ($SRG > SPV$).

The proposed hot tearing model by **Clyne and Davies**[27] is based on the theory that in the last stage of freezing, it is difficult for the liquid to move freely. Therefore, the strain applied during this stage cannot be accommodated by mass feeding. The hot tearing susceptibility is defined as the ratio between the vulnerable time period (t_V) and the time available for a stress-relief process (t_R). The vulnerable time period corresponds to the period of time, where the solid fraction of a volume element is in the range between 0.9 and 0.99. In the corresponding temperature range hot tears are generated, which cannot be refilled with residual liquid (*open hot tears*). The time period for the stress-relief process correlates to the movement of a considered volume element between a solid fraction of 0.4 and 0.9. In this range, hot tears can be refilled with residual liquid. The resulting expression can be written in terms of a hot tearing susceptibility (HCS) coefficient:

$$HCS = \frac{t_V}{t_R} = \frac{t_{0.99} - t_{0.9}}{t_{0.9} - t_{0.4}} \tag{3.36}$$

In Eq. 3.36, t is the time, the subscripts denote the fraction of solid.

The model according to **Katgerman**[72] combines the theoretical considerations of the previously presented hot tearing model and the approach of Feurer[84]. This model was intended to predict the hot tearing susceptibility during direct-chill casting of Al. The effects of casting speed, ingot diameter and alloy composition are considered. The hot tearing susceptibility is expressed by:

$$HCS = \frac{t_{0.99} - t_{LIT}}{t_{LIT} - t_{coh}} \tag{3.37}$$

The term $t_{0.99}$ corresponds to the time when the fraction of solid is 0.99, t_{coh} is the time when the fraction of solid is at the coherency point and t_{LIT} is the time when feeding becomes inadequate. The latter can be determined using Feurer's model and corresponds to the time for which $SPV = SRG$.

A hot tearing model considering shrinkage, the imposed strain rate and the (lack of) feeding as the main factors was developed by **Suyitno** *et al.*[73]. The model combines the critical feeding according to Feurer[84], the deformation rate suggested by Rappaz *et al.*[71] and the cavity formation. Additionally, the flow behavior of the semi-solid state is included as proposed by Braccini *et al.*[118]. Suyitno *et al.* suggest that a growing nucleus becomes either a micro-pore or a hot tear at the end of solidification, which is determined by the *Griffith* model for crack propagation. The description

of the cavity formation is based on an equiaxed structure at triple junctions between the grains as illustrated in Fig. 3.12. Cavity formation occurs if the volume changes due to local shrinkage and if external strain rates imposed by the mushy environment under the influence of the solidification are not counterbalanced by liquid feeding. It is assumed that the strain rate acts only perpendicular to the casting direction and feeding occurs only in the casting direction. The resulting transient mass conservation equation applied to the element in Fig. 3.12 leads to

$$\frac{\partial f_V}{\partial t} = -\left(\frac{\rho_S}{\rho_L} - 1\right) \cdot \frac{\partial (f_L)}{\partial t} + \left(\frac{\rho_S}{\rho_L}\right) \cdot f_S \cdot \dot{\varepsilon} - \frac{\partial (f_L\, u)}{\partial x} - \frac{\partial (f_L\, v)}{\partial y} \tag{3.38}$$

where f_S, f_L and f_V are solid, liquid and cavity fraction, respectively. The terms ρ_S and ρ_L denote the densities of solid and liquid, u and v are the velocities in x-direction and y-direction and t denotes the time.

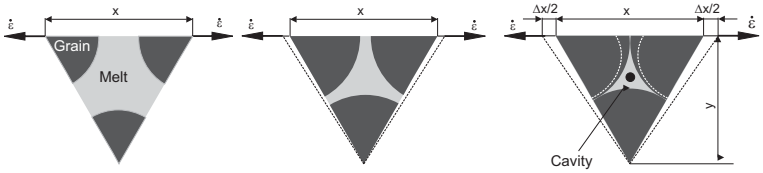

Figure 3.12: *Schematic model of the cavity formation during solidification according to Suyitno* et al.*[73]*

If Eq. 3.38 equals to zero or is negative, feeding is sufficient and a cavity is not formed. If this equation takes a positive value, it is a measure for cavity growth due to shrinkage and imposed deformation on the one hand and insufficient feeding on the other hand. The first and second term at the right-hand side are the contributions of shrinkage and deformation, respectively. The last two terms are the contributions from feeding in the two directions. Due to the above mentioned assumption (feeding only in casting direction), the term $\frac{\partial (f_L\, u)}{\partial x} = 0$. The remaining feeding term is calculated using Eq. 3.33 taken from Feurer[84].

In order to determine whether a micro-pore or a hot tear will form, it is assumed that the cavity shape is circular and a hot tear will develop if the diameter of the cavity d_{cavity} will be larger than the critical diameter d_C. The diameter of the cavity can be determined according to Suyitno *et al.* as follows:

$$\pi \cdot d_{cavity} = \sqrt{3} \cdot d_{grain}^2 \int_0^t \dot{\varepsilon} \cdot \mathrm{d}\tau \tag{3.39}$$

The final grain diameter is termed as d_{grain} and t is the time during solidification. Using the *Griffith* approach, the relation between the cavity diameter and the minimum stress σ_{min} necessary to propagate a crack is as follows (E is *Young's modulus* and γ_{LG} is the surface tension):

$$d_C = \frac{4 \cdot \gamma_{LG} \cdot E}{\pi \cdot \sigma_{min}} \tag{3.40}$$

Inserting the cavity diameter resulting from Eq. 3.39 into Eq. 3.40 allows the calculation of the minimum stress of crack propagation. If the stress within the mushy zone becomes equal to the minimum stress for crack propagation, the cavity has reached its critical diameter and a crack will develop. The stress within the mushy zone is calculated using the constitutive equation taken from Braccini *et al.*[118]:

$$\sigma = K \cdot \dot{\varepsilon}^{m^*} \tag{3.41}$$

In this equation, K is a constitutive parameter and m^* is the strain rate (sensitivity) exponent (for a detailed consideration of Eq. 3.41 see reference[118]).

3.5 Summary

In this chapter, a large number of hot tearing criteria from the literature were presented and summarised in Tab. 3.6. These models are based on different considerations, approaches and assumptions. In the field of continuous casting, the literature mainly provides criteria based on the comparison of the strain due to the process ε_P to a critical strain of hot tearing. The determined values of ε_C were illustrated in Section 3.2.2. Additionally, these values are the basis of the empirical equation proposed by Won *et al.*[8].

Stress-based criteria for the continuous casting process were developed mostly by Korean researchers. The necessary critical stress is calculated as a function of δ-Fe and γ-Fe based on constitutive equations of high temperature deformation. Other stress-based criteria consider the liquid film between grain boundaries or take into account a fracture mechanical approach.

The strain rate-based criteria were mainly developed in the field of aluminium alloys. Only one publication can be found in the field of continuous casting of steel. One of the presented models is based on the strain rates within the brittle temperature range, whereas the other two models consider liquid feeding and therefore only open hot tears.

With respect to criteria based on other principles, the approaches focus on mass feeding and/or shrinkage and the combination of feeding, deformation rate and cavity formation. The criterion defining a hot tearing susceptibility in terms of the ratio between the vulnerable time period and the time available for stress-relief process was also applied in the field of continuous casting of steel[35]. This model as well as the models proposed by Rogberg[20], Rappaz *et al.*[71] and Won *et al.*[8] are applied in the next chapter in order to predict the hot tearing tendency of steel as a function of the carbon content.

Researcher	Parameters	HCS	Tearing Condition
	Stress-Based Criteria		
Rogberg[20]	$\sigma_C = f(\gamma_{LG}, b, \lambda_2)$	σ_{max}/σ_C	$\sigma_P > \sigma_C$
Laheie and Bouchard[93]	$\sigma_C = f(\gamma_{LG}, b, \lambda_2, \varepsilon, f_S, m_p)$	σ_{max}/σ_C	$\sigma_P > \sigma_C$
Kim *et al.*[37]	$\sigma_C = f(\delta/\gamma - Fe, \varepsilon_C, \dot{\varepsilon})$	σ_{max}/σ_C	$\sigma_P > \sigma_C$
Kim[106]	${}^{T}S_C = f(A_m, t_C, S_C)$	${}^{T}S_C$	–
Won *et al.*[99]	${}^{S}S_C = f({}^{T}S_C, A_s, t_C)$	${}^{S}S_C$	–
Won *et al.*[8]	$W_{\Delta T_B} = f(\varepsilon_C, \sigma_{ZDT}, \sigma_{LIT})$	$W_{\Delta T_B}$	–
Williams and Singer[76]	$\sigma_C = f(G_{mod}, \gamma_{fr}, \nu, a)$	σ_{max}/σ_C	$\sigma_P > \sigma_C$
	Strain-Based Criteria		
Novikov and Grushko[109]	$p_r = f(T_{coh}, T_S, \varepsilon_C, \varepsilon_{sh})$	$1/p_r$	–
Magnin *et al.*[110]	$\varepsilon_{\theta\theta}$	$\varepsilon_{\theta\theta}/\varepsilon_C$	$\varepsilon_{\theta\theta} > \varepsilon_C$
Won *et al.*[8]	$\varepsilon_C = f(\Delta T_B, \dot{\varepsilon})$	$1/\varepsilon_C$	$\varepsilon_P > \varepsilon_C$
	Strain Rate-Based Criteria		
Prokhorov[30]	$\dot{\varepsilon}_{res} = f(\dot{\varepsilon}_{min}, \dot{\varepsilon}_{free}, \dot{\varepsilon}_{app})$	ε_{res}	$\varepsilon_{res} \leq 0$
Rappaz *et al.*[71]	$\dot{\varepsilon} = f(p_m, p_C, p_\varepsilon, p_{sh})$	$1/\dot{\varepsilon}_C$	$\Delta p > \Delta p_C$
Braccini *et al.*[118]	$\dot{\varepsilon}_C^{prop} = f(\dot{\varepsilon}_M, \dot{\varepsilon}_L, b, a)$	$1/\dot{\varepsilon}_C^{prop}$	$\dot{\varepsilon}_P > \dot{\varepsilon}_C^{init}$
	Other Criteria		
Feurer[84]	$SPV = f(\kappa, \eta, L, p_0, p_m, p_C)$ $SRG = f(\rho_L, \rho_S, f_L, f_S)$	–	$SRG > SPV$
Clyne and Davies[27]	t_V, t_R	t_V/t_R	–
Katgermann[72]	$t_{0.99}, t_{LIT}, t_{coh}$	$\frac{t_{0.99}-t_{LIT}}{t_{LIT}-t_{coh}}$	–
Suyitno *et al.*[73]	$d_C = f(E, \gamma_{LG}, \sigma)$ $d_{cavity} = f(d_{grain}, \dot{\varepsilon})$	–	$d_{cavity} > d_C$

Table 3.6: *Summary of existing hot tearing criteria from literature.*

4 Prediction of the Hot Tearing Tendency Using Models from Literature

It doesn't matter how beautiful your theory is, it doesn't matter how smart you are. If it doesn't agree with experiment, it's wrong.[a] RICHARD P. FEYNMAN

[a] Unsourced

Within the scope of the present thesis a large number of laboratory experiments were conducted in order to investigate hot tearing under continuous casting conditions. For this purpose, the SSCT-test was used. The principle of this experiment is illustrated in Chapter 7, the results will be presented in Chapter 8. In the following, selected criteria from literature will be applied to calculate the expected hot tearing tendency of steel of experiments varying only the carbon content. Therefore, solidification calculations in conjunction with a microsegregation analysis of the SSCT-test are necessary. The influence of the microsegregation analysis on the results of the hot tearing models are briefly discussed in the following. However, in this chapter a detailed description of the thermal analysis is not included. This will be done in Section 7.2. Nevertheless, all necessary parameters for calculating the hot tearing susceptibility are listed. Again, the aim of this chapter is not to explain the SSCT-test and the thermal analysis, but to present the calculation procedure, to identify the necessary model parameters and to illustrate the results of the different hot tearing criteria.

In the previous section, different hot tearing criteria from the literature were presented, which were classified into stress-based, strain-based and strain rate-based criteria as well as criteria based on other principles. In the following calculations, one model per classification will be used. In particular, these are the criteria proposed by Rogberg[20], Won *et al.*[8], Rappaz *et al.*[71] and Clyne and Davies[27]. In a previous publication[9] results of these selected criteria were presented. These calculations were based on the microsegregation analysis using the *IDS software*[120]. With the exception of the criterion of Rogberg, the other three criteria strongly depend on the applied microsegregation model. The results of the microsegregation analysis are reflected in

- the brittle temperature range necessary to calculate the critical strain,
- the solution of the integrals in the model of Rappaz *et al.* and

- the determination of t_V and t_R in the model proposed by Clyne and Davies.

In the present thesis, the microsegregation analysis according to Ueshima *et al.*[54] is used instead of the *IDS software*. This model is based on a one-dimensional direct finite-difference model, which is modified to determine f_S, the δ-phase solid fraction ($^{\delta}f_S$) and the γ-phase solid fraction ($^{\gamma}f_S$) in the mushy zone as a function of temperature. A detailed explanation of the microsegregation model, is included in Appendix A.

Steel No.	C	T_L	T_S	ΔT_{LS}	ΔT_B	t_f	R
1	0.05	1522	1491	31	11.6	5.86	0.30
2	0.08	1520	1475	45	14.8	7.44	0.30
3	0.12	1516	1453	63	22.7	10.14	0.30
4	0.16	1513	1441	72	28.5	11.02	0.31
5	0.30	1501	1407	94	39.2	13.02	0.32
6	0.50	1486	1363	123	49.1	15.16	0.35
7	0.70	1473	1321	152	57.5	16.34	0.34

Table 4.1: *Required parameters for the hot tearing models resulting from the thermal analysis: Liquidus temperature T_L (in °C), solidus temperature T_S (in °C), the solidification interval ΔT_{LS} (in °C), the local solidification time t_f (in s) and the solidification velocity R (in mm/s).*

In this chapter the hot tearing susceptibility as a function of the carbon content will be calculated. The carbon content is 0.05, 0.08, 0.12, 0.16, 0.30, 0.50 and 0.70 $wt.\text{-}\%C$ (0.30 $wt.\text{-}\%Si$, 1.30 $wt.\text{-}\%Mn$, 0.007 $wt.\text{-}\%S$ and 0.007 $wt.\text{-}\%P$). The main parameters resulting from the thermal analysis, necessary for the hot tearing criteria, are summarised in Tab. 4.1. The liquidus and solidus temperatures are calculated in the microsegregation analysis. The local solidification time t_f as well as the solidification velocity R are the result of the solidification calculations (shell thickness vs. solidification time). The latter two parameters change with solidification time. Therefore, t_f is determined for the solidification time when the tensile test starts and R represents an average solidification velocity of the dendrite tip during the hot tensile test. The brittle temperature range ΔT_B is determined according to Won *et al.*[8] between LIT ($f_S = 0.9$) and ZDT ($f_S = 0.99$).

4.1 A Stress-Based Hot Tearing Criterion

The model proposed by **Rogberg**[20] is based on the assumption that two grains are separated by a thin liquid film. The fracture stress σ_{fr} results from Eq. 3.5 as a function of the surface tension γ_{LG} and the thickness of the liquid film b . According to Keene[121,122] and Poirier[123] the surface tension can be calculated as a function of temperature. In addition, Keene summarised several studies on the influence of carbon content on the surface tension of iron. The effect of carbon is negative, which leads to the following expression:

$$\gamma_{LG} = 2.858 \; - \; 0.00051 \cdot T \; - \; 0.01424 \cdot C(at. - \%) \tag{4.1}$$

In Eq. 4.1, C denotes the carbon concentration in atom percentage and T is the temperature in K. By inserting the different carbon contents and the corresponding solidus temperature γ_{LG} can be calculated. Assuming an elliptical shape of the dendrites, the liquid film thickness can be calculated as follows:

$$b = \lambda_1 \cdot \left(1 - \sqrt{1 - f_L^2}\right) \tag{4.2}$$

In order to determine the primary dendrite arm spacing λ_1, the relationship $\lambda_1/\lambda_2 \cong 2.6$ is used. This value was estimated by Cicutti and Boeri[124] applying a simple mathematical model. The value is between 2 and 4, as proposed by Wolf[125]. A summary of empirically determined λ_2-relations, can for example be found in the work of Bernhard[126]. In the present thesis two different equations from literature together with experimentally determined λ_2-values[127] are used for the calculation of the liquid film thickness:

Based on published values of λ_2 in *A Guide of the Solidification of Steels*[128] published by Jernkontoret for different carbon steels and the corresponding local solidification time, a relationship between these parameters can be determined. This was carried out by Bernhard[126] resulting in Eq. 4.3:

$$\lambda_2 = M_{SDAS} \cdot t_f^{n_{SDAS}} = [6.1 + 3.6 \cdot C(wt.-\%)] \cdot t_f^{0.6-0.2 \cdot C(wt.-\%)} \tag{4.3}$$

$$\begin{aligned} \lambda_2 &= 148 \cdot \dot{T}^{-0.38} && 0 \leq C \leq 0.53 \\ \lambda_2 &= (21.53 - 9.40 \cdot C) \cdot t_f^{0.4+0.08 \cdot C} && 0.53 \leq C \leq 1.5 \end{aligned} \tag{4.4}$$

The latter equation (Eq. 4.4) is independent of the carbon content and was proposed by El-Bealy and Thomas[129] based on measurements conducted by Schwerdtfeger[130] and Suzuki[131]. Eq. 4.4 implies an increasing λ_2 with increasing carbon content under the prerequisite of a constant t_f. However, the local solidification time changes with the solidification interval if the cooling rate $\dot{T}$ is assumed to be constant. The relationship between cooling rate and local solidification time is $t_f = \Delta T_{LS}/\dot{T}$, with $\Delta T_{LS} = T_L - T_S$. These parameters are summarised in Tab. 4.1.

Based on the secondary dendrite arm spacing, the liquid film thickness and consequently the fracture stress can be calculated according to Eq. 3.1 (see Section 3.1). The hot tearing susceptibility can finally be determined as follows:

$$HCS = \frac{\sigma_{max}}{\sigma_{fr}} \tag{4.5}$$

In this equation, σ_{max} denotes the maximum measured stress during the SSCT-test. These values together with the measured λ_2-values are illustrated in Tab. 4.2. For the calculation of the liquid film thickness, a solid fraction of 0.9 is assumed resulting in reasonable values of σ_{fr}. Shin *et al.*[42] have

measured values of σ_{fr} as a function of carbon content in the range of $3-8\ N/mm^2$ (corresponding to $f_S = 1$). The calculated values using Eq. 3.1 are in the same order of magnitude. However, the experimentally determined σ_{fr}-values by Shin *et al.* are the result of a conventional hot tensile test where the steel sample is fully ruptured.

The results of the calculations using different values of the secondary dendrite arm spacing are illustrated in terms of a hot tearing susceptibility. Additionally, the resulting values of HCS using the experimentally determined fracture stress by Shin *et al.* are illustrated in Fig. 4.1b. In order to ensure comparability of the different results, a normalised HCS is used in Fig. 4.1.

Carbon Content	0.05	0.08	0.12	0.16	0.30	0.50	0.70
σ_{max}	4.33	6.50	6.94	6.92	7.5	8.39	8.43
λ_2	36	37	33	42	44	36	27
σ_{fr} [42]	3.2	4.0	5.5	6.2	7.0	7.6	8.5

Table 4.2: *Measured maximum stress σ_{max} (in MPa) and measured secondary dendrite arm spacing (in μm) from SSCT specimen as well as experimentally determined fracture stress σ_{fr} (in MPa) for different carbon contents.*

Fig. 4.1a shows the results of HCS as a function of carbon content calculated using Eq. 4.3 to Eq. 4.5. As expected, different values of the secondary dendrite arm spacing strongly influence the hot tearing susceptibility. Generally, the hot tearing susceptibility tends to increase with increasing carbon content. This is in contrast to the curve of HCS determined with the measured values of λ_2, which is illustrated in Fig. 4.1b. In this case, a maximum of the hot tearing tendency is obtained at a carbon content of 0.30 $wt.$-$\%C$. The most different trend is determined by inserting the experimentally measured values of the fracture stress into Eq. 4.5.

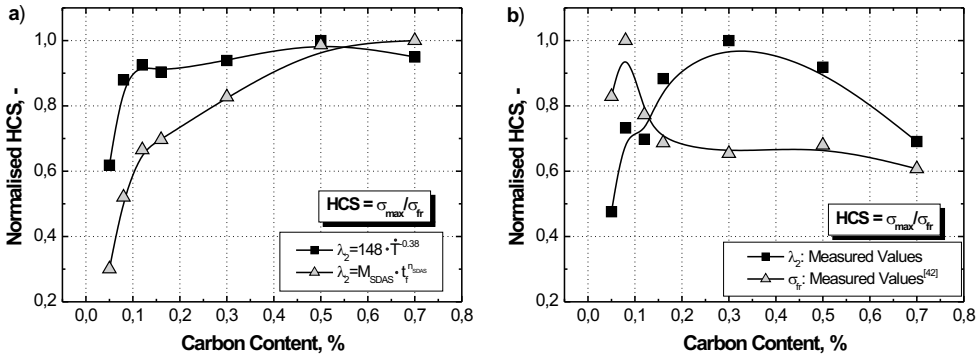

Figure 4.1: *Calculated normalised HCS as a function of carbon content using a) two different equations of λ_2 and b) measured values of λ_2 and σ_{fr}*

Summarising, the results of the hot tearing susceptibility calculated with the stress-based hot tearing model proposed by Rogberg[20] strongly depend on the liquid film thickness between den-

drites or grains and consequently on the structure parameter (i.e. secondary dendrite arm spacing under the assumption of an interdendritic fracture).

4.2 A Strain-Based Hot Tearing Criterion

Won *et al.*[8] consider the brittle temperature range and the strain rate to define an empirical equation of the critical strain of hot tearing. The authors use numerous experimental data of critical strain, which were determined, in particular, under continuous casting conditions. Thus, the necessary fitting parameters φ, m^* and n^* can be determined considering the brittle temperature range and the strain rate. The latter can be taken from the experiment, but the brittle temperature range needs to be calculated using a microsegregation analysis.

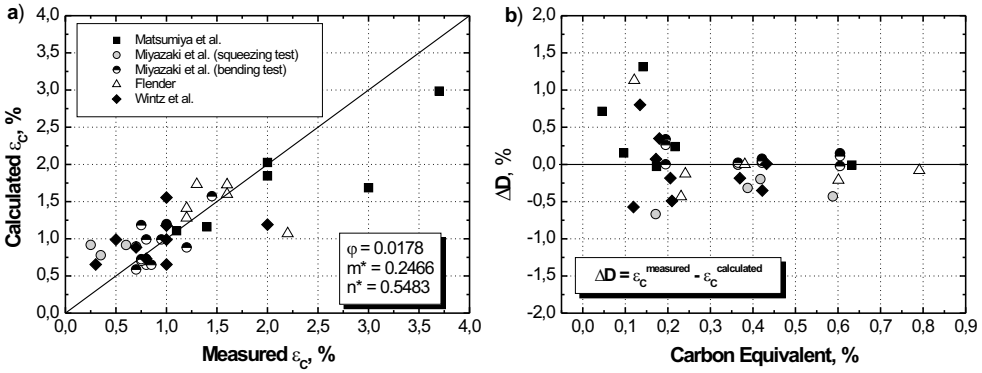

Figure 4.2: *a) Calculated versus measured critical strain of hot tearing and b) the difference between these two values as a function of the carbon equivalent.*

The results from Eq. 3.18 strongly depend on ΔT_B and thus on the applied microsegregation model. This can be clarified by the following example. Won *et al.* determined a ΔT_B of 21 K for a 0.12 $wt.\text{-}\%C$ steel (0.03 $wt.\text{-}\%Si$, 0.4 $wt.\text{-}\%Mn$, 0.01 $wt.\text{-}\%P$ and 0.02 $wt.\text{-}\%S$). Using the *software* IDS[120] a ΔT_B of 13 K is calculated. Inserting these two values in Eq. 3.18 together with a strain rate of 0.001 s^{-1} results in critical strains of 1.8 % and 2.7 %, respectively. An application of calculated critical values of hot tearing must therefore be done very carefully, using either the same microsegregation model as applied by Won *et al.* or by fitting the parameters φ, m^* and n^* to the corresponding microsegregation analysis. Taking the reciprocal value of ε_C as a measure of HCS does not show a significant influence regarding the trend of HCS. However, the prediction whether hot tears will form or not requires the adjustment of the fitting parameters on the microsegregation analysis.

The determination of these fitting parameters according to the used microsegregation model is the first step of the present thesis. Using results from the literature (see Fig. 3.9) together with the corresponding strain rate and the calculated brittle temperature range leads to $\varphi = 0.0178$, $m^* = 0.2466$ and $n^* = 0.5483$. Fig. 4.2a shows the results of the calculated and measured values

of ε_c. The difference between the calculated and measured values is illustrated in Fig. 4.2b. It can be seen that especially at lower carbon contents a major scatter band appears. Nevertheless, a hot tearing susceptibility can be calculated using Eq. 3.18 together with the above illustrated fitting parameters:

$$HCS = \frac{1}{\varepsilon_C} \tag{4.6}$$

For the calculation of the critical strain, a strain rate of $2 \cdot 10^{-2}$, $2 \cdot 10^{-3}$ and $2 \cdot 10^{-4}$ s^{-1} is used. According to Won *et al.*, the brittle temperature range is defined as the difference between the liquid impenetrable temperature ($LIT = T(f_S = 0.9)$) and the zero ductility temperature ($ZDT = T(f_S = 0.99)$), values of ΔT_B can be found in Tab. 4.1. The calculated critical strain using the empirical relationship proposed by Won *et al.* is illustrated in Fig. 4.3a.

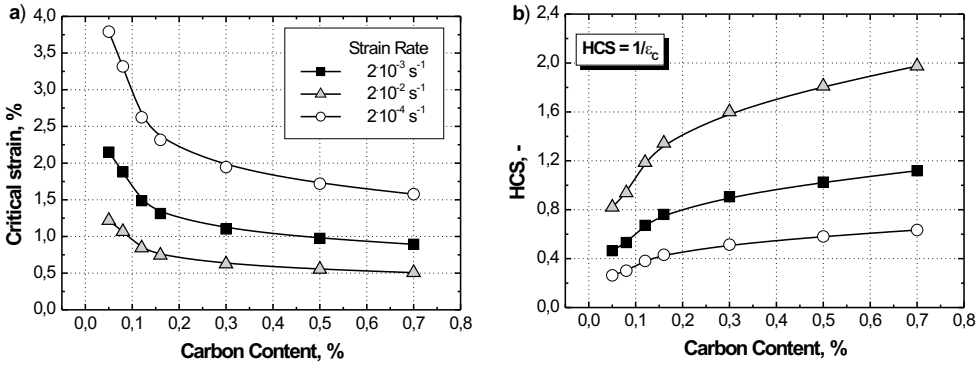

Figure 4.3: *a) The calculated critical strain as a function of carbon content and b) the hot tearing susceptibility in terms of the reciprocal critical strain for three different strain rates.*

It can be seen that with increasing carbon content the critical strain decreases. Furthermore, the influence of the strain rate is clearly visible. These results are reflected in Fig. 4.3b. Hence, the hot tearing tendency increases with increasing carbon content and strain rate.

4.3 A Strain Rate-Based Hot Tearing Criterion

The model proposed by **Rappaz** *et al.*[71] is chosen as an example for the strain rate-based hot tearing criterion. This model states that once the pressure $p = p_m - \Delta p_{sh} - \Delta p_\varepsilon$ falls below the cavitation pressure p_C a hot tear forms. The metallostatic pressure can easily be computed by $p_m = \rho \cdot g \cdot h$, the equations for calculating Δp_ε (Eq. 3.24) and p_{sh} (Eq. 3.25) can be found in section 3.3. In their publication, Rappaz *et al.*[71] assumed a constant cavitation depression $\Delta p_C = 2000\ Pa$ in order to investigate hot tearing of Al-Cu alloys. A detailed review of the literature shows that the model of Rappaz *et al.* is built upon the model of Feurer[84] and incorporates Fisher's criterion[132] for liquid fraction[70]. Fisher proposed a critical fracture pressure required

for homogeneous nucleation of one pore as follows (k is Boltzmann's constant, N is Avogadro's number and h is Planck's constant):

$$p_C = -\left[\frac{16 \cdot \pi}{3 \cdot k \cdot T} \cdot \frac{\gamma_{LG}}{ln(N \cdot k \cdot T/h)}\right]^{1/2} \tag{4.7}$$

This equation can be reduced to approximately $-37.7(\gamma_{LG}^3/T)^{1/2}$ for temperatures between 100 and 2000 °C[63]. Applying this approximation leads to values of p_C of about -77000 to $-84000\ Pa$ in the range of 0.05 to 0.70 $wt.\text{-}\%C$. However, experimental measurements for fracture pressures typically show orders of magnitude smaller than the predicted values[70]. The reasons for that are dissolved gases in the melt and heterogeneous nucleation (e.g. inclusions or oxide films). According to Campbell[63], the fracture pressure under the assumption of heterogeneous nucleation, p'_C can be approximated by $p'_C/p_C = 1.12 \cdot \phi^{1/2}$ for temperatures between 1 and 10000 °C, where $\phi = (2 - \cos\theta_C)(1 + \cos\theta_C)^2/4$. In Campbell's study θ_C is the contact angle, which corresponds to the already discussed dihedral angle in conjunction with hot tearing (see Fig. 2.5). This angle strongly influences the results of p_C and must therefore be known for reasonable calculations.

Hence, the cavitation or fracture pressure is calculated using the equation suggested by Feurer[84] (Eq. 3.34), where p_C is a function of the secondary dendrite arm spacing and the solid-liquid interfacial energy γ_{SL}. In order to determine the latter parameter, Tyson and Miller's[133] approach is used. They defined the ratio between solid to liquid energies:

$$\alpha = \frac{\gamma_{SL}}{\gamma_{SG}} = \frac{\gamma_{SL}}{\gamma_{GB}} \cdot \frac{\gamma_{GB}}{\gamma_{SG}} \tag{4.8}$$

Taking values of $\gamma_{SL}/\gamma_{GB} = 0.45$ and $\gamma_{GB}/\gamma_{SG} = 0.33$ as typical values of all metals leads to $\alpha = 0.15$[133]. Furthermore, Tyson and Miller suggested a ratio of the solid-gas surface energy and the liquid-gas surface tension. It is assumed that at the melting point the surface consists of either a thin liquid-like layer or a crystallographically roughened layer of the same energy ($\gamma_{SG} = \gamma_{SL} + \gamma_{LG}$). Hence, γ_{SL}/γ_{LG} have a value of 1.18. This value is in good agreement with the literature, where such empirical or semi-empirical estimations of the ratio γ_{SL}/γ_{LG} range between $1.09 - 1.33$[134]. Finally, the solid-liquid interfacial energy can be determined for the different carbon steels based on γ_{LG} calculated using Eq. 4.1. Tab. 4.3 summarises these values as well as all necessary parameters for calculating the critical strain rate of hot tearing $\dot{\varepsilon}_C$ using the model proposed by Rappaz *et al.*.

Carbon Content	0.05	0.08	0.12	0.16	0.30	0.50	0.70
γ_{SL}	0.3460	0.3471	0.3487	0.3493	0.3507	0.3524	0.3540
η	5.702	5.826	5.874	5.966	6.709	8.063	9.251
G	15.1	16.2	16.5	16.7	17.1	16.9	17.4

Table 4.3: *The solid-liquid interfacial tension γ_{SL} (in mN/m), viscosity η (in $mPas$) and thermal gradient G (in K/mm) within the mushy zone.*

The solidification shrinkage factors β_{sh}^{δ} and β_{sh}^{γ} are approximately 3.6 % and 5.1 % for steels[55]. Considering the equations for Δp_{ε} and Δp_{sh}, the integral between the temperature range of T_L and the coalescence temperature T_{coal} has to be solved. This is a modification of the original model, as this criterion is applied to continuous casting[117]. According to Kurz and Fisher[55], T_{coal} typically corresponds to a solid fraction of 0.99 between two different grains and to 0.95 for two different dendrites of the same grain. With respect to favoured hot tearing at grain boundaries a value of $f_S = 0.95$ is used.

Fig. 4.4a shows the result of the two different pressure drop contributions due to shrinkage and deformation. The secondary dendrite arm spacing, necessary for the calculation of these two parameters, is calculated using Eq. 4.3. It can be seen that Δp_{sh} has a local maximum of around 5000 Pa at a carbon content of 0.12 $wt.\text{-}\%C$. For the calculation of Δp_{ε} three different strain rates are assumed. The pressure drop due to deformation clearly increases with increasing strain rate. Under the present conditions these two contributions have the same order of magnitude up to a carbon content of 0.30 $wt.\text{-}\%$ at the very high strain rate of $2 \cdot 10^{-2}$ s^{-1} (please note the different scale of the y-axes). At the lower strain rates Δp_{ε} shows clearly lower values than the pressure drop due to shrinkage. Fig. 4.4b shows the resulting critical strain rate calculated using Eq. 3.23. For the calculation of the metallostatic pressure, the parameter h is 50 mm according to the conditions during the SSCT-test. The calculated values of p_C are in the range of -77000 to -45000 Pa, depending on the carbon content. It is interesting to note that inserting these values into the approximation $p'_C/p_C = 1.12 \cdot \phi^{1/2}$, proposed by Campbell, results in contact (dihedral) angles between 45 and 75°.

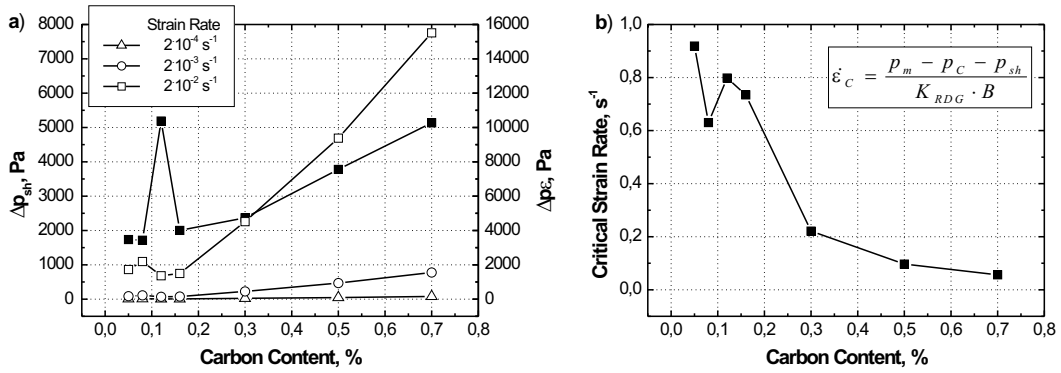

Figure 4.4: *a) Calculated pressure drop contribution due to shrinkage and deformation and b) calculated critical strain rate as a function of carbon content.*

The calculated values of the critical strain rate seem exceedingly high. The model is based on the mass balance, i.e. the liquid flow has to compensate for deformation and shrinkage (feeding). Therefore, the calculated critical strain rate applies for the formation of open hot tears. However, it can be seen that the progression of the curve is similar to the characteristic of the critical strain,

which decreases with increasing carbon content. Finally, Rappaz *et al.* propose to calculate the hot tearing susceptibility as follows:

$$HCS = \frac{1}{\dot{\varepsilon}_C} \tag{4.9}$$

The results are illustrated in Fig. 4.5 for the measured and calculated (Eq. 4.3) values of the secondary dendrite arm spacing. The hot tearing susceptibility shows no significant difference for the two different λ_2-values: Up to a carbon content of 0.16 $wt.$-% the HCS remains nearly constant, after that it sharply increases.

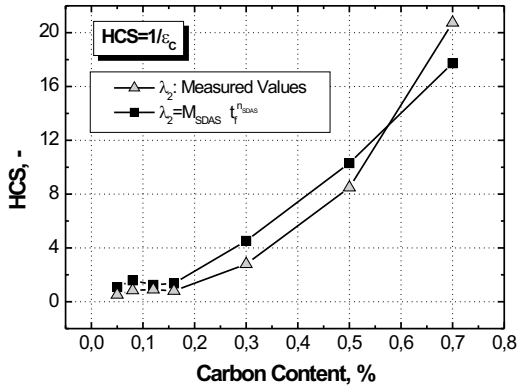

Figure 4.5: *Calculated hot tearing susceptibility as a function of carbon content for calculated and measured values of λ_2.*

4.4 A Criterion Based on Other Principles

An example for a hot tearing model which is based on other principles was published by **Clyne and Davies**[27]. The authors defined the hot tearing susceptibility as the ratio of the vulnerable time period and the time available for a stress-relief process (see Eq. 3.36). The necessary parameters for calculating HCS are determined from the results of the thermal analysis (shell thickness as a function of solidification time) and are summarised in Tab. 4.4.

Carbon Content	0.05	0.08	0.12	0.16	0.30	0.50	0.70
t_V	2.76	3.56	4.94	6.08	8.00	9.66	11.12
t_R	3.34	4.36	5.32	4.92	4.84	6.54	7.20

Table 4.4: *The parameters of t_V and t_R necessary for the calculation of HCS according to the hot tearing model by Clyne and Davies.*

Fig. 4.6 shows the calculated HCS according to the criterion proposed by Clyne and Davies. The equation for the hot tearing susceptibility is also illustrated in Fig. 4.6. It can be seen that the hot tearing susceptibility starts to increase at a carbon content of 0.12 $wt.$-%C. After reaching a maximum at 0.30 $wt.$-%C, the HCS tends to decrease.

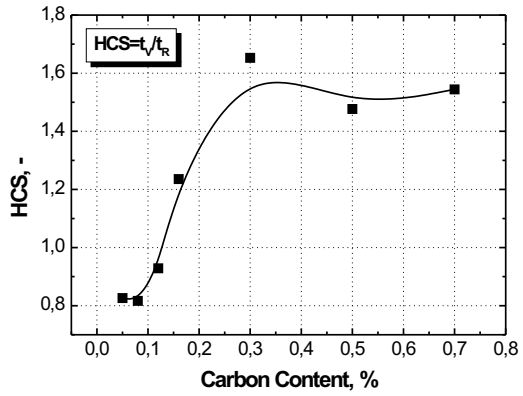

Figure 4.6: *Calculated hot tearing susceptibility as a function of carbon content according to Clyne and Davies.*

4.5 Summary

The results of the calculations using these four different hot tearing criteria can now be summarised. The stress-based model proposed by Rogberg strongly depends on the secondary dendrite arm spacing. Fig. 4.1 shows the results of the normalised HCS using different λ_2-relations, measured values of λ_2 and the curve obtained by inserting measured values of the fracture stress. Using λ_2-relations from the literature, the hot tearing susceptibility tends to increase with increasing carbon content. Using measured values of λ_2 leads to a maximum hot tearing susceptibility at a carbon content of 0.30 $wt.$-%C. The measured values of the fracture strain according to Shin [42] result in a higher hot tearing susceptibility at carbon contents up to 0.12 $wt.$-%C. From a carbon content of 0.16 $wt.$-%C the hot tearing susceptibility remains nearly constant.

The strain-based criterion according to Won *et al.* leads to an increasing hot tearing susceptibility with increasing carbon content. Calculating the hot tearing susceptibility according to Rappaz *et al.* results also in an increasing tendency of hot tearing with increasing carbon content. In comparison to the Rogberg model, the secondary dendrite arm spacing shows no significant influence on the calculation results.

Finally, the hot tearing susceptibility coefficient suggested by Clyne and Davies shows a similar curve as the stress-based model using measured values of the secondary dendrite arm spacing. The hot tearing tendency increases up to a carbon content of 0.30 $wt.$-%C, which remains fairly constant above 0.30 $wt.$-%C.

5 Requirements to a Process Related Hot Tearing Criterion

...Wer aber Bücher und Abhandlungen nach ihren Titeln und die Menschen nach ihren Kleidern beurteilt, handelt gleich voreilig, denn hinter beiden steckt oft ganz etwas anderes, als man dem ersten Anschein nach vermuthet.[a] CHRISTIAN DOPPLER

[a] Österreichische Blätter für Literatur und Kunst, Nr. 15, (1844).

In the summary of Chapter 2 the definition of hot tearing during continuous casting according to Bernhard *et al.*[18] is presented. This definition is the initial point of the following chapter. Based on the considerations of hot tearing in the continuous casting process and the resulting consequences, this definition will be modified.

In the literature, many hot tearing criteria can be found (see Chapter 3 *Hot Tearing Criteria*). Generally, these criteria can be used to estimate the hot tearing susceptibility as a function of the steel composition. However, the question if hot tears affect the quality of the cast product remains unanswered. In the following, the relationship between the casting process, the material properties, the subsequent processing and the properties of the product will be illustrated. Consequently, the demands on a process related hot tearing criterion will be deduced.

Hot tears can develop near the surface of the cast product during the initial solidification and can propagate up to the product surface. However, hot tears are mainly found inside the cast product. Therefore, the following section basically distinguishes between *Subsurface Hot Tears* and *Internal Hot Tears*[17].

5.1 Types of Hot Tears in the Cast Product

Considering ***subsurface hot tears***, a distinction with respect to the cast product (slab, bloom, billet or round) is necessary. Subsurface hot tears are mainly found in slabs, blooms and billets at the vicinity of the corner. The cracks are formed within or directly below the mould associated with the deformation of the solidified shell. Cracks below the mould result from bulging in conjunction with off-corner depressions, the raising of the edges from the mould wall associated

with strain development and the rhomboidal deformation of the solidified shell framework at billet casting. Subsurface hot tear formation during continuous casting of rounds mainly occurs below depressions. The development of such depressions is strongly influenced by the phase transformation (shrinkage/contraction) near the solidus temperature and just below this temperature. Peritectic steel grades are therefore particularly affected[135]. Fig. 5.1 shows an example of hot tearing below a depression[17]. It can be seen clearly that the weakening of the steel shell (thinner shell thickness, higher temperature) results in numerous initiations of hot tears. A major requirement to initiate hot tears are stresses within the mushy zone generated, for example, by friction forces within the mould or by reheating of the strand surface below the mould.

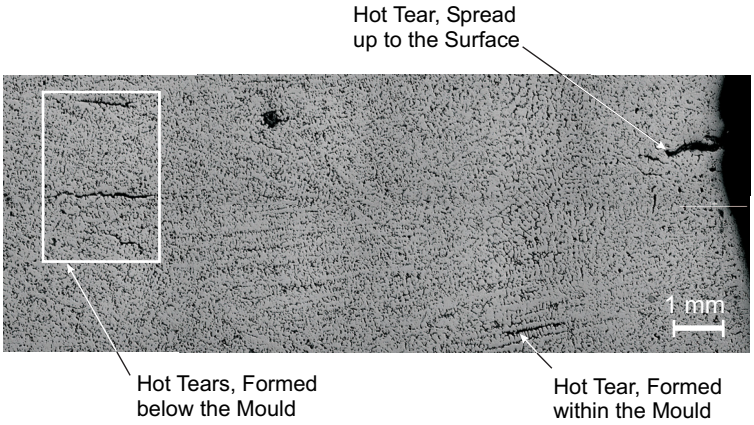

Figure 5.1: *Hot tearing below a depression of continuously cast rounds (0.12 wt.-%C)[17].*

Generally, subsurface hot tears are very harmful because these cracks can propagate up to the surface during the continuous casting process, which might result in a breakout. During hot forming these cracks can also grow up to the surface, leading to surface defects in the product. Surface defects represent a quality loss of nearly all products, certainly depending on the requirement of the surface quality.

Additionally, segregated hot tears are a serious problem in steel products. Applying a high degree of deformation, such segregated hot tears can propagate up to the surface. For example, manganese-sulfide (MnS) bands within segregated hot tears can lead to a quality loss in a cold rolled strip. Furthermore, segregated hot tears result in a banded structure. This banded structure together with MnS bands causes a response of the ultrasonic test at subsequent processing. Thus, the harmfulness of hot tears strongly depends on the subsequent processing and the required product quality. It can be summarised that the hot tearing susceptibility is not only influenced by the material but also by process parameters, in particular, in the case of subsurface cracks. Fig. 5.2 shows an example of the concentration distribution of Si and P in a segregated hot tear. In addition, the MnS precipitations can be seen clearly[126].

Crack formation in the continuous casting process due to bending, bulging, straightening, strand treatment (thermal or mechanical soft reduction) or reheating of the strand surface within the strand are often referred to as ***internal cracks*** in the relevant literature[136–138]. These cracks are

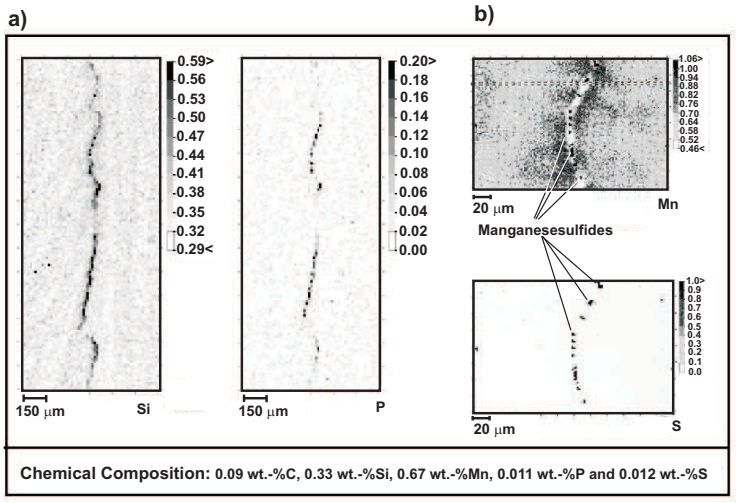

Figure 5.2: *a) Concentration distribution of Si and P within a segregated hot tear and b) a magnification of the concentration distribution of Mn and S together with MnS precipitation*[126].

mainly midway (halfway) cracks, triple-point cracks and diagonal cracks. The formation of such cracks corresponds to the classical theory of hot tearing along interdendritic paths or along grain boundaries, respectively.

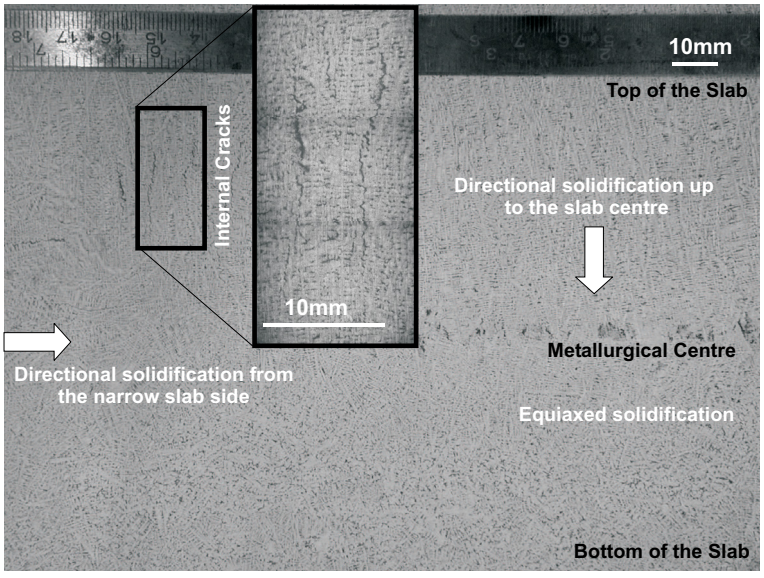

Figure 5.3: *Etched slab containing a segregated hot tear and characterisation of the solidification morphology (0.17 wt.-%C)*[17].

Within slabs typical solidification structures can be found. These structures show differences between the upper and lower part of the slab, which can be seen in Fig 5.3[17]. At the top of the slab a directional solidification occurs up to the metallurgical center of the slab. The latter is shifted slightly in the direction of the upper part of the slab. Concerning the lower part of the slab,

fragments of dendrites lead to a more or less developed transition from directional to equiaxed solidification. However, hot tears can only be found in directionally solidified areas of the cast product, where the load acts perpendicular to the main direction of crystallisation.

Considering the product quality, internal cracks far inside the cast product clearly show a less negative influence. Certainly, the degree of deformation at subsequent processing has to be taken into account. Enrichments of segregating elements within segregated hot tears result in a change of the phase transformation behavior, most notably when applying small degrees of deformation (e.g. heavy plates).

Concluding, hot tear formation is influenced by the continuous casting machine in conjunction with the system configuration, the maintenance of the equipment and certainly the cast material. In addition, the general trend towards higher casting speed and the increasing production of steel grades with unfavorable material properties increase the hot tearing susceptibility. Therefore, the development of a process related hot tearing criterion is an important demand for improving the quality of the continuous casting product. In the present section, the interrelation between process, material and subsequent processing with respect to hot tearing was illustrated. The following section will focus on the conclusions that can be drawn from these considerations on hot tearing criteria.

5.2 Outcome

Hot tearing criteria available in the literature enable either a qualitative assessment of the hot tearing susceptibility or a quantification mostly in terms of critical values (stress or strain). In all cases, these criteria are related to the material. Several models are based on the limit of liquid feeding, which can lead to a limitation because of the potentially harmful effect of segregated hot tears, as pointed out above.

The demands on a hot tearing criterion depend on the use of the cast product. Most importantly, a hot tearing criterion should take into account aspects of quality assurance. Moreover, a hot tearing criterion should give an indication on the expected problems when casting new steel grades. A highly-developed hot tearing criterion should provide solutions in order to optimise steel grade specific production specifications. With respect to the development and the initial operation of new plants, a hot tearing criterion should also allow a steel grade-dependent quantification of the expected hot tear formation.

In order to meet the requirement of ***considering the process***, a hot tearing model cannot be restricted to the description of material properties. As pointed out above, the process plays an important role especially for the formation of subsurface hot tears. Hot tearing is strongly influenced by the formation of weak points (e.g. depressions) that are further stressed. Therefore, the formation of weak points at defined conditions must be considered, because only at that time the hot tearing susceptibility plays a decisive role.

The consideration of the process is already done by thermo-mechanical computational models. Hence, the strain and strain rates in the mushy zone due to the process can be described very exactly based on sophisticated strand mechanics. Thus, a strain-based criterion would be sufficient to consider the phenomenon of hot tearing in continuous casting of steel[17].

A further important demand is the ***consideration of the microstructure***. The term microstructure is related to the solidification structure and therefore not only to the consideration of dendrites, but also that of primary grains. Primary grains are defined as regions showing the same spatial orientation with primary grain boundaries between the grains. Primary grain boundaries are considerably broader than the interdendritic distance, which results in a greater amount of segregated residual liquid due to longer back-diffusion paths.

Fig. 5.4 shows an example of the position of hot tears perpendicular to the main solidification direction of a 0.17 $wt.\text{-}\%C$ steel. The hot tears are generated by means of a laboratory experiment with the main load direction as illustrated in Fig. 5.4. It can be seen that cracks preferentially extend along primary grain boundaries, which are perpendicularly orientated to the main load direction[18].

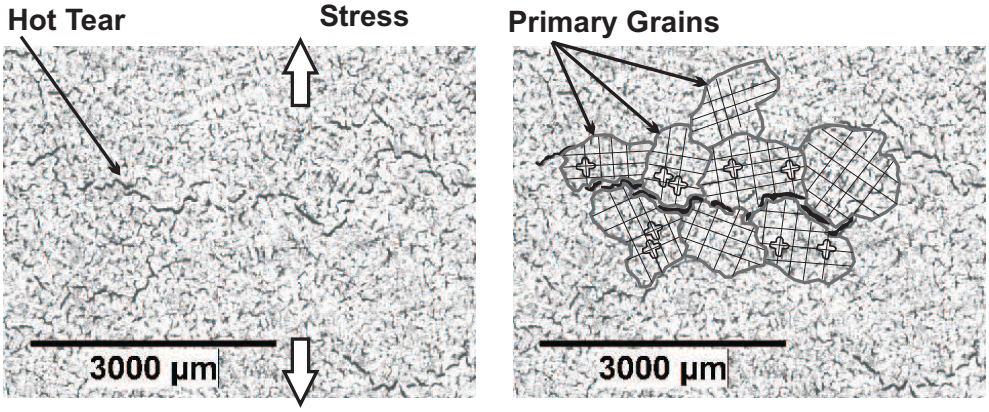

Figure 5.4: *Primary etching of a 0.17 wt.-% carbon steel perpendicular to the solidification direction (distance from the interface: 6.8 mm), without (left) and with marked primary grain boundaries (right)[18].*

Generally, the microstructure (columnar or equiaxed) as well as the formation of the microstructure (fine or coarse) show an influence on crack initiation and crack propagation. This was shown by Mori[139] using results from a convectional hot tensile test. Fig. 5.5* shows the ductility near the solidus temperature for steel samples with 0.15 to 0.18 $wt.\text{-}\%C$. The samples were taken from different positions of a continuously cast slab. The ductility of an equiaxed structure is zero at a temperature which is clearly higher compared to samples showing a columnar structure. Regarding the columnar structure, samples with a finer structure (near the surface) show higher temperatures of zero ductility than samples with a coarse structure. Based on these results the following conclusions can be drawn with respect to hot tearing. The hot tearing tendency increases in the sequence equiaxed – columnar fine – columnar coarse. Results from previous investigations using the SSCT test clearly show the influence of different cooling rates during solidification and therefore

*Original Source: Fujii *et al.* Tetsu-to-Hagane, **63** (1977)

the influence of microstructure on hot tearing[1]. The tests at the higher cooling rate, corresponding to a fine microstructure, are obviously less crack-sensitive. As a result of these considerations the demand of coupling a hot tearing model to a microstructure model can be deduced. Particulary in the vicinity of the center of a cast product only few coarse grains exist. Thus, the applied total strain is concentrated at few primary grain boundaries, resulting in a higher local strain at these boundaries. This explanation is also used by Campbell[16], who points out that with an increasing amount of residual liquid and finer grains, more strain can be accumulated by grain boundary sliding. Additionally, for the deformation of grains a plastic work is necessary. Therefore, it can be concluded that the high temperature behaviour near T_S also contributes to a description of the phenomenon of hot tearing. Thus, the distinction between the two occurring Fe-phases during solidification plays an important role.

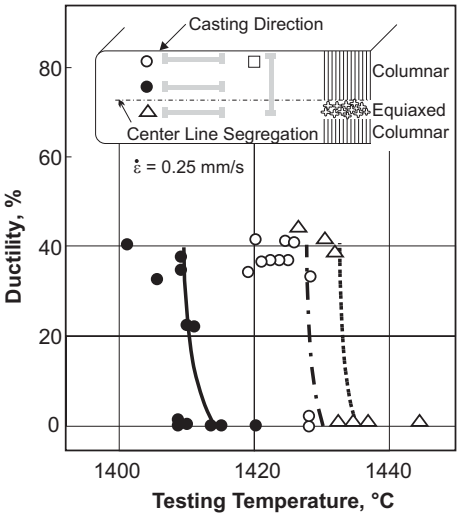

Figure 5.5: *Results of hot tensile tests of samples taken from different positions of a continuously cast slab* $(0.15 - 0.18\ wt.\text{-}\%C)$ *[139].*

Finally, the ***consideration of the steel composition*** is an important feature of a hot tearing criterion. In an already published paper[9] four selected criteria were applied to the results of the SSCT test (see also Chapter 4). It was shown that the different models tend to agree with the measurements up to a carbon content of 0.30 $wt.$-%. However, none of the used criteria can reproduce the measured decreasing hot tearing susceptibility above this carbon content. These calculations were based on the microsegregation analysis using the *IDS software*[120]. In Chapter 4, the calculations of the above mentioned models were illustrated in detail.

5.3 Summary and Conclusion

This chapter illustrated the complex interplay between the continuous casting process and the material properties. The occurrence of hot tears is not necessarily connected to a quality loss of the continuously cast product. The demands on the product as well as the subsequent processing must be considered. Hot tears can be found in different positions of the cast product, generally

subsurface hot tears are more critical. Both open and segregated hot tears can degrade the quality of the final product. In certain cases segregated hot tears may have an even more negative effect on the quality than open hot tears.

Taking these facts into account, the definition of hot tearing with respect to continuous casting according to Bernhard[18] must be modified as follows:

> *In continuous casting, hot tearing generally results from an overcritical, perpendicularly oriented tensile straining of a columnar solidifying mushy zone. The hot tears initiate within the mushy zone and propagate along primary grain boundaries resulting in open or in hot segregated hot tears.*

The aim of the present thesis is a considerable advancement of the description of hot tearing in the continuous casting process. For this purpose, the above illustrated requirements to a process related hot tearing criterion should be considered. Since the strain and strain rate generated through the process can be calculated using strand mechanics, a strain-based hot tearing criterion will be developed. Therefore, the requirement of considering the process (e.g. formation of weak points which are stressed) is fulfilled. In a first approach, the consideration of the steel composition is the main parameter of the criterion. In the next chapter the basic concept of the model is illustrated. The main part of the present thesis focuses on the experimental investigation of the problem of hot tearing. In order to take into account that both open and segregated hot tears may degrade the quality of the final cast product, no distinction is made between these types of hot tears. The description of the laboratory experiment and the evaluation of hot tearing are illustrated in Chapter 7. The results of a large number of experiments will be presented in Chapter 8. Furthermore, the developed model will be applied to these results. The application of the model to the experimentally determined results of hot tearing under continuous casting conditions enables the consideration of the demands on the final product quality.

6 Concept Behind the Model

Each time new experiments are observed to agree with the predictions the theory survives, and our confidence in it is increased; but if ever a new observation is found to disagree, we have to abandon or modify the theory.[a]
STEPHEN HAWKING

[a] A Brief History of Time, Bantam Books, (1988).

The previous chapter *Requirements to a Process Related Hot Tearing Criterion* pointed out that a hot tearing criterion for continuous casting of steel cannot be restricted to the description of material parameters (e.g. steel composition). Important requirements include the consideration of the microstructure and the process. The latter is of particular importance because hot tearing is also strongly influenced by the formation of weak points during the process. The degree of damage by hot tearing depends on the property demands on the final product and/or on further processing routes. Both open and segregated hot tears have to be seen as a defect in the casting.

Hot tearing criteria from the literature (see Chapter 3) have advantages and disadvantages. In the majority of the cases, these models allow an indication of the hot tearing susceptibility and/or the definition of quantitative limits. However, the quantitative prediction of hot tearing – mostly achieved by comparing the stress or strain due to the process to critical values – strongly depends on critical values of hot tearing. The hot tearing model for continuous casting, described in the following section, is based on a critical strain criterion. The main reasons for this can be summarised as follows:

- A critical strain criterion allows the quantitative definition of a deformation limit and can be coupled with FE strand mechanics easily,
- it allows the accumulation of tensile strain in certain parts of the mushy zone over time, making the criterion dependent on steel composition, strain rate, solidification velocity and temperature gradient and
- the thermal contraction during solidification can be considered.

As summarised in Chapter 2, Pellini[58] was the first to investigate hot tearing of steel. Pellini's *Strain Theory*, explaining the mechanism of hot tearing, was already illustrated in detail. However,

Pellini did not follow up these concepts in detail, and over the years the model has almost been forgotten. More recently, Yamanaka *et al.*[22,81] found out that hot tearing occurs when the total amount of strain within a certain critical (or brittle) temperature range exceeds the critical strain, independent of strain rate and manner of deformation. Yamanaka *et al.* pointed out that hot tearing in continuous casting should be assessed through the accumulated strain within the brittle temperature range resulting from bulging, bending, et cetera.

Following this theory of an accumulated strain, the realisation of a strain-based hot tearing criterion for the continuous casting process can be done in a first step by comparing the accumulated strain due to the process to a critical strain of hot tearing:

$$\varepsilon_{P,A} > \varepsilon_{C,A} \tag{6.1}$$

Thus, Eq. 6.1 states that hot tears will form if the accumulated strain due to the process exceeds a critical value of hot tearing. The following two sections will illustrate in detail the determination of both the accumulated strain as well as the critical strain.

6.1 The Accumulated Strain due to the Process

Following the fact that hot tears are generated by an overcritical deformation of the mushy zone, it must be considered that in continuous casting the mushy zone moves with the shell growth from the surface to the centre of the casting. Not only the position, but also the width of the mushy zone changes due to the variation of the solidification parameters over the metallurgical length. This is illustrated in Fig. 6.1a, which shows the position of the mushy zone in view of the normalised solidification time (t/t_S) and the width w of the mushy zone, expressed by the normalised shell thickness (s/s_0). The mushy zone is highlighted at two different positions ($t/t_S = 0.2$ and $t/t_S = 0.8$) within the casting machine. Assuming a squared bloom with $s_0 = 250\ mm$, the width of the mushy zone of w_1 is 40 mm and w_2 is 70 mm, respectively.

The extent of tensile straining during solidification results from the combination of material and the casting process. The continuous casting of steel is characterised by a large quantity of possible degrading effects, such as bulging of the shell between guiding rolls or unbending of the only partly solidified strand. According to the theory of strain accumulation, it is assumed that only a part of the total strain within a certain temperature range of the mushy zone will contribute to the formation of hot tears. This temperature range is denoted as temperature range of preferable strain accumulation ΔT_{SA} and is defined between the temperatures $T_A(f_S = f_{S,A})$ and $T_S(f_S = 1)$. This range is also illustrated in Fig. 6.1a, together with the associated residence time t_A^i of a volume element i. The parameter t_A corresponds to the time period, where the solid fraction of a volume element is in the range of $f_S = f_{S,A}$ and $f_S = 1$. The resulting curve of t_A as a function of the normalised solidification time ($\widehat{=}$ strand length) can be seen in Fig. 6.1b.

As a result of a thermal analysis, the time during which each element i can accumulate strain within the preferable range of strain accumulation can be computed by[140]

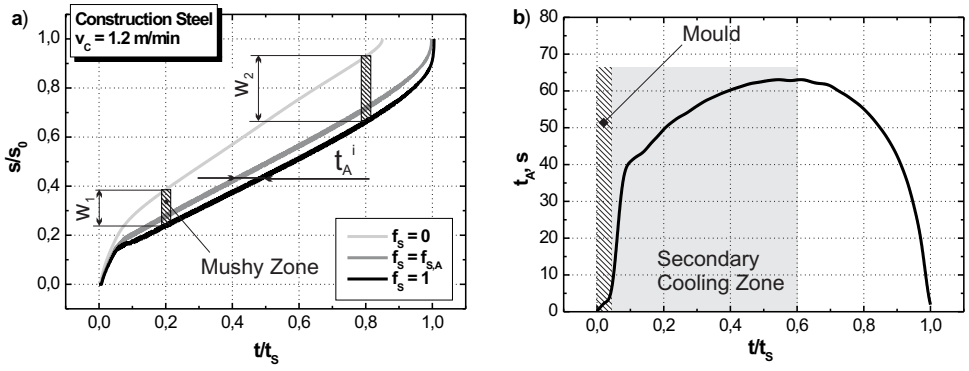

Figure 6.1: *a) Shell thickness as a function of normalised solidification time for a construction steel and b) the determined time of strain accumulation t_A within the temperature range of preferable strain accumulation[140].*

$$t_A^i = t_2^i - t_1^i \tag{6.2}$$

where the time step t_1^i represents the time when the element first reaches $f_{S,A}$ and t_2^i denotes the time when the volume element is fully solidified (i.e. $f_S = 1$). Thus, Eq. 6.2 is valid, where $s(t)$ is the strand shell thickness as a function of time for different fractions of solid:

$$t_2^i : s_{f_{S,A}}(t_1^i) = s_{f_S=1}(t_2^i) \tag{6.3}$$

The time t_A only represents the time period of a certain volume element within a certain temperature range within the mushy zone. The magnitude of this parameter is in no relation to the hot tearing tendency if no strain appears in the process. If the solidifying steel shell is strained, the accumulated strain due to the process $\varepsilon_{P,A}$ can be calculated as a function of t_A as follows:

$$\varepsilon_{P,A} = \int_{t_A} \dot{\varepsilon} \cdot \mathrm{d}t \tag{6.4}$$

In Eq. 6.4, $\dot{\varepsilon}$ denotes the total strain rate as the sum of all strain rates resulting from the deformation of the solidifying shell in the process and the thermal contraction during solidification. The parameter t_A does not only depend on the steel composition ($\widehat{=}$ the width of ΔT_{SA}) but also on the solidification velocity of the solidus isotherm R_S (in mm/s) and the temperature gradient within the mushy zone G (in K/mm). Assuming in a first step that R_S is constant within t_A, the following estimation of t_A can be used:

$$t_A = \frac{\Delta T_{SA}}{R_S \cdot G} \tag{6.5}$$

Eq. 6.5 is a simplification and in practice it will be replaced by a numerical solution of a thermal analysis of the continuous casting process as illustrated above (see Eq. 6.2 and Eq. 6.3).

Employing the enthalpy conservation, the shell growth as a function of solidification time can be calculated for selected casting parameters. Results of these calculations were already published [140]. Fig. 6.1 taken from this publication shows the result of a casting speed of 1.2 m/min. Fig. 6.1b illustrates that the time of strain accumulation increases sharply immediately below the mould. A maximum of t_A is reached at the end of the secondary cooling zone and subsequently decreases to very small values towards the end of solidification due to the accelerated final solidification. Elements which solidify at the end of the secondary cooling zone can accumulate substantially more strain than other elements. This means that it is more likely for those elements to exceed a given critical strain than elsewhere (see Eq. 6.1). Therefore, the occurrence of hot tears is also more likely in this region – consequently at higher values of t_A.

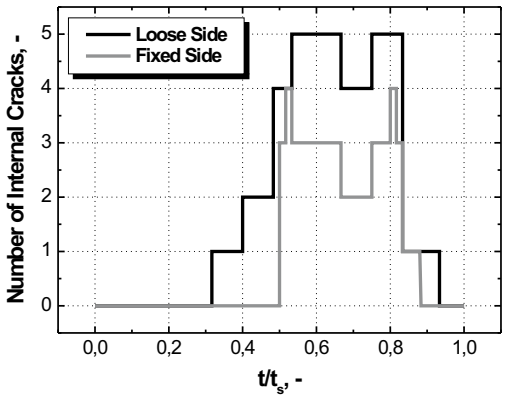

Figure 6.2: *Number of internal cracks vs. normalised solidification time of a slab of 220 x 2000 mm^2 with 0.20 wt.-%C from data according to Vaterlaus und Wolf[141].*

Vaterlaus and Wolf[141] found a very similar distribution of the number of internal cracks over the normalised solidification time, as shown in Fig. 6.2. The illustrated values result from both, solidification conditions and mechanic loads. Fig. 6.2 also shows the differences in crack formation for the fixed and loose side of the slab which result from the different directions of strain application.

Using sophisticated thermo-mechanical analysis, the accumulated strain due to the process (left hand term of Eq. 6.1) within a certain temperature range (preferable range of strain accumulation) of the mushy zone can be calculated. However, the quality of this strain-based criterion strongly depends on the critical strain of hot tearing (right hand term of Eq. 6.1). The determination of $\varepsilon_{C,A}$, therefore plays an important role and forms the main focus of the present thesis.

6.2 The Strain-Based Hot Tearing Criterion

In the previous section, the principle of strain accumulation within a certain temperature range applied on the continuous casting process was introduced. In the following section, the concept of this hot tearing criterion will be specified. It is assumed that the accumulation of strain in a certain part of the mushy zone causes the continuous separation of primary grains or dendrites. The probability for the formation of an overcritical intergranular enrichment (segregated hot tear) or an open hot tear increases with rising accumulated strain. Fig. 6.3 illustrates the process of the initiation of a hot tear. Fig. 6.3a schematically shows the columnar microstructure in a solidifying shell. Due to the solidification process in time, the mushy zone moves towards the centre of the casting product. Fig. 6.3b shows a detail with a primary grain boundary between two grains with a misorientation angle θ. The illustration indicates the comparably higher enrichment of segregating elements between primary grains due to the longer diffusion path.

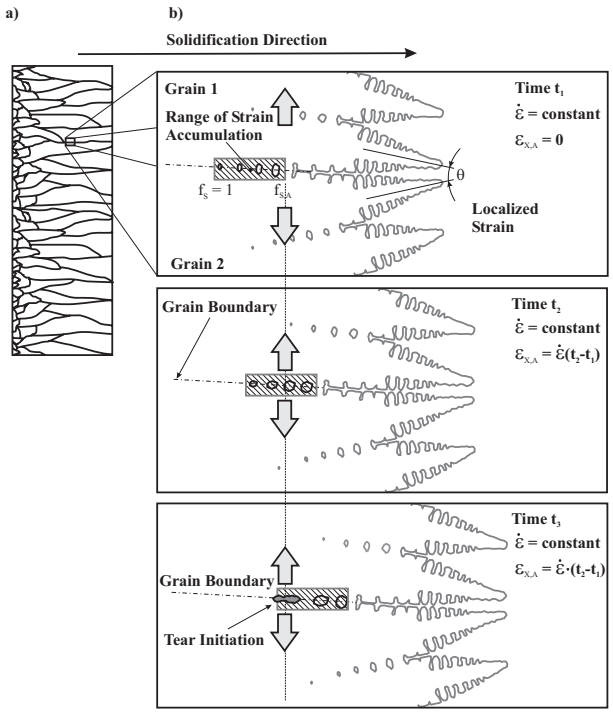

Figure 6.3: *Schematic illustration of hot tear initiation due to strain accumulation within a certain range of the mushy zone during columnar solidification.*

Assuming that hot tears are generated within a range of preferable strain accumulation in the mushy zone, that the primary grain boundaries are the favourable locations for hot tearing and that tear initiation is the result of strain accumulation, the strain-based criterion can be described as follows. At the time t_1 tensile straining starts at a strain rate $\dot{\varepsilon}$. During the time interval $t_X = t_2 - t_1$ solidification proceeds, and a volume element, corresponding to the solid fraction $f_{S,A}$, accumulates the strain $\varepsilon_{X,A} = \dot{\varepsilon} \cdot t_X$. The only partly solidified microstructure will be widened, but as long as the resulting segregation (segregated hot tear) or the extent of the deformation (open hot tear) remains below the critical limit, no hot tears will be detected. During the time interval

$t_{C,A} = t_3 - t_1$ the tensile strain will be further accumulated until either the volume element is totally solidified (no crack formation), or the extent of grain separation causes a hot tear (*tear initiation*). The concurrently accumulated strain is defined as the critical strain of hot tearing, $\varepsilon_{C,A} = \dot{\varepsilon} \cdot t_{C,A}$. Further straining causes a widening of the defects (*tear propagation*), increasing the probability of the detection as well as the extent of quality deterioration.

The determination of the accumulated strain within a certain temperature range of the continuous casting process is done by calculating the time of strain accumulation t_A and the appearing strain rates during the process. However, these calculations are not part of the present thesis. Instead it focuses on the determination of the right term in Eq. 6.1 – the critical accumulated strain of hot tearing – as well as on tear propagation. In order to investigate the influence of the accumulated strain on the extent of hot tearing, an experimental apparatus was employed. A detailed description of this experiment is given in the next chapter.

The determination of the accumulated strain appearing during the laboratory test is schematically shown in Fig. 6.4a. It shows the calculated shell growth* as a function of solidification time for the isotherms corresponding to $f_S = 1$, $f_S = f_{S,A}$ and $f_S = 0$. After a certain holding time, the tensile test starts at a constant strain rate. The range of straining the solidifying steel shell is also illustrated in the diagram together with the range of strain accumulation (grey area). The totally accumulated strain in every volume element within this defined range is illustrated in Fig. 6.4b. The maximum accumulated strain $\varepsilon_{A,max}$ is only 1.4 %, compared with the total global strain of 2 %. Again, the ratio between the accumulated strain and the total strain depends on the steel composition (width of the accumulation range, ΔT_{SA}), the strain rate and the solidification conditions.

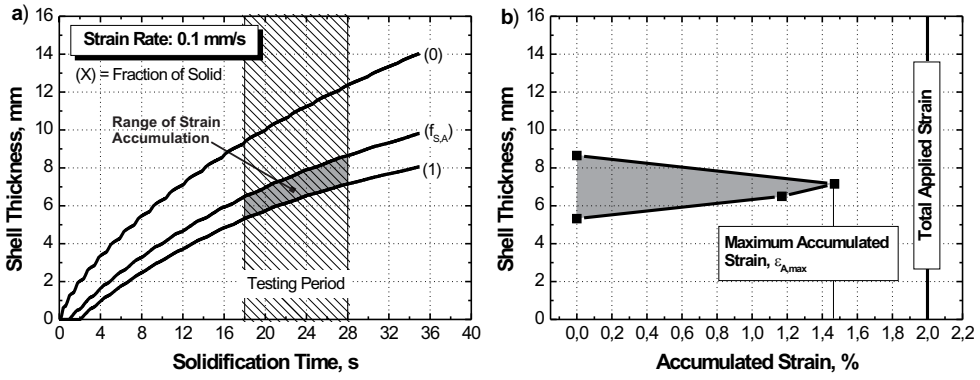

Figure 6.4: *a) Shell growth as a function of time and b) the resulting accumulated strain within a certain temperature range at a strain rate of* $2 \cdot 10^{-3}\ s^{-1}$.

Due to the specific testing conditions (hindered shrinkage/contraction) of the SSCT-test, the strain resulting from volume changes caused by both temperature differences and phase transformation contributes to the deformation of the solidifying steel shell. Generally, a distinction must

*The detail description of the thermal analysis is illustrated in Chapter 7

be made between the terms *shrinkage* and *contraction*. In the literature the following definition can be found [142]:

> *For the 100 %-solid steel, contraction takes place due to the decreasing of temperature and corresponding reduction in elementary volume, while another process (shrinkage) takes place in the mushy zone owing to the transition of steel from liquid to solid phase.*

However, in the present thesis the strain due to temperature differences and phase transformation within ΔT_{SA} is referred to as thermal strain ε_{th}. Thus, the effective strain ε_{eff} that will be accumulated within this temperature range results from the accumulated strain and the thermal strain according to:

$$\varepsilon_{eff} = \varepsilon_{th} + \varepsilon_A \tag{6.6}$$

The primary objective of this study is to define the severity of hot tearing as a function of this effective strain. Thus, mainly the influence of carbon content – certainly the most important alloying element in steel – on hot tearing will be investigated. This will be realised by distinguishing between tear initiation and propagation. However, not only a critical strain of tear initiation will be considered, but also the evolution of the hot tears in view of the number of hot tears (NHT) with increasing effective strain. Thus, the criterion enables the definition of critical values of the effective strain – the tolerable strain ε_{tol} – depending on product quality and Eq. 6.1 can be modified:

$$\varepsilon_{P,A} > \varepsilon_{tol}(NHT) \tag{6.7}$$

If the accumulated strain due to the process is greater than a predefined tolerable strain, the extent of hot tearing lies below an acceptable limit. Furthermore, tear growth and consequently a generated average tear length strongly influence the severity of hot tearing. Thus, a relation must be found, which enables the estimation of the expected average tear length.

Chapter 8 illustrates the determination of the preferable range of strain accumulation as well as the determination of the above mentioned parameters. Based on the experimentally measured strain-dependent extent of hot tearing the above illustrated considerations will be defined and presented.

7 The Experiment

Since the measuring device has been constructed by the observer ... we have to remember that what we observe is not nature itself but nature exposed to our method of questioning.[a] WERNER HEISENBERG

[a] Physics and Philosophy: The Revolution in Modern Science. Harper, New York (1958).

The following section gives an overview of the laboratory experiment used in this study to investigate hot tearing under continuous casting conditions. The principle and the relevant parts of the **S**ubmerged **S**plit **C**hill **T**ensile (SSCT) apparatus were adopted from EPF Lausanne. This university mainly carried out studies investigating the deformation behavior of solidifying Al-alloys[143,144]. At the department of Metallurgy in Leoben the experiment was applied on solidifying steel, continuously modified and improved and the testing procedure was systematised. Since numerous publications[145–147,135,148–150] already focus on this topic, the following section only concentrates on the essential parameters necessary for the interpretation of hot tear formation during the experiment.

7.1 Test Arrangement

A proper laboratory simulation for investigating hot tearing under continuous casting conditions needs to fulfil the following demands:

1. The existence of a deformable mushy zone together with a columnar grain structure,
2. the conformity of the microstructure with that of a continuous casting shell, and
3. main load directions are perpendicular to the main dendrite growth axis.

Fig. 7.1 shows a schematic view of the SSCT test method and the solidification conditions compared to the continuous casting process. Keeping the above mentioned demands in mind, the testing procedure of the SSCT test can be summarised as follows. A steel shell solidifies around a solid test body – split in two halves – with a columnar grain structure perpendicular to the interface (Demand 1). The surface of the test body is spray-coated with a thin zirconium oxide

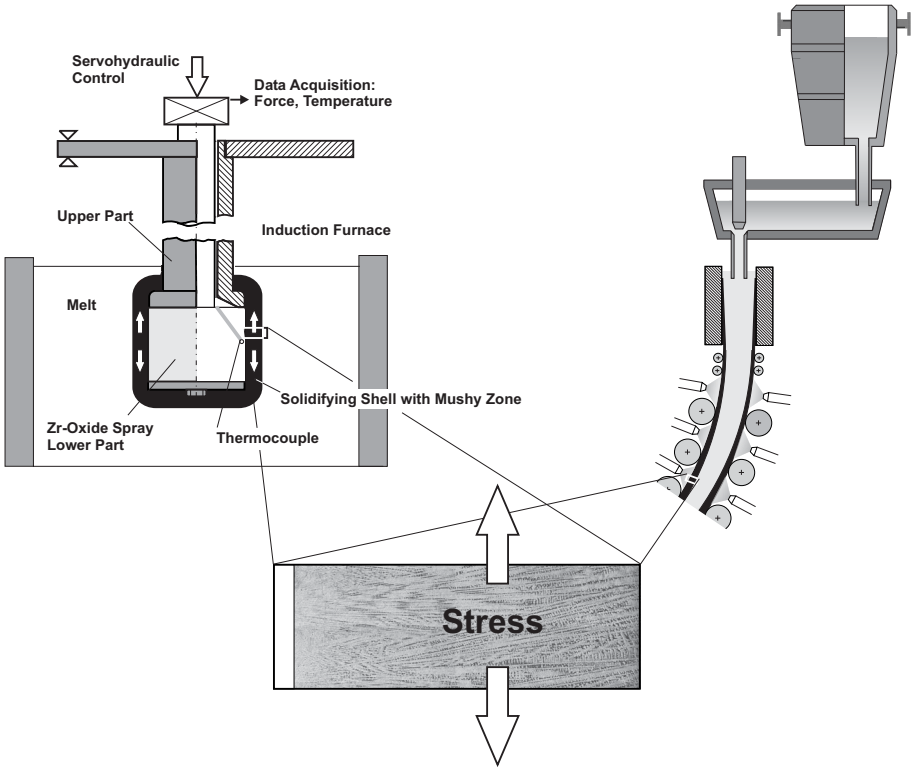

Figure 7.1: *Schematic illustration of the SSCT test and solidification conditions during the laboratory test ant the continuous casting process.*

layer in order to control the cooling conditions and the microstructure (Demand 2). After a certain holding time, the lower part of the test body moves downwards. In doing so, the solidifying steel shell is subjected to a tension perpendicular to the main growth axis, in correspondence with shell deformation in continuous casting (Demand 3).

During the tensile test, the force between the upper and lower parts of the test body is measured by a load cell, the position of the lower part by an inductive position sensor. After tensile testing, the test body together with the solidified steel shell emerge immediately out of the melt. In addition to the measurements of the force-elongation curves, the temperature increase inside the test body and the temperature of the melt are measured. These temperature measurements provide important data for the thermal analysis of the SSCT test, which will be described in the following section.

In this laboratory experiment the following testing parameters can be varied:

- ***Steel bath temperature:*** the initial temperature of the steel bath (T_{SB}). This temperature is held constant in the present study with values of 20 to 30 °C above the liquidus temperature of the tested steels.

- ***Cooling rate:*** This parameter is controlled by the thickness of the coating. The coating thickness influences the heat flux density. An increasing coating thickness affects primarily the maximum of the heat flux density. A detailed illustration of the relationship between coating thickness and heat flux density in conjunction with the characterisation of the cool-

ing conditions is given by Bernhard[126]. In this study, the characterisation of the cooling conditions was done by means of determing of the primary dendrite spacing (λ_1 or PDS) and the secondary dendrite arm spacing (λ_2 or SDAS). In the present study, mainly a coating thickness of $0.40\,mm$ is applied, which corresponds to the cooling conditions in a slab caster (maximum heat flux of $1.7\,MW/m^2$ and a mean heat flux of $1.25\,MW/m^2$).

- ***Holding time:*** The thickness of the shell and the temperature distribution inside the shell can be varied via the holding time. Due to the heat balance within the induction furnace, the total testing time is limited to approximately $35\,s$. In a first test series this parameter was varied between 4 and $12\,s$, in all other cases the holding time is $16\,s$.

- ***Strain rate and strain:*** In order to apply strain rates corresponding to the appearing strain rates of the continuous casting process, this parameter is $2 \cdot 10^{-3}\ s^{-1}$ ($\widehat{=} 0.1\ mm/s$). For the determination of the preferable temperature range of strain accumulation, additionally strain rates greater than $2 \cdot 10^{-3}\ s^{-1}$ are used. The total applied strain is a very important parameter of the study and was varied between 0 % and 3 %.

- ***Chemical composition:*** With an induction furnace any steel composition can be alloyed. In order to reduce the testing parameters, a basic steel composition is investigated varying only the carbon content.

The main focus of the present thesis is to investigate the phenomenon of hot tearing depending on the carbon content under continuous casting conditions, and to develop and validate the model of an accumulated strain within a certain temperature range of the mushy zone. Therefore, different testing parameters were varied, which are summarised in Appendix B for every conducted experiment.

7.2 Thermal Analysis

An important requirement to interpret the test results is the detailed knowledge of the temperature distribution inside the steel shell and the shell growth during solidification. For this purpose the increase of temperature inside the test body is recorded in a defined distance from the chill-shell interface by means of thermocouples. As a result, the heat flux density q can be calculated at the interface between the liquid melt and the solid steel test body using an inverse algorithm for the solution of the heat-conduction equation. The calculation procedure is based on a maximum-a-posteriori method and is described in detail in the literature[151]. The careful thermal analysis of the experiment is carried out by determining the enthalpy distribution between the chill surface and the inner side of the induction furnace using one-dimensional heat conduction. In order to consider the axisymmetric geometry of the test body, Eq. 7.1 is written in cylindrical coordinates:

$$\frac{\partial}{\partial t}(\rho \cdot H) = \frac{1}{r} \cdot \frac{\partial}{\partial r}\left(r \cdot k \cdot \frac{\partial T}{\partial r}\right) \tag{7.1}$$

where ρ is the temperature-dependent density, H denotes the enthalpy, k stands for the temperature-dependent thermal conductivity, r is the radius and t is the time. The enthalpy $H(T)$ is given by the following equation, where ΔH_{LS} is the latent heat:

$$H(T) = \int_0^T c_P(T') \cdot \mathrm{d}T' + (1 - f_S) \cdot \Delta H_{LS} \tag{7.2}$$

The following initial and boundary conditions can be defined from the initial temperature of the steel bath T_{SB}, the radius of the test body r_{tb}, the inner radius of the induction furnace r_0 and the heat flux density q at the chill surface:

$$\begin{aligned} &\text{Initial Conditions :} \\ &T = T_{SB}, \qquad r_{tb} \leq r \leq r_0, \qquad t = 0 \end{aligned} \tag{7.3}$$

$$\begin{aligned} &\text{Boundary Conditions :} \\ &k \cdot \frac{\partial T}{\partial r} = -q, \qquad r = r_{tb}, \qquad t > 0 \\ &k \cdot \frac{\partial T}{\partial r} = 0, \qquad r = r_0, \qquad t > 0 \end{aligned} \tag{7.4}$$

The solution of Eq. 7.1 is achieved with a numerical approach. A detailed description of these procedure is given by Xia[152].

In the following section, the whole procedure of the thermal analysis is presented in detail for a 0.16 $wt.\text{-}\%C$ steel (0.30 $wt.\text{-}\%Si$, 1.35 $wt.\text{-}\%Mn$, 0.007 $wt.\text{-}\%P$ and 0.007 $wt.\text{-}\%S$). The initial steel bath temperature T_{SB} is 1540 $°C$. Fig. 7.2a shows the measured temperatures during the SSCT-test. The temperature increase inside the test body, recorded via two thermocouples (THC01 and THC02) serves as the input data for the calculation of the heat flux density. The results of this calculation are illustrated in Fig. 7.2b. It can be seen that the heat flux densities are in good agreement with the above mentioned values (maximum heat flux of 1.7 MW/m^2 and a mean heat flux of 1.25 MW/m^2) of a slab caster. The black curve represents the smoothed mean values of the two calculated heat flux densities, which are used in the following solidification calculation. The result of this calculation is the temperature distribution in the melt during the SSCT test, as illustrated in Fig. 7.2c. Node number 1 represents the interface between the chill surface of the test body and the melt, the solidification time is 30 s. This temperature distribution as a function of time in connection with the results from a microsegregation model (fraction of solid vs. temperature) allows the calculation of shell growth during the experiment. In present study the microsegregation model proposed by Ueshima[54] is applied (Appendix A). Fig. 7.2d shows the calculated fraction of solid, fraction of δ-phase and γ-phase as a function of temperature.

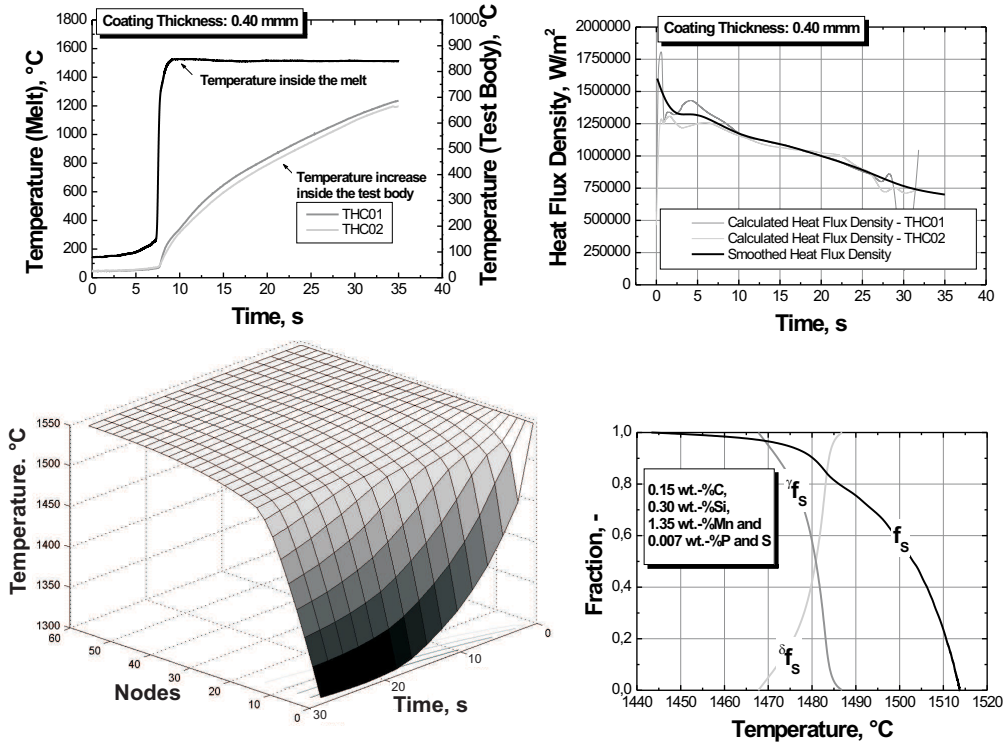

Figure 7.2: *a) Measured temperatures during the SSCT test, b) calculated heat flux density as a function of time, c) temperature distribution between chill surface and the inner side of the induction furnace and calculated fraction of solid, fraction of δ-phase and γ-phase d), respectively for a* 0.15 *wt.-%C steel.*

Finally, this calculation procedure enables the determination of the shell growth during the SSCT test. Fig. 7.3 illustrates the calculated shell growth as a function of solidification time for the isotherms corresponding to solid fractions of 0 and 1. In addition, the measured shell thickness together with the scatter band of the measurement is illustrated. In previous studies it was shown that the measured shell thickness is in good agreement with a solid fraction of approximately 0.2. In addition to the comparison of the measured and calculated temperature of the melt, the comparison of measured and calculated ($f_S = 0.2$) shell thickness is an important basis for the reliability of the thermal analysis.

The duration of submerging as well as the duration of emerging is 2 s. The holding time for this experiment is 16 s and the total strain ε_{tot} is 1.5 %. Thus, applying a strain rate $\dot{\varepsilon}$ of $2 \cdot 10^{-3}$ s^{-1} ($\widehat{=} 0.1$ mm/s) the testing time results in 7.5 s, which leads to a total solidification time of 27.5 s. This situation (different stages during the experiment) is also illustrated in Fig. 7.3. The time range of the tensile test is highlighted to underline the shell growth during the test and therefore the non-isothermal conditions similar to the continuous casting process.

This section illustrated that the mathematical determination of the temperature distribution within the shell as well as the determination of the solidification progress require considerable

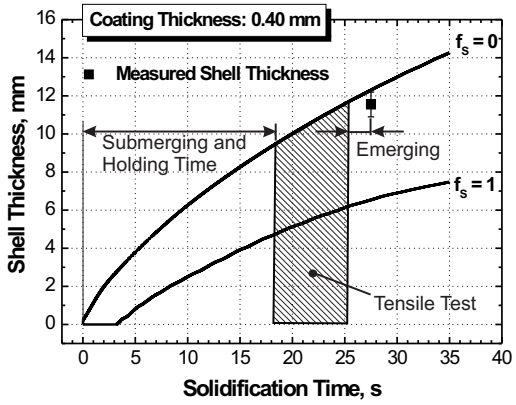

Figure 7.3: *Calculated and measured shell thickness as a function of solidification time together with the different stages during the SSCT test of a* $0.15wt.\text{-}\%C$ *steel (*$T_{SB} = 1540$ °C, $\varepsilon_{tot} = 1.5$ %, $\dot{\varepsilon} = 2 \cdot 10^{-3}\ s^{-1}$*).*

effort. However, contrary to conventional hot tensile tests, the non-isothermal conditions of the SSCT test are closer to the conditions of the continuous casting process.

7.3 Metallographic Analysis

The evaluation of hot tears is done by separating the solidified shell from the test body. In doing so, 16 samples are cut from the circumference of the shell and are finally polished and etched. This procedure is schematically shown in Fig. 7.4 (left hand side). The solidified steel shell around the test body is illustrated together with the samples and the polished and etched metallographic specimen. Eight of these 16 specimen are finally investigated in a metallographic examination in which the hot tears are counted (**N**umber of **H**ot **T**ears, NHT) and their length (**L**ength of **H**ot **T**ears, LHT) is measured. In addition, the distance from the chill-shell interface (**D**istance **f**rom **I**nterface, DfI) is determined.

The evaluation procedure of these parameters is illustrated in Fig. 7.4 (right hand side). The determination of NHT and LHT is performed according to the following equations:

$$NHT = \frac{1}{N_{Micrograph}} \cdot \sum_{i}^{k} N_i \tag{7.5}$$

$$LHT = \frac{1}{N_{Micrograph}} \cdot \sum_{i}^{k} L_i \tag{7.6}$$

In these two equations, $N_{Micrograph}$ is the number of analysed micrographs (mainly eight micrographs) and k denotes the individual hot tear. In addition, the ratio LHT/NHT can be determined, which represents the average tear length ATL. These parameters together with the calculated standard deviation (SD) for every analysed experiment are summarised in Section B.2 (Appendix B).

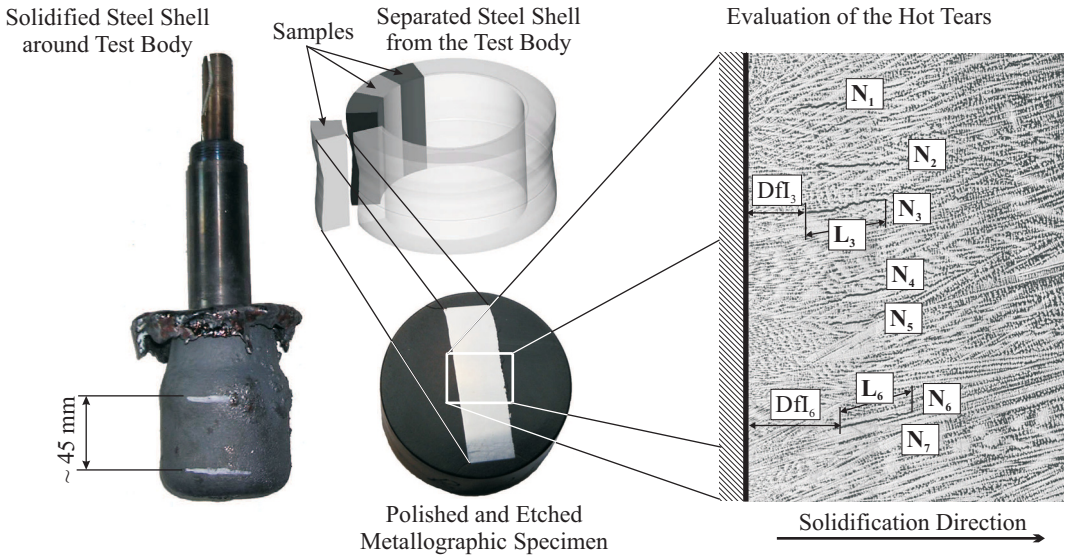

Figure 7.4: *Schematic illustration of the making of the metallographic specimen and a detailed view of a micrograph including hot tears, whereby the evaluation parameters are additionally illustrated.*

Hot tearing represents the phenomenon of crack formation within the mushy zone. Therefore, the analysis of the above mentioned parameters considers only cracks which are within the range of the mushy zone during the tensile test. This can also be formulated vice versa: The determination of the position of the cracks provides information, whether cracks are generated within the mushy zone or not. These kinds of cracks can therefore be treated as hot tears. Again, no distinction is made between open or segregated hot tears.

7.4 Summary

The SSCT testing method is very complex. Thus, the test and the evaluation of the test must be carried out very accurately. The results are substantially influenced by the testing parameters. Therefore, the validation of the solidification conditions is an important feature of the SSCT-test. In a previous study [126], it was shown that the conditions of the above described laboratory experiment are similar to those of the continuous casting process. The main demands – a deformable mushy zone with columnar grain structure, an adjustable microstructure and a load direction perpendicular to the dendrite growth axis – are fulfilled.

The thermal analysis is essential in the interpretation of hot tearing, the metallographic analysis is carried out in view of the number and length of hot tears, the average tear length and the distance from interface. In Appendix B, all results of the thermal and metallographic analysis are summarised.

8 Hot Tearing Under Continuous Casting Conditions

A hot tear does not always appear under apparently identical conditions; in fact it seems subject to a considerable degree of randomness in relation to its appearance or non-appearance, and to its extent.[a].
JOHN CAMPBELL

[a]Castings, Butterworth-Heinemann (1991)

Chapter 8 presents the results of the experimental investigations of hot tearing using the SSCT-test for different steel grades. In addition, the previously presented model of an accumulated strain within a certain range of the mushy zone is applied and the consequences are discussed.

An important point in this investigation was the question whether the SSCT-test is an appropriate tool for investigating the phenomenon of hot tearing of steel. According to the definition of hot tearing, the generation of hot tears takes place during solidification within the mushy zone. Therefore, the aim of the first test series was to clarify if it is possible to generate hot tears within the mushy zone. An important point was the position of the hot tears within the sample. The following section summarises the results of a test series applying different testing parameters (holding time, strain rate and cooling rate) at a constant chemical composition (construction steel) and constant total strain ε_{tot}.

8.1 Hot Tearing of a Construction Steel under Different Testing Conditions

The first test series (*Test Series A*) was performed using a typical construction steel ($0.16-0.20$ $wt.\text{-}\%C$, $0.20-0.40$ $wt.\text{-}\%Si$, $1.30-1.50$ $wt.\text{-}\%Mn$, <0.025 $wt.\text{-}\%P$ and <0.01 $wt.\text{-}\%S$), the as-is analysis of the tested steels is summarised in Tab. B.1. Additionally, the measured initial steel bath temperature T_{SB}, the used coating thickness s_{coat} and strain rate $\dot{\varepsilon}$ as well as the respective holding time HT are listed in Tab. B.1. The total applied strain is 2.4 % in all cases. As it can be seen from this table, three different holding times ($HT = 4,\ 8$ and $12\ s$), two different strain rates ($\dot{\varepsilon} = 2 \cdot 10^{-3}$ and $6 \cdot 10^{-3}\ s^{-1}$) and two different cooling rates ($s_{coat} = 0.40$ and $0.15\ mm$)

were investigated. As mentioned in Chapter 7, a coating thickness of 0.40 mm corresponds to the cooling conditions in a slab casting mould (maximum heat flux of $\sim$ 1.7 MW/m^2 and a mean heat flux of $\sim$ 1.25 MW/m^2), whereas a coating thickness of 0.15 mm corresponds to the cooling conditions in a bloom casting mold (maximum heat flux of $\sim$ 2.4 MW/m^2, and a mean heat flux of $\sim$ 1.45 MW/m^2).

Test series A included 13 tests, test number A09/1 and A09/2 are two experiments using the same testing parameters. All other experiments differ in their testing parameters. The first step in every individual experiment is the thermal analysis. In Chapter 7 an example of a thermal analysis was illustrated in detail. Therefore, the thermal analysis of every experiment will not be described in the following section.

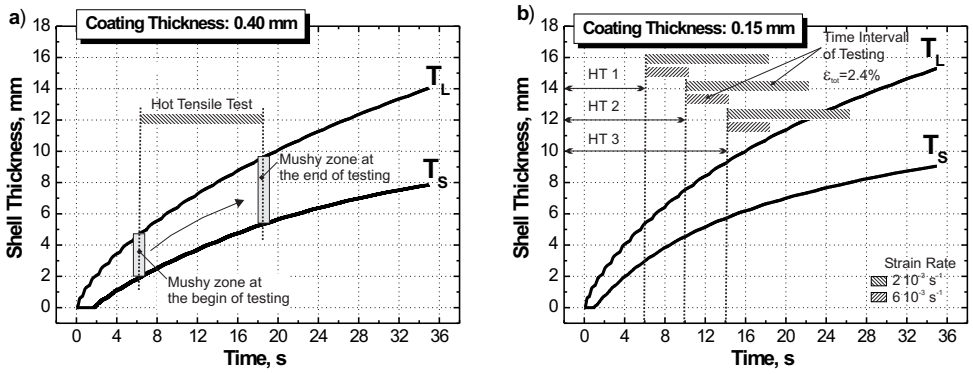

Figure 8.1: *Calculated shell thickness as a function of time for two different coating thicknesses.*

The result of the thermal analysis is the shell growth as a function of solidification time during the SSCT-test (see Fig. 7.3). This is an important requirement for the coming accurate hot tearing analysis. Two examples of the calculated shell growth as a function of solidification time are illustrated in Fig. 8.1 for two different cooling rates. These calculations were carried out by applying an average time-dependent heat flux density and an average initial steel bath temperature of the different experiments illustrated in Tab. B.1. These diagrams are only used in the following to explain the different testing conditions for the different testing parameters. For the detailed consideration of every experiment a careful analysis – as illustrated in the section *Thermal Analysis* – is applied.

When comparing the two diagrams, it can be seen that the higher cooling rate ($s_{coat} = 0.15\ mm$) results in a higher time-dependent shell thickness. Furthermore, the different holding times are illustrated, resulting in different shell thicknesses at the beginning of testing. According to the two different strain rates and the constant total strain of 2.4 %, the time interval of testing is 4 and 12 s, respectively. This is also illustrated in the figures by means of different hatched rectangles. The position of the deformed (strained) mushy zone changes with solidification time and testing conditions (holding time, strain rate and cooling rate). Considering, for example, the lower cooling rate ($s_{coat} = 0.40\ mm$), the shortest holding time and the lower strain rate, Fig. 8.1a shows that the position of the strained mushy zone moves during testing. The position of the mushy zone

during the straining process plays an important role as will be seen also later in the present thesis. The results of the thermal analysis (shell thickness vs. solidification time) for every experiment of *test series A* are summarised in Appendix B. Furthermore, the comparison of the calculated and measured shell thickness is illustrated in Fig. B.10 in Appendix B. The good correspondence of the calculated and measured shell thickness is apparent and is an important requirement for further investigations.

First of all it is necessary to clarify whether the SSCT-test represents an appropriate tool to investigate hot tearing and whether it is possible to generate hot tears within the mushy zone. In order to answer these questions, the position of hot tears within the solidified steel shell was determined as described in Section 7.3. The grey bars in Fig. 8.2a show the position of the mushy zone during the hot tensile test as described above for a strain rate of $2 \cdot 10^{-3}\ s^{-1}$ (deformation rate: 0.1 mm/s) and the different testing parameters of holding time and cooling rate. In addition, the minimum/maximum position from the interface of the determined hot tears is illustrated. It can clearly be seen that the position of the occurring hot tears is situated within the mushy zone during testing. Moreover, the occurrence of hot tears can further be narrowed within the mushy zone. The illustrated range (minimum/maxium value) of the determined hot tears in Fig. 8.2a requires a closer examination. Therefore, Fig. 8.2b shows an example for the distribution of the number of hot tears* for steel A01 ($s_{coat} = 0.40\ mm$ and $HT = 4\ s$) and A06 ($s_{coat} = 0.15\ mm$ and $HT = 12\ s$), respectively. Fig. 8.2b shows a typically trend of the detected number of hot tears with a maximum of detected hot tears at a certain position from the interface.

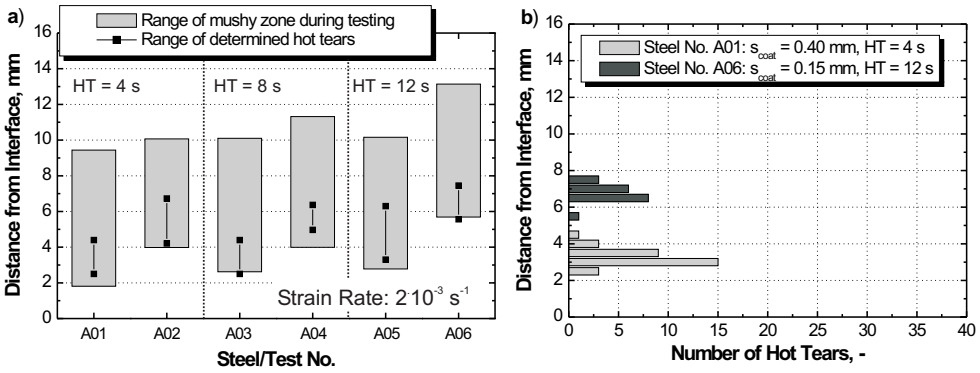

Figure 8.2: *a) Range of mushy zone during tensile testing together with the position of the detected hot tears within the solidified shell and b) the distribution of the number of hot tears at defined distances from the chill-shell interface for a strain rate of* $2 \cdot 10^{-3}\ s^{-1}$.

Fig. 8.3a shows the same situation for a strain rate of $6 \cdot 10^{-3}\ s^{-1}$ (deformation rate: 0.3 mm/s). Similar to the results of the lower strain rate, the range of the detected hot tears lies within the position of the mushy zone during testing. However, it can be seen that the minimum position of the generated hot tears lies slightly below the position of the mushy zone at the beginning of

*Please note that this distribution only refers to the starting point – by means of the measured DfI – of the detected hot tears.

testing. The results of the holding time of 4 s are not considered because of a fully disrupted shell at both cooling rates. Fig. 8.3b again shows the distribution of the number of hot tears. The trend is similar as the trend obtained by a strain rate of $2 \cdot 10^{-3}$ s^{-1} with a clear maximum of the detected number of hot tears in a certain position from the interface.

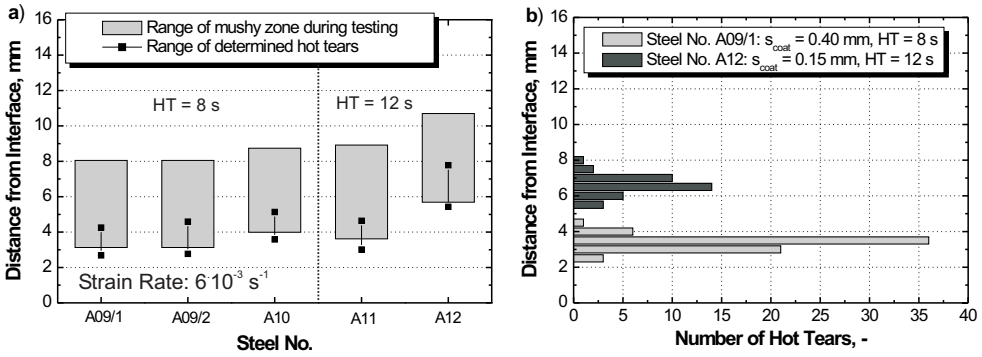

Figure 8.3: *a) Range of mushy zone during tensile testing together with the position of the detected hot tears within the solidified shell and b) the distribution of the number of hot tears at defined distances from the chill-shell interface for a strain rate of* $6 \cdot 10^{-3}$ s^{-1}.

The determined distribution of the number of hot tears for every test illustrated above is summarised in Appendix B. It can be seen from these figures that the obtained characteristics can be approximated using a Gauss fit. Thus, the essential information regarding these investigations can be summarised as follows. The results show that the SSCT-test can generate hot tears within a certain range of the mushy zone during solidification. Applying different testing conditions, especially different cooling rates, leads to different positions of the strained mushy zone. The position of the detected hot tears corresponds very well to the position of the mushy zone in all cases. Furthermore, the investigated steels show a uniform trend regarding the distribution of the number of hot tears within the solidified shell.

Apart from the number of hot tears and the corresponding position from the interface, also the length of the hot tears and the average tear length were determined (see Section *Metallographic Analysis*). The results of these investigations are listed in Tab. B.3 (see Appendix B) together with the corresponding standard deviation and the parameters centre and width resulting from the Gauss fit.

The results of the number of hot tears, length of hot tears and the average tear length together with the standard deviation resulting from a total strain of 2.4 % are illustrated in the following figures. Fig. 8.4 shows the results of the number of hot tears for the two different strain rates. From Fig. 8.4a it can be concluded that a higher cooling rate ($s_{coat} = 0.15$ mm) results in a smaller number of hot tears in all cases. The different applied holding times show no effect on this parameter. Contrary to the higher cooling rate, the number of hot tears tends to augment with increasing holding time at the lower cooling rate ($s_{coat} = 0.40$ mm). Applying the higher strain rate of $6 \cdot 10^{-3}$ s^{-1} (Fig. 8.4b) basically results in higher values for the number of hot tears at both

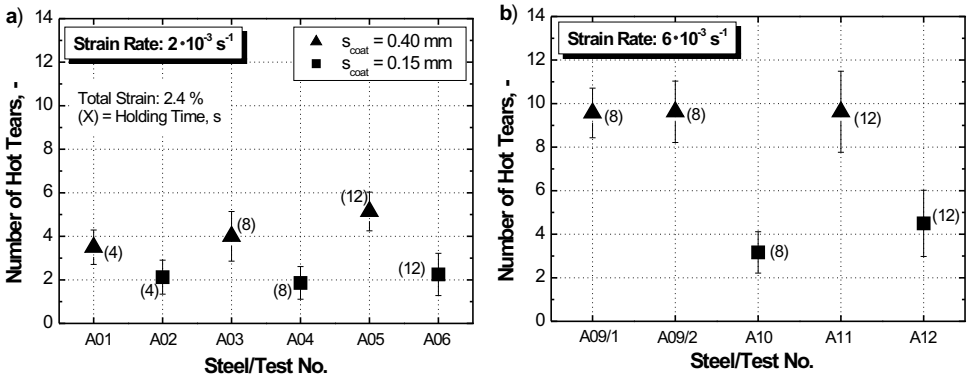

Figure 8.4: *Detected number of hot tears for the tested construction steel under different testing conditions (holding time and cooling rate) for a strain rate of a)* $2 \cdot 10^{-3}\ s^{-1}$ *and b)* $6 \cdot 10^{-3}\ s^{-1}$.

lower and higher cooling rates. Considering the lower cooling rate, no influence of the holding time can be observed. However, increasing the holding time at the higher cooling rate leads to a higher number of hot tears.

The same situation is illustrated in Fig. 8.5 for the experimentally determined length of hot tears for the two different strain rates. Considering the results of the lower strain rate, illustrated in Fig. 8.5a, the same tendency as found for the number of hot tears can be seen. With increasing holding time the values of the length of hot tears tends to increases for the lower cooling rate. At the higher cooling rate clearly smaller values are determined, showing no influence with increasing holding time. At the higher strain rate (see Fig. 8.5b), a slight increase of the length of hot tears can be seen at both the lower and higher cooling rates. Compared to the number of hot tears, it is interesting to note that the higher strain rate results only in a minor increase of the length of hot tears.

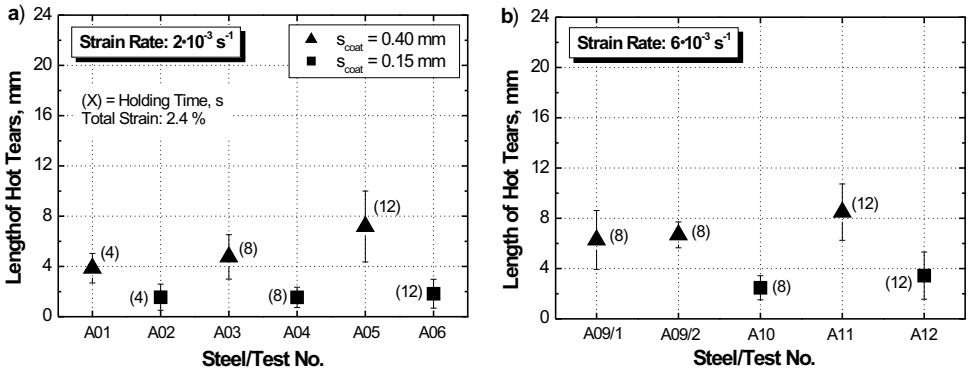

Figure 8.5: *Detected length of hot tears for the tested construction steel under different testing conditions (holding time and cooling rate) for a strain rate of a)* $2 \cdot 10^{-3}\ s^{-1}$ *and b)* $6 \cdot 10^{-3}\ s^{-1}$.

A further parameter resulting from the metallographic analysis is the average tear length. This parameter is the mean value of all detected hot tears of the investigated micrographs (generally eight micrographs per experiment). The determined values are illustrated in Fig. 8.6a for the lower cooling rate and in Fig. 8.6b for the higher cooling rate. Considering the lower cooling rate, it can be seen that the higher strain rate leads to shorter hot tears. The average tear length tends to increase with higher holding times. However, with respect to the high cooling rate, the measured values of the average tear length remain constant, independent of holding time and strain rate.

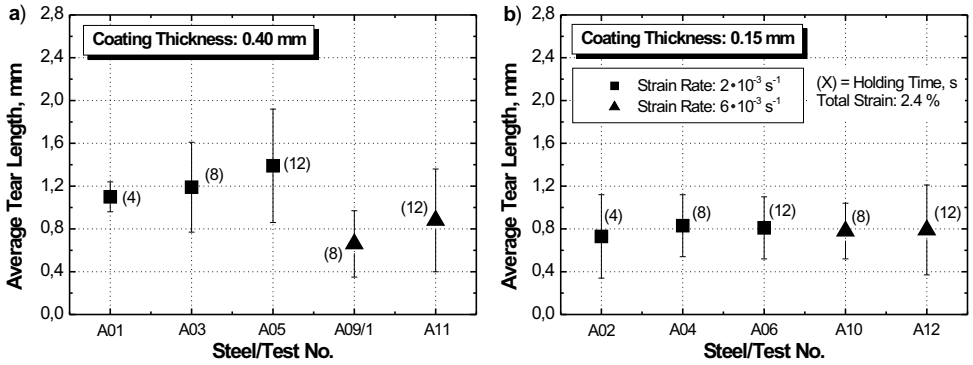

Figure 8.6: *Detected average tear length for the tested construction steel under different testing conditions (holding time and strain rate) for a) the lower cooling rate ($s_{coat} = 0.40\ mm$) and b) for the higher cooling rate ($s_{coat} = 0.15\ mm$).*

Tab. 8.1 summarises the influence of strain rate, cooling rate and holding on the results of the experimentally determined parameters of the number of hot tears, length of hot tears and the average tear length. Both the strain rate and the cooling rate show a significant influence in view of the number of hot tears. A higher cooling rate reduces the number of hot tears, whereas a higher strain rate increases the number of hot tears. This also applies for the length of hot tears. However, the effect of the strain rate on the length of hot tears is much smaller. The average tear length decreases with increasing strain rate at the lower cooling rate, but shows no effect on this parameter at the higher cooling rate. Generally, an increasing holding time augments the values of all three determined parameters. An exception are the measured numbers of hot tears at the higher strain rate in conjunction with the lower cooling rate and the entire values of the average tear length at the higher cooling rate.

Parameter	Number of Hot Tears	Length of Hot Tears	Average Tear Length
Strain Rate	↑	–	↓–
Cooling Rate	↓	↓	↓–
Holding Time	↑–	↑–	↑–

Table 8.1: *Effect of strain rate, cooling rate and holding time on the experimentally determined parameters (↑ increase, ↓ decrease and – no influence).*

It can be concluded that the strain rate and cooling rate show the expected effect on hot tearing and corresponds with the literature. However, an increasing number and length of hot tears as well as a slight increase of the average tear length, especially at the lower cooling rate, was measured although the total strain was held constant. Due to the formation of hot tears within the mushy zone during solidification the holding time should not affect the hot tearing susceptibility. Therefore, these finding are of particular interest and will be discussed later.

Test series A was also carried out to provide results for the validation of a fully coupled, thermal-stress analysis using the software package ABAQUS[153] and a decoupled thermal and mechanical analysis using the software package COMSOL Multiphysics[154]. The goal of these simulations was to evaluate the stress and strain distribution within the test specimen and furthermore, to improve the general understanding of the SSCT-test. However, this is not part of the present thesis, more information on this is provided in the literature[1,155,156].

After these investigations using different testing conditions on a constant chemical composition (construction steel), the influence of the carbon content on hot tearing was examined. The next section illustrates the results of seven test series (*test series B - test series H*), the individual test series were performed with different carbon contents.

8.2 Metallographic Results of Hot Tearing of Different Carbon Steels

In order to investigate the influence of carbon, all other alloying elements (Si, Mn, P and S) were held constant with contents equal to a typical construction steel ($0.20-0.40$ $wt.\text{-}\%Si$, $1.30-1.50$ $wt.\text{-}\%Mn$, ~ 0.007 $wt.\text{-}\%P$ and ~ 0.007 $wt.\text{-}\%S$). The different carbon contents was 0.05, 0.08, 0.12, 0.16, 0.30, 0.50 and 0.70 $wt.\text{-}\%C$, the coating thickness was 0.40 mm (lower cooling rate according to a slab caster) and the holding time was defined as 16 s. The as-is analysis of all conducted experiments and the corresponding initial steel bath temperature are listed in Appendix B (see Tab. B.2) together with the applied total strain and strain rates. The summary of the testing parameters from the test series and the calculated liquidus and solidus temperatures are illustrated in Tab. 8.2

A very important result of the Finite Element (FE) calculations regarding stress and strain distribution within the solidifying steel shell and of the *test series A* was that the hazard of a disrupted steel shell decreases with increasing holding time. The reason can be explained by a higher shell thickness at the beginning of testing. Therefore, the experiments presented in the following section refer to a holding time of 16 s in all cases. The previous section described an increasing hot tearing tendency with increasing holding time. This fact is not neglected in the following section, but the reason for the slight increase of hot tearing with increasing holding time will be discussed later in conjunction with the model of an accumulated strain.

As already mentioned, is the thermal calculation the first step in analysing the experiments (see Section 7.2). The results of these calculations – the shell growth (shell thickness vs. solidification time) – are summarised in Appendix B. Fig. B.10 in Appendix B shows the comparison of calculated

		Testing Parameters			*Microsegregation Analysis*	
Test Series	C	Deformation Rate	HT	s_{coat}	T_L	T_S
B	0.05	0.1/0.3/0.6	16	0.40	1522	1491
C	0.08	0.1/0.3	16	0.40	1520	1475
D	0.12	0.1/0.3	16	0.40	1516	1453
E	0.16	0.1	16	0.40	1513	1441
F	0.30	0.1	16	0.40	1501	1407
G	0.50	0.1	16	0.40	1486	1363
H	0.70	0.1	16	0.40	1473	1321

Table 8.2: *Indication of test series with corresponding carbon content(in wt.-%), applied deformation rates (in mm/s), holding time (HT, s) and coating thickness (s_{coat}, mm) as well as liquidus (T_L) and solidus (T_S) temperature (in* ℃*) resulting from microsegregation analysis.*

and measured shell thickness of all conducted test series. Again, the calculated shell thickness corresponds to a solid fraction of 0.2. The diagrams in Fig. B.10 show that this value of f_S results in a very good correlation between measured and calculated shell thickness.

A further important calculation is the microsegregation analysis, which was carried out adopting the microsegregation model proposed by Ueshima *et al.*[54] (see Appendix A). Fig. 8.7 shows the results of these calculations for the tested steel grades containing different carbon contents. In addition, the resulting liquidus and solidus temperatures are illustrated. From these figures it follows that the 0.05 and 0.08 $wt.\text{-}\%C$ steels solidify in the δ-Fe phase. The solidification range ΔT_{LS} is 31 ℃ and 42 ℃, respectively. As expected, the tested steel grades containing 0.12, 0.16 and 0.30 $wt.\text{-}\%C$ show a δ-γ transformation during solidification. Regarding the occurrence of the δ-γ transformation the following conclusions can be drawn from the microsegregation analysis. The δ-γ transformation of the 0.12 $wt.\text{-}\%C$ steel starts at a temperature of 1483 ℃, which corresponds to a solid fraction of approximately 0.9. The end of the transformation coincides with the solidus temperature, which results in a temperature range ($\Delta T_{\delta-\gamma}$) of 30 ℃. Considering the 0.16 $wt.\text{-}\%C$, it follows that the δ-γ transformation starts at a solid fraction of approximately 0.79 and is finished at 0.98. Hence, the temperature range $\Delta T_{\delta-\gamma}$ is 19 ℃, which is clearly lower compared to the 0.12 $wt.\text{-}\%C$ steel. The δ-γ transformation of the 0.30 $wt.\text{-}\%C$ steel already occurs at a very early stage during solidification ($f_S = 0.42$). As can be seen from Fig. 8.7e, the transformation takes place in a rather small temperature range of $T_{\delta-\gamma} = 3$ ℃. Finally, the 0.50 and 0.70 $wt.\text{-}\%$ carbon steel show pure austenitic solidification, with values of ΔT_{LS} of 123 ℃ and 153 ℃, respectively.

The results of these calculations in conjunction with the thermal analysis lead to the shell growth of the different tested steels. Evidently, the determined solidus temperature plays an important role. However, the validation of this temperature is still a great challenge. One possibility is the comparison of the calculated solidus temperature to the measured zero ductility temperature from hot tensile tests. As illustrated in Chapter 2, this parameter corresponds to a solid fraction of 0.99 or 1 according to the literature. In order to review the applied microsegregation model major effort was taken to compare values from literature to corresponding calculated values[157].

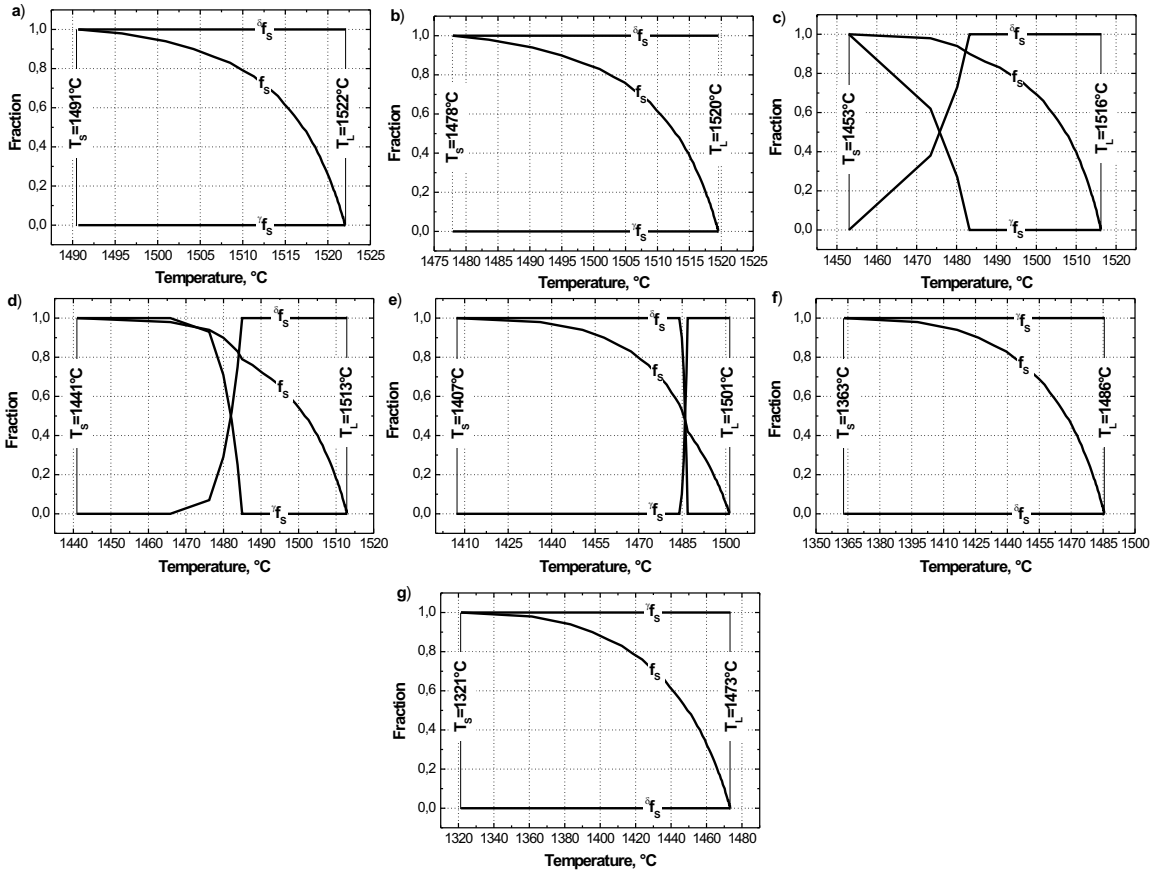

Figure 8.7: *Calculated solid fraction, δ-Fe fraction in the solid phase and γ-Fe fraction in the solid phase as a function of temperature at carbon contents of a) 0.05, b) 0.08, c) 0.12, d) 0.16, e) 0.30, f) 0.50 and g) 0.70 wt.-%.*

8.2.1 Position of Detected Hot Tears

Section 8.1 already pointed out the importance of the position of the detected hot tears. In this section, the results of the different test series will be illustrated. Fig. 8.8 summarises the results of these investigations.

The investigation of the 0.05 *wt.-%C* steel includes five tests (*test series B*). The determined values of the number and length of hot tears and the average tear length are listed in Tab. B.4. As can be seen in this table, applying a strain rate of $2 \cdot 10^{-3}$ s^{-1} and a total strain of 2 and 3 % (B01 and B02) results in no hot tearing. Therefore, Fig. 8.8a only considers the test with the higher strain rates (B03 – B05). The range of generated hot tears tends to agree with the position of the mushy zone during testing. However, the minimum position of detected hot tears lies below the mushy zone during straining. In comparison to the results of the construction steel, this phenomenon also appears at the higher strain rate (see Fig. 8.3) but not at a strain rate of $2 \cdot 10^{-3}$ s^{-1}. Please note that the illustrated distance from the interface of the determined hot tears (black rectangles) represents the minimum and maximum values. The detailed distribution within

the shell in view of the number of hot tears for all experiments of *test series B* to *H* is summarised in Appendix B.

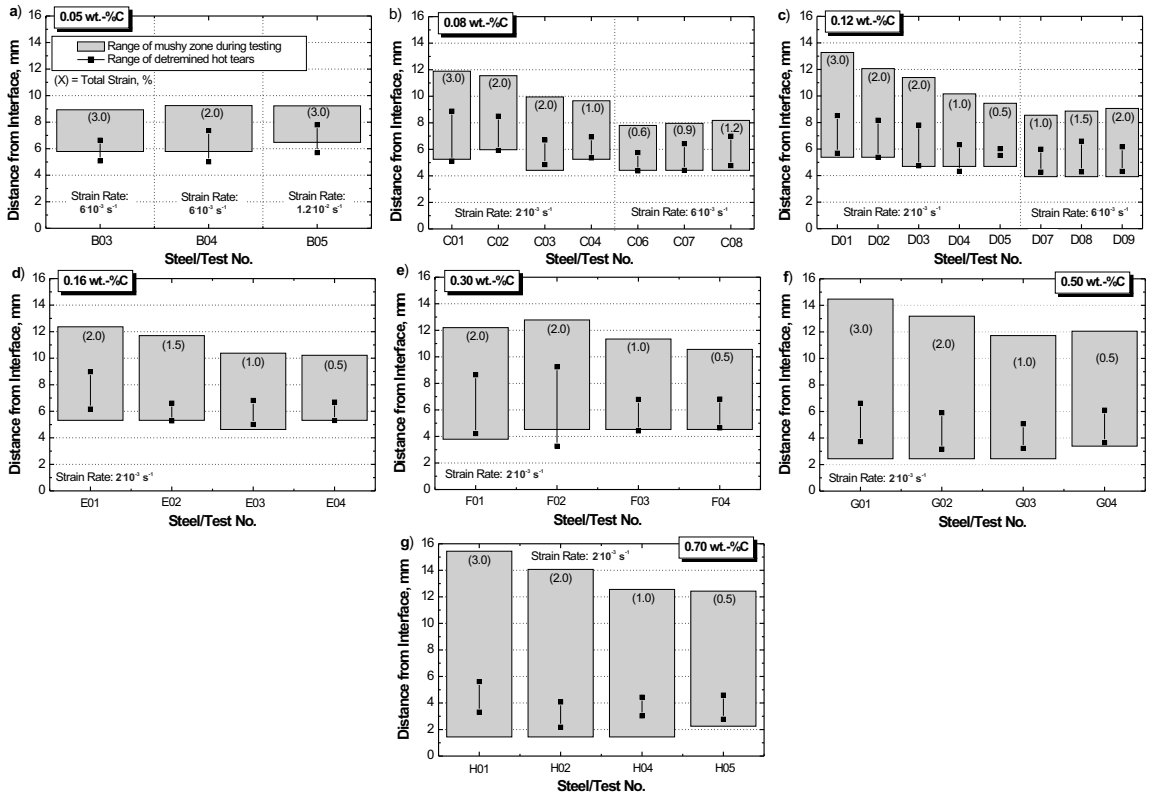

Figure 8.8: *Range of mushy zone during tensile testing together with the position of the detected hot tears within the solidified shell for test series B – H.*

In order to investigate the 0.08 and 0.12 *wt.-%C* steel (*test series C* and *D*), two different strain rates were applied. The experiments with the higher strain rate were conducted to determine the range of preferred strain accumulation according to the presented model in Chapter 6. The detailed consideration will be done in a subsequent section, however, the results are already included in Fig. 8.8b and c. The detected hot tears of all experiments are within the mushy zone during testing, and they are generally situated in the lower half of the mushy zone. Contrary to the higher strain rates of *test series B*, the position of the detected hot tears of these two test series at the higher strain rate are also within the mushy zone.

Fig. 8.8d to Fig. 8.8g again show the range of the detected hot tears within the shell in terms of the distance from the interface. It can clearly be seen that the generated hot tears are within the range of the mushy zone during testing. This applies for all tested steels except for steel F02, where the minimum value is below the mushy zone. As previously discussed, the hot tears tend to occur at higher amounts of solid fractions. The detailed characteristics of the distribution of the number of hot tears is of particular interest. These results are summarised in Appendix B (Fig. B.13 to Fig. B.19). Considering these figures a general tendency of the number of hot tears

as a function of the distance from the interface can be observed. At a certain distance from the interface a maximum of the number of hot tears are detected. Fitting this trend using a Gauss model, this distance can be determined in terms of the Gaussian mean (GM). This parameter is summarised in Tab. B.4.

It can be concluded that the detected hot tears within the micrograph can be clearly related to the position of the mushy zone during testing. Moreover, the range of the occurring hot tears can further be narrowed within the mushy zone. The detailed consideration of this fact takes place later in conjunction with the determination of a preferable range of strain accumulation. A further interesting result is the trend of the tear distribution.

Apart from the evaluation of the position of the hot tears, the number and length of hot tears as well as the average tear length are measured for every experiment. The summary of these investigations can also be found in Appendix B.

8.2.2 Number of Hot Tears

The diagrams in Fig. 8.9 show the results of the number of detected hot tears per micrograph with the corresponding standard deviation for all experiments investigating the influence of carbon content. The aim of this investigation is the determination of hot tearing sensitivity as a function of strain and the carbon content. Furthermore, the presented model will be applied to the results. First of all, only the measured values resulting from the metallographic analysis are presented.

Fig. 8.9a shows the detected number of hot tears as a function of the total applied strain (2 and 3 %) and the strain rate for the 0.05 $wt.$-%C steel. A strain rate of $2 \cdot 10^{-3}$ s^{-1} does not cause any tear formation. Applying a higher strain rate of $6 \cdot 10^{-3}$ s^{-1} results in the values illustrated in Fig. 8.9a. These values increase with increasing total strain. However, increasing the strain rate once more ($12 \cdot 10^{-3}$ s^{-1}) does not lead to an increase of the number of hot tears (see B05 and B04 at a total strain of 3 %).

At the *test series* C and D (0.08 and 0.12 $wt.$-%C) two different strain rates were investigated. The purpose of testing a strain rate of $6 \cdot 10^{-3}$ s^{-1} is the determination of the range of preferred strain accumulation within the mushy zone. Considering Fig. 8.9b it can be seen that steel C05 does not feature an applied total strain. The experiments without external deformation (straining) were carried out for 0.08, 0.12, 0.16, 0.30, 0.50 and 0.70 $wt.$-%C. Since the 0.05 $wt.$-%C steel showed no hot tearing at total strains of 2 and 3 %, this steel grade was not tested without straining. The reason for investigating no external load (strain) lies in the specific conditions of the SSCT-test. Because of the hindered shrinkage during the total test, the question arises if the material specific contraction (shrinkage) can already lead to hot tearing. Hence, tests without straining the solidifying steel were additionally carried out in order to consider only the effect of steel shrinkage on hot tearing. The results of the 0.08 $wt.$-%C steel can be summarised as follows. An increasing total strain results in an increase of the number of hot tears at both strain rates. When conducting the experiment without tensile testing (C05), no hot tearing takes place. Further, the higher strain rate changes the increase of number of hot tears to lower values of the total strain. Generally, this

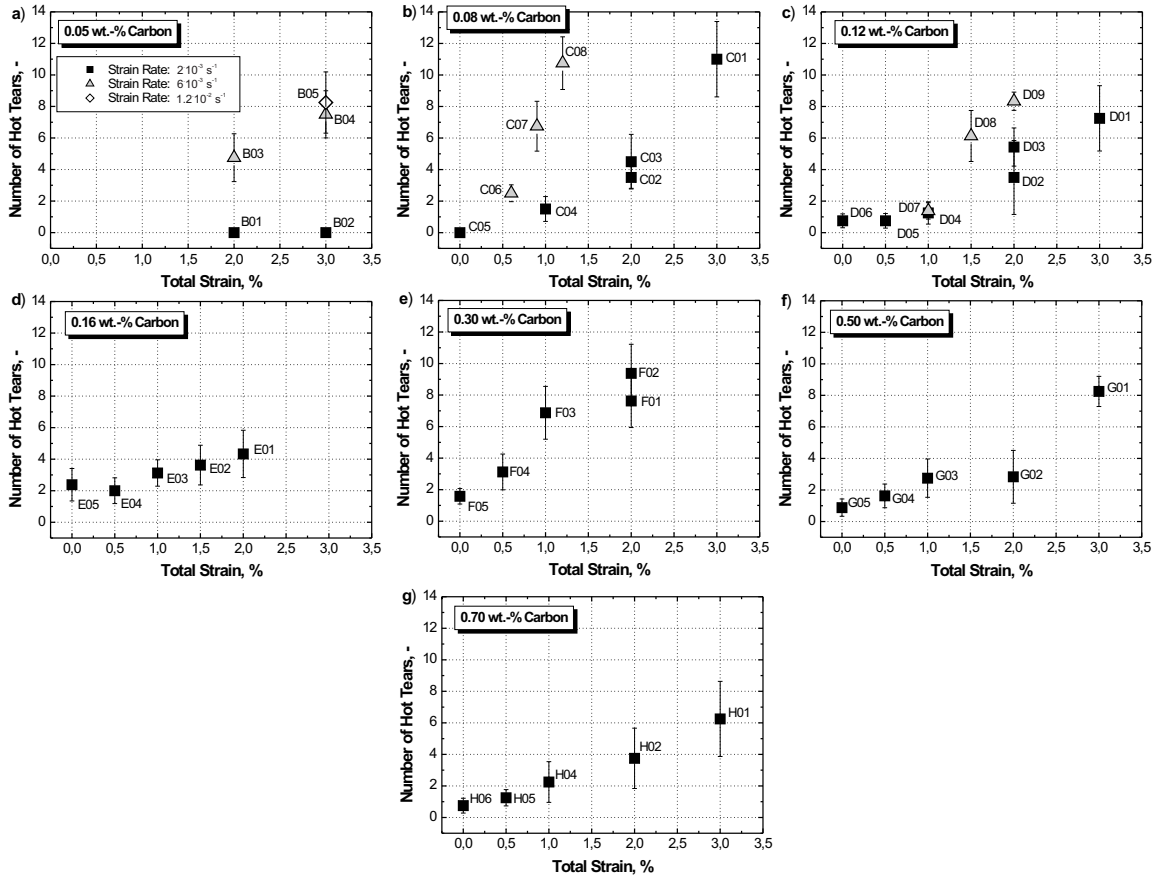

Figure 8.9: *Number of hot tears as a function of applied total strain for the a) 0.05 wt.-%, b) 0.08 wt.-%, c) 0.12 wt.-%, d) 0.16 wt.-%, e) 0.30 wt.-%, f) 0.50 wt.-% and g) 0.70 wt.-% carbon steels.*

behaviour can also be observed at the 0.12 $wt.\text{-}\%C$ steel, which is illustrated in Fig. 8.9c. Contrary to the 0.08 $wt.\text{-}\%C$ steel, which shows only a δ-Fe solidification (see Fig. 8.7b and c), a small number of hot tears is determined at the experiment without straining (D06). The measured values of the number of hot tears at a total strain of 0.0 and 0.5 % are nearly identical. The detection of the number of hot tears of approximately one per micrograph lies within the scatter band of the metallographic analysis. A further point of interest regarding the results of the 0.12 $wt.\text{-}\%C$ steel concerns the detected number of hot tears applying two different strain rates at a total strain of 2 % (D03/D02 and D09) and 1 % (D04 and D07). It can be seen that the higher strain rate leads to a higher number of hot tears at a total strain of 2 %. However, at a total strain of 1 %, the results of the number of hot tears are nearly identical at these two strain rates. The *test series C* and *D* include two experiments applying the same testing parameters (C03/C02 and D02/D03). From both test series it follows that the values of the number of hot tears lie within the range of the standard deviation and show a good reproducibility.

The steels containing 0.16, 0.30, 0.50 and 0.70 $wt.\text{-}\%C$ were investigated applying only a strain rate of $2 \cdot 10^{-3}\ s^{-1}$. The diagrams in Fig. 8.9 illustrate that the 0.16 $wt.\text{-}\%C$ steel already shows an observable degree of hot tearing at the experiment without straining (E05), but a relatively small increase of the number of hot tears with increasing total strain. In addition, the 0.30 $wt.\text{-}\%C$ steel shows hot tearing merely due to shrinkage during solidification (F05). However, contrary to the 0.16 $wt.\text{-}\%C$, the number of hot tears considerably increases with total strain. Finally, the results of the 0.50 and 0.70 $wt.\text{-}\%C$ steels are very similar, with a small value at the tests without straining and a more or less moderate increase of hot tears with increasing total strain.

8.2.3 Length of Hot Tears

In addition to the number of hot tears, the length of each detected tear within 8 micrographs is measured. The testing parameters of the results illustrated in Fig. 8.10 correspond to those of the previously illustrated results of the number of hot tears. The experiments containing 0.05, 0.08 and 0.12 $wt.\text{-}\%C$ were conducted applying different strain rates, whereas the 0.16, 0.30, 0.50 and 0.70 $wt.\text{-}\%C$ steels were tested at a strain rate of $2 \cdot 10^{-3}\ s^{-1}$.

Fig. 8.10 shows that the characteristics of the length of hot tears in all cases is very similar to the characteristics of the number of hot tears. Hence, the facts pointed out in the previous section also apply for the length of hot tears. With increasing total strain the length of hot tears increases for all tested steel grades. Generally, a higher strain rate results in an increasing hot tearing tendency. However, increasing the strain rate rate (B04, B05) shows no effect on hot tearing, neither on the number nor on the length of hot tears. Regarding the tests C03/C02 and D02/D03 clear reproducibility can be seen from Fig. 8.10b and Fig. 8.10c. Considering the tests F01/F02, it seems that steel F01 is a maverick.

8.2.4 Average Tear Length

The diagrams in Fig. 8.11 illustrate the measured values of the average tear length. Considering the results of the 0.05 $wt.\text{-}\%C$ steel (Fig. 8.11a), it can be observed that the detected hot tears nearly show the same value, independent of strain and strain rate. Regarding the 0.08 $wt.\text{-}\%C$ steel, the higher strain rate shows no effect on the average tear length with values approximately in the same range as steel C04 (lower strain rate). At the lower strain rate, this parameter tends to increase with increasing total strain. Additionally, the scatter band of the average tear length significantly increases with the total applied strain, demonstrating the higher variation of tear lengths at higher strains. Fig. 8.6 shows the results of the 0.12 $wt.\text{-}\%C$ steel. At both strain rates a slight increase with increasing total strain can be seen, whereas the average tear length of the higher strain rate shows lower values than those of the lower strain rate. The results of the remaining test series generally show the same trend, i.e. a slight increase with increasing total strain.

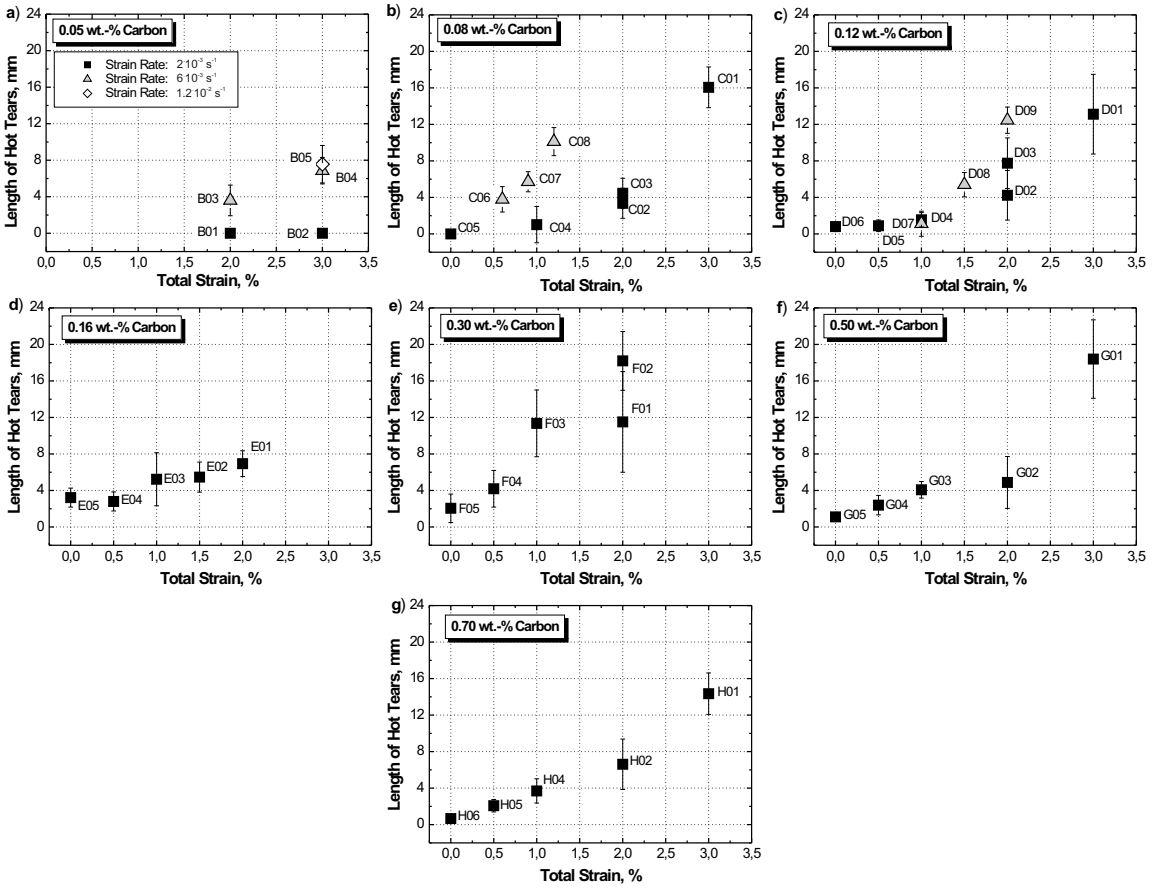

Figure 8.10: *Length of hot tears as a function of applied total strain for the a) 0.05 wt.-%, b) 0.08 wt.-%, c) 0.12 wt.-%, d) 0.16 wt.-%, e) 0.30 wt.-%, f) 0.50 wt.-% and g) 0.70 wt.-% carbon steels.*

8.3 The Effect of Carbon Content on the Hot Tearing Tendency

In the previous section, the results from the metallographic analysis were presented for each investigated carbon steel. In the following section, these results are illustrated as a function of the carbon content and the applied total strain to point out the measured hot tearing susceptibility in view of the number and length of hot tears and the average tear length.

The diagrams in Fig. 8.12 show the measured values of the number of hot tears for the experiments applying no external strain (total applied strain = 0.0 %) and the results applying 0.5, 1.0 and 2.0 % strain. The values of the 0.05 $wt.\text{-}\%C$ steel for 0.0, 0.5 and 1.0 % total applied strain have been assumed to be zero in all cases. Since no hot tears occurred during the experiments with 2 and 3 % total strain, this assumptions seems to be adequate. In addition, an average value is used in the figures for the experiments with the same testing conditions (e.g. C02 and C03).

Fig. 8.12 summarises the results of the number of hot tears as a function of carbon content. Considering the experiments without applying an external deformation (Fig. 8.12a), hot tearing is observed above a carbon content of 0.12 $wt.\text{-}\%$. At a carbon content of 0.16 $wt.\text{-}\%$, a maximum

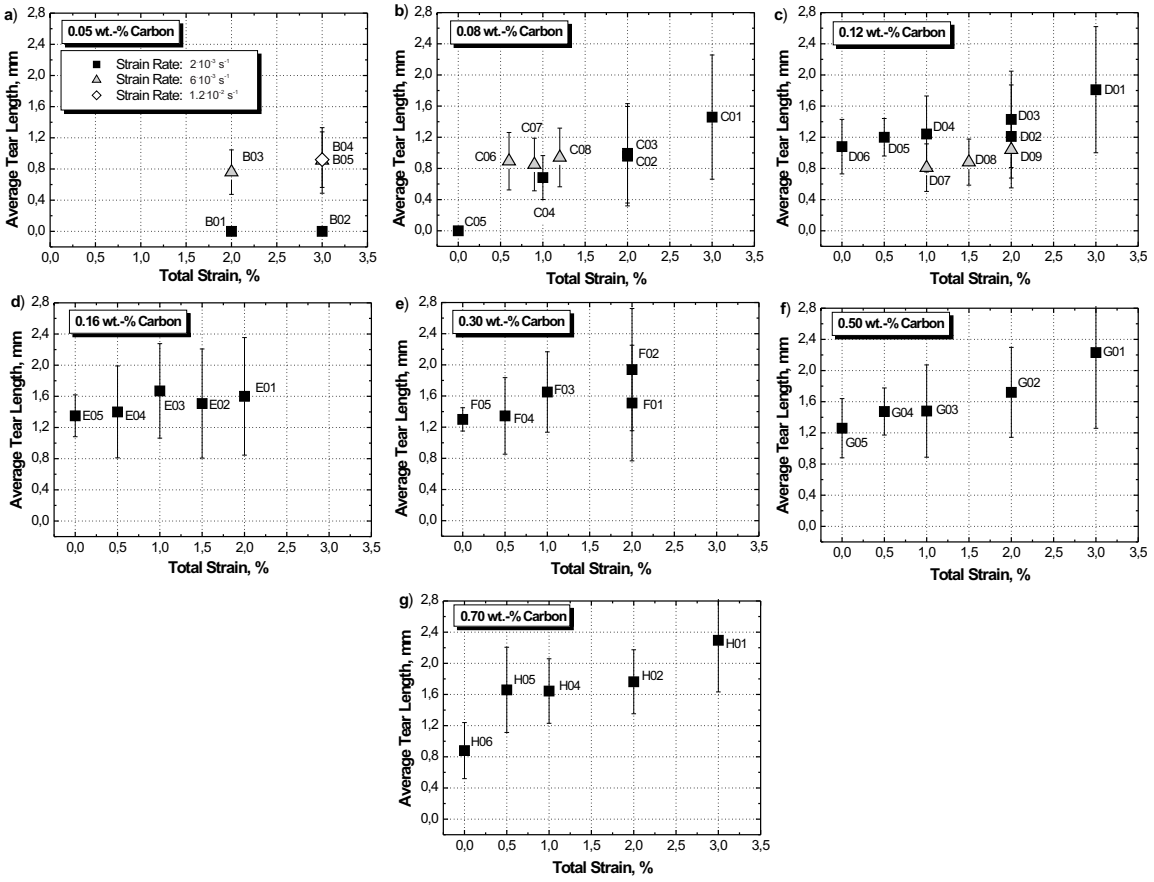

Figure 8.11: *Average tear length as a function of applied total strain for the a) 0.05 wt.-%, b) 0.08 wt.-%, c) 0.12 wt.-%, d) 0.16 wt.-%, e) 0.30 wt.-%, f) 0.50 wt.-% and g) 0.70 wt.-% carbon steels.*

of the number of hot tears is detected. After this maximum value the determined number of hot tears continuously decreases. Applying a total strain of 0.5 % slightly increases the number of hot tears. However, the maximum of the number of hot tears changes from a carbon content of 0.16 to 0.30 *wt.*-%.

These results in view of the number of hot tears can also be applied to the determined values of the length of hot tears, which are summarised in Fig. 8.13. If no tensile test is performed, a maximum value of the length of hot tears is determined at a carbon content of 0.16 *wt.*-%. At a total applied strain of 0.5, 1.0 and 2.0 %, the length of hot tears increases from 0.05 to 0.30 *wt.*-%C. A higher total strain results in a considerable trend of the maximum value at 0.30 *wt.*-%C. At a carbon content of 0.50 and 0.70 *wt.*-%C the length of hot tears decreases.

The results of the average tear length differ from the results of the number and length of hot tears. Considering the results of the different applied total strains, the average tear length as a function of carbon content shows a similar trend. An exception are the experiments without straining, where the values tend to decrease after reaching a maximum value at 0.16 *wt.*-%C. In all other cases (0.5, 1.0 and 2.0 % total strain), the carbon content shows no significant effect on the average tear length

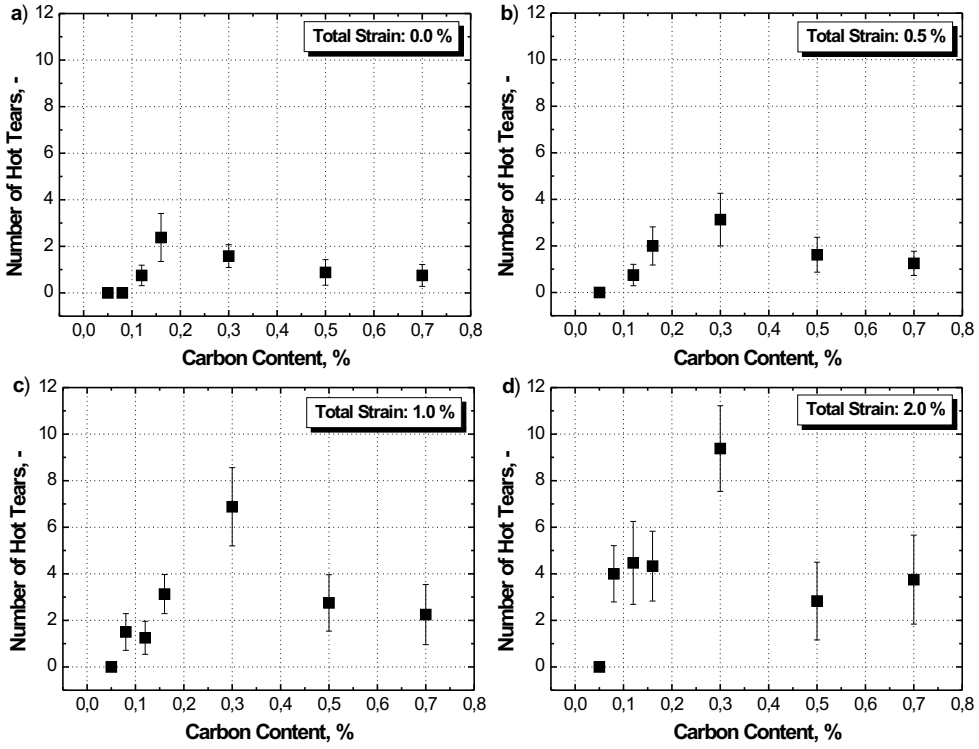

Figure 8.12: *Number of hot tears as a function of carbon content for a total strain of a) 0.0 %, b) 0.5 %, c) 1.0 % and d) 2.0 % (strain rate:* $2 \cdot 10^{-3}\ s^{-1}$*).*

at carbon contents greater than 0.16 *wt.*-%. However, up to this carbon content, the average tear length shows a considerable increase.

8.4 Determination of a Preferable Range of Strain Accumulation

The basic concept of accumulation of strain within a certain temperature range ($\Delta T_{SA} = T_A - T_S$) in the mushy zone is based on the assumption that there is a temperature T_A (solid fraction $f_{S,A}$, respectively) where the strain starts to accumulate. Thus, the amount of the effective strain ε_{eff} ($\varepsilon_{eff} = \varepsilon_{th} + \varepsilon_A$) strongly depends on this temperature range. The determination of $f_{S,A}$ is an important step and was carried out for the 0.08 and 0.12 *wt.*-%C steel. Considering the figures in the section *Position of Detected Hot Tears* (Fig. 8.8), the occurrence of hot tears can be approximately narrowed between $f_{S,A} > 0.9$ and $f_S = 1$. In order to determine $f_{S,A}$ in detail, the following considerations are made.

According to the definition of the effective strain, the thermal strain and the accumulated strain must be calculated within ΔT_{SA}. However, these calculations require the unknown parameter of the fraction of solid $f_{S,A}$. It is assumed that the strain rate affects only the magnitude of the effective strain. Therefore, Fig. 8.9b and Fig. 8.9c illustrate the number of hot tears for the 0.08

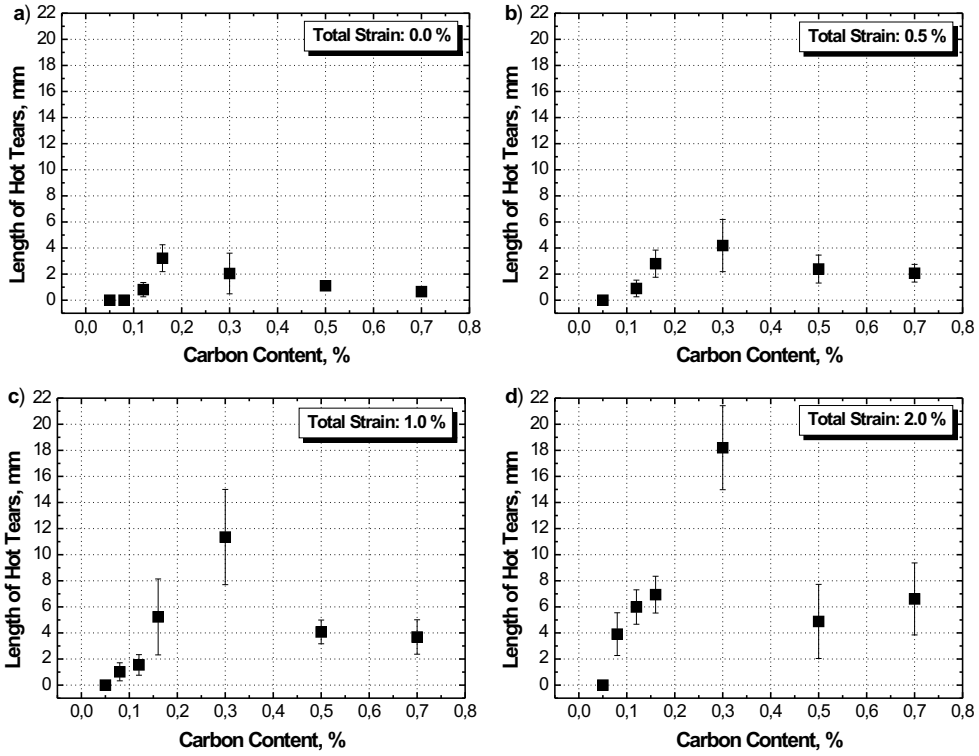

Figure 8.13: *Length of hot tears as a function of carbon content for a total strain of a) 0.0 %, b) 0.5 %, c) 1.0 % and d) 2.0 % (strain rate:* $2 \cdot 10^{-3}\ s^{-1}$*).*

and the 0.12 $wt.\text{-}\%C$ steel which were gained by various experiments and the variation of the total strain and two different strain rates. In these figures two different trends of the number of hot tears as a function of the total strain can be observed for a strain rate of $2 \cdot 10^{-3}$ and $6 \cdot 10^{-3}\ s^{-1}$, respectively. Determining the effective strain depending on f_S for all experiments should result in a uniform trend of the number of hot tears as a function of ε_{eff}. The reason for this is that the accumulated strain already considers the strain rate. The corresponding f_S is assumed to be $f_{S,A}$. The calculation of the effective strain is therefore done for different values of $f_{S,A}$ (0.8, 0.9, 0.93, 0.96 and 0.99), determining the thermal and accumulated strain.

The strain resulting from volume changes caused by both, temperature differences and phase transformation must be considered. The **thermal strain** is a direct result from the density ρ via the following equation[158]:

$$\varepsilon_{th}(T) = \sqrt[3]{\frac{\rho(T_0)}{\rho(T)}} - 1 \tag{8.1}$$

Using this equation it is essential to define the density for δ-Fe and γ-Fe as a function of temperature T and carbon content[159,160]:

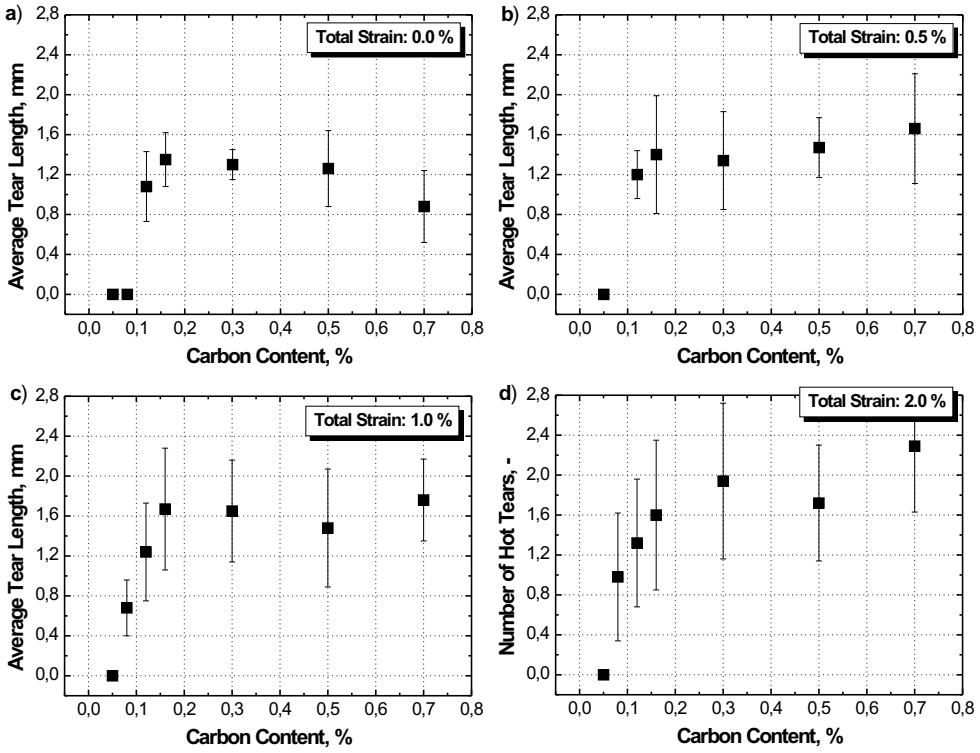

Figure 8.14: *Average tear length as a function of carbon content for a total strain of a) 0.0 %, b) 0.5 %, c) 1.0 % and d) 2.0 % (strain rate:* $2 \cdot 10^{-3}\ s^{-1}$*).*

$$\rho_\delta = (8010.71 - 0.4724 \cdot T) \cdot (1 + \frac{\%C}{100 - \%C}) \cdot (1 + 13.43 \cdot 10^{-3} \cdot \%C)^{-3} \tag{8.2}$$

$$\rho_\gamma = (8105.91 - 0.5091 \cdot T) \cdot (1 + \frac{\%C}{100 - \%C}) \cdot (1 + 8.317 \cdot 10^{-3} \cdot \%C)^{-3} \tag{8.3}$$

$$\rho_L = 7100 - 73 \cdot \%C - (0.8 - 0.09 \cdot \%C) \cdot (T - 1550) \tag{8.4}$$

A simple mixture rule can be used to determine the overall density from the values of the different phases ($^\delta f_S$, $^\gamma f_S$ and f_L):

$$\rho = \frac{1}{^\delta f_S/\rho_\delta + ^\gamma f_S/\rho_\gamma + f_L/\rho_L} \tag{8.5}$$

Based on the results of the microsegregation analysis (see Fig. 8.7), the thermal strain can be calculated for the 0.08 and 0.12 $wt.$-$\%C$ steel between $f_S = 1$ ($T_0 = T_S$) and different values of $f_{S,A}$ (0.8, 0.9, 0.93, 0.96 and 0.99). The results of these calculations - the thermal strain within a certain temperature range - are illustrated in Fig. 8.15.

Fig. 8.15 shows that the thermal strain increases with an increasing temperature range within the mushy zone (decreasing f_S). It can further be seen that the thermal strain of the 0.12 $wt.$-$\%C$ steel

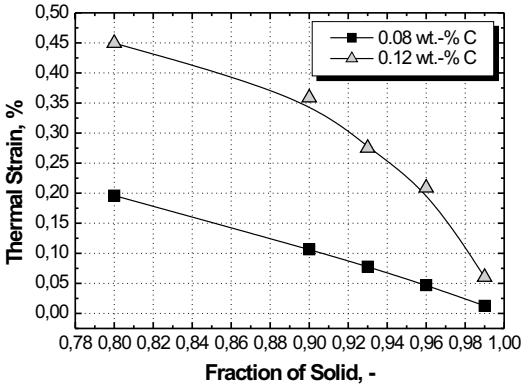

Figure 8.15: *Thermal strain as a function of f_s for the 0.08 and* 0.12 *wt.-%C steel.*

shows higher values due to higher values of ΔT_{SA} and particularly due to the δ-γ transformation during solidification.

The **accumulated strain** is determined directly from the results of the thermal analysis. This is illustrated in Fig. 8.16a for the 0.08 *wt.-%C* steel and a total applied strain of 2 % (Steel No. C02). According to the used strain rate ($2 \cdot 10^{-3}$ s^{-1}) the testing time is 10 s. Additionally, the certain temperature range of strain accumulation $\Delta T_{SA} = T_A(f_S = f_{S,A}) - T_S(f_S = 1)$ is illustrated. Due to the solidification process this results in an accumulated strain curve, which is illustrated in Fig. 8.16b for different values of $f_{S,A}$. With increasing values of $f_{S,A}$ (decreasing ΔT_{SA}) the accumulated strain decreases. The maximum values of the accumulated strain $\varepsilon_{A,max}$ for the different values of $f_{S,A}$ are found at the same position within the shell. Furthermore, the values of $\varepsilon_{A,max}$ are below the total strain of 2 % in all cases. Considering Fig. 8.16a at the beginning of the test, the first accumulating volume elements show values of f_S greater than $f_{S,A}$. Subsequently, volume elements reach $f_{S,A}$ due to the solidification progress and start to accumulate strain. At a certain position within the shell, these volume elements reach a maximum value ($\varepsilon_{A,max}$). This maximum value appears at the position where the final volume element can move from $f_{S,A}$ to $f_S = 1$ during straining.

Fig. 8.17 shows the values of the calculated maximum accumulated strain for the 0.08 (C02) and the 0.12 *wt.-%C* steel (D02). The curves are similar to that obtained for the thermal strain. With decreasing $f_{S,A}$ the values of $\varepsilon_{A,max}$ increase. The reason for the higher accumulated strain of the 0.12 *wt.-%C* steel is the wider ΔT_{SA}. The values of the maximum accumulated strain result from the thermal analysis of the experiments C02 and D02, respectively. Thus, the results also include the influence of the solidification conditions.

For the calculation of the effective strain, the maximum accumulated strain and the thermal strain must be determined as illustrated above. In doing so, the effective strain can be calculated for every conducted experiment of *test series C* and *D* (0.08 and 0.12 *wt.-%C*). However, the aim of this step is to determine $f_{S,A}$ by means of calculating ε_{eff} as a function of the different fraction

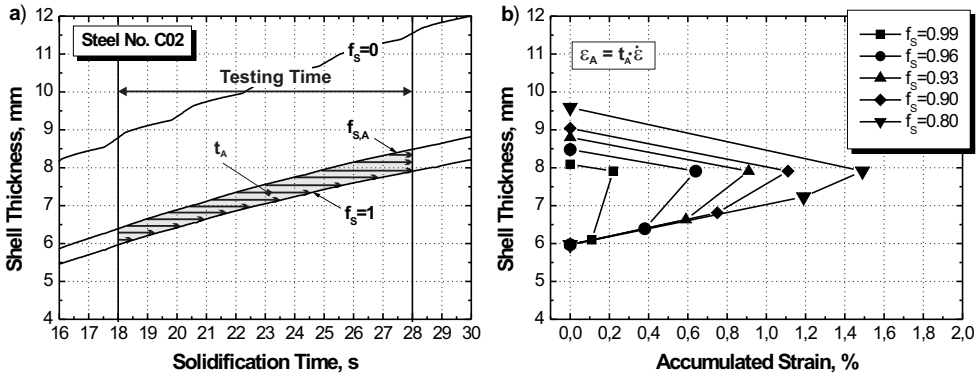

Figure 8.16: *a) Shell growth during testing together with a certain temperature range of strain accumulation and b) the resulting characteristic of the accumulated strain for different values of* $f_{S,A}$.

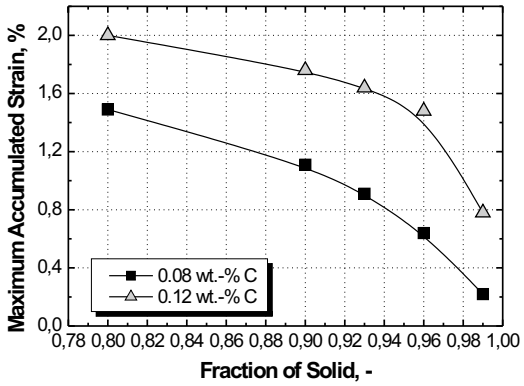

Figure 8.17: *Accumulated strain as a function of* f_s *for the 0.08 and* 0.12 *wt.-%C steel.*

of solids. As illustrated in Fig. 8.18, a solid fraction of 0.96 leads to a very good correlation of the detected number of hot tears as a function of effective strain at both steel grades.

The transparent squares represent the results of the lower strain rate ($2 \cdot 10^{-3}\ s^{-1}$) at the total applied strain. Due to the consideration of the accumulated strain within a certain part of the mushy zone, the effective strain clearly lies at lower values (black squares). Because of the higher strain rate ($6 \cdot 10^{-3}\ s^{-1}$), the accumulated strain corresponds to the total strain at these experiments. At both steel grades, the number of generated hot tears as a function of the effective strain lies on the same curve at a solid fraction of 0.96. According to the above made assumptions and considerations, the solid fraction at which strain accumulation within the mushy zone starts is $f_{S,A} = 0.96$. Hence, the range of a preferable strain accumulation is found between $\Delta T_{SA} = T_A(f_S = 0.96) - T_S(f_S = 1)$.

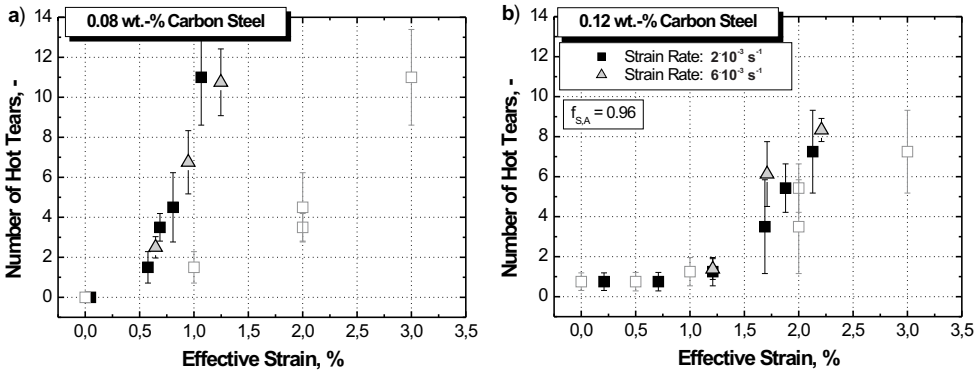

Figure 8.18: *Number of hot tears as a function of the effective strain for the 0.08 and* 0.12 *wt.-%C steel.*

8.5 Application of the Model and Discussion of the Results

In the previous section, the preferred range of strain accumulation was determined for the 0.08 and 0.12 $wt.\text{-}\%C$ steels. In a first assumption, this range is used for the calculation of the effective strain for all tested steels. The position of the detected hot tears within the mushy zone was already illustrated in Section 8.2.1 (see Fig. 8.8). In this figure the range of the determined hot tears is illustrated for minimum and maximum values of the distance from the interface. Fig. 8.19 corresponds to this illustration, the preferable range of strain accumulation is also highlighted. Contrary to Fig. 8.8 the position of the detected hot tears is displayed via the determined Gaussian mean and the standard deviation (see also Fig. B.11 - Fig. B.19 in Appendix B). From the diagrams in Fig. 8.19 it can clearly be seen that the position of the detected hot tears is within ΔT_{SA} – a very important result regarding the verification of this range.

Regarding the position of the detected hot tears within the steel shell (hot tear distribution) in conjunction with the curve of the accumulated strain, the following results can be observed. Fig. 8.20 shows the hot tear distribution together with the acting accumulated strain within ΔT_{SA} for the steel C01. In order to illustrate tendencies of the position of the appearing hot tears as a function of the carbon content, the parameter Δd_{HT} is defined, which is also illustrated in Fig. 8.20. This parameter represents the difference between the Gaussian mean from the hot tear distribution and the position of $\varepsilon_{A,max}$ ($d_2 = DfI(GM) - DfI(\varepsilon_{A,max})$).

In conjunction with the position of the maximum number of hot tears within the shell (Gaussian mean) it is investigated whether this position corresponds to the position of the maximum accumulated strain. For this purpose, the results of the determined parameter Δd_{HT} are summarised in Fig. 8.21. From the diagrams it can be seen that the position of the Gaussian mean coincides well with the arising maximum accumulated strain. Fig. 8.21b shows the results of Δd_{HT} in view of the mean value and standard deviation for the different carbon contents. The values increase from approximately -1.0 to $+1.0$ mm with increasing carbon content, the steels up to 0.12 $wt.\text{-}\%C$

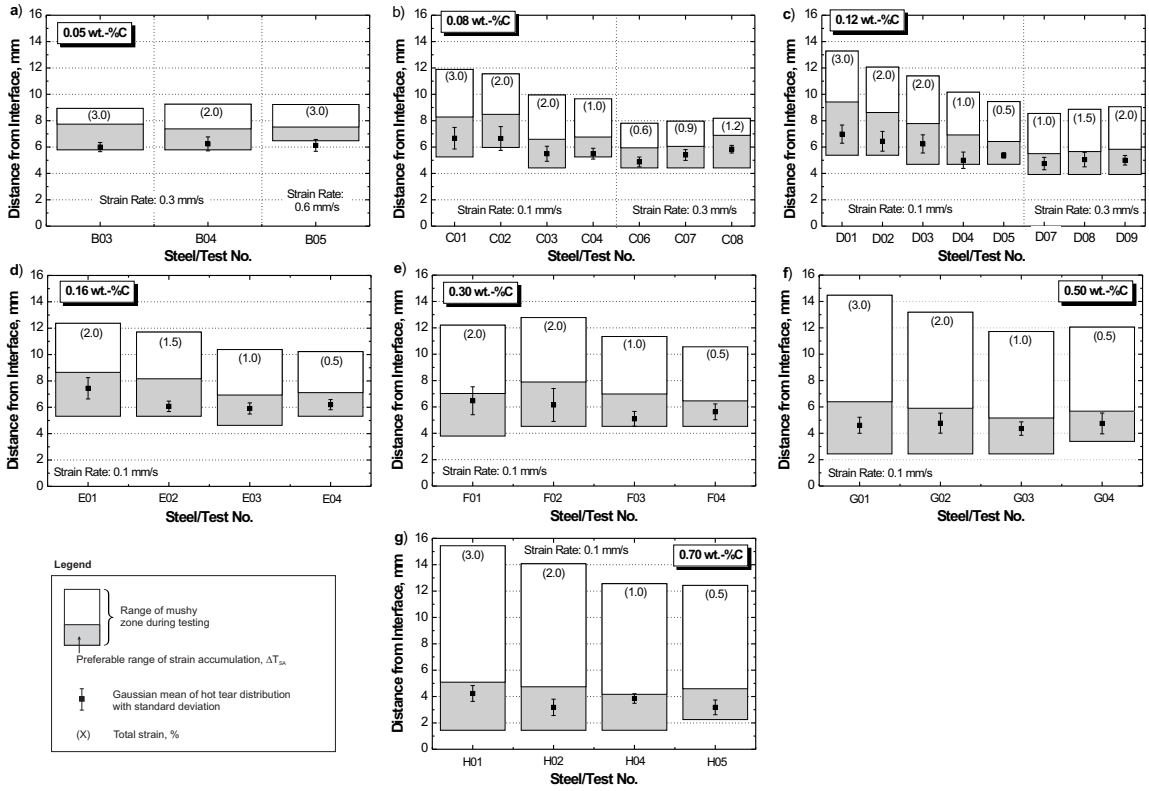

Figure 8.19: *Range of mushy zone during tensile testing, the preferable range of strain accumulation and the position of the detected hot tears in terms of the Gaussian mean and the standard deviation for test series B – H.*

show negative values and the steels above 0.16 $wt.\text{-}\%C$ have positive values. A possible explanation for this is given by the microsegregation analysis. As was shown in Fig. 8.16, the position of $\varepsilon_{A,max}$ does not change with different values of f_S. However, the position of this parameter changes with the curve of f_S as a function of temperature, which strongly depends on the microsegregation calculation and the used model parameters. Thus, it seems that the micosegregation analysis underestimates the segregation at lower carbon contents and overestimates it at higher carbon contents.

Nevertheless, it can be concluded that the determined preferred range of strain accumulation corresponds very well to the position of the detected hot tears within the steel shell for all tested steels. However, the determination of ΔT_{SA} is based on solidification calculations (thermal analysis) using the modified microsegregation model according to Ueshima *et al.*. Other microsegregation models may change the above illustrated results. Furthermore, only the carbon content was varied in the present study. Based on these facts the preferred range of strain accumulation is valid for a carbon content between 0.05 and 0.70 $wt.\text{-}\%$ and a constant chemical composition of 0.30 ± 0.04 $wt.\text{-}\%Si$, 1.30 ± 0.05 $wt.\text{-}\%Mn$, 0.006 ± 0.001 $wt.\text{-}\%P$ and 0.007 ± 0.001 $wt.\text{-}\%S$:

$$\Delta T_{SA} = T(f_S = 0.96) - T(f_S = 1) \tag{8.6}$$

Considering hot tearing, two features must be taken into account: first, the hot tearing sensitivity or susceptibility and second, the characteristic of tear growth/propagation. The former can be described by the number of hot tears and the latter by the average tear length. Following these considerations two extreme cases may occur. Few hot tears (low hot tearing sensitivity) showing high values of tear length (high tendency of tear propagation) or many hot tears (high hot tearing sensitivity) which are rather short (low tendency of tear propagation). Basically, few long cracks are more harmful than many short cracks. Depending on the definition of a crack index† or on the quality demands on the final cast product both, the number of hot tears as well as the average tear length have to be considered.

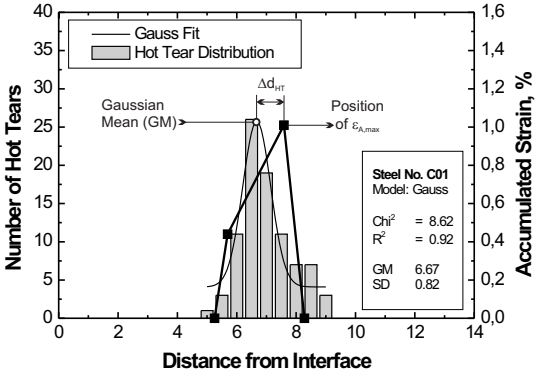

Figure 8.20: *Distribution of hot tears and accumulated strain within the steel shell for steel No. C01.*

In other words, the phenomenon of hot tearing must be investigated in view of tear ***initiation*** and ***propagation***. This will be done in the following section in conjunction with the effective strain. The determination of this parameter (ε_{eff}) was already demonstrated taking into account the thermal strain as well as the maximum accumulated strain within ΔT_{SA}. As pointed out in Chapter 6, hot tearing occurs if the effective strain reaches a critical value – the critical strain of hot tearing ε_C. Therefore, the tear initiation can be described by means of ε_C. The corresponding parameter from the metallographic analysis illustrates the number of hot tears. After initiating hot tears, tear growth takes place with increasing strain. A measure of the tendency of tear propagation illustrates the average tear length.

Before starting with the determination of a critical strain of hot tearing as well as the illustration of the tendency of tear propagation as a function of carbon content, it should be mentioned that in this study the tested steels show mainly segregated hot tears. As pointed out in a previous section, no distinction is made between open and segregated hot tears.

†The crack index proposed by Wünnenberg and Flender[5], for example, puts more focus on the number of hot tears (hot tearing sensitivity).

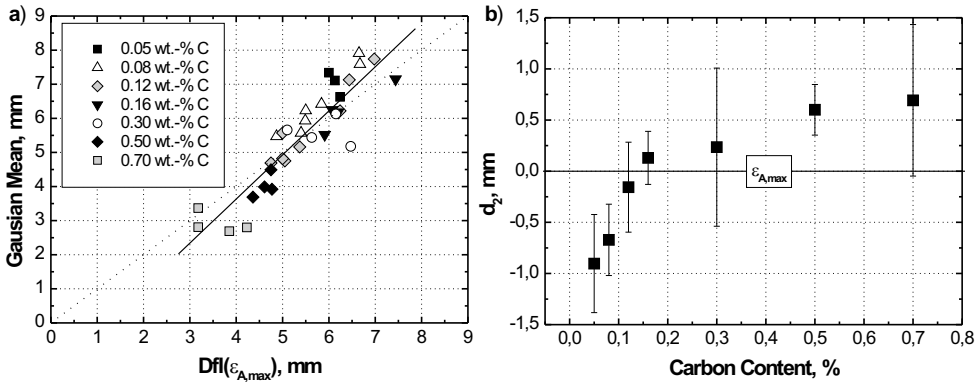

Figure 8.21: *a) Gaussian mean versus the position of $\varepsilon_{A,max}$ for all tested steels and b) mean values with standard deviation of the parameter d_2 as a function of carbon content.*

Due to the different solidification sequence regarding the appearing Fe-phases, three different steel grades are defined (see also Fig. 8.7): Steel grade **Type A** solidifies only in the δ-phase. The transformation into austenite takes place below the solidus temperature (*test series B* and *C*). The steels of **Type B** show a δ-γ transformation during solidification, which applies for the 0.12, 0.16 and 0.30 $wt.$-$\%C$ steels (*test series D, E* and *F*). Finally, the steels of **Type C** show no δ-Fe during solidification (carbon contents above 0.50 $wt.$-$\%C$, *test series G* and *H*).

This classification is used in the illustration and discussion of the results as depicted in Fig. 8.22. In the respective diagrams for the different carbon contents, the number of hot tears are illustrated as a function of the effective strain. A careful and critical analysis of the measured values in Fig. 8.9 allows the detection of possible mavericks (such as steel No. G02), which are highlighted in the diagrams.

The diagrams in Fig. 8.22 show the evolution of the number of hot tears with increasing effective strain. The determined linear equations for each carbon content are also illustrated. Discussing the resulting gradient m_{init}, the steels of the respective steel types show a similar gradient. This means that type A steels (0.05 and 0.08 $wt.$-$\%C$) show a high gradient ($m_{init} \geq 8$), type B steels point at gradients between 4 and 6 and the 0.50 and 0.70 $wt.$-$\%C$ steels show m_{init}-values smaller than 3. A high gradient implies that with increasing effective strain the number of hot tears increases significantly. A lower gradient leads to lower values of the number of hot tears with increasing effective strain. Thus, the parameter m_{init} represents the sensitivity of hot tearing (in terms of the number of hot tears) as a function of the effective strain, a very important result of these depictions. The trend of the gradient m_{init} is summarised in Fig. 8.23a as a function of carbon content.

The results of Fig. 8.22 allow the determination of a critical strain of hot tearing. According to the results of the number of hot tears as a function of effective strain, the hot tear formation cannot be described by means of a *Heaviside Step Function*. However, considering two different cases allows the determination of a critical strain of hot tearing ($\varepsilon_C = (NHT - d_{init})/m_{init}$):

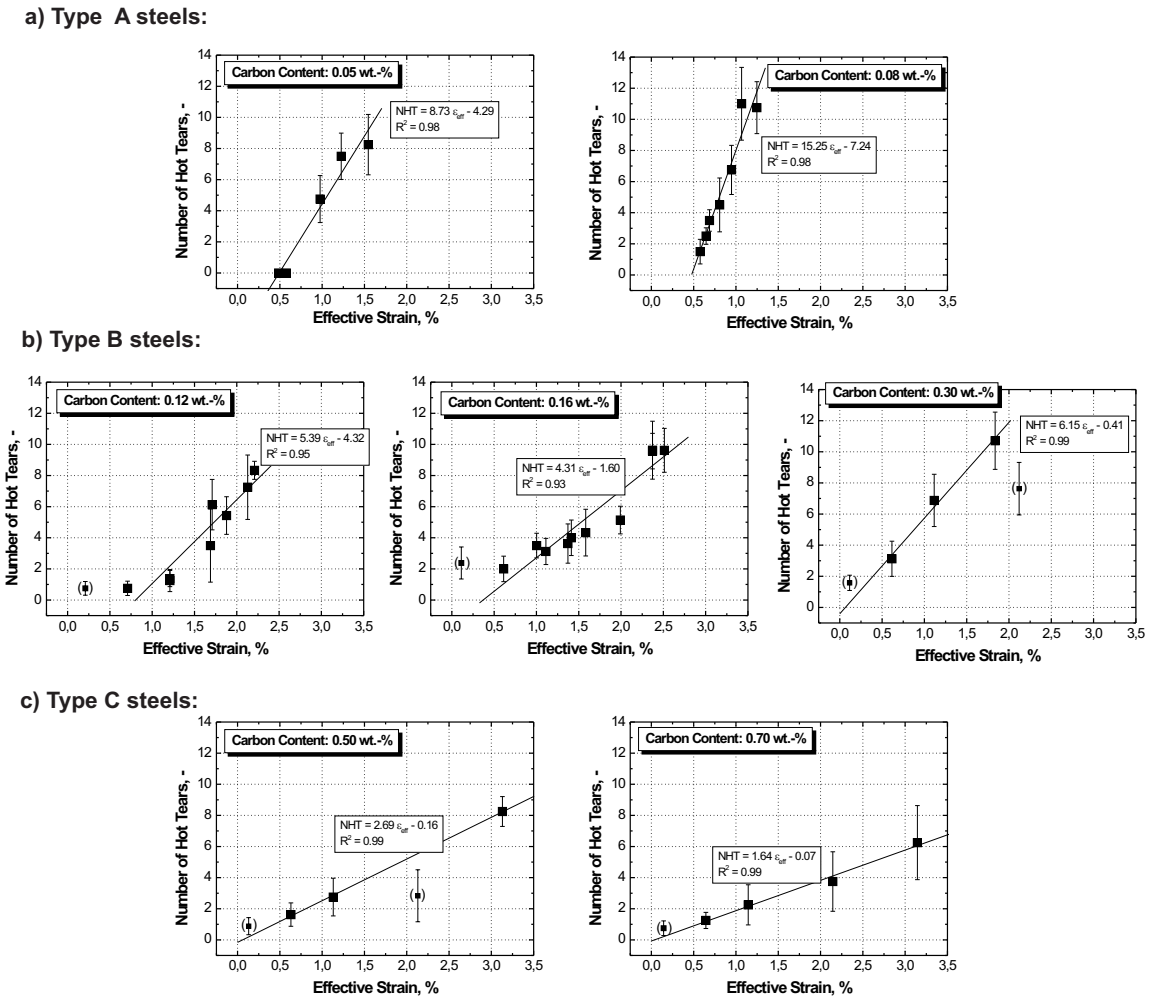

Figure 8.22: *Number of hot tears as a function of the effective strain for type A, B and C steels.*

- **Case 1:** The requirement of no hot tears within the steel shell ($NHT = 0$) leads to $\varepsilon_{C,0}$ by determining the point where the line (linear fit) crosses the abscissa ($\varepsilon_{C,0} = -d_{init}/m_{init}$). Therefore, hot tearing occurs if $\varepsilon_{eff} > \varepsilon_{C,0}$.
- **Case 2:** Assuming that ε_C corresponds to one generated hot tear as a critical value ($NHT = 1$) leads to $\varepsilon_{C,1} = (1 - d_{init})/m_{init}$. Thus, this criterion states that no hot tearing takes place if $\varepsilon_{eff} < \varepsilon_{C,1}$.

Fig. 8.23b shows the results of these two different approaches. It can be seen that the critical strain of hot tearing of type A steels is approximately 0.5 for Case 1 and 0.6 for Case 2. Type B steels strongly depend on the carbon content. With increasing carbon content the critical strain decreases from about 0.70 to < 0.10 (case 1) and from 1.10 to 0.20 (Case 2), respectively. A nearly constant critical strain is determined for type C steels, with a value of less than 0.10 for case 1 and approximately 0.50 for case 2. Regarding the specification of a critical amount of hot tearing, these two cases clearly illustrate the difficulty in defining a critical limit of hot tearing. Besides other

reasons, this fact explains the great scatter band of critical strain values from literature. Case 2 (one generated hot tear) is the more reasonable approach. The determined values are more realistic than the very low values of ε_C at higher carbon contents. Hence, the determined critical strain $\varepsilon_{C,1}$ corresponding to one generated hot tear (Case 2) is used in conjunction with tear initiation ($\varepsilon_C = \varepsilon_{C,1}$).

Due to the different evolution of the number of hot tears with increasing effective strain is is not sufficient to consider the critical strain of tear initiation only. Therefore, the present thesis defines critical values as a function of the numbers of hot tears. Thus, the criterion can take into account the extent of hot tearing and consequently the quality demands on the final product:

$$\varepsilon_{tol}[\%] = \varepsilon_{C,0}[\%] + \frac{NHT}{m_{init}} \tag{8.7}$$

In this equation, the term tolerable strain ε_{tol} is introduced. The parameters m_{init} and $\varepsilon_{C,0}$ were already illustrated in Fig. 8.23 and are finally listed in Tab. 8.3.

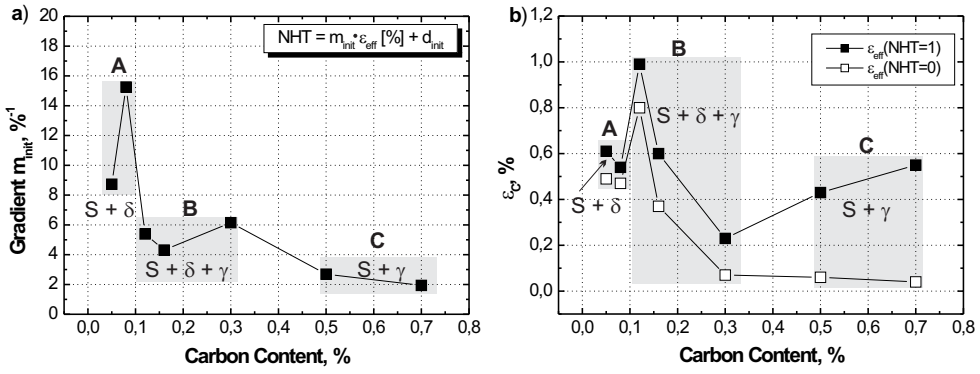

Figure 8.23: *a) The gradient m_{init} resulting from the linear regression and b) the critical strain as a function of carbon content.*

The results of these considerations can be summarised as follows. Type A steels are more likely to show a medium value of the critical strain but with increasing effective strain the extent of hot tearing increases considerably(high m_{init}). Type C steels show a critical strain in the same order of magnitude compared to Type A steels. With increasing effective strain a rather moderate hot tearing sensitivity is determined (low m_{init}). Steels with a δ-γ transformation (Type B) clearly differ from the previous ones. The 0.12 $wt.$-$\%C$ steel shows the highest value of critical strain. With increasing carbon content up to 0.30 $wt.$-%, the critical strain decreases to a minimum. Regarding the degree of hot tearing with increasing effective strain, Type B steels are between the fully δ-ferritic and austenitic solidifying steels and show no significant differences as a function of the carbon content.

Investigations of hot tearing considering the tear propagation can be done by introducing and determining the propagation velocity v_{prop}. In doing so, the results of the average tear length as

a function of the time t_{prop} are of particular interest and relevance. In Fig. 8.24, the two different mechanisms of hot tearing – tear initiation and propagation – are illustrated for the 0.12 $wt.\text{-}\%C$ steel and for two strain rates[‡]. At the higher strain rate the effective strain is equal to the total applied strain, whereas at the lower strain rate the effective strain lies below ε_{tot}. In both cases, hot tears will be initiated when the strain is equal to the critical strain of hot tearing. Subsequently, hot tears grow with a certain velocity as long as a strain acts and/or the effective strain is reached. The time interval of propagation t_{prop} is also illustrated in the diagrams.

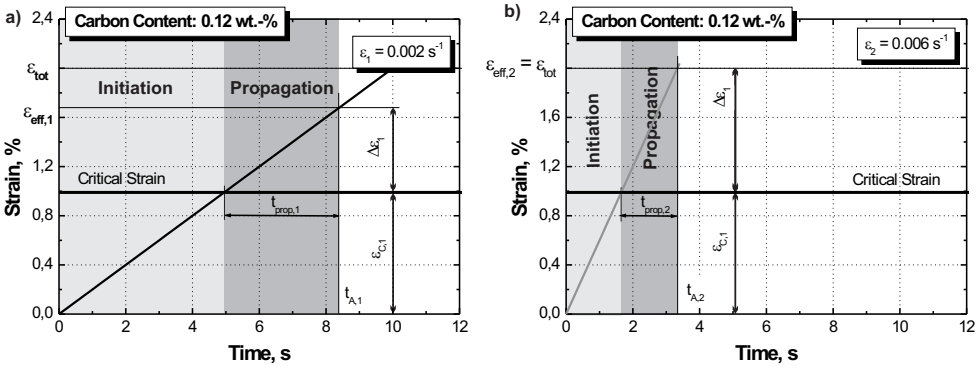

Figure 8.24: *Tear initiation and propagation of a 0.12 wt.-%C steel for two different strain rates.*

By using the values of t_{prop} and the experimentally measured average tear length, the propagation velocity v_{prop} can be determined. This is illustrated in Fig. 8.25 for the different carbon contents. In addition, the determined linear equations ($ATL = ATL_0 + v_{prop} \cdot t$) for each carbon content are illustrated in Fig. 8.25. If the critical strain is reached, a hot tear occurs with a certain length ATL_0 (initial tear length). Fig. 8.26a illustrates the initial tear length as a function of the carbon content. With increasing carbon content the initial tear length tends to increase. The determined propagation velocity of the hot tears is illustrated in Fig. 8.26b, showing a decreasing trend of the values between 0.05 and 0.16 $wt.\text{-}\%C$ and nearly constant values of v_{prop} above 0.16 $wt.\text{-}\%C$.

Summarising, Type A steels show the lowest values of initial tear length of about 0.6 mm and the highest propagation velocity of approximately 0.3 mm/s. Type C steels show the opposite behaviour (high initial tear length: ~ 1.4 mm, low propagation velocity: 0.05 mm/s). The initial tear length of Type B steels tends to increase from 0.9 to 1.4 mm with increasing carbon content. The propagation velocity of the 0.12 $wt.\text{-}\%C$ steel is 0.14 mm/s, whereas the 0.16 and 0.30 $wt.\text{-}\%C$ steels show values similar to Type C steels.

Additionally to the hot tearing sensitivity expressed by the number of hot tears including the evolution of this parameter with increasing effective strain (see Eq. 8.7), the expected average tear length can be estimated using the following relation:

[‡]Please note that the thermal strain which also contributes to the effective strain is not considered in this figure

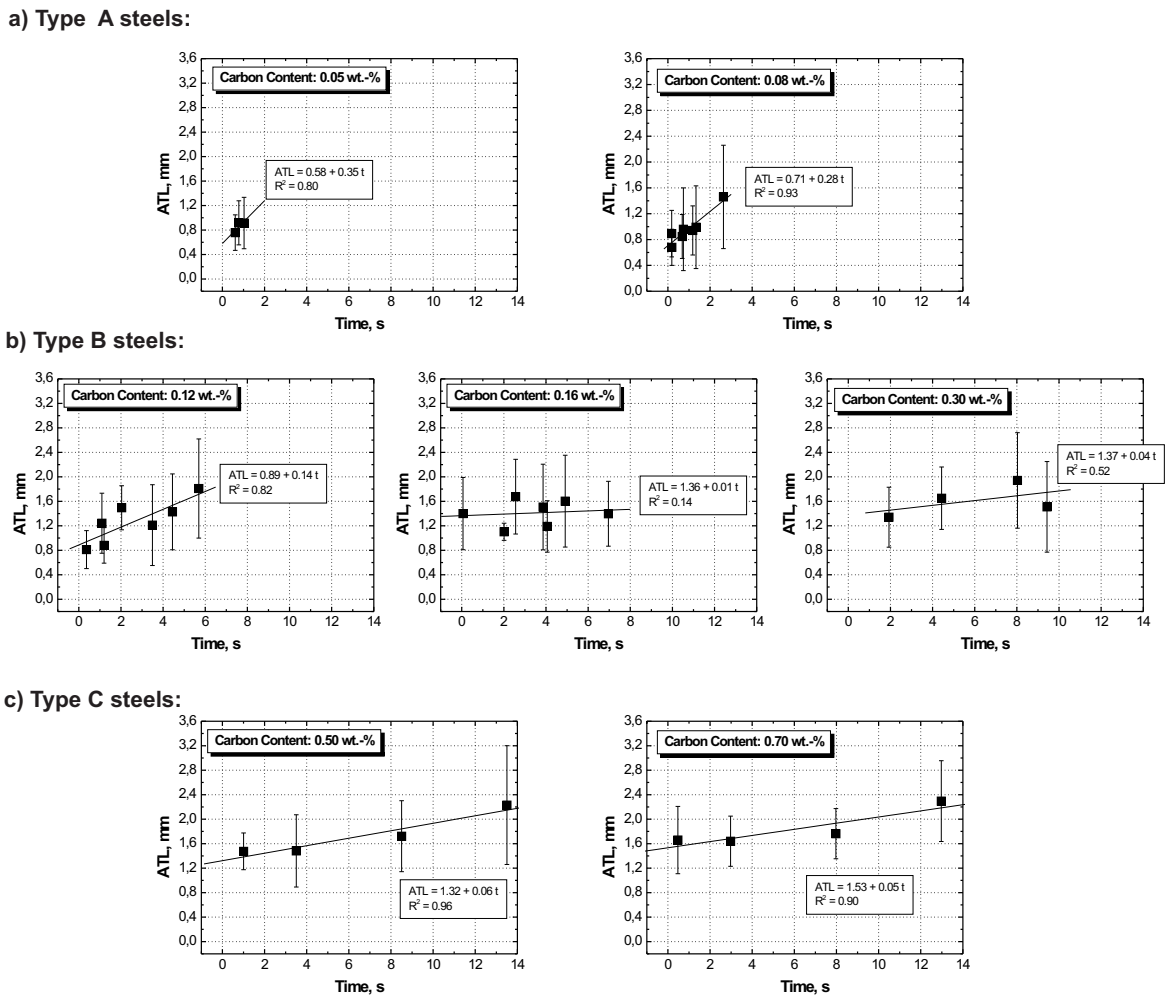

Figure 8.25: *Average tear length as a function of time for the 0.05, 0.08, 0.12, 0.16, 0.30, 0.50 and 0.70 wt.-% carbon steels.*

$$ATL = ATL_0 + v_{prop} \cdot \frac{\varepsilon_{eff} - \varepsilon_C}{\dot{\varepsilon}} \qquad \varepsilon_{eff} \geq \varepsilon_C \tag{8.8}$$

The initial tear length ATL_0 as well as the propagation velocity v_{prop} were already illustrated in diagrams and are summarised in Tab. 8.3. This equation considers the influence of the strain rate on the tear length. According to Eq. 8.8, the average tear length decreases with increasing strain rate. This is in accordance with the findings of Yamanaka *et al.*[22], which show shorter tear lengths with higher strain rates. At a strain rate of $2 \cdot 10^{-4}\ s^{-1}$, a tear length of up to 20 mm was measured, whereas the measured tear length amounts to only 3 mm[22] at four times higher strain rates.

As already mentioned, the number of hot tears as well as the average tear length are very important parameters in the consideration of the demands on the product quality. The above determined relations of NHT and ATL enables an estimation of the extent of hot tearing as a function of the effective strain. In the following, an example will be presented to underline the

Carbon Content	0.05	0.08	0.12	0.16	0.30	0.50	0.70
$\varepsilon_{C,0}$	0.49	0.47	0.80	0.37	0.07	0.06	0.04
m_{init}	8.73	15.25	5.39	4.31	6.15	2.69	1.94
ATL_0	0.58	0.71	0.89	1.36	1.37	1.32	1.53
v_{prop}	0.35	0.28	0.14	0.01	0.04	0.06	0.05
Range of Validity: ε_{eff}	<1.6	<1.4	<2.4	<2.6	<2.0	<3.4	<3.4

Table 8.3: *The determined parameters $\varepsilon_{C,0}$ (in %), m_{init} (in $\%^{-1}$), the initial tear length ATL_0 (in mm) and the propagation velocity v_{prop} (in mm/s) for different carbon contents of the tested steel grades.*

advancement of using the results of the present thesis. Considering, for example the 0.08 and the 0.30 $wt.$-%C steel, the first steel ($\varepsilon_C = 0.54$ %) has a higher critical strain than the latter ($\varepsilon_C = 0.20$ %). However, the severity of hot tearing can be much higher for the 0.08 $wt.$-%C steel. An effective strain of 1.4 % would, for instance, result in 14 hot tears with an average tear length of 1.9 mm for the 0.08 $wt.$-%C steel. The same effective strain causes 8 hot tears with an average tear length of 1.6 mm for the 0.30 $wt.$-%C steel.

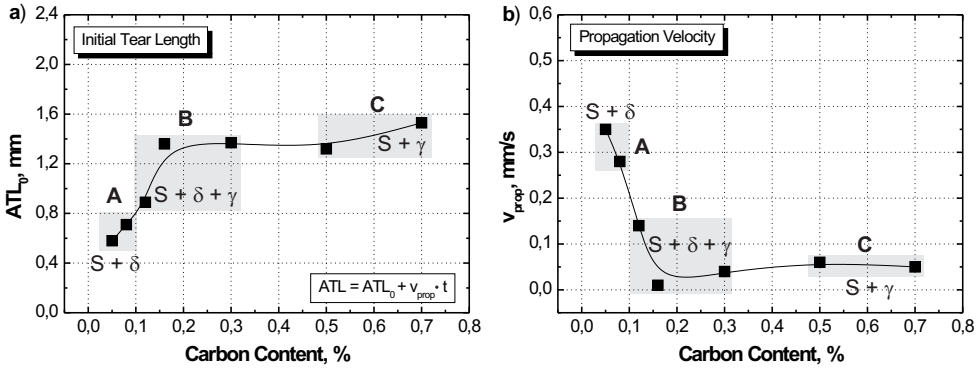

Figure 8.26: *The determined initial tear length ATL_0 and the propagation velocity v_{prop} as function of the carbon content.*

The above illustrated example clearly shows the advancement not only considering the critical strain but also the evolution of the extent/severity of hot tearing with an acting strain. It was shown that this evolution is very different for the respective carbon content. Depending on the quality demands on the final cast product, a tolerable strain ε_{tol} can be defined as a function of the acceptable extent of hot tearing (in terms of NHT and ATL). Therefore, the results of the present study provide an important basis and a step forward in the consideration of hot tearing in the continuous casting process. However, these results are only valid for the tested steel grades with carbon contents of 0.05, 0.08, 0.12, 0.16, 0.30, 0.50 and 0.70 $wt.$-%C and $0.20 - 0.40$ $wt.$-%Si, $1.30 - 1.50$ $wt.$-%Mn, ~ 0.007 $wt.$-%P and ~ 0.007 $wt.$-%S and for the investigated parameters.

8.6 Summary

This chapter showed that the SSCT-test is an appropriate tool to investigate hot tearing under continuous casting conditions. Applying different testing conditions on a construction steel, it could be shown that the position of generated hot tears is in good agreement with the position of the mushy zone during testing. Furthermore, the influence of the strain rate and the cooling rate were illustrated. The increasing hot tearing tendency with increasing holding time indicates that a strain-based hot tearing criterion must consider the solidification conditions.

After that, the results of the position of the detected hot tears within the mushy zone, the number and length of hot tears as well as the average tear length were presented. Regarding the position of the detected hot tears, hot tears are more likely to occur in a small range above the solidus temperature. The number and length of hot tears show a clear tendency, to increase with increasing total applied strain. Generally, the average tear length also tends to increase with increasing total strain.

The influence of carbon content on hot tearing in view of the number and length of hot tears can be summarised as follows. Between a carbon content of 0.05 and 0.30 $wt.\text{-}\%C$, the hot tearing sensitivity increases, reaching a maximum at 0.30 $wt.\text{-}\%C$ and decreases at carbon contents of 0.50 and 0.70 $wt.\text{-}\%C$. An interesting result was gained from the experiments applying no external strain. Steels which pass through a δ-γ transformation during solidification already show a minor hot tear formation. A maximum value was found at a carbon content of 0.16 $wt.\text{-}\%C$. However, these results must be interpreted very carefully, because the number of hot tears are in the same order of magnitude as the standard deviation.

According to the introduced concept of an accumulated strain within a certain part of the mushy zone, the determination of this temperature range (ΔT_{SA}) was of major importance. Considering the accumulated strain and the thermal strain, ΔT_{SA} was determined between a solid fraction of 0.96 and 1 for the 0.08 and 0.12 $wt.\text{-}\%C$ steels. The defined effective strain ε_{eff} using the proposed model takes into account the influence of chemical composition (width of ΔT_{SA}), strain rate and solidification conditions (time for strain accumulation, t_A).

Finally, the model of an accumulated strain was applied, illustrated and discussed for all results. The comparison of the position of the detected hot tears within the steel corresponds very well to the position of ΔT_{SA} during tensile testing. The description of hot tearing was carried out by distinguishing tear initiation and propagation. The determination of the critical strain was carried out for two cases ($NHT = 0$ and $NHT = 1$), illustrating the uncertainty and difficulty of the determination of this parameter. It was found that the critical strain of steels which solidify purely in the δ-Fe (Type A steels) or γ-Fe (Type C steels) phase is in the same order of magnitude, whereas the critical strain of steels with a δ-γ transformation (Type B steels) changes considerably with carbon content. Besides the critical value of hot tearing it could also be shown that the evolution of the extent of hot tearing is influenced by the carbon content. Type A steel grades show a sharp increase of the extent of hot tearing with increasing effective strain, whereas the extent of hot tearing increases rather moderately with increasing effective strain at Type C steel grades. Type

B steel grades lie between Type A and C steels. The consideration of tear propagation was done by determining the initial tear length and the propagation velocity. It was shown that the initial tear length tends to increase with increasing carbon content. Hence, the width of the preferable temperature range of strain accumulation ΔT_{SA} and the initial tear length show a correlation. The propagation velocity showed an inverse trend as a function of the carbon content. Between 0.05 and 0.16 $wt.\text{-}\%C$ the propagation velocity sharply decreased and remained constant afterwards.

In order to consider the demands on the quality of the final cast product, the criterion of a critical strain was advanced in terms of a tolerable strain ε_{tol} and the estimation of an average tear length as a function of the effective strain. By this, the evolution of hot tearing is considered, ensuring flexibility of the criterion with respect to the final product quality requirements.

9 Summary, Conclusion and Outlook

You know that I write slowly. This is chiefly because I am never satisfied until I have said as much as possible in a few words, and writing briefly takes far more time than writing at length.[a] Carl Friedrich Gauss

[a] In G. Simmons Calculus Gems, New York, McGraw Hill Inc., 1992

9.1 Summary and Conclusion

The presented thesis deals with the phenomenon of hot tearing and the development of an efficient hot tearing criterion in continuous casting of steels. In a comprehensive review of the literature different definitions were presented, the suggested mechanisms were explained and the main influencing parameters were pointed out. According to the *Shrinkage-Brittleness Theory* hot tearing takes place by separating solid-solid bridges. The *Strain Theory* describes hot tearing by the separation of a solid-liquid mass in the absence of solid-solid bridges, whereas the *Generalised Theory* tries to combine the previous two theories. The *initiation* and *propagation* of hot tears along *primary grain boundaries* represent an important element in the phenomenon of hot tearing. In addition, the wettability of the grain boundaries by the liquid is described in the relevant literature. A further point of interest is the similarity of hot tearing and liquid metal embrittlement. In the field of continuous casting, hot tearing is mainly associated with the *brittle temperature range* considering the influence of chemical composition.

Numerous hot tearing criteria based on stress, strain and strain rates or based on other principles were illustrated in detail. Many of these criteria are rather new in the field of continuous casting of steel because they were mainly developed in the field of aluminium alloys or have their origin in the field of welding. However, hot tearing in steel and other materials or in casting and welding represents the same phenomenon. Some of the criteria define a critical value of hot tearing, e.g. in terms of a critical strain or stress. Others define a hot tearing susceptibility in order to describe mainly the influence of the chemical composition. Hot tearing criteria in continuous casting of steels are mainly strain-based models, which compare the strain due to the process to a critical strain of hot tearing. Generally, the critical strain of hot tearing of steels decreases with increasing

carbon content and strain rate. However, regarding the strain rate different research findings are published. Here, the results of Yamanaka[22,81] are of special relevance. Hot tearing occurs when the total amount of strain within a certain critical temperature range exceeds the critical strain, independent of strain rate and manner of deformation.

In order to predict the expected hot tearing tendency of the tested steel grades in a laboratory experiment, four different criteria from the literature were applied. The stress-based model proposed by Rogberg[20] strongly depends on the secondary dendrite arm spacing. Using values of this parameter determined from micrographs of the SSCT-test leads to an increasing hot tearing tendency between 0.05 and 0.30 $wt.\text{-}\%C$. After 0.30 $wt.\text{-}\%C$ the hot tearing tendency decreases. This trend is very similar to the results of the present thesis in view of the number and length of hot tears at different applied total strains. Both criteria, the empirical equation of the critical strain proposed by Won *et al.*[8] and the strain rate-based model published by Rappaz *et al.*[71] show an increasing hot tearing susceptibility with increasing carbon content. The Clyne and Davies[27] approach results in a similar trend as the stress-based criteria. These results indicate the major influence of the microstructure (secondary dendrite arm spacing in the Rogberg criterion) and the consideration of the residence time of a volume element in a certain part of the mushy zone.

The requirements on a hot tearing criterion in the field of continuous casting were also illustrated, which represented the initial point of the development of a process related hot tearing criterion. Based on the distinction between *subsurface hot tears* and *internal hot tears*, it appears that the consideration of the process, the microstructure and the steel composition are the main demands on a process related hot tearing criterion. Furthermore, both open and segregated hot tears may degrade the quality of the final product. The occurrence of hot tears is not necessarily connected to a quality loss of the final product. Additionally, it was shown that the cracks preferably extend along primary grain boundaries, which are orientated perpendicular to the main load direction. As a result of these considerations, the definition of hot tearing was specified.

In order to consider also steel composition, strain rate, solidification velocity, thermal contraction during solidification and the quantification of deformation limits a hot tearing criterion based on an accumulated strain within a certain part of the mushy zone was developed. In doing so, the accumulated strain due to process is compared to an effective strain. This effective strain comprises of the accumulated strain and the thermal strain within a preferable temperature range of strain accumulation. By introducing a tolerable strain as a function of the hot tearing susceptibility quality demands on the final cast product can be considered.

A major part of the presented thesis focuses on laboratory experiments (SSCT-test). After demonstrating the main features of this test, the thermal and metallographic analysis were presented. These two procedures are essential for an accurate interpretation of the results.

According to the experimental investigation of hot tearing, it was first shown that the position of generated hot tears is in good agreement with the position of the mushy zone during testing. The experiments for this were carried out using a typical construction steel and different testing parameters (strain rate, cooling rate and holding time). Based on this steel composition the in-

vestigations focused on the influence of carbon content on hot tearing. The cooling rate (coating thickness: 0.4 mm) and the holding time (16 s) were held constant. For the most part the strain rate has $2 \cdot 10^{-3}$ s^{-1}, whereas at certain steel grades the strain rate was increased to $6 \cdot 10^{-3}$ and $1.2 \cdot 10^{-2}$ s^{-1}. The results of the position of the detected hot tears within the mushy zone, the number and length of hot tears as well as the average tear length were presented. By comparing the position of the detected hot tears with the position of the mushy zone during testing, it could be shown that hot tears are more likely to occur in a small range above the solidus. The number and length of hot tears clearly increase with increasing total applied strain, whereas this behaviour could not be demonstrated clearly for the average tear length. The trend of the number and length of hot tears – the hot tearing susceptibility – as a function of the carbon content can be summarised as follows. If no external deformation is applied a maximum value of the hot tearing susceptibility was found at a carbon content of 0.16 $wt.\text{-}\%C$. With increasing total strain this maximum is shifted to a carbon content of 0.30 $wt.\text{-}\%C$. This is in contradiction to the general findings of the relevant literature which mainly describe increasing hot tearing susceptibility with increasing carbon content.

The model of an accumulated strain is based on a preferable temperature range of strain accumulation within the mushy zone ($\Delta T_{SA} = T_A - T_S$). Therefore, the determination of this certain range was necessary. According to the definition and basic understanding of hot tearing, the generation of the cracks takes place at temperatures above solidus representing the lower boundary of the preferable temperature range of strain accumulation. The upper boundary (T_A) is the temperature and the corresponding solid fraction where strain accumulation starts. The determined value of this solid fraction is $f_{S,A} = 0.96$ for the 0.08 and 0.12 $wt.\text{-}\%C$ steels. Again, $f_{S,A}$ strongly depends on the microsegregation analysis and consequently on the used model and model parameters.

In a first assumption, this value was applied to all tested steel grades resulting in an effective strain (= accumulated strain + thermal strain) within the preferable temperature range of strain accumulation. It could be shown that the occurrence of hot tears corresponds very well to the defined position of the preferable temperature range of strain accumulation during tensile testing. The characterisation of hot tearing was carried out by considering both, tear initiation and propagation. Thus, the phenomenon of tear initiation was described by a critical strain, whereas tear propagation was specified by an average propagation velocity. It was found that steels which solidify purely in the δ-Fe phase show nearly the same critical value ($\varepsilon_C \sim 0.5$ %). This value was also found for steels that solidify purely in the γ-Fe phase. Steels with a δ-γ transformation show a decreasing critical strain (0.12 $wt.\text{-}\%C$: $\varepsilon_C = 1.0$ %, 0.16 $wt.\text{-}\%C$: $\varepsilon_C = 0.6$ % and 0.30 $wt.\text{-}\%C$: $\varepsilon_C = 0.2$ %) with increasing carbon content. However, the definition of a critical strain of hot tearing is not sufficient. This can be confirmed by the findings of the present thesis regarding the evolution of the extent of hot tearing in view of the number of hot tears and the average tear length (propagation) with increasing effective strain. The 0.05 and 0.08 $wt.\text{-}\%C$ steels show a sharp increase of the number of hot tears with increasing effective strain, whereas the extent of hot tearing increases rather moderately with increasing effective strain at the 0.50 and 0.70 $wt.\text{-}\%C$. For the 0.12, 0.16 and 0.30 $wt.\text{-}\%C$ steels the evolution of hot tears was found to be between the above

mentioned steel grades. It was also found that the initiated hot tears show an initial tear length, which increases with increasing carbon content. With respect to tear propagation, a decreasing propagation velocity with increasing carbon content was determined.

Based on these findings, the present thesis defined two relations in order to estimate the expected quantity and length of hot tears as a function of the effective strain. A further improvement resulting from these considerations is the possibility of defining critical strain values taking into account the demands on the final cast product. Finally, the presented approach together with the experimentally determined results offer a more accurate consideration of the problem of hot tearing in the continuous casting process of steel.

9.2 Outlook

Conclusions that can be drawn from the performed experiments and the presented model seem to provide promising perspectives for further work using the SSCT-test and the presented approach of an accumulated strain within a preferable temperature range of the mushy zone. In the following section, some additional questions and further necessary considerations for a deeper fundamental understanding of hot tearing shall be sketched:

- It is still an open question whether hot tearing takes place by separating solid-solid bridges, separating a continuous liquid film between primary grain boundaries or whether both phenomena are possible. The key for answering this question can certainly be found in the metallographic analysis by means of a detailed investigation of generated hot tears.
- As a further step, the mechanism of the generation of open or segregated hot tears must be studied in order to provide a criterion distinguishing between these two types of hot tears. Therefore, experiments should be carried out with the aim to create these kinds of hot tears. In combination with metallographic analysis, a criterion considering open and segregated hot tears can be developed.
- With respect to segregated hot tears and the severity in the final product, deformation experiments should be carried out to investigate the behaviour of segregated hot tears at the subsequent processing.
- As shown, hot tears preferably occur at primary grain boundaries. In this context, the morphology (grain boundary cohesion) in view of the coherency temperature, coalescence temperature and microsegregation behaviour should be described. In this case, also the metallographic analysis could be an important tool to provide clues regarding the role of primary grain boundaries in hot tearing.
- A further important parameter concerning hot tearing is the microstructure. The influence of this parameter was investigated in Chapter 5. The presented results mainly refer to constant cooling conditions. However, it appears that the hot tearing tendency of the construction

steel is clearly lower at a higher cooling rate (coating thickness of 0.15 mm) in comparison to lower cooling rate (coating thickness of 0.40 mm). Therefore, the presented results of hot tearing are only valid for the used cooling rate. Further investigations should focus on the influence of the microstructure, e.g. by introducing a microstructure parameter in the model.

- Finally, the role of precipitations and/or of microporosity in the face of tear initiation should be examined.

The presented strain-based approach of an accumulated strain within a certain temperature range constitutes a step forward in the consideration of hot tearing in continuous casting. This concept together with the above sketched necessary improvements could provide a further step forward to avoid the undesirable phenomenon of hot tearing in the continuous casting process.

Bibliography

[1] C. Bernhard, R. Pierer, A. Tubikanec, and C. Chimani, *Experimental characterization of crack sensitivity under continuous casting conditions*, Proceedings of the CCR'04 - Continuous Casting and Hot Rolling Conference (Linz, Austria), 2004, 6.3.

[2] J. Miyazaki, T. Mori, K. Narita, and T. Ohnishi, *Influence of deformation on the internal crack formation in continuously cast bloom*, 2nd Process Technology Conference Proceedings (Chicago, USA), 1981, 35–43.

[3] S. Nagata, T. Matsumiya, K. Ozawa, and T. Ohashi, *Estimation of critical strain for internal crack formation in continuously cast slabs*, Tetsu-to-Hagané (Journal of Iron and Steel Institute Japan) **76** (1990), No. 2, 214–221.

[4] T. Matsumiya, M. Ito, H. Kajioka, S. Yamaguchi, and Y. Nakamura, *An evaluation of critical strain for internal crack formation in continuously cast slabs*, Transactions Iron and Steel Institue Japan **26** (1986), No. 6, 540–545.

[5] K. Wünnenberg and R. Flender, *Investigation of internal crack formation in continuous casting, using a hot model*, Ironmaking and Steelmaking **12** (1985), No. 1, 22–29.

[6] R. Flender, *Untersuchung zur Innenrissbildung beim Stranggießen*, Ph.D. Thesis, University of Clausthal, 1983.

[7] M. Wintz, M. Bodadilla, and J. M. Jolivet, *Hot cracking during solidification of steel: effect of carbon, sulphur and phosphorus*, La Revue de Métallurgie **91** (1994), No. 1, 105–114.

[8] Y. M. Won, T. J. Yeo, D. J Seol, and K. H. Oh, *A new criterion for internal crack formation in continuously cast steels*, Metallurgical and Materials Transactions B **31** (2000), No. 4, 779–794.

[9] R. Pierer, C. Bernhard, and C. Chimani, *A contribution to hot tearing in the continuous casting process*, La Revue de Métallurgie (2007), No. 2, 72–83.

[10] Verein Deutscher Eisenhüttenleute, *Stahl-Eisen-Prüfblätter*, 1992.

[11] *The appearance of cracks and fractures im metallic materials*, Verlag Stahleisen GmbH, Düsseldorf, 1996.

[12] R. Mitsche, F. Jeglitsch, S. Stanzl, and H. Scheidl, *Anwendung des Rasterelektronenmikroskops bei Eisen- und Stahlwerkstoffen*, Radex-Rundschau **3** (1978), No. 4.

[13] H. Riedel, *Fracture at high temperatures*, Springer Verlag, Berlin-Heidelberg-New York, 1987.

[14] J. Langlais and J. E. Gruzleski, *A novel approach to assessing the hot tearing susceptibility of aluminum alloys*, International Symposium on Light Metals (Quebec City, Canada), 1999, 247–263.

[15] D. G. Eskin, Suyitno, and L. Katgerman, *Mechanical properties in the semi-solid state and hot tearing of aluminium alloys*, Progress in Material Science **49** (2004), No. 5, 629–711.

[16] J. Campbell, *Castings*, Butterworth-Heinemann, Oxford, 1991.

[17] C. Bernhard, *Anforderungen an prozessorientierte Heißrissbildungsmodelle*, BHM **149** (2004), No. 3, 90–95.

[18] C. Bernhard, R. Pierer, and C. Chimani, *A new hot tearing criterion for the continuous casting of steel*, 5th Decennial International Conference on Solification Processing (Sheffield, UK), 2007, 525–530.

[19] D. G. Eskin and L. Katgerman, *A quest for a new hot tearing criterion*, Metallurgical and Materials Transactions A **38** (2007), No. 7.

[20] B. Rogberg, *An investigation on the hot ductility of steels by performing tensile tests on in situ solidified samples*, Scandinavian Journal of Metallurgy **12** (1983), No. 2, 51–66.

[21] J. A. Spittle and A. A. Cushway, *Influence of superheat and grain structure on hot tearing susceptibilities of Al-Cu alloy castings*, Metals Technology **10** (1983), No. 1, 6–13.

[22] A. Yamanaka, K. Nakajima, and K. Okamura, *Critical strain for internal crack formation in continuous casting*, Ironmaking and Steelmaking **22** (1995), No. 6, 508–512.

[23] J. Verö, *The hot shortness of aluminium alloys*, Met. Ind. **48** (1936), 431–442.

[24] A. R. E. Singer and P. H. Jennings, *Hot shortness of aluminium-silicon alloys of commercial purity*, Journal of the Institute of Metals **74** (1947), 197–212.

[25] A. R. E. Singer and S. A. Cottrell, *Properties of aluminium-silicon alloys at temperatures in the region of the solidus*, Journal of the Institute of Metals **73** (1947), 33–54.

[26] D. C. G. Lees, *The hot tearing tendencies of aluminium casting alloys*, Journal of the Institute of Metals **72** (1946), 358–364.

[27] T. W. Clyne and G. J. Davies, *Comparison between experimental data and theoretical predictions relating to dependence of solidification cracking on composition*, Solidification and Casting of Metals (Sheffield, England), 1979, 275–278.

[28] B. Forest and S. Bercoivici, *Experimental study of mechanical properties of aluminium alloys during controlled solidification: application to hot tearing*, Solidification Technology in the Foundry and Cast House (Coventry, England), 1980, 607–612.

[29] N. Wang, S. Mokadem, M. Rappaz, and W. Kurz, *Solidification cracking of superalloy single- and bi-crystals*, Acta Materialia **52** (2004), No. 11, 3173–3182.

[30] N. N. Prokhorov, Russian Castings Production **2** (1962), 172–175.

[31] N. N. Prokhorov, *The technological strength of metals whilst crystallising during welding*, Welding Production **9** (1962), 1–5.

[32] N. N. Prokhorov, *Problems of strength of metals in the process of solidification during welding*, Welding Production **6** (1956), 5–11.

[33] N. N. Prokhorov and M. P. Bochai, *The mechanical properties of alluminium alloys in the crystallising range during welding*, Welding Production **6** (1956), 5–11.

[34] F. Weinberg, *The ductility of continuously-cast steel near the melting point – hot tearing*, Metallurgical and Materials Transactions B **10** (1979), No. 2, 219–227.

[35] T. W. Clyne, M. Wolf, and W. Kurz, *The effect of melt composition on solidification cracking of steel, with particular reference to continuous casting*, Metallurgical and Materials Transactions B **13** (1982), No. 2, 259–266.

[36] K.-H. Kim, T.-J. Yeo, K. H. Oh, and D. N. Lee, *Effect of carbon and sulphur in continuously cast strand on longitudinal surface cracks*, ISIJ International **36** (1996), No. 3, 284–289.

[37] K. Kim, H. N. Han, T. Yeo, Y. Lee, K. H. Oh, and D. N. Lee, *Analysis of surface and internal cracks in continuously cast beam blank*, Ironmaking and Steelmaking **24** (1997), No. 3, 249–256.

[38] H. G. Suzuki, S. Nishimura, and S. Yamaguchi, *Characteristics of hot ductility in steels subjected to melting and solidification*, Transactions Iron and Steel Institute Japan **22** (1982), No. 1, 48–56.

[39] M. M. Wolf, *Fine intergranular surface cracks in bloom casting*, Transactions Iron and Steel Institute Japan **24** (1984), No. 5, 351–358.

[40] B. G. Thomas, I. V. Samarasekera, and J. K. Brimacombe, *The formation of panel cracks in steel ingots: a state of the art review*, ISS Transactions **7** (1986), 7–20.

[41] T. Nakagawa, T. Umeda, J. Murata, Y. Kamimura, and N. Niwa, *Deformation behavior during solidification of steels*, ISIJ International **32** (1995), No. 6, 723–729.

[42] G. Shin, T. Kajitani, T. Suzuki, and T. Umeda, *Mechanical properties of carbon steels during solidification*, Tetsu-to-Hagané (Journal of Iron and Steel Institute Japan) **78** (1992), 587–593.

[43] R. Steffen, W. Dahl, R. Flesch, H. Litterscheidt, F. Radowski, P. Scheller, and E. Sowka, *Hochtemperatureigenschaften und Rissbildung beim Stranggießen*, Tech. Report, European Commission, Bruxelles, Belgium, 1999.

[44] T. W. Clyne and G. J. Davies, *The influence of composition on solidification cracking susceptibility in binary alloy systems*, The British Foundryman **74** (1981), No. 4, 65–73.

[45] S. Kobayashi, Tetsu-to-Hagané (Journal of Iron and Steel Institute Japan) **73** (1987), No. 12, 896.

[46] E. Schmidtmann and F. Rakoski, *Einfluss des C-Gehalts von 0.015 bis 1 % und der Gefügestruktur auf das Hochtemperaturfestigkeits- und -zähigkeitsverhalten von Baustählen nach der Erstarrung aus der Schmelze*, Archiv Eisenhüttenwesen **54** (1983), No. 9, 357–362.

[47] E. Schmidtmann and F. Rakoski, *Einfluss von S und Mn sowie der Abkühlbedingungen auf die Gefügestruktur und die Zähigkeitseigenschaften von Baustählen nach der Erstarrung aus der Schmelze*, Archiv Eisenhüttenwesen **54** (1983), No. 9, 363–368.

[48] K. H. Kim, H. N. Han, T. J. Yeo, Y. G. Lee, K. H. Oh, and D. N. Lee, *Heat flow, deformation behavior and crack formation during continuous casting of beam blank*, Melt Spinning, Strip Casting and Slab Casting (Anaheim, California, USA), 1996, 87–102.

[49] E. Scheil, *Bemerkungen zur Schichtkristallbildung*, Zeitschrift für Metallkunde **70** (1942), No. 3, 70–72.

[50] H. D. Brody and M. C. Flemings, *Solute redistribution in dendritic solidification*, Transaction of the Metallurgical Society AIME **236** (1966), No. 5, 615–624.

[51] T. W. Clyne and W. Kurz, *Solute redistribution during solidification with rapid solid-state diffusion*, Metallurgical and Materials Transactions A **12** (1981), No. 6, 965–971.

[52] I. Ohnaka, *Mathematical analysis of solute redistribution during solidification with diffusion in solid phase*, Transactions Iron and Steel Institute of Japan **26** (1986), No. 12, 1045–1051.

[53] S. Kobayashi, *Mathematical analysis of solute redistribution during solidification based on a columnar dendrite model*, Transactions Iron and Steel Institute of Japan **28** (1988), No. 9, 728–735.

[54] Y. Ueshima, S. Mizoguchi, T. Matsumiya, and H. Kajioka, *Analysis of solute distribution in dendrites of carbon steel with delta/gamma transformation during solidification*, Metallurgical and Materials Transactions B **17** (1986), No. 4, 845–859.

[55] W. Kurz and D. J. Fischer, *Fundamentals of solidification*, Trans Tech Publications LDT, Uetikon-Zuerich, Switzerland, 1984.

[56] J. Zhang and R. F. Singer, *Hot tearing of nickel-based superalloys during directional solidification*, Acta Materialia **50** (2002), No. 7, 1869–1879.

[57] K. Heck, J. R. Blackford, and R. F. Singer, *Castability of directionally solidified nickel base superalloys*, Materials Science and Technology **15** (1999), No. 2, 213–220.

[58] W. S. Pellini, *Strain theory of hot tearing*, Foundry (1952), 125–199.

[59] H. F. Bishop, C. G. Ackerlind, and W. S. Pellini, *Metallurgy and mechanics of hot tearing*, AFS Transactions **60** (1952), 818–833.

[60] H. F. Bishop, C. G. Ackerlind, and W. S. Pellini, *Investigation of metallurgical and mechanical effects in the development of hot tearing*, AFS Transactions **65** (1957), 247–258.

[61] J. C. Borland, *Generalised theory of super-solidus cracking in welds and casting: an initial development*, British Welding Journal **7** (1960), 508–512.

[62] N. Wang, *Grains, phases and interfaces: As interpretation of microstructure*, Metal Technology **15** (1948), No. 4, 1–37.

[63] J. Campbell, *Dihedral angles and the equilibrium morphology of grain-boundary phases*, Metallography **4** (1971), No. 3, 269–278.

[64] S. P. Tucker and F. G. Hochgraf, *Equilibrium morphology of grain boundary phases*, Metallography **6** (1973), No. 6, 457–464.

[65] P. Wray, *The geometry of two-phase aggregates in which the shape of the second phase is determined by its dihedral angle*, Acta Materialia **24** (1976), No. 2, 125–135.

[66] J. C. Borland, *Fundamentals of solidification cracking in welds. Part 1*, Welding and Metal Fabrication **47** (1979), No. 1, 19–29.

[67] J. C. Borland, *Suggested explanation of hot cracking in mild and low alloy steel welds*, British Welding Journal **8** (1961), 526–540.

[68] J. C. Borland, *Fundamentals of solidification cracking in welds. Part 2*, Welding and Metal Fabrication **47** (1979), No. 2, 99–107.

[69] H. Fredriksson and B. Lehtinen, *Continuous observation of hot crack formation during deformation and heating in SEM*, Solidification and Casting of Metals (Sheffield, UK), 1979, 260–267.

[70] C. E. Cross, *On the origin of weld solidification cracking*, 3–18, Springer-Verlag Berlin Heidelberg, 2005.

[71] M. Rappaz, J.-M. Drezet, and M. Gremaud, *New hot-tearing criterion*, Metallurgical and Materials Transactions A **30** (1999), No. 2, 449–455.

[72] L. Katgerman, *A mathematical model for hot cracking of aluminium alloys during DC casting*, Journal of Materials (JOM) **34** (1982), No. 2, 46–49.

[73] Suyitno, W. H. Kool, and L. Katgerman, *Micro-mechanical model of hot tearing at triple junctions in DC casting*, Materials Science Forum **393-402** (2002), 179–184.

[74] C. Monroe and C. Beckermann, *Development of a hot tear indicator for steel castings*, Materials Science and Engineering A **413-414** (2005), 30–36.

[75] B. Burton and G. W. Greenwood, *Limits of the linear relation between stress and strain rate in the creep of copper and copper-zinc alloys*, Acta Metallurgica **18** (1970), No. 12, 1237–1242.

[76] J. A. Williams and A. R. E. Singer, *Deformation, strength, and fracture above the solidus temperature*, Journal of the Institute of Metals **96** (1968), No. 1, 5–12.

[77] I. I. Novikov and F. S. Novik, *Nature of fracture of aluminium alloys in the solid-liquid state*, Russian Metallurgy **2** (1967), 44–47.

[78] D. Warrington and D. G. McCartney, *Development of a new hot-cracking test for aluminium alloys*, Cast Metals **2** (1989), No. 3, 134–143.

[79] V. D. E. L. Davies, *Influence of grain size on hot tearing*, The British Foundryman **63** (1970), No. 4, 93–101.

[80] H. Mizukami, K. Murakami, and T. Mitagawa, *Characteristics of embrittlement of continuously cast steel near the solidification temperature*, Tetsu-to-Hagané (Journal of Iron and Steel Institute Japan) **81** (1995), 792–797.

[81] A. Yamanaka, K. Nakajima, K. Yasumoto, H. Kawashima, and K. Nakai, *New evaluation of critical strain for internal crack formation in continuous casting*, La Revue de Métallurgie **89** (1992), No. 7-8, 627–633.

[82] C. H. Yu, M. Suzuki, H. Shibata, and T. Emi, *Simulation of crack formation on solidifying steel shell in continuous casting mold*, ISIJ International **36** (1996), 159–162.

[83] G. K. Sigworth, *Hot tearing of metals*, Transactions of the American Foundrymen's Society (Philadelphia, USA), Vol. 104, 1996, 1053–1062.

[84] L. Feurer, *Mathematisches Modell der Warmrißneigung von binären Aluminiumlegierungen*, Gießereiforschung **28** (1976), No. 2, 75–80.

[85] E. Niyama, *Some considerations on internal cracks in continuously cast steel*, Proceedings of the Japan-US Joint Seminar on Solidification of Metals and Alloys (Tokyo, Japan), 1977, 271–282.

[86] B. Joseph, M. Picat, and F. Barbier, *Liquid metal embrittlement: A state-of-the-art appraisal*, The European Physical Journal Applied Physics **5** (1999), 19–31.

[87] W. Rostoker, J. M. McCaughey, and H. Markus, *Embrittlement by liquid metals*, Reinhold Publishing Corp., New York, 1960.

[88] M. J. Kelley and N. S. Stoloff, *Analysis of liquid metal embrittlement from a bond energy viewpoint*, Metallurgical and Materials Transactions A **6** (1975), No. 1, 159–166.

[89] N. S. Stoloff and T. L. Johnson, *Crack propagation in a liquid metal enviroment*, Acta Metallurgical **11** (1963), No. 4, 251–256.

[90] Suyitno, W. H. Kool, and L. Katgerman, *Hot tearing criteria evaluation for direct-chill casting of an Al-4.5 % Cu alloy*, Metallurgical and Materials Transactions A **36** (2005), No. 6, 1537–1546.

[91] V. N. Saveiko, *Theory of hot tearing*, Russian Castings Production **8** (1961), 453–456.

[92] C. H. Dickhaus, L. Ohm, and S. Engler, *Models to reflect the mechanical properties of solidifying shells during continuous casting*, Metall (Germany) **46** (1992), No. 2, 581–58.

[93] D. J. Lahaie and M. Bouchard, *Physical modeling of the deformation mechanisms of semisolid bodies and a mechanical criterion for hot tearing*, Metallurgical and Materials Transactions B **32** (2001), No. 4, 697–705.

[94] D. Larouche, J. Langlais, W. Wu, and M. Bouchard, *A constitutive model for the tensile deformation of a binary aluminum alloy at high fractions of solid*, Metallurgical and Materials Transactions B **37** (2006), No. 3, 431–443.

[95] C. D. Drucker, *Engineering and continuum aspects of high-strength materials*, High-strength materials (John Wiley & Sons INC., New York), 1964, 795–833.

[96] M. Kinefuchi, T. Nakagawa, N. Kakehana, K. Tanigaw, and M. Kimura, *Measurement of critical strain for initiation of internal cracks during continuous casting process*, CAMP-ISIJ **8** (1995), 150.

[97] B. G. Thomas, I. V. Samarasekera, and J. K. Brimacombe, *Mathematical model of the thermal processing of steel ingots. II. Stress model*, Metallurgical and Materials Transactions B **18** (1987), No. 1, 131–147.

[98] J. E. Kelly, K. P. Michalek, T. G. O'Connor, and B. G. Thomas, *Initial development of thermal and stress fields in continuously cast steel billets*, Metallurgical and Materials Transactions A **19** (1988), No. 10, 2589–2602.

[99] Y. M. Won, H. N. Han, T. J. Yeo, and K. H. Oh, *Analysis of solidification cracking using the specific crack susceptibility*, ISIJ International **40** (2000), No. 2, 129–136.

[100] Lee D. N and H. S. Kim, *Plastic yield behavior of porous metals*, Powder Metallurgy (UK) **35** (1992), No. 4, 275–279.

[101] D. J. Seol, Y. M. Won, T. J. Yeo, K. H. Oh, J. K. Park, and C. H. Yim, *High temperature deformation behavior of carbon steel in the austenite and delta-ferrite regions*, ISIJ International **39** (1999), No. 1, 91–98.

[102] D. J. Seol, Y. M. Won, K. H. Oh, Y. C. Shin, and C. H. Yim, *Mechanical behavior of carbon steels in the temperature range of mushy zone*, ISIJ International **40** (2000), No. 4, 356–363.

[103] H. N. Han, Y. G. Lee, K. H. Oh, and D. N. Lee, *Analysis of hot forging of porous metals*, Materials Science and Engineering A **206** (1996), No. 1, 81–89.

[104] F. Garofalo, *An empirical relation defining the stress dependence of minimum creep rate in matals*, Transaction of the Metallurgical Society AIME **227** (1963), No. 2, 351–355.

[105] M. Uehara, I. V. Samarasekera, and J. K. Brimacombe, *Mathematical modeling of unbending of continuously cast steel slabs*, Ironmaking and Steelmaking **3** (1986), No. 3, 138–153.

[106] K. H. Kim, Ph.D. Thesis, Seoul National University, 1996.

[107] R. Eborall and P. Gregory, *The mechanism of embrittlement by a liquid phase*, Journal of the Institute of Metals **84** (1955), 88–90.

[108] Y. A. Skok, *Fracture of steel at temperatures close to solidus*, Stal **3** (1994), 40–43.

[109] I. I. Novikov and O. E. Grushko, *Hot cracking susceptibility of Al-Cu-Li and Al-Cu-Li-Mn alloys*, Materials Science and Technology **11** (1995), No. 9, 926–932.

[110] B. Magnin, L. Katgerman, and B. Hannart, *Physical and numerical modeling of thermal stress generation during DC casting of aluminum alloys*, Modeling of Casting, Welding and Advanced Solidification Processes VII (London, UK), 1995, 303–310.

[111] L. Zhao, N. Wang, V. Sahajwalla, and R. D. Pehlke, *The rheological properties and hot tearing behaviour of an Al-Cu alloy*, International Journal of Cast Metals Research **13** (2000), No. 3, 167–174.

[112] W. Poppmeier and B. Tarmann, *Étude de la formation des fissures lors de la coulée continue de billettes et de brames*, La Revue de Métallurgie **65** (1968), No. 2, 113–119.

[113] K. Schwerdtfeger, *Rissanfälligkeit von Stählen beim Stranggießen und Warmumformen*, Verlag Stahleisen GmbH, Düsseldorf, 1994.

[114] K. Nakayama, M. Kinefuchi, and T. Tsutsumi, *A measurement of critical strain for internal crack in continuously cast slabs*, Proceedings of the Modeling of Casting, Welding and Advanced Solidification Processes VIII (San Diego, USA), 1998, 915–923.

[115] H. Mizukami, K. Murakami, and T. Kitagawa, *Characteristics of embrittlement of continuously cast steel near the solidification temperature*, Tetsu-to-Hagané (Journal of Iron and Steel Institute Japan) **81** (1995), No. 8, 792–797.

[116] A. A. Howe, *Segregation and phase distribution during solidification of carbon, alloy and stainless steel*, Tech. Report, ECSC, EUR 13303, Luxembourg, 1991.

[117] Drezet J.-M., M. Gremaud, and M. Gäumann, *A new hot-tearing criterion for steel*, Proceedings of the 4th European Continuous Casting Conference (Birmingham, UK), 2002, 755–763.

[118] M. Braccini, C. L. Martin, and M. Suery, *Relation between mushy zone rheology and hot tearing phenomena in al-cu alloys*, Proceedings of the Modeling of Casting, Welding and Advanced Solidification Processes IX (Aachen, Germany), 2000, 18–24.

[119] M. Braccini, M. Suery, C. Laguerre, and M. Stucky, *Influence of grain refinement on hot tearing in aluminium-cooper alloys used in foundry industries*, La Revue de Métallurgie **100** (2003), No. 2, 157–164.

[120] J. Miettinen, *Mathematical simulation of interdendritic solidification of low-alloyed and stainless steels*, Metallurgical and Materials Transactions A **23** (1992), No. 4, 1155–1170.

[121] B. J. Keene, *Review of data for surface tension of iron and its binary alloys*, International Materials Reviews **33** (1988), No. 1, 1–37.

[122] B. J. Keene, *Review of data for the surface tension of pure metals*, International Materials Reviews **38** (1993), No. 4, 157–192.

[123] D. R. Poirier, H. Yin, M. Suzuki, and T. Emi, *Interfacial properties of dilute Fe-O-S melts on alumina substrates*, Stal **38** (1998), No. 3, 229–238.

[124] C. Cicutti and R. Boeri, *On the relationship between primary and secondary dendrite arm spacing in continuous casting products*, Scripta Materialia **45** (2001), No. 12, 1455–1460.

[125] M. M. Wolf, *Effect of solidification rate on microstructure*, Continuous Casting, Volume Nine, Initial Solidification and Strand Surface Quality of Peritectic Steels (Warrendale, USA), 1997, 69–78.

[126] C. Bernhard, *Mechanische Eigenschaften und Rissanfälligkeit erstarrender Stähle unter stranggießähnlichen Bedingungen*, Ph.D. Thesis, University of Leoben, 1998.

[127] M. Hanel, *Bestimmung von λ_2-Beziehungen für Stähle mit unterschiedlichen Kohlenstoffgehalten*, Baccalaureate Thesis, Department of Metallurgy, University of Leoben, 2007.

[128] *A guide to the solidification of steels*, Jernkontoret, Stockholm, 1977.

[129] M. El-Bealy and B. G. Thomas, *Prediction of dendrite arm spacing for low alloy steel casting processes*, Metallurgical and Materials Transactions B **27** (1996), 688–693.

[130] K. Schwerdtfeger, *Effect of solidification rate on microsegregation and interdendritic precipitation of manganese sulphide inclusions in a steel containing manganese and carbon*, Archiv Eisenhüttenwesen **41** (1970), No. 9, 923–937.

[131] A. Suzuki, T. Suzuki, Y. Nagaoka, and Y. Iwata, *On secondary dendrite arm spacing in commercial carbon steels with different carbon contents*, Tetsu-to-Hagané (Journal of Iron and Steel Institute Japan) **32** (1968), No. 12, 1301–1305.

[132] J. C. Fisher, *The fracture of liquids*, Journal of Applied Physics **19** (1948), 1062–1067.

[133] W. R. Tyson and W. A. Miller, *Surface free energies of solid metals – estimation from liquid surface tension measurements*, Surface Science **62** (1977), No. 1, 267–276.

[134] J. W. Taylor, *An evaluation of interface energies in metallic systems*, Journal of the Institute of Metals **86** (1957-58), 456–463.

[135] C. Bernhard, H. Hiebler, and M. M. Wolf, *Experimental simulation of subsurface crack formation in continuous casting*, La Revue de Métallurgie **97** (2000), No. 3, 333–344.

[136] G. VanDrunen, J. K. Brimacombe, and F. Weinberg, *Internal cracks in strand cast billets*, Ironmaking and Steelmaking **2** (1975), No. 2, 125–133.

[137] Y. Morita, H. Kawashima, and M. Nakamura, *Strain analysis on internal cracks in continuously cast steel slabs*, The Sumitomo Search **30** (1985), 19–30.

[138] Z. Han, K. Cai, and B. Liu, *Prediction and analysis on formation of internal cracks in continuously cast slabs by mathematical models*, ISIJ International **41** (2001), No. 12, 1473–1480.

[139] T. Mori, *High temperature deformation behaviour on solidification*, Transactions Iron and Steel Institute of Japan **25** (1985), No. 7, 648–652.

[140] R. Pierer, S. Michelic, C. Bernhard, and C. Chimani, *A hot tearing criterion for the continuous casting process*, METEC InSteelCon, Third International Conference on New Developments im Metallurgical Process Technologies (Düsseldorf, Germany), 2007, 893–900.

[141] A. Vaterlaus and M. M. Wolf, 7th Concast Technology Convention (Zürich, Switzerland), 1984.

[142] D. Sediako, O. Sediako, and K. J. Lin, *Some aspects of thermal analysis and technology upgrading in steel continuous casting*, Canadian Metallurgical Quarterly **38** (1999), No. 5, 377–385.

[143] P. Ackermann, W. Kurz, and W. Heinemann, *In situ tensile testing of solidifying aluminium and Al-Mg shells*, Materials Science and Engineering **75** (1985), No. 1-2, 79–86.

[144] J. D. Wagnieres and P. Ackermann, *Le laboratoire d'aujourd'hui pour les brames de demain*, La Revue Politechnique **6** (1985), 669–673.

[145] C. Bernhard, H. Hiebler, and M. M. Wolf, *The effect of P and B on crack susceptibility: new results of the SSCT test*, Proceedings of the Second International Conference on Continuous Casting of Steel in Developing Countries (Wuhan, China), 1997, 224–229.

[146] C. Bernhard, H. Hiebler, and M. M. Wolf, *Shell strength versus P and B content measured by the SSCT test (Prevention of inner crack formation in continuous casting)*, 134th ISIJ Meeting (Senda, Japan), 1997, 972.

[147] C. Bernhard and M. M. Hiebler, H. Wolf, *Simulation of shell strength properties by the SSCT test*, ISIJ International, Suppl. Science and Technology of Steelmaking **36** (1996), 163–166.

[148] C. Bernhard, H. Hiebler, and M. M. Wolf, *The influence of phosphorus on the mechanical properties of carbon steels near the melting point at low strain rate*, Belton Memorial Symposium Proceedings (Sydney, Australia), 2000, 263–272.

[149] H. Hiebler and C. Bernhard, *Mechanical properties and crack susceptibility of steel during solidification*, Steel Research **69** (1999), No. 8+9, 349–355.

[150] C. Bernhard, *Simulation of internal crack formation in continuous casting of steel*, BHM **145** (2000), No. 1, 22–29.

[151] S. Michelic, *Development of an inverse thermal model of the SSCT-test*, Baccalaureate Thesis, Department of Metallurgy, University of Leoben, 2004.

[152] G. Xia, *Untersuchung über das mechanische Verhalten von erstarrendem Sthal unter stranggußähnlichen Bedingungen*, Ph.D. Thesis, University of Leoben, 1992.

[153] ABAQUS, *Standard user's manual, version 6.1*, Hibbit, Kalsson & Sorensen Inc., 2003.

[154] COMSOL AB., *Comsol multiphysics modelling guide*, COMSOL AB., 2005.

[155] R. Pierer, C. Bernhard, and C. Chimani, *Experimental and analytical analysis of high-temperature mechanical properties of steel under continuous casting conditions*, Computational Methods and Experimental Measurements XII, CMEM (Malta), 2005, 757–768.

[156] J. Reiter and R. Pierer, *Thermo-mechanical simulation of a laboratory test to determine mechanical properties of steel near the solidus temperature*, FEMLAB Conference (Frankfurt, Germany), 2005, 247–253.

[157] H. Stocker, *Untersuchung unterschiedlicher Einflussfaktoren auf die Heißrissbildung von Kohlenstoffstählen*, Master's thesis, University of Leoben, 2007.

[158] A. Jablonka, K. Harste, and K. Schwerdtfeger, *Thermomechanical properties of iron and iron–carbon alloys: Density and thermal contraction*, Steel Research **62** (1991), No. 1, 24–33.

[159] K. Harste, *Untersuchungen zur Schrumpfung und zur Entstehung von mechanischen Spannungen während der Erstarrung und nachfolgender Abkühlung zylindrischer Blöcke aus Fe-C-Legierungen*, Ph.D. Thesis, University of Clausthal, 1989.

[160] I. Jimbo and A. A. W. Cramb, *The density of liquid iron-carbon alloys*, Metallurgical and Materials Transactions B **24** (1993), No. 1, 5–10.

[161] M. C. M. Cornellissen, *Mathematical model for solidification of multicomponent alloys*, Ironmaking and Steelmaking **13** (1986), 204–212.

[162] Y. Nakamura and H. Esaka, Tetsu-to-Hagané (Journal of Iron and Steel Institute Japan) **67** (1981), S140.

[163] G. Wieser, *Relation between local solidification time and secondary dendrite arm spacing*, Private Communication, 2003.

[164] F. Rakoski, *Einfluss von Mangan, Schwefel und Phosphor auf die Hochtemperaturfestigkeits- und -zähigkeitseigenschaften von Baustahl mit Kohlenstoffgehalten von 0.015 bis 1 % nach der Erstarrung aus der Schmelze*, Ph.D. Thesis, University of Aachen, 1984.

[165] H. G. Suzuki, S. Nishimura, and Y. Nakamura, *Improvement of hot ductility of continuously cast carbon steels*, Transactions Iron and Steel Institute of Japan **24** (1984), No. 1, 54–59.

List of Figures

List of Tables

A The Microsegregation Model

This seems to be one of the many cases in which the admitted accuracy of mathematical processes is allowed to throw a wholly inadmissible appearance of authority over the results obtained by them. Mathematics may be compared to a mill of exquisite workmanship, which grinds your stuff of any degree of fineness; but, nevertheless, what you get out depends on what you put in; and as the grandest mill in the world will not extract wheat flour from peascods, so pages of formulae will not get a definite result out of loose data.[a]

THOMAS HENRY HUXLEY

[a]Quarterly Journal of the Geological Society, 25, 1869

The non equilibrium (true) solidus temperature – in the present thesis referred to as solidus temperature T_S – strongly depends on the cooling conditions. In fact, the solidus temperature can be calculated using empirical formulas. However, these equations do not consider the cooling conditions, which results in inaccurate values of T_S. Therefore, the microsegregation as well as the influence of the solidification conditions must be taken into account.

In Chapter 2, different microsegregation approaches[49–53] were already mentioned. The present study uses the model proposed by Ueshima *et al.*[54] to calculate the solute redistribution during solidification. The following assumption are made:

- The transverse cross section of the dendrites is approximated by a regular hexagon, which is schematically illustrated in Fig. A.1a.
- In the transverse section of the dendrites the concentrations of solutes in liquid are uniform, in axial direction of the dendrites the diffusion in solid and liquid is neglected. This results in a one-dimensional diffusion in the x direction as illustrated in Fig. A.1b.
- The development of the γ-phase occurs from the interface between δ and the liquid phase. At the interfaces (s/l and δ/γ), the solutes are distributed in equilibrium.

Using a finite difference method and applying the above mentioned assumptions, the diffusion and distribution of solutes can be calculated for three existing phases (δ, γ and liquid). Thus, the analysis can be done by dividing half the area of the secondary dendrite arm spacing λ_2 into k_N

nodes (see Fig. A.1b). In this figure, i is the node number and L_i denotes the length of the interface between the nodal areas i and $i+1$. The area of the i^{th} node is referred to as A_i with the width Δx. The rates of diffusion into solid and liquid phases are calculated using the following equations:

$$\text{In the } \delta - \text{phase } (2 \leq i \leq N^{\delta/\gamma}) \text{ and the } \gamma - \text{phase } (N^{\delta/\gamma}+1 \leq i \leq N^{\gamma/L}):$$
$$\frac{\Delta C_i^j}{\Delta t} = D^j \frac{L_i^j \cdot (C_{i+1}^j - C_i^j) - L_{i-1}^j \cdot (C_i^j - C_{i-1}^j)}{A_i \cdot \Delta x} \tag{A.1}$$

$$\text{In the } \delta - \text{phase } (i = 1):$$
$$\frac{\Delta C_1^\delta}{\Delta t} = D^\delta \frac{L_1 \cdot (C_2^\delta - C_1^\delta)}{A_1 \cdot \Delta x} \tag{A.2}$$

$$\text{At the } \delta/\gamma \text{ interface } (\delta - \text{phase}: \ i = N^{\delta/\gamma} - 1; \quad \gamma - \text{phase}: \ i = N^{\delta/\gamma}):$$
$$C^\gamma_{N^{\delta/\gamma}} = C^\delta_{N^{\delta/\gamma}-1} \cdot k^{\gamma/\delta} \tag{A.3}$$

In these equations, j is δ or γ phase, C is the solute concentration ($wt.$-%), D denotes the diffusion coefficient, $k^{\gamma/\delta}$ denotes the distribution coefficient between γ and δ phases, $N^{\delta/\gamma}$ and $N^{\gamma/L}$ are the interfaces between δ and γ phase and γ and liquid phase, respectively.

Applying a mass balance to the δ/γ interface results in the following equation:

$$\frac{\Delta C^\delta_{N^{\delta/\gamma}-1}}{\Delta t} = \frac{D^\gamma \cdot L_{N^{\delta/\gamma}} \cdot (C^\gamma_{N^{\delta/\gamma}+1} - C^\gamma_{N^{\delta/\gamma}}) - D^\delta \cdot L_{N^{\delta/\gamma}-2} \cdot (C^\delta_{N^{\delta/\gamma}-1} - C^\delta_{N^{\delta/\gamma}-2})}{(A_{N^{\delta/\gamma}-1} + A_{N^{\delta/\gamma}} \cdot k^{\gamma/\delta}) \cdot \Delta x} \tag{A.4}$$

Considering the mass balance of solid and liquid phases at the δ/L interface, the following equations can be written:

$$C^\gamma_{N^{\gamma/L}} = C^L \cdot k^{\gamma/L} \tag{A.5}$$

$$F_1 = C_0 - \sum_{i=1}^{N^{\gamma/L}-1} C_i \cdot A_i / \sum_{i=1}^{k_N} A_i \tag{A.6}$$

$$F_2 = \left(k^{\gamma/L} \cdot A_{N^{\gamma/L}} + \sum_{i=N^{\gamma/L}+1}^{k_N} A_i \right) / \sum_{i=1}^{k_N} A_i \tag{A.7}$$

$$C^L = \frac{F_1}{F_2} \tag{A.8}$$

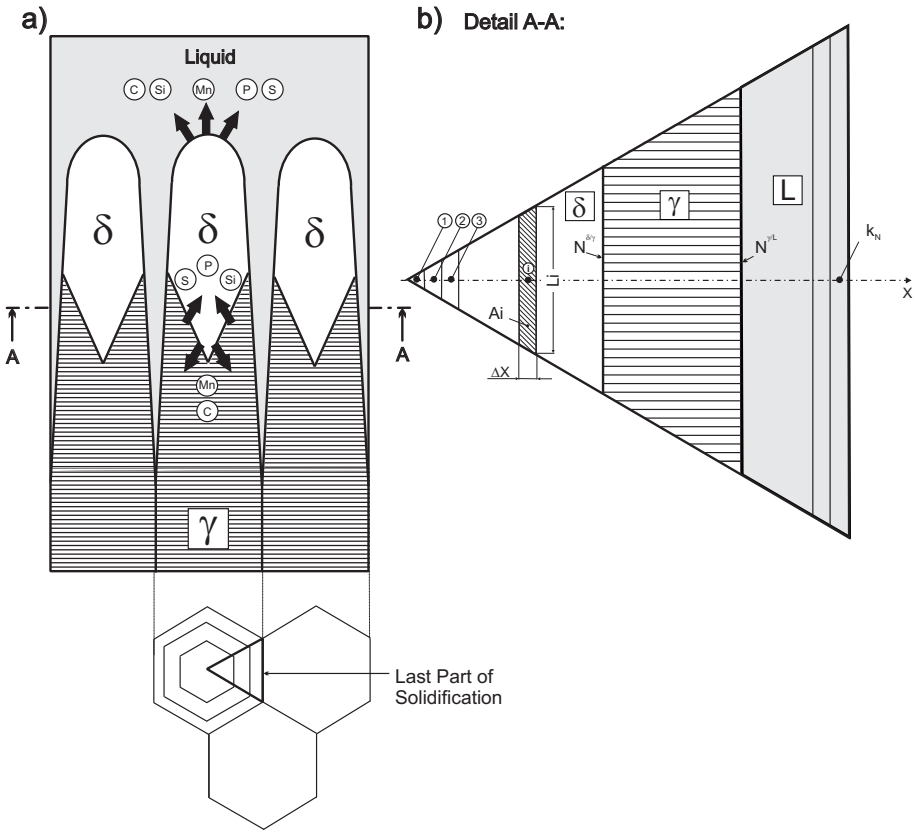

Figure A.1: *a) Longitudinal and transverse cross section of dendrites (schematically) and b) part of the transverse cross section together with numerical discretisation according to Ueshima* et al.*[54].*

In the above illustrated equations, $k^{\gamma/L}$ is the distribution coefficient between γ and liquid phases and C_0 is the average concentration.

A further assumption of the calculation procedure is the parabolic growth rate. In order to account for the shell growth rate, the local solidification time t_f must be determined. This is done by means of the empirical equation between t_f an λ_2, where the latter is used as an input parameter[163]:

$$\lambda_2 = 14.775 \cdot t_f^{0.475} \tag{A.9}$$

In the calculation procedure, the solidification or the $\delta - \gamma$ transformation in a given area is complete when the liquidus temperature T_L and the $\delta - \gamma$ transformation temperature $T_{\delta/\gamma}$ become equal to the actual temperature. These temperatures are given by:

$$T_L = T_L^j + \sum_i m_i^j \cdot C_i^0 \tag{A.10}$$

$$T_{\delta/\gamma} = T_{pure}^{\delta/\gamma} + \sum_i m_i^{\delta/\gamma} \cdot k_i^{\delta/L} \cdot C_{L,i} \tag{A.11}$$

In these equations, j is the δ or γ phase, i is the element and C^0 denotes the initial concentration. The liquidus temperature of the δ and γ phase is $T_L^\delta = 1536$ and $T_L^\gamma = 1525.4$ °C, respectively and the $T_{pure}^{\delta/\gamma}$ is the temperature of the $\delta-\gamma$ transformation of pure iron (1392 °C). The parameter m and the equilibrium distribution coefficients of the elements are summarised in Tab. A.1. Additionally, the diffusion coefficients* (cm^2/s) used in the calculations are illustrated in Tab. A.1. A further important point in the calculation procedure is the consideration of the MnS precipitation, which is not included in the original study of Ueshima *et al.*[54]. In order to determine the solubility product of MnS, the following relation is used in the present thesis:

$$\log K_{MnS} = -\frac{8750}{T(K)} + 4.63 \tag{A.12}$$

It is assumed that the MnS precipitation starts when $[Mn] \cdot [S] > K_{MnS}$. Thus, the MnS precipitation takes place until the stoichiometric equilibrium is reached.

Element	m^δ	m^γ	$m^{\delta/\gamma}$	$k^{\delta/L}$	$k^{\gamma/L}$	D^δ	D^γ
C	-82.7	-60.9	1122	0.19	0.34	$0.0127\exp(-19450/RT)$	$0.0761\exp(-32160/RT)$
Si	-9.0	-11.9	-60	0.77	0.52	$8.0\exp(-59500/RT)$	$0.3\exp(-60100/RT)$
Mn	-5.1	-4.2	12	0.76	0.72	$0.76\exp(-53640/RT)$	$0.055\exp(-59600/RT)$
P	-34	-33.4	-140	0.23	0.13	$2.9\exp(-55000/RT)$	$0.01\exp(-43700/RT)$
S	-40	-37.7	-160	0.05	0.035	$4.56\exp(-51300/RT)$	$2.4\exp(-53400/RT)$

Table A.1: *The liquidus line slopes m, the equilibrium distribution coefficients k [52,161,53] and the diffusion coefficients D [53,162] of the solute elements.*

It can be summarised that the determination of the fraction of solid as a function of temperature using microsegregation models is an important basis for the solidification calculations. The prediction as well as the validation of (true) solidus temperatures considering the cooling conditions is a complex task. The validation of microsegregation models can be done by comparing measured and calculated values of zero ductility temperatures. This was carried out within the scope of a master thesis[157] in conjunction with the present thesis using the above described and modified model[54]. Fig. A.2 shows the comparison of the measured[41,42,102,164,165] and calculated (according to a f_S of 0.99) zero ductility temperatures. Detailed considerations of these results are provided by Stocker[157]. Nevertheless, it can be seen that the calculated ZDT is in good agreement with the measured values.

The major parameters of the calculation are the equilibrium distribution coefficients, the diffusion coefficients of the solute elements and the input parameter λ_2. The first two coefficients are taken from literature. The used relation between local solidification time and secondary dendrite arm spacing results from λ_2-measurements of previously conducted SSCT experiments. The secondary dendrite arm spacing of the tested steel grades was assumed to be 30 μm. In a first step, this seems to be a sufficient assumption due to the applied constant cooling conditions. However, in order to

*Notes: In the equations of D, R is the gas constant (1.987 $cal/molK$) and T is the temperature in Kelvin

improve the quality of the calculations, recently a study was started with the aim of measuring secondary dendrite arm spacing as a function of the carbon content and the local solidification time using SSCT specimen of the present study. On completion of the present thesis, first results were available showing values of λ_2 between 20 and 50μm. However, the determined relations between local solidification time and secondary dendrite arm spacing could not be considered in the microsegregation analysis.

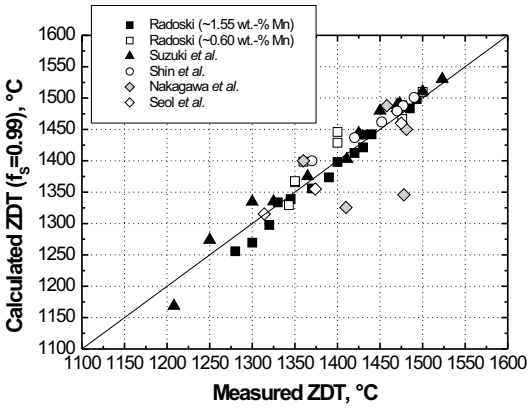

Figure A.2: *Comparison of measured and calculated ($f_S = 0.99$) ZDT using the modofied microsegregation model according to Ueshima* et al.*[54].*

Finally, the MnS precipitation must also be considered in the microsgregation analysis. Calculations without MnS precipitation would lead to very high enrichment of sulphur and consequently to very small values of the solidus temperature, which was shown in the literature[126].

B Experimental Data

Statistics are like a bikini. What they reveal is suggestive, but what they conceal is vital.[a]
Aaron Levenstein

[a]Unsourced

B.1 As-is Analysis and Testing Parameters of the Different Test Series

Test No.	C	Si	Mn	P	S	T_{SB}	s_{coat}	$\dot{\varepsilon}$	HT
A01	0.17	0.27	1.30	0.005	0.007	1539	0.40	0.002	4
A02	0.18	0.30	1.40	0.005	0.007	1541	0.15	0.002	4
A03	0.17	0.30	1.44	0.005	0.007	1544	0.40	0.002	8
A04	0.17	0.26	1.36	0.005	0.007	1542	0.15	0.002	8
A05	0.18	0.30	1.29	0.004	0.005	1550	0.40	0.002	12
A06	0.16	0.24	1.40	0.005	0.007	1542	0.15	0.002	12
A07	0.18	0.30	1.29	0.004	0.005	1550	0.40	0.006	4
A08	0.17	0.26	1.46	0.005	0.007	1548	0.15	0.006	4
A09/1	0.16	0.24	1.37	0.005	0.007	1547	0.40	0.006	8
A09/2	0.18	0.24	1.42	0.005	0.007	1543	0.40	0.006	8
A10	0.17	0.25	1.39	0.005	0.007	1539	0.15	0.006	8
A11	0.18	0.24	1.34	0.005	0.007	1541	0.40	0.006	12
A12	0.18	0.26	1.37	0.005	0.007	1543	0.15	0.006	12

Table B.1: *Chemical composition (as-is analysis in wt.-%) of the investigated carbon steel (construction steel), steel bath temperature (in* °C*), coating thickness (in mm), strain rate (in* s^{-1}*) and holding time (in s).*

Test No.	C	Si	Mn	P	S	T_{SB}	ε_{tot}	$\dot{\varepsilon}$
B01	0.05	0.25	1.30	0.006	0.007	1556	2	0.002
B02	0.05	0.21	1.13	0.005	0.008	1549	3	0.002
B03	0.06	0.26	1.27	0.004	0.005	1557	2	0.006
B04	0.05	0.29	1.28	0.004	0.005	1550	3	0.006
B05	0.05	0.30	1.29	0.004	0.005	1550	3	0.012
C01	0.08	0.26	1.20	0.007	0.008	1550	3	0.002
C02	0.08	0.30	1.36	0.007	0.008	1550	2	0.002
C03	0.08	0.29	1.16	0.004	0.006	1546	2	0.002
C04	0.08	0.30	1.29	0.004	0.006	1550	1	0.002
C05	0.08	0.30	1.27	0.004	0.005	1555	-	-
C06	0.08	0.29	1.31	0.003	0.005	1546	0.6	0.006
C07	0.09	0.28	1.33	0.003	0.005	1546	0.9	0.006
C08	0.07	0.28	1.30	0.003	0.005	1541	1.2	0.006
D01	0.12	0.30	1.35	0.007	0.008	1544	3	0.002
D02	0.12	0.28	1.34	0.007	0.007	1546	2	0.002
D03	0.12	0.32	1.25	0.004	0.007	1541	2	0.002
D04	0.12	0.28	1.26	0.005	0.007	1543	1	0.002
D05	0.12	0.29	1.33	0.004	0.006	1542	0.5	0.002
D06	0.12	0.34	1.27	0.004	0.005	1551	-	-
D07	0.12	0.28	1.35	0.004	0.006	1544	1	0.006
D08	0.12	0.28	1.33	0.004	0.006	1546	1.5	0.006
D09	0.12	0.27	1.31	0.004	0.006	1542	2	0.006
E01	0.16	0.31	1.28	0.006	0.007	1548	2	0.002
E02	0.15	0.26	1.32	0.007	0.007	1540	1.5	0.002
E03	0.16	0.30	1.27	0.005	0.007	1542	1	0.002
E04	0.15	0.27	1.31	0.004	0.007	1540	0.5	0.002
E05	0.16	0.30	1.28	0.004	0.005	1546	-	-
F01	0.29	0.28	1.33	0.007	0.007	1540	2.0	0.002
F02	0.30	0.27	1.26	0.008	0.007	1528	2.0	0.002
F03	0.31	0.34	1.28	0.005	0.008	1530	1	0.002
F04	0.30	0.28	1.32	0.004	0.007	1524	0.5	0.002
F05	0.30	0.29	1.29	0.004	0.007	1536	-	-
G01	0.50	0.26	1.30	0.008	0.007	1514	3	0.002
G02	0.51	0.29	1.28	0.007	0.007	1516	2	0.002
G03	0.47	0.32	1.31	0.005	0.008	1515	1	0.002
G04	0.48	0.29	1.33	0.004	0.009	1510	0.5	0.002
G05	0.51	0.29	1.28	0.004	0.008	1520	-	-
H01	0.70	0.27	1.32	0.009	0.008	1505	3.0	0.002
H02	0.70	0.25	1.34	0.007	0.007	1506	2.0	0.002
H03	0.66	0.29	1.32	0.008	0.008	1503	2.0	0.002
H04	0.66	0.31	1.36	0.005	0.009	1505	1.0	0.002
H05	0.69	0.29	1.41	0.004	0.009	1498	0.5	0.002
H06	0.70	0.29	1.29	0.004	0.010	1506	-	-

Table B.2: *Chemical composition (as-is analysis in wt.-%), steel bath temperature (in* °C*), applied total strain (in %) and strain rate (in* s^{-1}*) for test series B – H.*

B.2 Parameters of the Metallographic Analysis

	Data from Experiments						*Gauss fit*	
Test No.	NHT	SD	LHT	SD	ATL	SD	Gaussian Mean	Width
A01	3.50	0.79	3.86	1.18	1.10	0.14	3.15	0.59
A02	2.13	0.78	1.55	1.04	0.73	0.39	5.49	0.60
A03	4.00	1.14	4.76	1.77	1.19	0.42	4.33	3.56
A04	1.86	0.75	1.54	0.81	0.83	0.29	5.59	1.56
A05	5.14	0.89	7.18	2.82	1.39	0.53	3.81	1.21
A06	2.25	0.97	1.83	1.15	0.81	0.29	6.72	0.38
A09/1	9.57	1.14	6.28	2.34	0.66	0.31	3.36	0.62
A09/2	9.63	1.41	6.68	1.03	0.60	0.33	3.47	0.67
A10	3.17	0.95	2.47	0.96	0.78	0.26	4.09	1.19
A11	9.62	1.86	8.49	2.24	0.88	0.48	3.20	1.71
A12	4.50	1.52	3.44	1.88	0.79	0.42	3.82	2.53

Table B.3: *Number of hot tears (NHT), length of hot tears (LHT, mm), average tear length (ATL, mm) and standard deviation (SD) as well as the Gaussian mean (in mm) and width (in mm) resulting from the Gauss fit of the tear distribution within the shell (test series A).*

	Data from Experiments						*Gauss fit*	
Test No.	NHT	SD	LHT	SD	ATL	SD	Gaussian Mean	Width
B01	0	0	0	0	0	0	0	0
B02	0	0	0	0	0	0	0	0
B03	4.75	1.51	3.60	1.68	0.76	0.29	6.00	0.54
B04	7.50	1.49	6.86	1.44	0.91	0.42	6.24	0.99
B05	8.25	1.94	7.57	2.05	0.92	0.36	6.13	0.84
C01	11.00	2.34	16.06	2.23	1.46	0.80	6.67	0.94
C02	3.50	0.69	3.36	1.64	0.96	0.64	6.65	0.33
C03	4.50	1.73	4.46	1.64	0.99	0.64	5.49	4.29
C04	1.50	0.79	1.02	0.69	0.68	0.28	4.39	1.53
C05	0.00	0.00	0.00	0.00	0.00	0.00	0.00	0.00
C06	2.50	0.53	2.23	1.39	0.89	0.36	4.87	0.58
C07	6.75	1.58	5.72	1.10	0.85	0.34	5.40	0.94
C08	10.75	1.67	10.11	1.54	0.94	0.38	5.84	0.88
D01	7.25	2.07	13.12	4.37	1.81	0.81	6.98	0.90
D02	3.50	2.35	4.24	2.72	1.21	0.66	6.44	0.58
D03	5.43	1.21	7.75	2.77	1.43	0.62	6.24	0.38
D04	1.25	0.71	1.55	0.79	1.24	0.49	5.00	0.15
D05	0.75	0.46	0.90	0.64	1.20	0.24	5.37	0.29
D06	0.75	0.44	0.81	0.55	1.08	0.35	-	-
D07	1.38	0.52	1.12	1.37	0.81	0.31	4.75	0.46
D08	6.13	1.62	5.39	1.33	0.88	0.29	5.05	1.12
D09	8.33	0.58	12.46	1.44	1.04	0.36	5.00	0.59
E01	4.33	1.50	6.94	1.41	1.60	0.75	7.59	3.30
E02	3.63	1.26	5.47	1.65	1.51	0.70	6.07	3.15
E03	3.13	0.84	5.23	2.91	1.67	0.61	5.91	0.59
E04	2.00	0.82	2.80	1.04	1.40	0.59	6.20	0.34
E05	2.38	1.03	3.22	1.04	1.35	0.27	-	-
F01	7.63	1.69	11.51	5.31	1.51	0.74	6.47	3.60
F02	9.38	1.84	18.20	3.22	1.94	0.78	6.15	1.81
F03	6.88	1.68	11.35	3.65	1.65	0.51	5.10	0.73
F04	3.13	1.13	4.19	2.00	1.34	0.49	5.63	1.51
F05	1.58	0.49	2.05	1.56	1.30	0.15	-	-
G01	8.25	0.96	18.40	4.29	2.23	0.97	4.61	0.83
G02	2.83	1.67	4.88	2.84	1.72	0.58	4.77	1.83
G03	2.75	1.21	4.08	0.91	1.48	0.59	4.36	0.72
G04	1.62	0.75	2.39	1.07	1.47	0.30	4.75	0.54
G05	0.88	0.55	1.11	0.30	1.26	0.38	-	-
H01	6.25	2.38	14.35	2.27	2.29	0.66	4.23	0.91
H02	3.75	1.91	6.61	2.76	1.76	0.41	3.18	2.35
H03	-	-	-	-	-	-	-	-
H04	2.25	1.29	3.69	1.32	1.64	0.41	3.85	0.44
H05	1.25	0.52	2.07	0.68	1.66	0.55	3.18	0.52
H06	0.75	0.47	0.66	0.19	0.88	0.36	-	-

Table B.4: *Number of hot tears (NHT), length of hot tears (LHT, mm), average tear length (ATL, mm) and standard deviation (SD) as well as the Gaussian mean (in mm) and width (in mm) for test series B-H.*

B.3 Shell Growth of the Tested Steel Grades

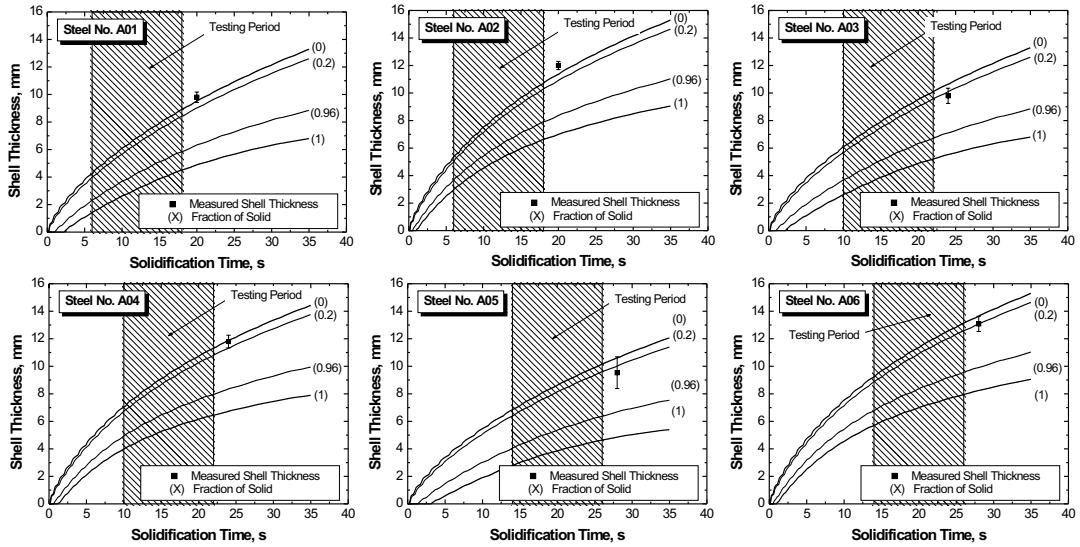

Figure B.1: *Calculated shell growth for a solid fraction of 0, 0.2, 0.96 and 1, measured shell thickness and range of straining for the test series A (strain rate:* $0.002\ s^{-1}$*).*

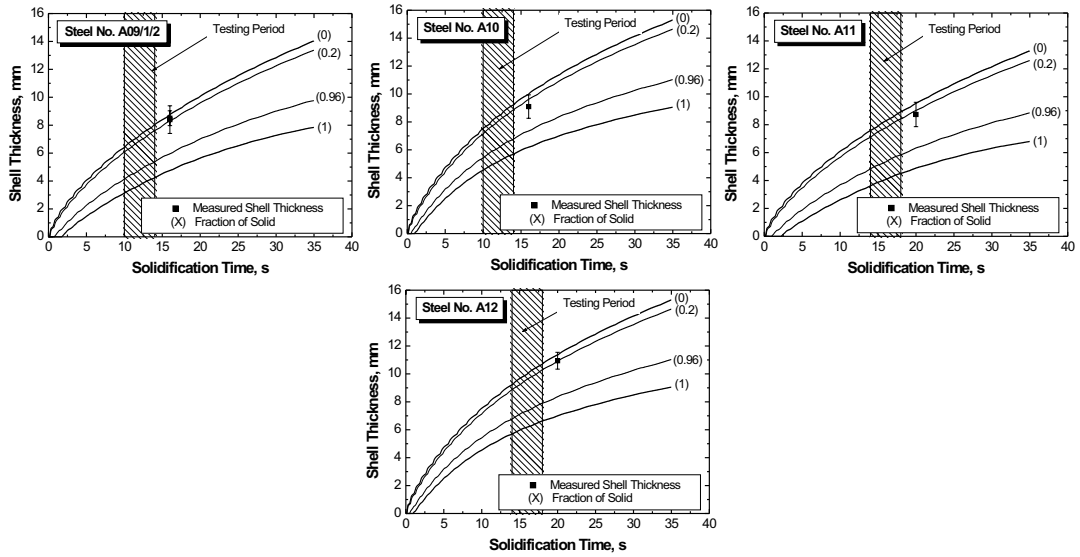

Figure B.2: *Calculated shell growth for a solid fraction of 0, 0.2, 0.96 and 1, measured shell thickness and range of straining for the test series A (strain rate:* $0.006\ s^{-1}$*).*

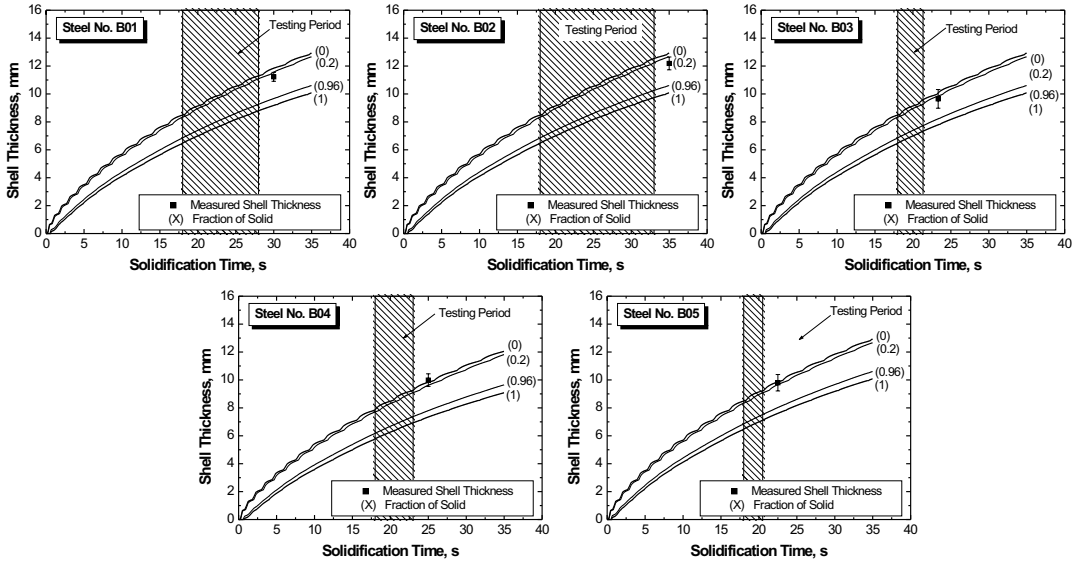

Figure B.3: *Calculated shell growth for a solid fraction of 0, 0.2, 0.96 and 1, measured shell thickness and range of straining for the 0.05 wt.-%C steel.*

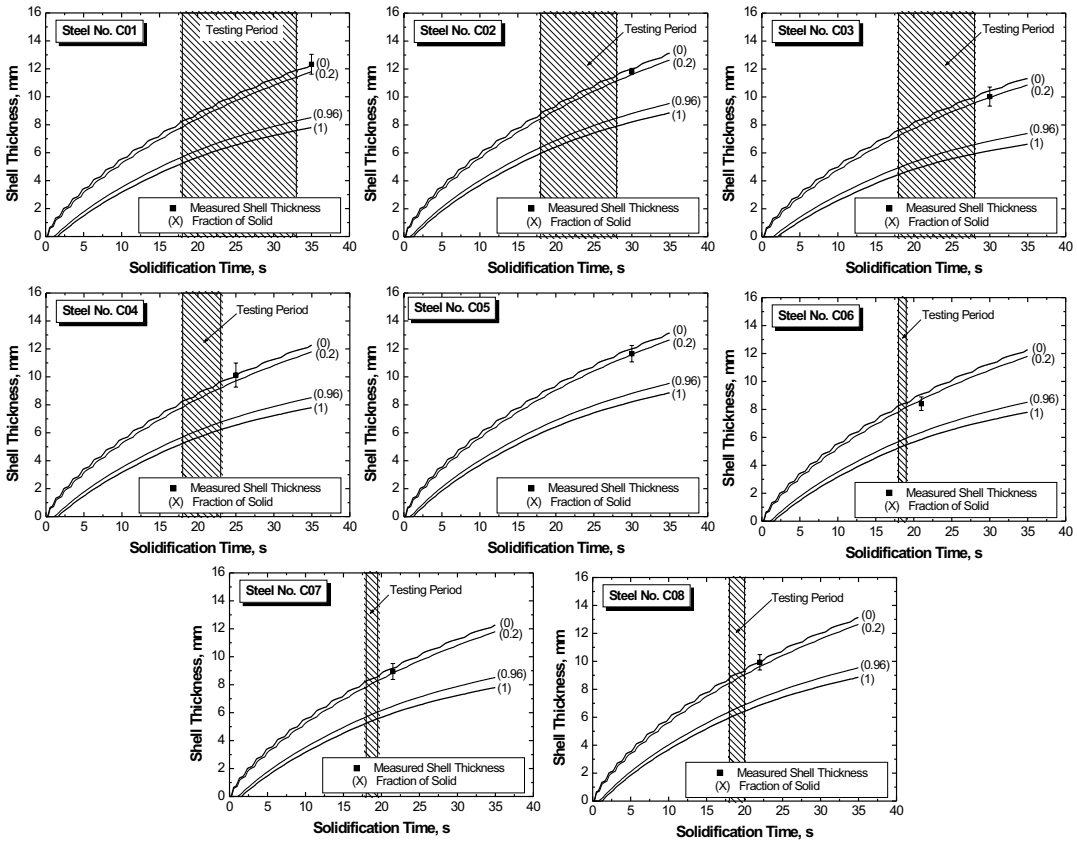

Figure B.4: *Calculated shell growth for a solid fraction of 0, 0.2, 0.96 and 1, measured shell thickness and range of straining for the 0.08 wt.-%C steel.*

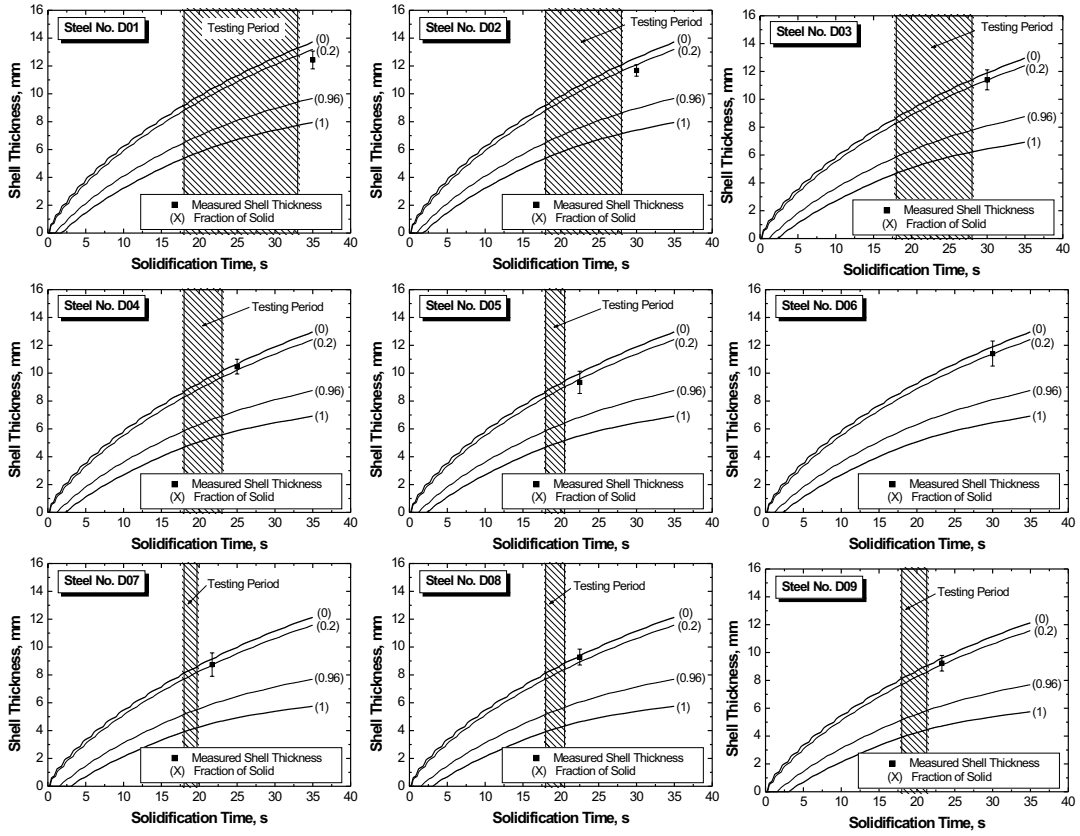

Figure B.5: *Calculated shell growth for a solid fraction of 0, 0.2, 0.96 and 1, measured shell thickness and range of straining for the 0.12 wt.-%C steel.*

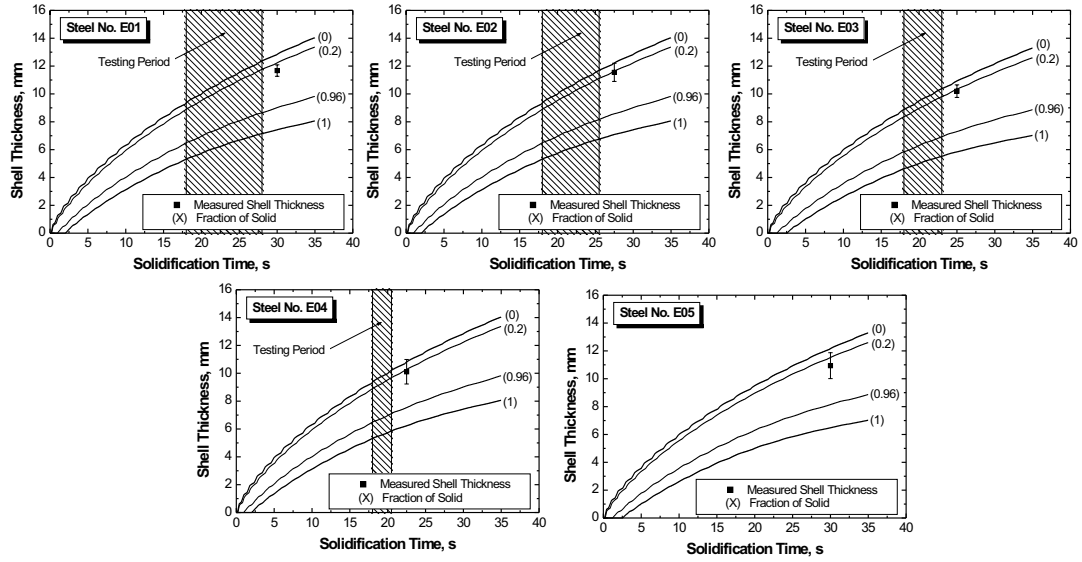

Figure B.6: *Calculated shell growth for a solid fraction of 0, 0.2, 0.96 and 1, measured shell thickness and range of straining for the 0.16 wt.-%C steel.*

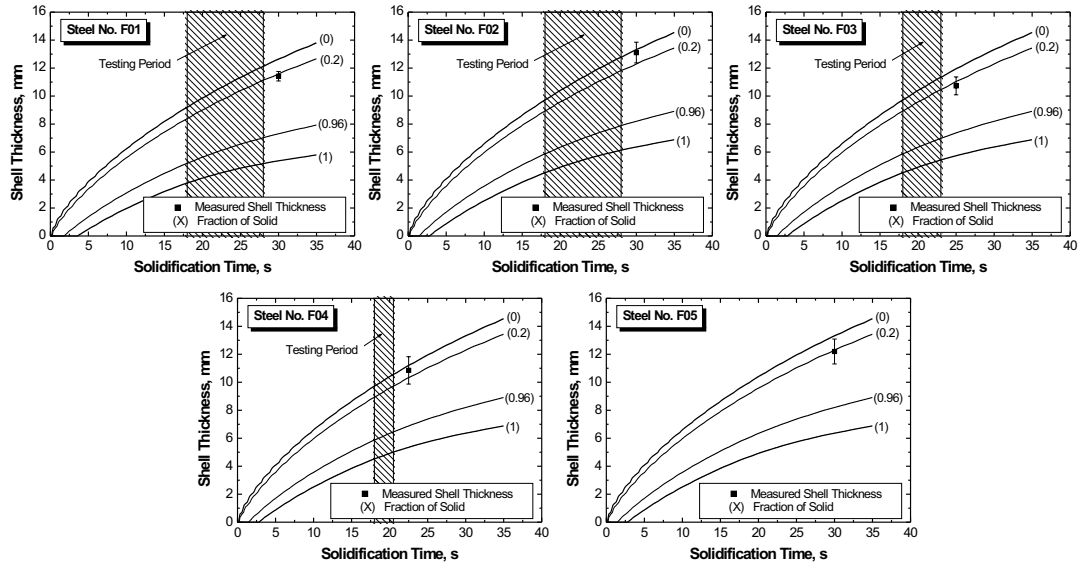

Figure B.7: *Calculated shell growth for a solid fraction of 0, 0.2, 0.96 and 1, measured shell thickness and range of straining for the 0.30 wt.-%C steel.*

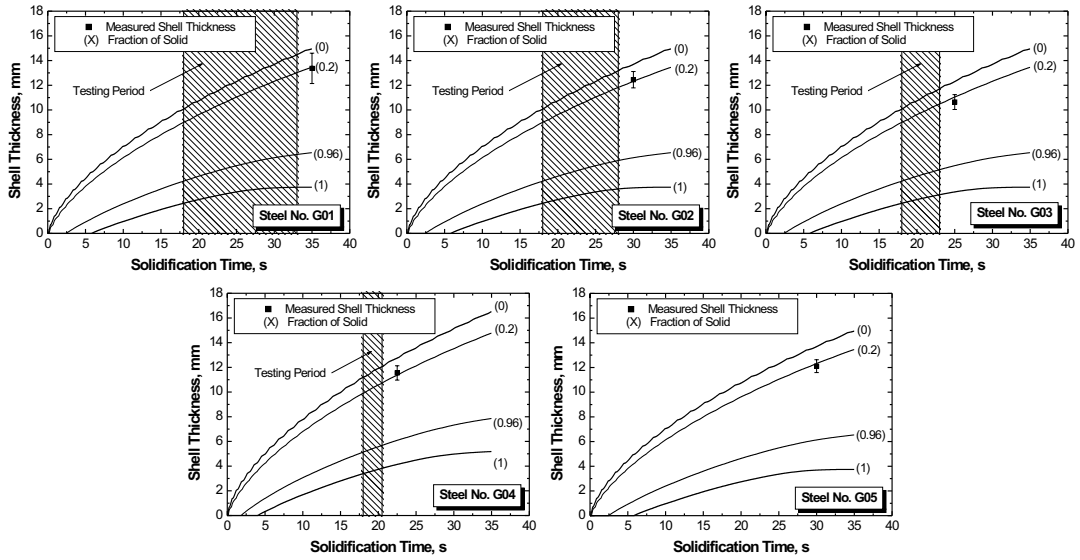

Figure B.8: *Calculated shell growth for a solid fraction of 0, 0.2, 0.96 and 1, measured shell thickness and range of straining for the 0.50 wt.-%C steel.*

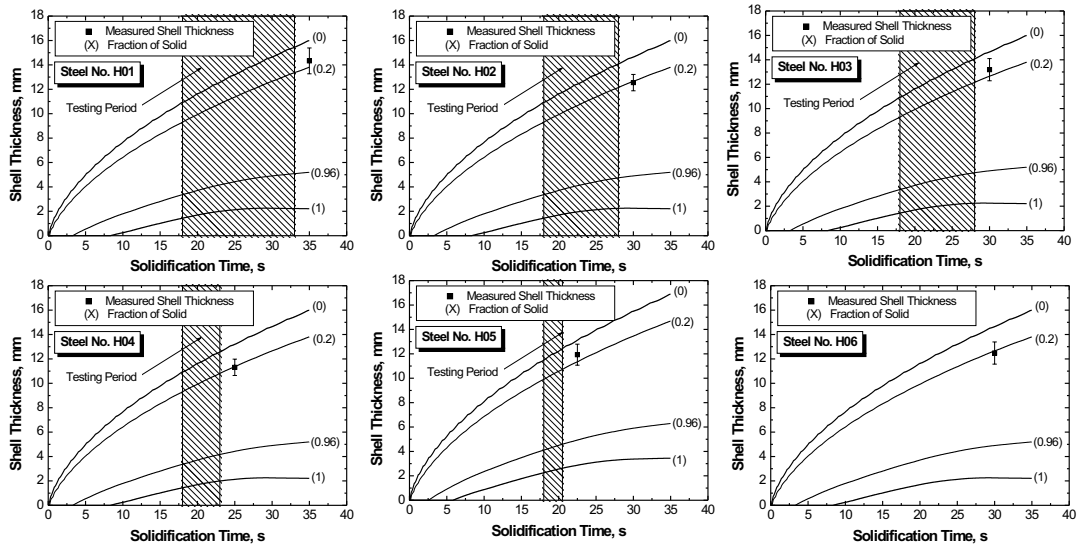

Figure B.9: *Calculated shell growth for a solid fraction of 0, 0.2, 0.96 and 1, measured shell thickness and range of straining for the 0.70 wt.-%C steel.*

B.4 Measured versus Calculated Shell Thickness

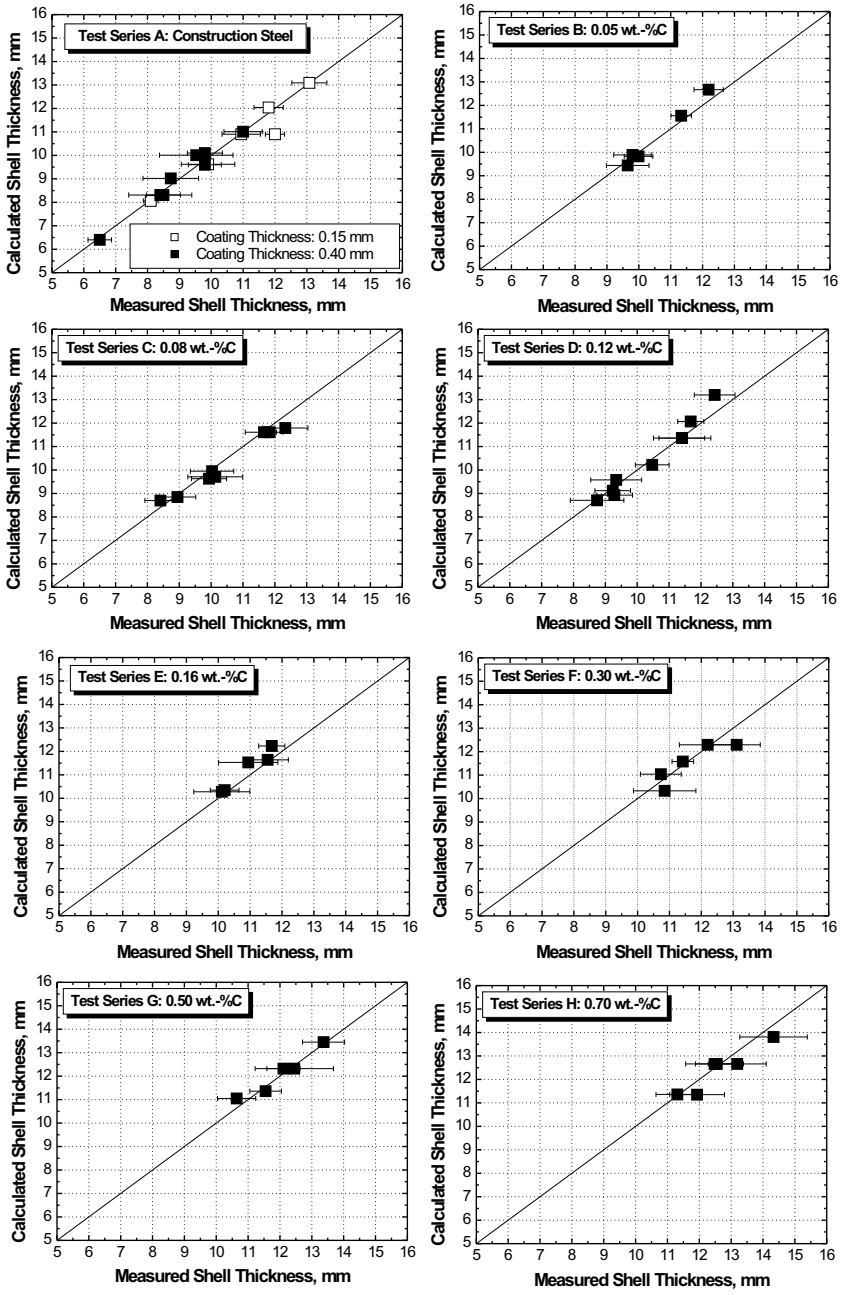

Figure B.10: *Calculated shell thickness versus measured shell thickness for all test series.*

B.5 Distribution of Detected Number of Hot Tears for all Test Series

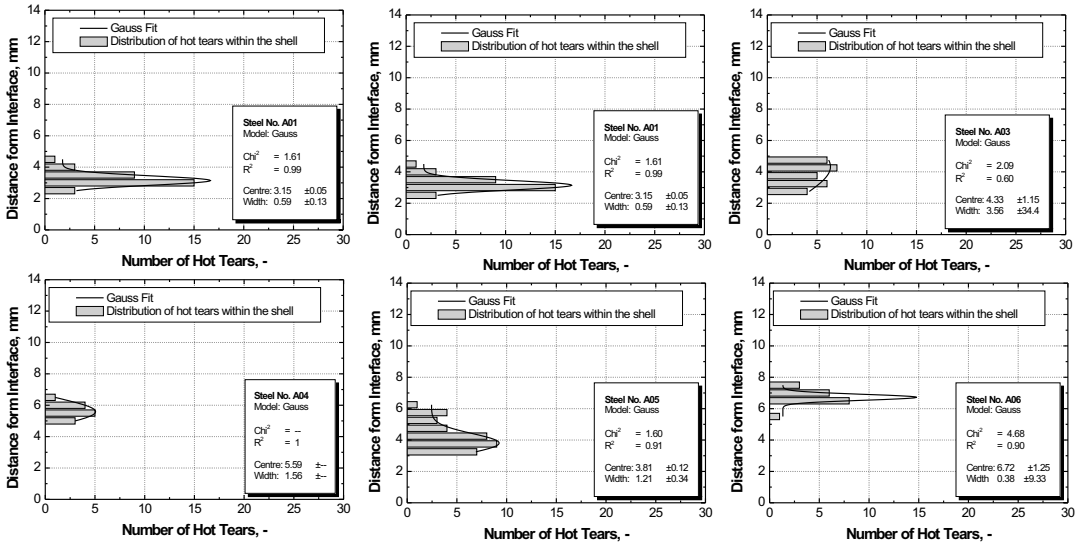

Figure B.11: *Distribution of detected number of hot tears for test series A (strain rate:* $0.002\ s^{-1}$*).*

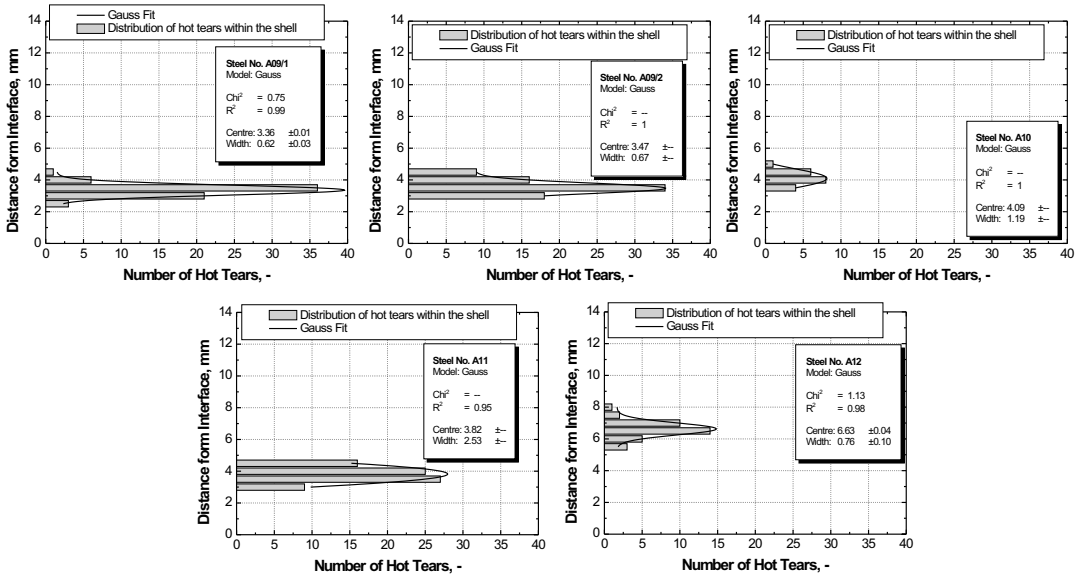

Figure B.12: *Distribution of detected number of hot tears for test series A (strain rate:* $0.006\ s^{-1}$*).*

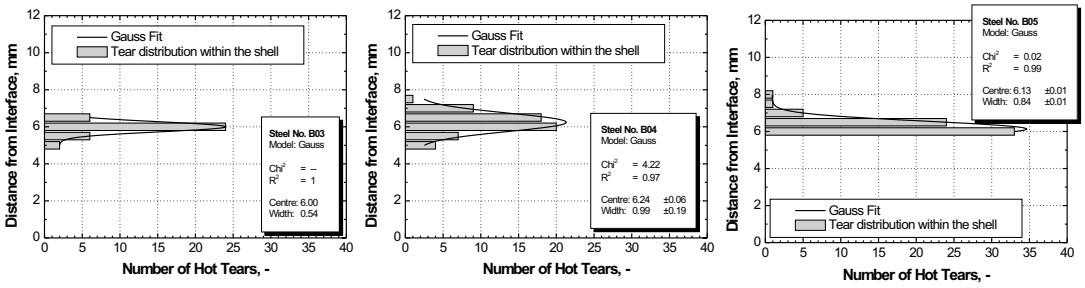

Figure B.13: *Distribution of detected number of hot tears for test series B.*

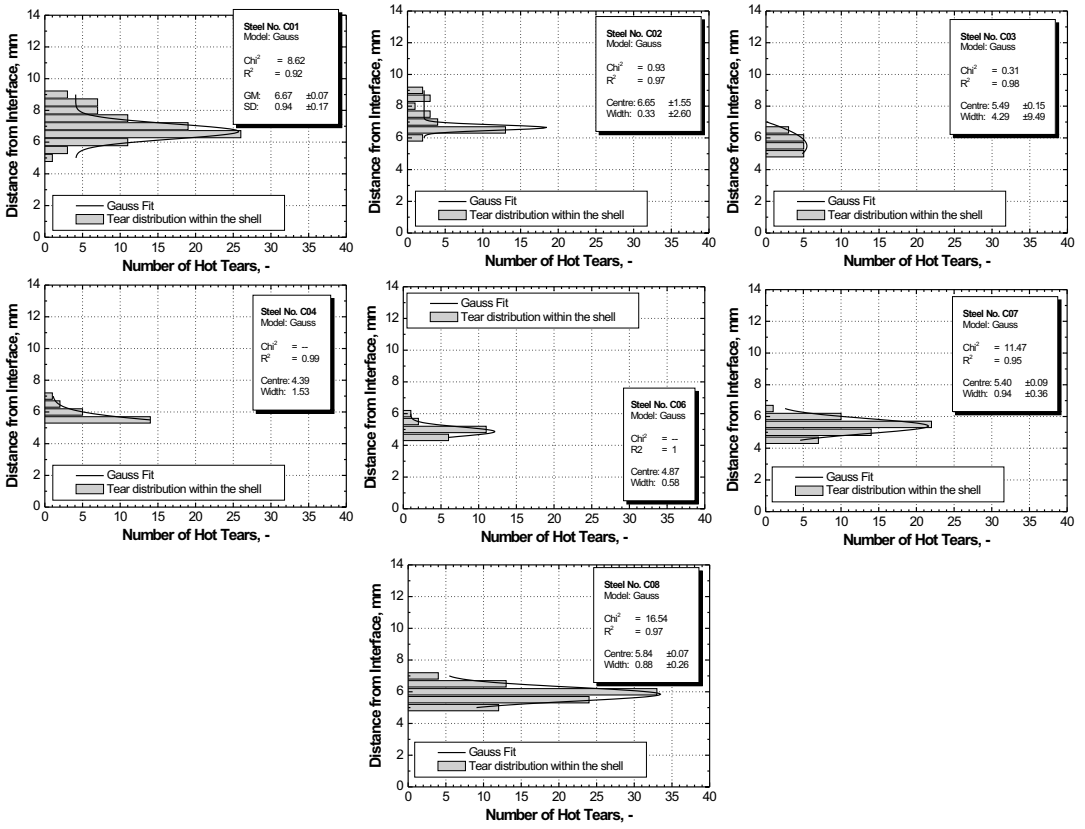

Figure B.14: *Distribution of detected number of hot tears for test series C.*

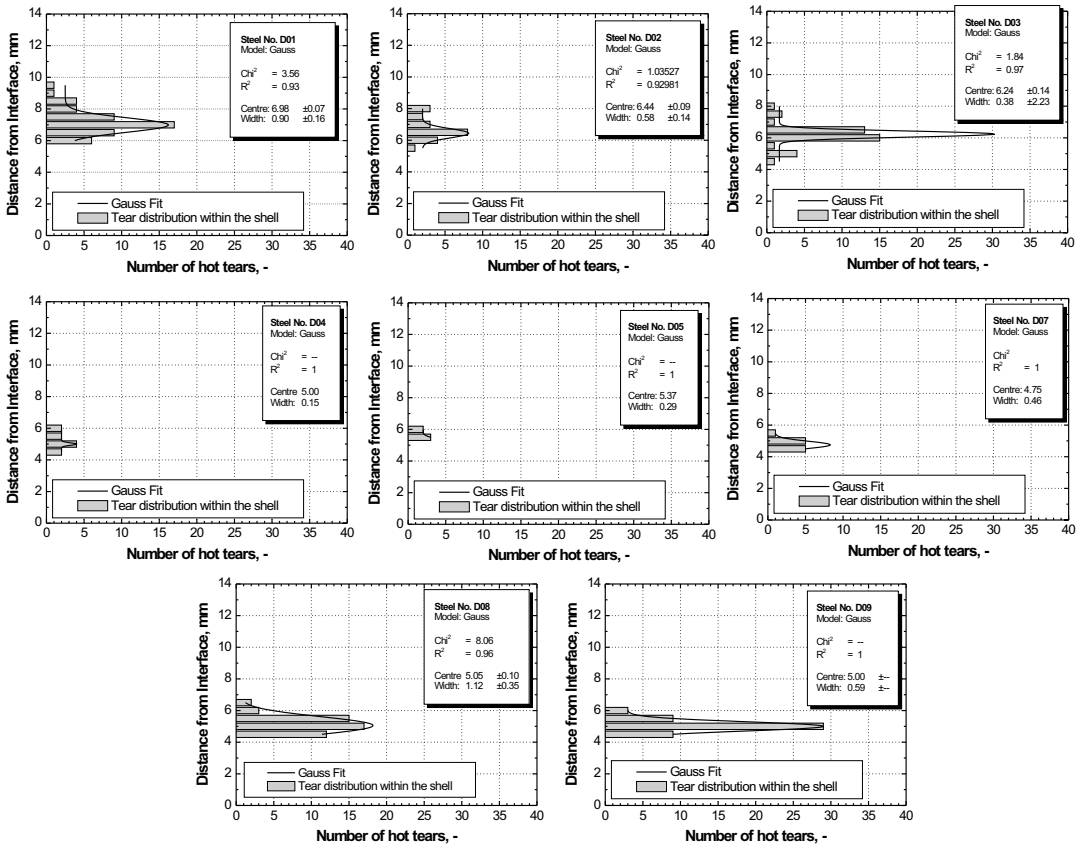

Figure B.15: *Distribution of detected number of hot tears for test series D.*

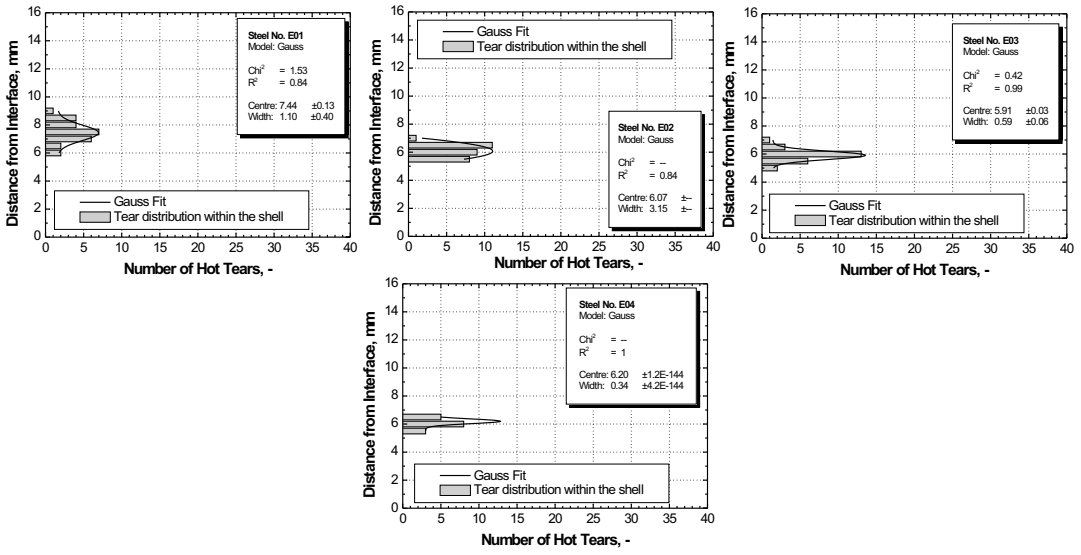

Figure B.16: *Distribution of detected number of hot tears for test series E.*

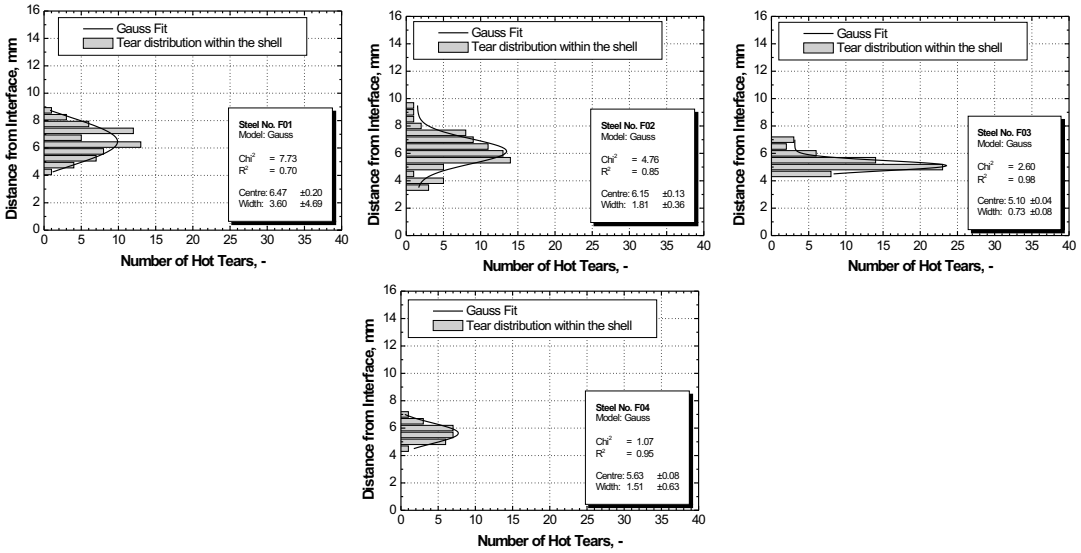

Figure B.17: *Distribution of detected number of hot tears for test series F.*

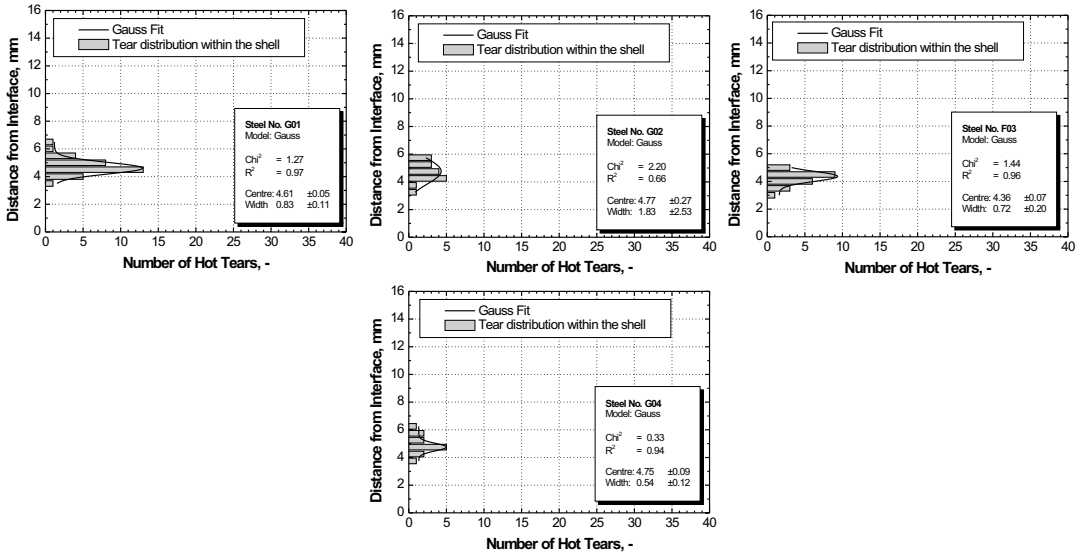

Figure B.18: *Distribution of detected number of hot tears for test series G.*

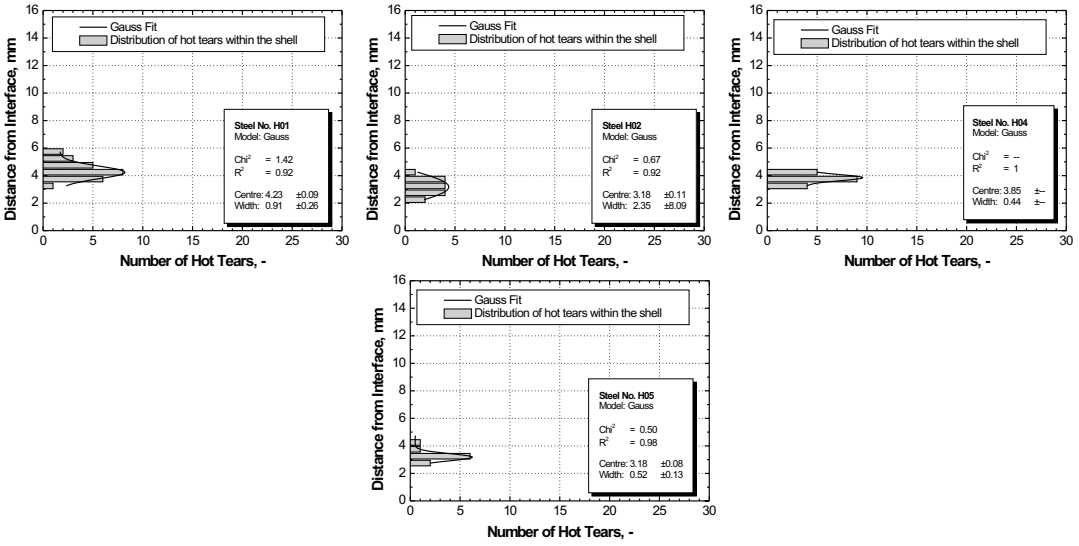

Figure B.19: *Distribution of detected number of hot tears for test series H.*